PHD THESIS

NEW DESIGNS OF THIN COATINGS FOR FIRE PROTECTION

Submitted to and defended at

UNIVERSITY OF LILLE
Ecole doctorale Sciences de la Matière, du Rayonnement et de l'Environnement
Unité Matériaux et Transformations, UMR CNRS 8207, ENSCL

For the degree of

Doctor of Philosophy

In Condensed Matter and Molecules
Specialty: Materials Chemistry

By
Anne-Lise DAVESNE

Supervised by

Prof. Serge BOURBIGOT and Prof. Maude JIMENEZ

Defended on the 22nd of October 2020 before the following PhD committee:

Prof. Frédéric SANCHETTE	Université de Technologie de Troyes, France	President
Prof. Jenny ALONGI	University of Milan, Italy	Reviewer
Prof Marianne COCHEZ	Université de Lorraine, France	Reviewer
Dr Fabienne SAMYN	Centrale Lille Institut, France	Examiner
Dr Sophie SENANI	SAFRAN Tech	Examiner
Prof Serge BOURBIGOT	Centrale Lille Institut, France	Supervisor
Prof Maude JIMENEZ	Université de Lille, France	Co-supervisor

THESE DE DOCTORAT

CONCEPTION DE NOUVEAUX REVÊTEMENTS FINS POUR LA PROTECTION CONTRE LE FEU

Présentée et soutenue publiquement à

L'UNIVERSITE DE LILLE
Ecole doctorale Sciences de la Matière, du Rayonnement et de l'Environnement
Unité Matériaux et Transformations, UMR CNRS 8207, ENSCL

Pour obtenir le grade de

Docteur

En Molécule et Matière Condensée
Spécialité : Chimie des Matériaux

par
Anne-Lise DAVESNE

Thèse dirigée par

Prof. Serge BOURBIGOT et Prof. Maude JIMENEZ

Soutenue le 22 octobre 2020 devant la Commission d'Examen composée de :

Prof. Frédéric SANCHETTE	Université de Technologie de Troyes, France	Président du jury
Prof. Jenny ALONGI	University of Milan, Italy	Rapporteur
Prof Marianne COCHEZ	Université de Lorraine, France	Rapporteur
Dr Fabienne SAMYN	Centrale Lille Institut, France	Examinatrice
Dr Sophie SENANI	SAFRAN Tech	Examinatrice
Prof Serge BOURBIGOT	Centrale Lille Institut, France	Directeur de thèse
Prof Maude JIMENEZ	Université de Lille, France	Co-directrice de thèse

A ma famille.

Acknowledgments

En tout premier j'aimerais remercier chaleureusement le Pr Alexandre Legris, ancien directeur de l'UMET, et Pr. Patrice Woisel, directeur actuel, pour m'avoir donné l'opportunité de rejoindre le laboratoire pour y travailler.

I am very grateful to Prof Jenny Alongi, Prof Marianne Cochez, Prof Frédéric Sanchette and Dr Sophie Senani for accepting to review this manuscript and be a part of the jury, thank you very much.

Un grand merci très chaleureux à Serge, Maude et Fabienne pour m'avoir accepté sur ce projet, et surtout pour leur supervision, pour les discussions, scientifiques ou non, pour leurs idées, leur aide précieuse et les opportunités qu'ils m'ont offertes.

Ce travail fait partie du projet FIREBAR Concept (ERC Advanced Grant Agreement no. 670747), qui n'aurait pas pu être réalisé sans le financement du conseil européen de la recherche, qui est ici grandement remercié.

Un remerciement tout spécial à Laura : je pense que l'expérience de la thèse aurait été moins supportable sans ton soutien constant et ta bonne humeur. On s'est tenu les coudes jusqu'au bout pendant trois ans et ça n'est pas rien ! Merci pour les petites séances zumba pendant et après les manips, la papote, les comptes rendus des reportages 7 à 8 après le week-end, et les petits verres remonte-moral à la fin des vacances ! Merci aux autres doctorants du projet ERC pour avoir rendu plus tolérable les réunions mensuelles de cinq heures, et pour l'aide précieuse. Merci Aditya pour ton aide, ta disponibilité et pour les blagues qui me font toujours rire. Roland, merci pour ta bonne humeur, tes conseils, et pour avoir été le meilleur vis-à-vis de bureau. Tatenda, merci pour ta force tranquille et ta gentillesse.

C'est important d'avoir un groupe soudé lorsqu'on fait une thèse, alors j'aimerai remercier très chaleureusement tous les autres doctorants, qu'ils soient déjà docteurs ou en passe de l'être, merci d'avoir rendu l'ambiance au labo aussi amusante, agréable et stimulante : Manon pour les gâteaux délicieux, la papote, le rire et les conseils zéro-déchets, Sophie pour toujours nous avoir rappelé qu'il fallait manger (très important), pour avoir essayé de m'apprendre l'arabe et pour faire la même taille que moi pour les séances de sport. Merci aux collègues du bureau 9bis, Angeline pour toutes nos conversations du matin et pour les petits dîners, et Alexandre pour les

discussions, et pour toujours partager tes chocolats et gâteaux. Merci à Charlotte pour ta bonne humeur et ton humour, et enfin merci à Elodie, Chi, Mariette, Louis, Nittaya, Agnès, Sawsen (merci énormément pour ton aide et tes conseils qui ont été très précieux au début de la thèse), Maryem, et enfin Xiao Dong pour les conversations du lundi matin en anglais et pour m'avoir appris un peu de chinois. Je vous souhaite à tous le meilleur.

A big thank you in English to Simone for having collaborated with me and having been so nice to work with. Thank you to Profs Jaime Grunlan and Federico Carosio for collaborating with me on the layer-by-layer project.

Un grand merci au trio technique, toujours là pour aider et toujours disponibles et gentils : Pierre, Benjamin et particulièrement Johan pour avoir été d'un si grand support pour les tests, l'extrusion et les mesures d'émissivité. Merci beaucoup à Tsilla pour son aide précieuse pour les mesures d'émissivité.

Enfin, merci beaucoup à tous les autres membres de l'équipe, qu'ils soient encore présents ou déjà partis : Pauline pour m'avoir accueillie si gentiment, Jérôme pour ton soutien et ta gentillesse, Guillaume, Morgane et Sophie.

J'aimerais également remercier Frédéric Sanchette pour avoir accepté de collaborer avec nous sur ce projet, une grosse partie de cette thèse n'aurait pas été possible sans ça. Merci beaucoup également à Fabrice Parent qui a fait tous les dépôts en PVD.

Je suis extrêmement reconnaissante à Séverine pour son expertise en microscopie, sa disponibilité, son implication et pour m'avoir aidée et conseillée pour les observations au MET, MEB et EPMA. Je souhaite également remercier chaleureusement Bertrand Revel et Bertrand Doumert pour leur support, leurs conseils et leur implication pour toutes les mesures de RMN du solide. Merci également à Florent Blanchard pour m'avoir consacré du temps pour m'aider sur la DRX.

Je voudrais finir en remerciant tout particulièrement mes parents Pascal et Evelyne pour leur soutien et globalement pour tout, c'est grâce à eux que je suis arrivée là. Merci aussi à mon frère Alexandre et à Lara pour m'avoir maintes fois hébergée quand j'étais sur Paris (et pour tout le reste aussi). Enfin merci à Lucas d'être toujours là pour moi depuis bientôt 6 ans, de m'écouter, de me soutenir, de me faire rire tout le temps, et pour tous les autres petits riens qui font tout.

Table of Content

List of Figures

List of Tables

List of abbreviations

Alg	Alginate
APP	Ammonium Polyphosphate
APTES	(3-Aminopropyl) Triethoxysilane
ATH	Aluminum Trihydroxide
BL	Bilayer
BPEI	Branched Polyethylenimine
CelNF	Cellulose Nanofibers
CH	Chitosan
CNF	Carbon Nanofibers
CP	Cross Polarization
DEPAL	Aluminum Diethylphosphate
DEPETS	Diethylphosphatoethyltriethoxysilane
DNA	Desoxyribonucleic Acid
DOPO	9,10-Dihydro-9-Oxa-10-Phosphaphenanthrene-10-Oxide
DPTES	Diethylphosphatoethyltriethoxysilane
EG	Expandable Graphite
EPMA	Electron Probe Micro-Analysis
ERC	European Research Council
FPUF	Flexible Polyurethane Foam
FR	Fire Retardant
FTIR	Fourier Transform Infrared
GO	Graphene Oxide
HAL	Halloysite
h-BN	Hexagonal Boron Nitride
HFT	Horizontal Flame Test
HG	Hydrogel
HMDSO	Hexamethyldisiloxane
HRC	Heat Release Capacity
HRR	Heat Release Rate

IR	Infrared (NIR, MIR Or FIR: Near, Mid Or Far Infrared)
LAP	Laponite
LbL	Layer-By-Layer
LDH	Layered Double Hydroxide
LOI	Limited Index Oxygen
MAS	Magic Angle Spinning
MCC	Microscale Combustion Calorimetry
MDH	Magnesium Dihydroxide
MLC	Mass Loss Cone Calorimeter
MMT	Montmorillonite
MPP	Melamine Polyphosphate
MTMS	Methyltrimethoxysilane
MWCNT	Multi Wall Carbon Nanotube
Na-PSS	Sodium Poly(Styrene Sulfonate)
NC	Nanocomposite
NMR	Nuclear Magnetic Resonance
OP	Exolit OP1311, Mixture Of DEPAL And MPP
OPC	OP And Cloisite
PA	Phytic Acid
PA6	Polyamide 6
PA66	Polyamide 66
PAA	Polyacrylic Acid
PAH	Poly(Allylamine Hydrochloride)
PAN	Polyacrylonitrile
PC	Polycarbonate
PCFC	Pyrolysis Combustion Flow Calorimeter
PDADMAC	Poly(Diallyldimethylammonium Chloride)
PE	Polyester
PEI	Polyethylenimine
PET	Polyesterterephtalate
pHRR	Peak Of Heat Release Rate
PLA	Polylactic Acid
PMMA	Poly(Methyl Methacrylate)

POSS	Polyhedral Oligomeric Silsesquioxane
PP	Polypropylene
PS	Polystyrene
PSP	Poly(Sodium Phosphate)
PUF	Polyurethane Foam
PVA	Polyvinyl Alcohol
PVD	Physical Vapor Deposition
PVP	Poly(Vinylphosphonic Acid)
QCM	Quartz Crystal Microbalance
QL	Quadlayer
rGO	Reduced Graphene Oxide
RPUF	Rigid Polyurethane Foam
SEM	Scanning Electron Microscopy
SEP	Sepiolite
SWCNT	Single Wall Carbon Nanotube
TEOS	Tetraethoxysilane
TEP	Triethylphosphate
TGA	Thermogravimetric Analysis
THR	Total Heat Release
TL	Trilayer
TMOS	Tetramethoxysilane
TSR	Total Smoke Release
TTI	Time To Ignition
UV	Ultra Violet
VFT	Vertical Flame Test
VMT	Vermiculite
VTS	Vinyl Trialkoxysilane

General introduction

The ever-increasing demand for high performance systems has led to an extensive use of combustible materials, mainly organic. This poses a huge threat on human lives and infrastructures integrity because of their high flammability, as attested by the many catastrophes occurring regularly (the fire of the Grenfell Tower for example is still fresh in the collective mind). The fire retardancy of those systems is therefore a necessity. It is the objective of the FireBar project (ERC-AdG funded, grant agreement n°670647/FireBarConcept/2014-2020) to design new materials with low flammability and restraining fire spread thanks to a better fundamental understanding of the mechanisms of fire protection, and a multi-disciplinary approach combining modelling and simulation, the development of new experimental protocols and multi-material designs.

There are three ways to lower the flammability of combustible materials. The first one is to synthesize intrinsically fire retardant polymers, or to graft active functions on the backbone of existing polymers. The second one is to add fire retardant molecules in the polymer matrix. Finally, a protective coating can be added that will act as a barrier for the mass and heat transfer responsible for the combustion. This work focuses on the last option which is very promising, as it allows to concentrate the action of the protective system on the surface of the flammable substrate (or in other words where it is needed). In addition, the processing is relatively easy, with few compatibility issues, and it has a minimal impact on the functional properties of the material.

A review of the literature shows the increasing interest for this approach, with a variety of systems explored. The most promising ones are those allowing an adequate protection, while maintaining thicknesses ranging from a dozen nanometers to a few microns, thanks to processing methods using sol-gel, plasma or layer-by-layer technologies. Layer-by-layer thin coatings, especially, have been extensively studied because of their high efficiency in reducing the flammability of a large variety of substrates, as well as their low thicknesses, versatility, ease of use and environmental-friendliness. Their mode of action is however still poorly understood, even if some thoughts have been given in the literature about it.

The objective of this work is therefore to first gain a detailed understanding of the mechanism of protection of layer-by-layer coatings. It is then expected that this understanding will give new insights for the development of innovative thin coatings designs.

In a first chapter, a state of the art of fire retardancy of polymers by surface treatment approaches is reported. Especially, the existing literature for layer-by-layer coatings is detailed and fully commented. In addition, new promising strategies for the development of new designs of thin coatings for fire protection are identified thanks to an interdisciplinary literature review. It also appears that each approaches are adapted to various kind of substrates, which are studied in each section of this manuscript.

The second chapter is dedicated to the determination of the mechanism of action of layer-by-layer coatings applied on polyurethane foams. Two systems were studied, the first one consisting in alternative layers of chitosan and vermiculite platelets, and the second in a single bilayer of polyethyleneimine and hexagonal boron nitride.

The understanding of the mode of action of these systems allowed to develop new systems based on composite hydrogels with a high filler content for the fire protection of textiles. PA66 fibers were coated with alginate/clay systems in a simple one-pot procedure, which is described in a third chapter.

In a fourth chapter, a new system was designed limiting radiative heat transfer. Coatings based on a metallic layer protected by a dielectric were deposited on PA6 plates in order to reflect incident radiation coming from the heat source. The combination of these protected mirrors with bulk fire retardant molecules was also examined to reach a complementary effect.

Finally, the materials and methods used in this project are presented at the end of this manuscript, after a general conclusion summarizing the different results of this work and the outlooks that can be envisioned is provided.

Chapter 1 . Thin coatings for fire protection: state of the art

In this section, an overview of the state of the art concerning flame retardant surface treatment is given. At first, basics on polymer combustion and the different strategies to fire retard polymers are described. Then, the interests of thin surface treatments as a strategy to fire protect various substrates are described, and the different methods are discussed.

I. Polymers combustion and fire retardancy

Polymers, in general, are widely used due to their specific advantageous properties. They are light, durable, resistant to corrosion and they offer mechanical properties unreachable with other classes of materials. They are present everywhere in our daily environment, in indoor furniture and upholstery, household appliances, building insulation, electric cables insulation, outdoor infrastructures and furniture or disposable tableware and containers. They are also used in more technical applications such as airplanes, automotive, rail, energy or space industries, raw or as composites. However, their organic nature makes them highly inflammable, and several catastrophes can attest of the danger their use can pose if this property is not properly considered. Statistics for the year 2018 in France show that 305 500 of safety interventions were due to fires, causing 26 253 victims including 262 deaths.[1] World's statistics compiled from 34 countries by the CTIF report 3,2 million fires in 2017, resulting in 16 900 fire deaths.[2] The Grenfell tower tragedy that costed 72 lives in June 2017 is still fresh in the minds of people living in Occidental Europe.

Polymer combustion is a complex and self-sustaining mechanism, involving reactions both in the condensed and gas phase, that is driven by heat and mass transfer at the interface between the material and the flame. Under high temperatures, polymers undergo thermal decomposition. Thermo-oxidative reactions also take place in presence of oxygen. Both yield small volatile molecules as well as radical species, highly likely to be very reactive, especially those evolved from the reaction with oxygen. When they are released into gas phase, they form an inflammable mixture with air, which will combust if the temperature is high enough (above ignition temperature) or in the presence of an external source of energy such as a spark or an electric arc for example. Combustion of the reactive species with oxygen creates light (which emission spectrum depends on the species present in the flame) and is exothermic. The resulting heat feedback to the material will help sustaining the polymer combustion reaction until oxygen or flammable mass are depleted. Further products of the thermal and thermo-oxidative reactions might not be volatile, which can contribute to limit the amount of flammable products, mainly by forming a stable carbonaceous layer called char. The combustion process of polymers is summarized in Figure 1.

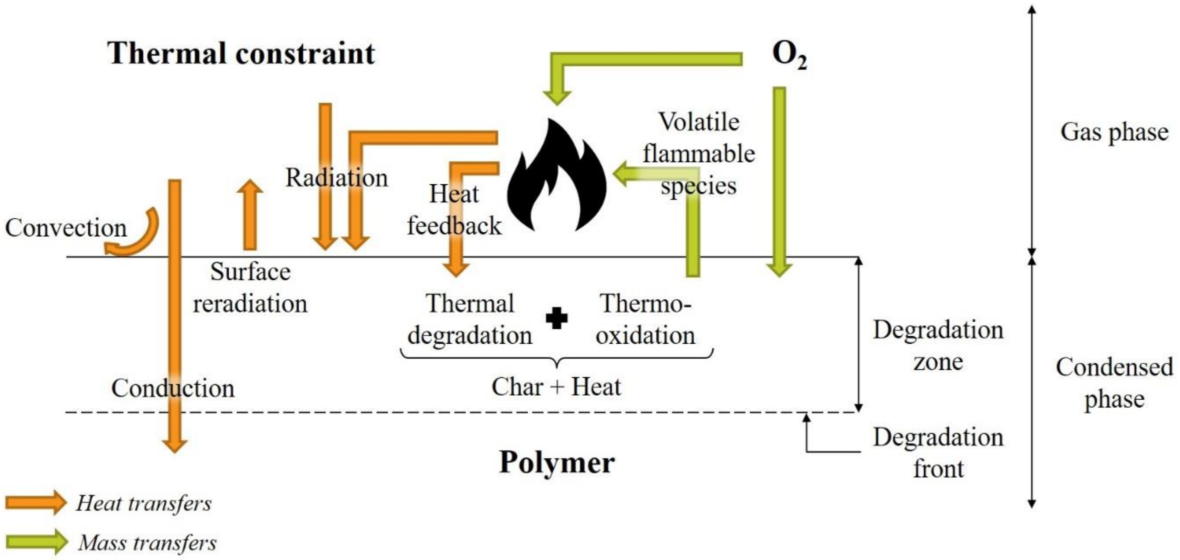

Figure 1. Polymer combustion mechanism.

Methods to fire protect polymers act on at least one of the elements of the diagram. The first method consists in synthetizing a polymer intrinsically resistant to thermal decomposition, or whose decomposition yields a thermally stable residue. For example, high performance polymers, such as PolyEther Imide, PolyEtherEtherKetone (PEEK), PolyImide (PI), PolyBenzOxazole (PBO), etc., have high decomposition temperatures, as well as in some cases a high char yield, which makes them intrinsically fire resistant.[3] Another approach consists in modifying already-existing polymers by grafting active functions on the polymer backbone or by modifying the monomer with potentially fire-active functions before polymerization. Functions containing P, S, N, B, Si or other compounds have been grafted on various polymers to limit their flammability.[4] For example, phosphorus groups have been added to polyamide[5] or polystyrene[6] chains to produce fire retardant polymers. Because of its complexity, high costs, and often processing difficulty of the resulting materials, this method is usually restricted to highly technical applications.

The second method consists in incorporating fire retardant (FR) additives into the polymer matrix. This is the most commercially used method as processing is easy and low-cost. Problems to care for are the compatibility of fillers with the matrix. Also, high loadings are sometimes required, which can impact the mechanical properties of the polymer. Nevertheless, many systems have proven to be efficient. Chemistry of the fire retardant molecule or system is what drives its performance. Traditional FRs rely on chlorinated or brominated components, for example Tetrabromobisphenol A or hexabromocyclododecane.[7] They act mainly in the gas phase by inhibiting the radical reactions during the combustion. However, they are under scrutiny because of their suspected toxicity.[8] Due to their small size, they tend to migrate out of the polymer matrix and pollute the environment or cause risks to human health. A solution to this problem was the development of brominated and chlorinated polymers. But, in addition, the corrosive gases emitted during a fire still raise health and environmental concern. Despite their high efficiency, they are therefore being replaced by other solutions. Organophosphorus compounds have shown their effectiveness, especially when combined with other elements such as nitrogen. They limit fuel output by enhancing char forming ability leading to thermally stable residues. They can also act in the gas phase by poisoning combustion reactions. Nitrogen fire retardants act mainly in the gas phase by releasing nonflammable NH_3 gas and diluting the active species in the flame. However, they are mostly used as synergists in combination with other fire retardants, as their effect is limited. Metal hydroxides and carbonates have also been proven to be efficient, but only at high loadings, which usually modify the mechanical properties of the final material. For example, $Al(OH)_3$ and $Mg(OH)_2$ act by decomposing and releasing H_2O. This endothermic reaction cools the material and the release of H_2O smoothers the flame. They also act in condensed phase by forming a ceramic barrier. Then, mineral fillers such as talc, silicon, silicon oxides, boron compounds or transition metal oxides have shown interesting fire retardant (char formation enhancement, catalysis of char formation, synergists, formation of ceramic barriers…) and smoke-suppressing properties.[8] Nanocomposites are also a class of materials having good fire properties, and have been studied a lot since their discovery. They act by forming a protective mineral layer upon heat exposure, acting as heat and mass transfer barrier.

Interesting fire performances are seen with intumescent systems (from the latin word *intumescere*, “to swell up”). Intumescent materials are composed of an acid source, a blowing agent and a carbon source. Upon heat exposure, the acid source decomposes and reacts with the carbon source to form a stable viscous cross-linked carbonaceous material. The blowing agent decomposes by releasing gases which will be trapped in the char and form an insulating carbon foam which protects the underlying polymer. The formulation can include nano- and/or micro-fillers as synergists (e.g. zeolites and clays). They either help the char formation or strengthen it to avoid the formation of cracks due to internal and external stresses.[9]

Intumescent systems have also been used as coatings, which is the last possible method to protect a polymer against fire. Although it also has some drawbacks (adhesion and durability being the main ones), adding a protective coating has several advantages when compared to the other two methods. First, the FR properties are concentrated at the surface, where the fire hits first, and there is less compatibility issues with the matrix. Finally, the functional properties of the materials are not or barely impacted. On a more fundamental point of view, it allows to act directly as a barrier against the mass and heat transfer driving the combustion process.[4]

In this work, the use of thin coatings has been investigated. Coatings with very low thicknesses have attracted a lot of the attention, mainly because they allow using a minimal amount of materials while still providing an efficient protection. Plasma, sol-gel, and others have been conducted to make thin coatings for many applications, including fire protection, with great success. [10], [11]

II. Flame retardant surface treatments

1) Sol-gel synthesis of fire protective thin coatings

The sol-gel process was introduced several decades ago and has been extensively studied ever since. It has focused a lot of interest, especially because it is carried out in soft conditions (low temperature, ambient pressure…) and because the processing of materials (particles, coating or monolith) is relatively easy. The process can be divided in three steps (see Figure 2). First, metal alkoxides $M(OR)_z$ (where M is a metal and R an alkyl group) are dispersed in a solvent to form a stable suspension of colloidal particles called a sol. Second, the metal alkoxides are hydrolyzed. This step is catalyzed by an acid or a base. Afterwards, it is followed by a condensation step.

The resulted product is a vitreous network (the gel). Its composition depends on the reaction conditions and on the nature of metallic precursors. Hybrid organic-inorganic coatings can be produced depending on their chemistry. Usually silicon alkoxides such as tetramethoxysilane (TMOS) or tetraethoxysilane (TEOS) are used as precursors to give silica-like structures, but other metal alkoxides from Al, Ti etc. can be used, which gives access to a wide range of properties.[12]–[14]

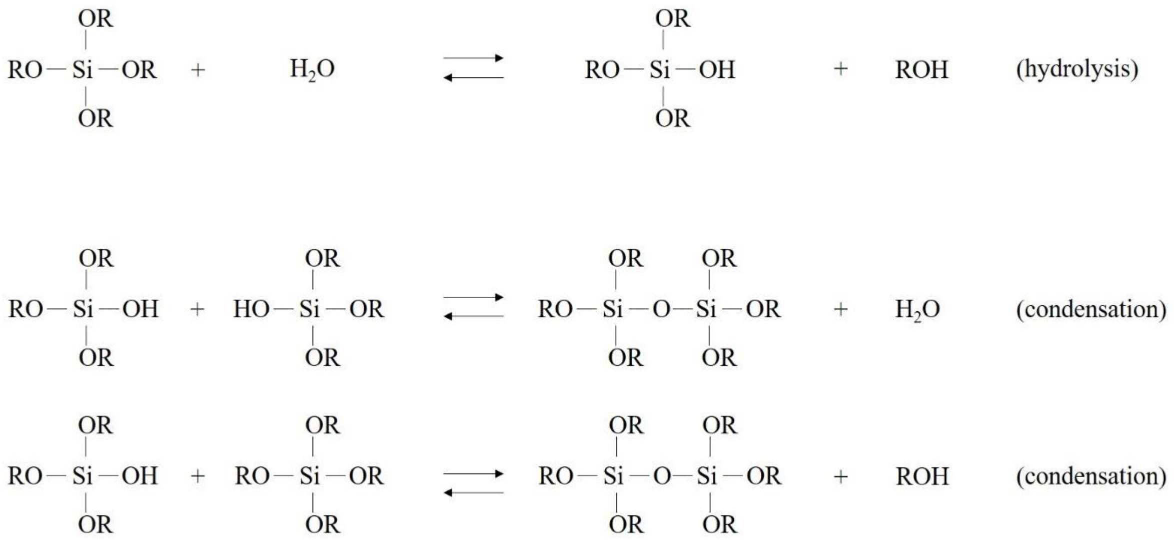

Figure 2. Sol-gel process. (example of silicon alkoxides)

Once dried, monoliths are usually fragile and broken down in powders, but thin functional sol-gel coatings have been developed throughout the years for various applications, including fire protection. First, sol-gel network can be used as additives in fire retardant coating formulations. They have been included in UV-curable resins for coatings which show potential for fire retardant applications.[15]–[21] They can also be casted as thin coatings on various substrates. They are applied either by dip-coating, spin coating, or by simply letting the water of a pool of gel evaporate.

The first records of sol-gel treatments for fire protection showed the potential of the approach for reducing the flammability of combustible materials. A coating of TEOS or a γ-triethoxysilane terminated poly(1-caprolactone) was deposited on poly(methyl methacrylate) (PMMA) and increased the time to ignition by 55% in a glow wire test. The protective effect was attributed to the accumulation of SiO_2 particles on the surface upon burning.[22]

Additionally, a hybrid coating of poly(metacrylic acid), TEOS and perfluoroalkyltriethoxy-silane on nylon carpeting gave good results in a pill test.[23]

Most sol-gel thin coatings for fire protection are applied on cotton fabrics, even if some studies mention their interest for Polyurethane foam (PUF) substrates,[24] expanded polystyrene (PS) foam,[25] polycarbonate (PC) panels[26] or wood.[27] All studies report either self-extinguishment, increase in Limited Index Oxygen (LOI), or decrease in peak of Heat Release Rate (pHRR), Total Heat Release (THR) and Total Smoke Release (TSR), depending on the tests performed. They also report the necessary synergism with other flame retardants such as phosphorus-based compounds.

Indeed, studies reporting the coating of polymers with silicon alkoxides only show either limited decrease of their flammability [28]–[30] or worsened combustion behavior, even if the time-to-ignition is sometimes longer.[31] Even if they don't provide significant protection, a silica coating can still enhance the charring of cotton when a small flame is applied,[32]–[36] and reduce its pHRR significantly (up to 35%).[37], [38] On synthetic fabrics such as PET and PA66, a silica coating can prevent melt-dripping, which is a huge fire hazard,[39], [40] but also enhance the durability of other surface flame retardant treatments.[41]

As a matter of fact, the fire protective properties of sol-gel coatings are usually enhanced by taking advantage of the synergism existing between silicon and other compounds, by adding fire retardants in the sol formulation, or both. For example, interesting fire behavior was obtained by using phosphorus-doped sol-gel precursors, especially for cotton. Using diethylphosphatoethyltriethoxysilane (DPTES), for instance, enhanced the charring of cotton in a vertical fire test and reduced the pHRR and the TSR respectively by 52 and 56% at cone calorimeter test.[42], [43] It was found that if the effect of silica was more prominent against a small flame, the synergism with P was necessary to improve the combustion behavior in a radiative scenario.[44], [45] Other strategies to use P and Si synergism is to treat the cotton by phosphorylation [34] or phenylphosphonic acid padding.[36] More commonly, phosphorous-containing molecules are added in the sol, such as aluminum phosphinate,[46], [47] phytic acid,[48]–[50] diethylphosphite,[33] ammonium polyphosphate,[51], [52] ammonium hexametaphosphate,[53] phenylphosphonic dichloride,[54] triphenylphosphate [55] or 9,10-dihydro-9-oxa-10-phosphaphenanthrene-10-oxide (DOPO).[56] The combination reduces the pHRR and THR in MLC and brings self-extinguishment behavior, which can be further enhanced by the addition of a molecule containing nitrogen, in order to obtain a P-Si-N synergism.[33], [34], [47], [49], [57] For example, DPTES on cotton mixed with monoethanolamine rises the LOI of the fabric up to 29%.[58] Phosphoramidate siloxane (DTSP) on cotton increases the LOI up to 30%. The coatings enhance char formation, leading to self-extinguishment behavior in a vertical flame test (VFT), while the pHRR and THR are reduced by 68% and 49% respectively at mass loss calorimeter test (MLC).[59] Other flame retardants such as alumina particles [60] ZnO, [61] boric acid, borax, or boron-containing additives [55], [62], [63] have also successfully been used to bring self-extinguishment to the fabrics.

Sol-gel treatments have also shown promising effects on synthetic fibers. PA66 fabrics grafted with a phosphorylated chitosan and coated with a sol-gel coating of (3-aminopropyl) triethoxysilane (APTES) stopped the melt-dripping against a small flame and reduced the pHRR by 30%.[39] Thanks to enhanced charring, the melt-dripping of PA6 fibers was also suppressed thanks to a TEOS sol-gel coating doped with 9,10-dihydro-9-oxa-10-phosphaphenanthrene-10-oxide-modified vinyl trialkoxysilane (DOPOeVTS).[64] The synergism between P, N and Si in a sol-gel methyltrimethoxysilane (MTMS) coating containing urea and phosphoric acid also suppressed the melt-dripping of PET and raised its LOI up to 28%.[65]

2) Plasma-aided formation of fire protective thin coatings

Plasma is a gas containing neutral species (atoms, molecules) and ions, either in their fundamental state or in an excited state, which emit electrons and photons during their de-excitation. It can be used to functionalize the surface of materials, either as a pre-treatment to enhance the adhesion of a coating or a finish, to induce the polymerization of active species or to deposit functional molecules. Cold plasma in particular has gained interest as it avoids using thermal treatment or extensive amount of solvents. The development of atmospheric plasma also allows to get rid of expensive vacuum equipment.

Plasma pre-treatment of flammable substrates has been mainly used to graft and polymerize fire retardant molecules on textiles. Plasma polymerization of phosphate-containing monomers was first carried out by Akovali et al. on polyacrylonitrile (PAN) and PET fabrics.[66], [67] While keeping the thickness of the added layer below 10 µm, they observed an increase in LOI and a slight decrease of the burning rate of the fabrics. However, they state that the fire-retardant species added must be efficient at small intake, otherwise the detrimental effect of the cross-linking of the fibers induced by plasma treatment would predominate. Plasma-induced polymerization of monomers containing phosphorus and/or silicon is privileged. Silicon or organophosphorus silicon monomers such as 1,1,3,3-tetramethyldisiloxane have been polymerized via plasma-assisted grafting on PA6 or PA6 powders, which increased the LOI by a few percent and reduced the pHRR and the THR respectively by 30 and 26% at mass loss cone test.[68]–[71] Diethylphosphatoethyltriethoxysilane (DEPETS)[72] or hexamethyl-disiloxane (HMDSO)[73] have been deposited respectively on PA6 and PC, and PA66 substrates. While with DEPETS the TTI was increased by 143%, HMDSO reduced the TTI and decreased the pHRR by 30% in mass loss cone calorimetry, without any change in THR and mass loss. However, the performance of silicon coatings can be improved by adding phosphorus molecules, for example triethylphosphate (TEP) with HDMSO on PC or PA6,[74] or vinyl phosphonic acid with cyclotetrasiloxane on cotton fabric.[75] The enhancement of the performance is believed to be due to condensed phase reactions as well as to a synergism between P and Si. A protective char layer is formed as a result, which helps reducing the pHRR and increasing the LOI considerably. But the particular interest of plasma-deposited fire retardant coatings is that they can enhance the performance of fire retardant substrates. For example, the fire performances of Proban and Nomex (commercial fire retardant fabrics) in a flash fire scenario were enhanced with a plasma-deposited HDMSO film.[76] The plasma-grafting of 1,1,3,3-tetramethyldisiloxane coating increased the LOI of PA6 nanocomposite from 22% to 42% and decreased the pHRR and THR by 41% and 33% respectively.[77] Several other studies are focused on the grafting of phosphate or phosphonate-functionalized acrylate monomers on PAN fabrics,[78] cotton,[79] silk[80], [81] or polyethylene substrates.[82] The grafting of fire retardant precursors has also been carried out on Polyurethane Foam (PUF) substrates. A durable diethylvinylphosphonate coating, cross-linked with 1,4 butanedioldiacrylate, prevented melt-dripping and gave self-extinguishment behavior to the PUF substrates. Boron and fluorine chemistries have also been tested on PP[83] and PA6[84] respectively.

Plasma treatment has also been used as a pre-treatment to enhance the adhesion of fire retardant molecules or coatings. A coating of montmorillonite platelets adsorbed thanks to the oxygen and radical species generated through plasma treatment increased the time to ignition of PET fabrics significantly.[85] Adhesion of organo-clay following the same principle (with an additional cross-linking step) decreased the pHRR of glass fibers reinforced epoxy composites.[86] The same principle was applied for the padding of polyester fabrics with alkyl-phosphonate, which allowed the LOI to reach values superior to 30%.[87] Additionally, a plasma-deposited coating of HDMSO also enhanced the adhesion of SiO_2 particles on PP and PS substrates.[88] Plasma treatments were also applied as post-treatment to increase the charring capacity and the durability of a coating via cross-linking.[89], [90]

Despite the interest of sol-gel and plasma approaches in bringing fire retardant properties to different materials, the most extensively studied method to make flame retardant materials via a surface treatment is by applying a layer-by-layer coating. Indeed, a layer-by-layer surface treatment has proven to be a very efficient, versatile and facile strategy for the fire protection of various substrates. These coatings are very interesting as their protective effect is high, even if the thickness of the coating is below 1 µm. Therefore, they are discussed in more details in the next paragraph.

III. Layer-by-layer coatings for fire protection

1) Generalities on nanocoatings made via layer-by-layer

Coatings made by layer-by-layer (LbL) have attracted a lot of interest since the technique was introduced in 1992 by Decher [91], [92] to improve the Langmuir-Blodgett technic and perfecting the work from Iler.[93] Layer-by-layer is a bottom-up nanofabrication technique for coatings or self-standing ultra-thin films (up to a few hundred micrometers). As opposed to the top-down method which relies on precise shaping of macroscopic materials into nanostructures, it uses physico-chemical processes to assemble elementary building blocks (polymers, nanoparticles, etc.) into macroscopic nanopatterned objects. Supramolecular chemistry is a famous example of a bottom-up method leading to complex structures by the self-assembly of molecules,[94] and despite it not being the original inspiration, some authors pointed out how similar this technic is to biological systems.[95], [96] The advantages of layer-by-layer in constructing thin films are multiple. First, it is an environmental-friendly process, as it is usually carried out in water. Then, it can be adapted to a wide range of substrates with complex structures, and it uses very little materials. The varieties of building blocks that can be used have also expanded the use of layer-by-layer coatings to many applications based on surface modification. The process relies on the self-assembly of two compounds driven by attractive forces. Commonly, electrostatic attraction between two compounds with opposite charges is what binds the layers together, but it was expanded to hydrogen bonding, covalent bonding, van der Walls forces, complexes formation... Basically, any type of acceptor/donor interactions. This results in coatings with controllable thickness and structures.

Using electrostatic interactions as an example, a charged substrate is immersed in a solution of ionic species of the opposite charge. At the surface, these are attracted by the substrate and form ionic complexes. Any excess or weakly adsorbed ions are rinsed by dipping the substrate in water, before immersing it once again (with an optional drying step) in a solution of ions of opposite charge, and rinsing it. This process creates a bilayer, and is repeated the necessary number of times to reach the required bilayer number or the required thickness. This is usually controlled by Quartz Crystal Microbalance (QCM) on silicon wafers, or by UV-Visible spectroscopy. The process is illustrated in Figure 3.

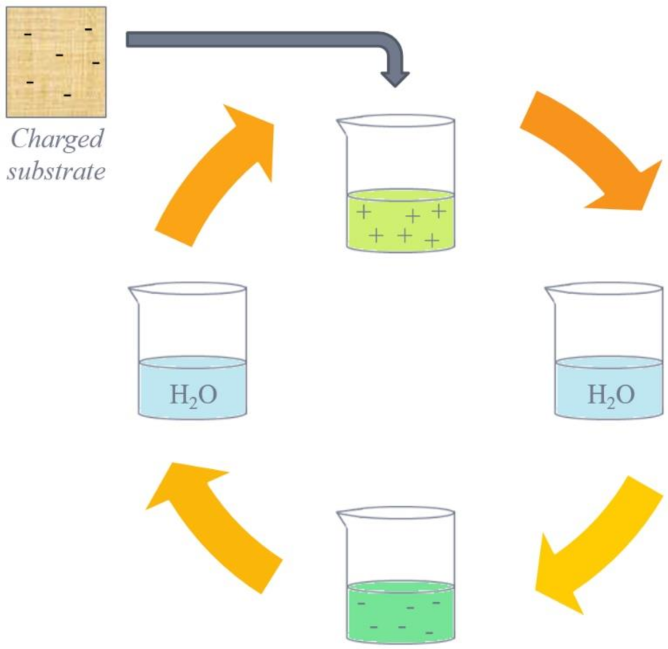

Figure 3. Schematic illustration of the layer-by-layer process (example of electrostatic interaction, with a negatively charged substrate).

The coating grows from the surface, and the growth profile depends on a lot of parameters. The charge density is important for instance, as well as the ionic force of the solution or the nature of the salt, which can induce more or less screening of the charge, and can cause coiling of polymers' chain, for example. Other parameters can influence the film's growth and morphology, such as the characteristics of the surface (charge density, roughness…), characteristics of the solution (concentration, pH, presence, nature and concentration of added salts…), or deposition conditions (time of adsorption, dipping speed, stirring, temperature, humidity of the environment, drying conditions, rinsing…).[92], [97] There are two growth profiles: linear and exponential. Linear growth happens when there is no diffusion at the interface. In that case, the deposition of a layer depends on its charge and on the charge of the surface, resulting in a thickness proportional to the number of layers. Exponential growth happens when there is diffusion at the interface. It is sometimes sought after because it means a higher thickness can be reached after fewer numbers of steps. First it was believed that the formation of coacervates, with a roughness increasing with the thickness, was responsible for this phenomenon, or a swelling and increased water absorption. However, it was proven that polycation diffusion in and out of the film was the cause.[98] Polycations diffuse in the film during cationic deposition, but out of the film during the rinsing steps and the polyanions deposition. There they form a complex with the incoming anions. Thickness was found to be proportional to the number of cations diffusing out of the coating.[99]

Layer-by-layer thin coatings can be built by a variety of techniques, including dip-coating, [100]–[107] spin-coating [108]–[113], spray coating [114], [115], roll-to-roll processes [116], [117]… depending on the scale, available instrumentation and substrate. For example, dip-coating is usually the preferred method for complex substrates such as foam or textiles, while roll-to-roll is adapted from textile finishing techniques; spin and spray-coating are usually used for flat surfaces. Automatic instrumentation and innovative processes are sought in order to reduce the deposition time and efforts. For example, Gittleson et al. conceived an automated spin-spray instrumentation,[118] Seo et al. an automatic spraying system,[119] while Prof Grunlan's group developed a continuous automatic dip-coating method for textile[120] as well as for various substrates[116]. Carosio et al. relied on padding to create efficient fire retardant layer-by-layer coatings on polyurethane foams within a matter of seconds[121].

As it was mentioned above, LbL allows for using a large variety of building blocks, from polymers to colloids or surfactants. PolyEthyleneImine (PEI), sodium Poly(Styrene Sulfonate) (Na-PSS), Poly(diallyldimethylammonium chloride) (PDADMAC), Poly (Acrylic Acid) (PAA), Poly(Allylamine Hydrochloride) (PAH) as polymer electrolytes have been used extensively since they can have high density charged according to pH. Biopolymers such as polysaccharides (chitosan, alginate…) have also been studied in layer-by-layer process because of their ionic nature (Table 1).

Table 1. Examples of polymers, synthetic and biobased commonly used in layer-by-layer processes

Type	Formula	Name
Synthetic polymers	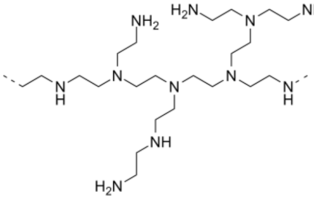	Branched Polyethyleneimine (BPEI)
	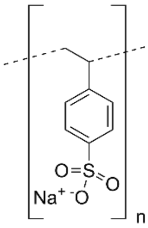	Sodium Poly(Styrene Sulfonate) (Na-PSS)
	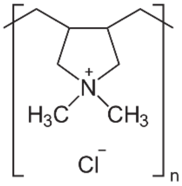	Poly(diallyldimethylammonium chloride) (PDADMAC)
	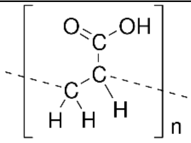	Poly (Acrylic Acid) (PAA)
	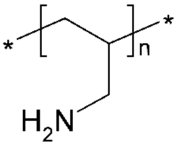	Poly(Allylamine Hydrochloride) (PAH)
Biosourced polymers	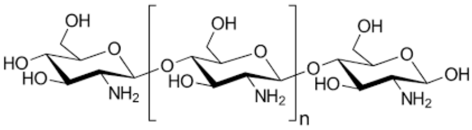	Chitosan
	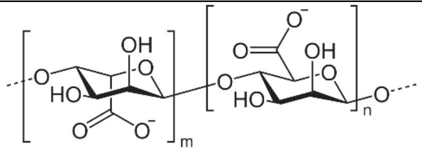	Alginate

Polyelectrolytes multilayer films as well as composite coatings have been fabricated by this method using an extensive amount of different nanoparticles, from silicon-based nanoparticles such as Polyhedral Oligomeric Silsesquioxane (POSS),[122]–[124] SiO_2 [125]–[127] to carbon-based nanoparticles and other inorganic species depending on the application and trends. In that case, polymers play the role of a binder between inorganic particles, even if some papers report the design of all-inorganic coatings.[128]

2) State of the art on layer-by-layer coatings for fire protection

Fire protection of flammable substrates by layer-by-layer coatings has been quite developed for a couple of decades. As mentioned in the paper by Holder et al.,[129] the first suggestion of using layer-by-layer coatings was made by Srikulkit et al. in 2006.[130] Despite the fact that they made no fire test, they demonstrated the interest of using such coatings for this purpose. 10 to 60 bilayers of Chitosan and Polyphosphoric acid were deposited on silk, and thermogravimetric analysis (TGA) at 10°C/min in air showed a delayed degradation starting from 30 bilayers as well as an increased residual mass. In 2009, Li et al. demonstrated their interest again by depositing 10 bilayers of branched polyethyleneimine (BPEI) and Laponite (LAP) on cotton fabrics and testing them with a vertical flame test. The idea was to mimic the behavior of flame retardant composites. During fire tests, the clay fillers tend to migrate to the exposed surface and form a protective ceramic barrier. Therefore, by forming the barrier from the get-go, the coating should protect the underlying substrate as it does for composite materials. In this study, the samples combusted completely but had a higher charring capacity, which increased with the thickness of the coating, here monitored by the pH of the laponite solution.[131] They then tested the same system by replacing laponite particles with montmorillonite platelets and obtained similar results. Quantitative results were given from a Microscale Combustion Calorimetry (MCC) test that showed a decrease in the Heat Release capacity (HRC) and in the Total Heat Release (THR).[132] The results are summarized in Table 2.

From then on, the number of articles published on the subject has grown up exponentially. The fact that impressive fire protective performances could be reached with only a few dozens of nanometers initiated lots of research. Most works focus on textile and polyurethane foam substrates, but some works have been done on polymer sheets or films. Different approaches are pursued. First, coatings consisting of polyelectrolytes multilayers have been extensively developed in an all-polymer approach, usually relying on intumescent mechanisms. Strict composite coatings as passive barriers have also been designed, as well as layer-by-layer systems based on a combination of both.[11]

Table 2. First Layer-by-layer fire protective coatings

Substrat	Material	System	Number of bilayers	Result	Reference
Textile	Silk	Chitosan/Phosphoric acid	30 to 60	TGA : delayed degradation	[130]
Textile	Cotton	BPEI/Laponite	10	VFT: complete combustion but higher charring capacity	[131]
Textile	Cotton	BPEI/Montmorillonite	10	VFT: complete combustion but higher charring capacity MCC: THR -20%; HRC-15%	[132]

a. All-polymer layer-by-layer fire protective coatings

i. Intumescent Polyelectrolytes

The first example of intumescent polyelectrolyte complex consisted in 20 bilayers of Poly(sodium Phosphate) (PSP) in combination with Poly(allylamine) (PAH), tested on a cotton substrate which acts as the carbon source. It showed great reduction in peak of heat release rate (-63%) and THR (-68%) using micro calorimetry, and quick extinction during the cone calorimeter test (reduction of 43% and 51% of the pHRR and THR respectively).[133] On PolyLactic Acid (PLA) sheets, the same system but reinforced with montmorillonite particles showed similar results using cone calorimetry.[134] It was then deposited on PA6,6 fabrics, which also improved their fire retardancy, however with less exciting results (reduction by 36% of pHRR) due to the coating not penetrating in between the fibers.[135] The addition of TiO_2 particles did not improve the performance.[136] On Polyester cotton blends, it was deposited as a polyelectrolyte complex in a one-pot process, which improved their flame retardant behavior (attributed to a higher nitrogen content) and their washing durability.[137] Their effectiveness, coupled with low weight gain, low thickness and the facile procedure, spurred on a lot of research. The scientific community strived to find new systems, that are either more efficient, that grow thicker or give equal to better results with a fewer number of layers, or that use renewable or bio-based resources. For example, cottons have been covered with 30 bilayers of chitosan (CH) and phytic acid (PA), showing great results for systems with the highest phosphorus content (pHRR and THR reduced by 60% and 76% respectively during cone calorimetry, and self-extinguishment during vertical fire test).[138] Pan et al. then added sulfonated melamine-formaldehyde to the phytic acid solution as a blowing agent, this system achieving self-extinguishment with only 10 bilayers.[139] The same system was deposited using layer-by-layer technology on PA66 fabrics, followed by borate cross-linking [140] or in combination with oxidized sodium alginate,[141] as well as on wool fabric in a one pot procedure as a polyelectrolyte complex, along with citric acid to increase durability.[142] Flammability of both systems was successfully decreased. Kundu et al. reported a 26% decrease in pHRR from mass loss cone experiments, with an increased LOI and a V-1 rating at UL94 test, while Cheng et al. reported a 39% pHRR reduction during microcalorimeter measurements, coupled with a decrease in THR, smoke density and an increased char yield.

Other examples of intumescent LbL coatings on textile have been carried out with different systems, researchers trying to find the most efficient one. Cotton is by far the most studied substrate, because of its high flammability and its extensive industrial use, however synthetic fibers (PA66 and Polyester fabrics) and natural fibers (Ramie) were also effectively protected by intumescent systems. With the constant concern of trying to find environmentally benign systems, bio-based materials are almost constantly used, with ionic chitosan being a major component used as a carbon source, and sometimes as both a carbon source and blowing agent, given by the presence of amino groups. It has been used in intumescent polyelectrolyte layer-by-layer assemblies in association with ammonium polyphosphate (APP) on cotton,[143], [144] polyester-cotton blends[145] and polyester fabrics (where the combination with guanidine sulfamate, urea and thiourea showed better flame retardancy, with fewer bilayers [146]) or with PU latex.[147] It was also combined with Poly(sodium Phosphate) [120], [148] (the addition of amine salts in the rinsing water thickens the coating and helps achieving good flame retardancy with fewer bilayers [149]), with phosphorylated chitin on cotton,[150] with phosphorylated chitosan on PA66,[151] or even with DNA on cotton [152] for fully renewable flame retardant coatings. Hypophosphorus acid-modified chitosan was deposited along with Polyethylenimine and genipin cross-linking which achieved self-extinguishment in horizontal flame test and a reduction of 73% and 80% of the pHRR and THR respectively in micro scale combustion calorimeter [153] (also on polyester-cotton blends, without genipin as cross-linker, and with similar vertical flame test results [154]). In addition to the previously-mentioned chitosan-phytic acid systems, phytic acid was used in combination with a sol-gel synthesized nitrogen modified silane on cotton,[155] with PEI and Melamine on cotton (pHRR reduced by 50% in MLC tests with an additional PDMS hydrophobic treatment [156]), and with polysiloxane on polyester fabric where it suppressed the dripping phenomenon, enhanced charring and reduced pHRR in MCC tests.[157] Then, Fang et al. focused on using polyhexamethylene guanidine phosphate (PHMGP) in a layer-by-layer intumescent assembly on cotton with potassium alginate,[158] Sodium Polyborate [159] and APP.[160] APP being a classic acid-source in intumescent systems, it was also extensively used, with BPEI on cotton[161] and on Ramie fabric [160],[161], or with Poly(Acrylic Acid) and Poly(diallydimethylammonium chloride) (PDADMAC) on cotton, polyester-cotton blend and polyester fabric,[164] for example. An original layer-by-layer system consisting in phosphonated oligoallylamines et oligoallylamines on cotton was also studied by Carosio et al.[165] NH_2-rich polysiloxanes with APP also gave good results in protecting Nylon-Cotton blends for military application, showing the versatility of the system and its large potential area of application.[166] All systems used to fire retard textiles with intumescent layer-by-layer coatings are gathered in Table 3.

Table 3. Intumescent layer-by-layer coating on textile

Material	System	Number of units	Result	Reference
Cotton	PSP/PAH	20	MCC: pHRR-63%; THR-68% MLC: pHRR-43%; THR-51%	[133]
Cotton	CH/PA	30	VFT: self-extinguishment MLC: pHRR-60%; THR-76%	[138]
Cotton	CH/(PA+sulfonated melamine formaldehyde)	10	VFT: self-extinguishment	[139]
Cotton	CH/APP	20	MCC: pHRR-80%; THR-82% VFT: enhanced charring, reduced burning time	[143], [144]
Cotton	CH/APP+UV-curable PU	3	LOI: 25% VFT: self-extinguishment MLC: pHRR-11%; THR-32%	[147]
Cotton	CH/PSP	30	VFT: self-extinguishment	[118]
Cotton	CH/PSP+sonication	17	VFT: Self-extinguishment MCC: pHRR-73%; THR-81%	[146]
Cotton	CH/PSP + amine salt treatment	10	VFT: self-extinguishment MCC: pHRR-73%; THR-78%	[149]
Cotton	CH/phosphorylated chitin	20	VFT: self-extinguishment MCC: pHRR-74%; THR-86%	[150]
Cotton	CH/DNA	20	VFT: self-extinguishment LOI: 24% MLC: pHRR-40%	[152]
Cotton	Hypophosphoric acid-modified CH/PEI	10	HFT: self-extinguishment MCC: pHRR-73%; THR-80%	[153]
Cotton	N-modified silane/PA	15	VFT: self-extinguishment MLC: pHRR-31%; THR-38%	[155]
Cotton	PEI+Melamine/PA	4	VFT: self-extinguishment MLC: pHRR-59%; THR-24%	[156]
Cotton	Potassium alginate/PHMGP	20	VFT: enhanced charring MCC: pHRR-29%; THR-24%	[158]

Cotton	Sodium polyborate/PHMGP	10	VFT: self-extinguishment LOI: 29% (20BL: 41%) MCC: pHRR-78%; THR-69%	[159]
Cotton	APP/PHMGP	10	VFT: enhanced charring	[160]
Cotton	APP/BPEI	PEC	HFT: self-extinguishment MLC pHRR-51%	[161]
Cotton	phosphonated oligoallylamines and oligoallylamines	5	VFT: enhanced charring and no afterglow	[165]
Cotton, PET, PET-Cotton	PDADMAC/PAA/PDADMAC/ APP	10	HFT: self-extinguishment VFT: enhanced charring MLC: reduced pHRR and THR for all substrates and for 25,35 and 50 kW/m^2	[164]
PET-cotton	Hypophosphorous acid-modified CH/BPEI	20	HFT: self-extinguishment	[154]
PET-Cotton	CH/APP	20	VFT: no afterglow, enhanced charring MLC: pHRR-24%; THR-22%	[145]
Nylon-cotton	NH2-rich polysiloxanes/APP	20	VFT: self-extinguishment	[166]
Ramie	PEI/APP	20 (dip-coating)	VFT: self-extinguishment MCC: pHRR-65%; THR-68% MLC: pHRR-42%; THR-25%	[160]
		20 (spray-coating)	VFT: self-extinguishment MCC: pHRR--74%; THR-60% MLC: pHRR-54%; THR-60%	[161]
Wool	CH/PA, citric acid crosslinking	PEC	MCC: pHRR-39; THR-41; reduction of smoke density	[142]
PA6.6	CH/PA+ borate cross-linking	10	LOI up to 21.5% MLC: pHRR-26% UL94: V1 rating	[140]
PA6.6	CH/PA/CH/oxidized alginate	5, 10, 15	5QL: MLC: pHRR-24% 10 and 15OL: VFT: suppressed melt-dripping LOI 21-22%	[141]
PA6.6	PSP/PAH	40	MLC: pHRR-60%	[135]
PA6.6	CH/phosphorylated CH+polyacrylate de sodium	10	LOI: 23% MLC: pHRR-25% UL94: V1 rating	[151]
PA6	PAH-PSP-PAH-TiO_2	15	MLC: pHRR-26%	[136]
PET			No effect in MLC	
PET	CH/APP with N or N and S based derivatives	10	MLC: pHRR-61.7% LOI 26% VFT: self-extinguishment	[146]
PET	Polysiloxane/PA	1,5	VFT: enhanced charring, reduced burning rate MLC: pHRR-65%;THR-59%;TSR-72% LOI 31.4	[157]

With the already mentioned exception of the work by Laachachi et al. on PLA films,[134] it seems that most intumescent all-polymer coatings have been deposited on textile fabrics. However, as gathered in Table 4, some works were also performed on PET, silicon and PU foams with relatively good results. APP combined with PDADMAC and PAA managed to suppress the melt-driping of the PET foam and to reduce the pHRR by 25% at MLC tests.[167] Combined with Chitosan on silicon foam, it decreased the pHRR and smoke release by 28% and 42% respectively.[168] On the PU foam, chitosan/phosphorylated cellulose as well as chitosan and poly(Phosphoric acid) suppressed melt-dripping and reduced the pHRR by around 30%. [121], [169]

Paper is also a flammable material that needs protection and LbL strategies were developed for this substrate (see Table 4). Xuan et al. directly coated paper and obtained self-extinguishment using a host-guest layer-by-layer self-healing coating of poly (acrylic acid)-adamantanamine/ammonium polyphosphate-cross-poly (ethylenimine)-β-cyclodextrin (PAA-AD/APP-co-PEI-β-CD)).[170] Some researchers prefer to directly treat the fibers before assembling them in a paper sheet. Chitosan combined with poly(vinyl phosphonic acid) (PVP) was used in a 20BL layer-by-layer treatment to coat wood fibers and make fire retardant paper, which reduced pHRR and THR by nearly half, and caused self-extinguishment in horizontal flame testing.[171] A high molecular weight PEI was found to adsorb more on the substrate and form a continuous coating with good coverage on cellulose fibers, which, combined with high quantity of sodium hexametaphosphate in a 3.5BL coating, gave a self-extinguishing behavior to the paper.[172] Same behavior and also reduced HRR in MCC test was obtained with PEI and Melamine deposited along with phytic acid.[173]

Table 4. Intumescent layer-by-layer coatings on other substrates

Substrate	Material	System	Number of units	Result	Reference
Polymer sheet	PLA	Poly(allylamine)/MMT	30 and 60	MLC (30): TTI+60%, pHRR-8%; THR-22% MLC (60): TTI+96%; pHRR-36%; THR+6%	[134]
		Poly(allylamine)/MMT + PsP		MLC (30): TTI+96%, pHRR-13%; THR-6% MLC (60): TTI+111%; pHRR-37%; THR+0%	
Foam	PET	PAA/PDADMAC/APP or DNA/PDADMAC	4	HFT: no dripping, self-extinguishment MLC: with APP pHRR-25%	[167]
	Si	CH/APP	7	LOI 23.8% MLC: pHRR-28%; THR-15%; TSR -42%	[168]
	PU	CH/phosphorylated cellulose nanofibers	5	HFT: no melt dripping MLC: pHRR-31%	[167]
	PU	CH/poly(phosphoric acid)	2	MLC: pHRR-33%	[119]
Paper		PAA-adamantine/APP-co-PEI-β-cyclodextrin	15	Self-extinguishment against the flame of a lighter	[170]
Fibers for paper making	Wood pulp	CH/poly(vinylphosphoric acid)	20	HFT: self-extinguishment; MLC: pHRR-49%; THR-33%	[171]
	cellulose	High molecular weight-PEI/sodium hexametaphosphate	3.5	HFT: self-extinguishment VFT: enhanced charring LOI: 25%	[172]
	paper	PEI+Melamine/PA	8	MCC: pHRR-43%; THR-49	[173]

These intumescent coatings usually form a stable char, and high residual masses are observed after fire test. Self-extinguishment characterizes the most efficient systems, smoke reduction as well as pHRR and THR reduction from MCC or MLC tests are also reported. SEM observations of the char show the presence of microbubbles characteristic of intumescence, however the terms “intumescent-like” or “catalytic charring” are more cautiously used and seem to be more accurate. Indeed, the presence of phosphate groups in large amount seems to favor the formation of the protective char, by catalyzing its formation. Whole and coherent coverage of the fabric seems to be the key element between complete combustion with “just” enhanced charring, and self-extinguishment with actual pHRR, THR and smoke reduction. In the paper by Jimenez et al., the term “micro-intumescence” is used to describe the phenomenon. Its mechanism was investigated, and it was found that the presence of phosphate groups catalyzes the dehydration of chitosan and cellulose fibers, leading to the decomposition of the LbL coating and the formation of a thermally stable char. According to TGA results, this step occurs at a lower temperature than the decomposition of cellulose, which explains the shorter time to ignition observed in cone calorimetry. The char acts as a barrier against heat transfer, effectively protecting the substrate, and traps the combustible gases formed, which results in the observed bubbles on the char. In addition, the dehydration step releases large quantities of water which extinguish the flame and cool the material. This explains the shorter burning time, as well as the enhanced charring and reduced HRR.[143]

ii. Non intumescent systems

In parallel, some research pointed out that an intumescing mechanism is not always necessarily needed to impart fire protection (see Table 5). On textile, coatings of PEI and alginate cross-linked with metal ions on cotton also showed enhanced charring, although not sufficient enough to reach good fire protection.[174] PEI and oxidized alginate crosslinked with hypophosphorus acid could also protect PET fabric by suppressing melt-dripping and reducing pHRR during cone calorimetry.[175] Combinations, applied on cotton, of starch and polyphosphoric acid,[176] chitosan with melamine and Poly(sodium Phosphate),[177] or polysiloxane and phytic acid with PEI [178] caused self-extinguishment with only a few bilayers. In all these systems, the presence of a char stable enough is necessary to reach good fire protection. These kinds of systems were also applied to protect foams. On PU foam substrates, a pHRR reduction of 52% was reached by taking advantage of the emission of large quantities of diluting gases (H_2O, SO_2, NH_3…) from a Chitosan/Poly(vinyl sulfonic acid sodium) 10 BL layer-by-layer coating.[179] Following the same principle, a pHRR reduction of 42% was reached with a Chitosan/Lignosulfonate 8BL coating.[180] Carosio et al chose to work with phosphorus filled coatings, with poly(phosphorus acid) or poly(allylamine diphosphonate) in association respectively with chitosan and polyacrylic acid assembled in quadlayers,[181] or with chitosan only.[182] Both systems could sustain high heat fluxes with great HRR reduction (both showed a 55% reduction in pHRR when exposed to a radiative 35kW/m² heat flux). All systems helped maintaining the polyurethane open-cell shape by forming an exoskeleton during fire test.

Table 5. All polymer non-intumescent layer-by-layer fire protective coatings

Substrat	Material	System	Number of units	Result	Reference
Textile	Cotton	PEI/alginate+metal ion cross-linking	10	VFT: With Ba ion, enhanced charring and reduced burning rate	[174]
		Starch/Poly(phosphoric acid)	2	HFT: Self-extinguishment MLC: pHRR and THR reduced by about 50% depending on the density of the cotton	[176]
		N-containing polysiloxane	30	LOI: 30% VFT: self-extinguishment	[178]
	PET-Cotton	CH+Melamine/sodium hexametaphosphate	15	VFT: self-extinguishment MCC pHRR-29%; THR-37%	[177]
	Polyacrylamide-grafted PET	PEI/oxidized alginate + hypophosphorous acid crosslinking	15	HFT: self-extinguishment MLC: pHRR-44%; THR-22%	[175]
Foam	PU	CH/poly(vinyl sulfonic acid)	10	Torch test: stops flame spread MLC: pHRR-52%	[179]
		CH/lignosulfate	8	HFT: no melt-dripping MLC: pHRR-42%	[180]
		PAA/CH/poly(phosphoric acid)/CH	5	HFT: Self-extinguishment MLC: pHRR -50 to 60% depending on heat flux Burn-through torch test: temperature on back side kept under 100°C LOI: 23%	[181]
		CH/poly(allylamine diphosphonate)	2	HFT: no melt-dripping MLC: pHRR-48%	[182]

iii. Other applications of Layer-by-layer all polymer coatings

The layer-by-layer coating technique was also employed, not to coat substrates, but to coat particles or fibers that would then be used either as filler or as composite reinforcement in a polymer matrix. These studies are usually carried out with LbL systems which have already been proven to be efficient in other studies on textile. For example, CH/lignosulfonate LbL system was used to coat hydroxyapatite to impart fire retardancy to PolyVinyl Alcohol (PVA) with very low loading.[183] Hollow mesoporous silica was coated with chitosan and phosphorylated chitosan in epoxy resin, reducing the pHRR by 51% thanks to a higher char yield.[184] Yan et al prepared flame retardant ramie fabric trough the deposition of poly(diphenolic acid-phenyl phosphate) and PEI, while Li et al chose APP and PEI, and included it in benzoxazine resin to prepare self-extinguishing laminates.[185]–[187] Layer-by-layer coating technique was also used for the fire retardancy of carbon fiber/epoxy composite through the functionalization of carbon fibers with one bilayer of PEI and PAA.[188]

b. All inorganic layer-by-layer fire protective coatings

Coatings made with bilayers of SiO_2 and alumina-coated SiO_2 on PET fabrics showed a decrease in pHRR of 38% for the best system, with no dripping and reduced burning and after-flame time. However, it was shown that only the coatings that managed to maintain a continuous coverage of the fabric could have an actual effect on the fire behavior.[189] This was achieved with horizontal spray layer-by-layer coating on cotton and PET fabric,[190], [191] which yielded a homogeneous and compact coverage of the fibers, highlighting the importance of the deposition technique. This led to a higher time to ignition, and lower pHRR, THR and smoke production. Similar results were obtained on PC sheets, where 20BL suppressed melt-dripping, lengthened the time to ignition, and reduced the HRR (the protection was however not enough for thicker PC substrates).[192] The only example of an all inorganic coating on foam that we are aware of was reported by Patra et al. and also relied on a clay sheets/metal-based particles combination. Vermiculite (VMT) platelets along with boehmite particles reduced pHRR and smoke release by around 50% with only a single bilayer. The only default was the coating fragility, which cracked easily during the test, however, it was not that critical and it still created a protective layer by keeping the foam skeleton intact.[128] The results from these works are summarized in Table 6.

Table 6. All-inorganic layer-by-layer fire protective coating.

Substrat	Material	System	Number of units	Result	Reference
Textile	PET	Cationic SiO_2/anionic SiO_2 Dip coating	5	MLC: TTI+45%; pHRR -20% VFT: no melt-dripping	[189]
		Cationic SiO_2/anionic SiO_2 Horizontal spray		MLC: TTI +21%; pHRR-34%; TSR-30%	[189]
	Cotton			MLC: TTI +27%; pHRR-20% VFT: increased residue	[188]
Polymer	0.2 mm PC	Cationic SiO_2/anionic SiO_2	5	MLC: pHRR-20%; THR-30% VFT: no melt-dripping at 20BL	[192]
	1 mm PC			No improvement of flammability	
Foam	PU	Vermiculite/Boehmite	1	MLC: pHRR-55%; TSR-50%%	[128]

c. *Layer-by-layer composite coatings*

i. Composite intumescent polyelectrolytes

The combination of intumescent layer-by-layer coating with nanoparticles has also been studied, with the idea of either providing an additional barrier, strengthening or reinforcing the char, or even catalyze its formation.

On textile (see Table 7), cotton substrates have been the most studied with the exception of one study on polyester-cotton blend [193], on PA66 and Polyester,[136] and two studies on ramie.[194], [195] Silicon-based particles such as clay [116], [196] or SiO_2 [105], [193], [197] have been used, as well as carbon based particle: graphene oxide (GO), single wall carbon nanotube (SWCNT) and multi wall carbon nanotubes (MWCNT).[198]–[201] α-ZrP sheets,[202] hydrotalcite particles [203] and TiO_2 particules [136] were also added in layer-by-layer coatings for fire protection. In some cases, the behavior was improved when compared to intumescent-only coatings, at two conditions. First, the presence of nanoparticle should not impart the intumescent properties of the coating [203] and then, there must be a good coverage.[136] Either previously mentioned systems were used, or intrinsically intumescing polymers were synthesized by grafting phosphorus-containing groups on the polymer backbone [196], [198].

Table 7. Composite intumescent layer-by-layer fire protective coating on textile.

Textile	System	Number of units	Result	Reference
Cotton	BPEI/APP+fluorinatedSiO2/PDMS	1	MCC: pHRR-86%; THR: -39% VFT: self-extinguishment	[103]
	BPEI+urea+diammonium phosphate/Kaolin	50	MCC: pHRR-72%; THR: -79% VFT: self-extinguishment	[116]
	FR-PAA/MMT	20	MLC: TTI+40%; pHRR-46%; THR-18%	[196]
	PEI-SiO$_2$/Poly(phosphoric acid)	Not mentioned	LOI: 28.2% VFT: self-extinguishment	[195]
	FR-polyacrylamide/GO	20	MLC: TII+56%; pHRR-50%; THR-22%	[196]
	Phosphorylated GO/PEI	10	MLC: pHRR-27%; THR-21% VFT: cohesive residue	[199]
	Polyhexamethylene guanidine phosphate (PHMGP)/potassium alginate-CNT	20	VFT: cohesive residue, no afterglow	[200]
	PHMGP/modified MWCNT	20	MCC: pHRR-35%; THR-37% VFT: cohesive residue, no afterglow	[199]
	PHMGP/APP/PHMGP/ZrP	20	MCC: pHRR-59%; THR-53% VFT: cohesive residue, no afterglow	[202]
	PDADMAC/DNA+hydrotalcite post-diffusion	10	HFT: self-extinguishment MCC : pHRR-33%	[203]
Ramie	PEI/ZrP+PEI/APP	5+5	MCC: pHRR-53%; THR-56% VFT: cohesive residue	[192]
	Amino-MWCNT/APP	20	MCC: pHRR-36%; THR-25% VFT: cohesive residue	[193]
PET-cotton	Cationic SiO$_2$/anionic SiO$_2$/CH/APP	10	MLC: TTI: +37%; pHRR-11%; THR-22% VFT: no afterglow	[191]
PET	PAH/PSP/PAHTiO$_2$	15	MCC: pHRR-14%	[136]
PA6.6			MCC: pHRR-26%	

On PUF substrates (see Table 8), the combination of inorganic particles yields great pHRR reduction from 39% for 2 Trilayer (TL) PEI/GO/Melanin nanoparticles [204] to 54% for 4TL PAH/PSP/MMT [205] and 67% for 5QL/CH/APP/CH/PAA-stabilized Kaolin.[206] It has been attributed to the formation of thermally stable, coherent, graphitized [204] and swollen chars that form exoskeletons able to retain the foam's shape. 5 quadlayer (QL) CH/sodium hexa-metaphosphate/CH/silicon-based nanoparticles was also applied on cellulose fibers to create fire retardant paper. Montmorillonite (MMT) platelets, Sepiolite (SEP) and colloidal silica were used and tested by horizontal flame testing and MLC. All three maintained the fiber shape upon burning while cotton was combusted underneath. MMT and SEP showed self-extinguishing behavior by forming a compact char layer, and pHRR reductions of 44 and 47% were observed, respectively. Smoke suppressing properties were obtained for SEP and SiO$_2$, though the low packing density of SiO$_2$ provoked worse fire behavior.[207] Combining a passive organic/inorganic barrier with an intumescent coating is also another strategy, where the inorganic barrier delays the degradation to give time for the intumescent system to react to the thermal constraint. This was applied with a 20BL CH/APP coating on top of a 4BL CH/VMT barrier.[208] Also, the combination of a passive CH/MMT barrier with a PDADMAC/Boehmite layer (aiming at releasing water to dilute the flame and cooling the material) and an APP/MMT coating applied on top was tested.[209] Both systems reduced the pHRR by 50% as well as smoke production during cone calorimetry, however the second made it with only 1TL. The application of a composite intumescent system to coat an inflammable aerogel should also be mentioned because of the exceptional protection the total system can provide, with an 80% reduction of pHRR during cone calorimetry. A cellulose nanofibrils aerogel was coated with a layer-by-layer coating made by CH, PVP and MMT platelets (see Table 8). A torch burn-through test revealed that the thermal gradient was 650°C with the foam retaining its shape and therefore keeping the barrier intact.[210]

Table 8. Composite intumescent layer-by-layer fire protective coating on foams.

Substrate	Material	System	Number of units	Result	Reference
Foam	PU	PEI/GO/Melamine nanoparticles	2	Torch test: Self-extinguishment MLC: pHRR-39%; THR-12%; TSR-59%	[204]
		MMT/PAH/PSP	4 to 10TL	Torch test: Self-extinguishment MLC: pHRR-54% to -62%; THR-8%	[205]
		CH/APP	5	Torch test: no melt-dripping MLC: pHRR-24%; increased TSR	[206]
		CH/PAA-Kaolin		Torch test: self-extinguishment MLC: pHRR-53%; THR-34%; TSR-76%	
		CH/APP/CH/PAA-Kaolin		Torch test: self-extinguishment MLC: pHRR-67%; THR-40%; TSR-59%	
		CH/sodium hexametaphosphate/CH/MMT	5	HFT: Self-extinguishment MLC: pHRR-44%; THR-22%; TSR+11%	[207]
		CH/sodium hexametaphosphate/CH/SEP		HFT: Self-extinguishment MLC: pHRR-47%; THR-14%; TSR-43%	
		CH/sodium hexametaphosphate/CH/SiO$_2$		HFT: no melt-dripping, enhanced charring MLC: pHRR-30%; THR-14%; TSR-27%	
		CH/APP	20	Torch test: no melt-dripping, enhanced charring MLC: pHRR-55%; THR-15%; TSR+113%	[208]
		CH/VMT	4	Torch test: Self-extinguishment MLC: pHRR-56%; THR-8%; TSR-57%	
		CH/VMT+CH/APP	4+20	Torch test: Self-extinguishment MLC: pHRR-66%; THR-11%; TSR+41%	
		PAA/MMT+PDADMAC/Boehmite +APP/MMT	1	HFT: Self-extinguishment MLC : pHRR-50%; TSR-34%;	[209]
Aerogel	Cellulose nanofibrils	CH/poly(vinylsulfonic acid)/CH/MMT	5	HFT: Self-extinguishment MLC: no ignition Burn-through torch test : back temperature maintained under 200°C	[210]

ii. Passive barrier coatings

Passive barrier coatings are coatings that do not react to fire in the way intumescent coatings do, and whose protective effect stems from the compact layer formed by the residue. These coatings are composed of inorganic particles at a very high loading, and of a polymer or an organic part that plays the role of a sort of glue (or binder) between the particles. As a consequence, they are usually referred to as “brick and mortar” structures.

It appears that composite coatings have been less studied on textiles and flat substrates, probably because the protection offered by an inorganic-organic barrier is usually not high enough. It is generally observed that the charring capacity is catalyzed and enhanced. The coating usually forms a coherent residue maintaining the shape of the substrate. Nevertheless, the polymer underneath is completely consumed. However, this barrier yields good results in the fire protection of foam substrates, therefore, a major part of the literature focuses on the protection of flexible polyurethane foams with layer-by-layer passive composite coatings.

Carbon-based particles (see Table 9), metal-based particles (see Table 10) and silicon-based particles (see Table 12) were used, but one or two papers reported more exotic chemistries (see Table 11).

The exciting thing about carbon-based nanoparticles such as graphene or carbon nanotube is that they are highly conductive, and as such, multifunctional materials are easily obtained with just one treatment, with electrical conductivity being the main property, and fire retardancy a welcome side-effect. But probably because of their high cost or difficult synthesis, carbon-based nanoparticles have been relatively less used than others, although they reach good fire retardant properties when used in passive layer-by-layer coating. For example, Davis et al used PEI-stabilized carbon nanofibers (CNF) and multi-wall carbon nanotubes (MWCNT) in a 4BL layer-by-layer assembly with PAA on barrier fabrics and on polyurethane foam. It was found detrimental to HRR when applied to barrier fabric.[211] However, it led to a pHRR reduction of about 40% on PUF and prevented pool fire in a MLC test.[212], [213] With MWCNT this result was further improved by using pyrene-modified PEI, with a reduction of pHRR of 68%, as well as reduced and slowed down flame spread in both horizontal and vertical flame tests, using a 6BL coating. It shows how the chemistry of the mortar can impact the protective behavior of the coating.[214] A similar result was obtained with 8TL of chitosan-stabilized CNT, alginate, and MMT.[215]

Graphene oxide (GO) as a 2D material was also investigated to flame retard PUF. Its thermal stability as well as its potential high coverage attracted attention. Enhancing its solubility and its dispersion stability in water requires to use a dispersant such as PEI or sodium alginate before using it in a layer-by-layer process. All studies report pHRR reduction of at least 50% with a few numbers of layers. For example, alginate-stabilized GO sheets layer alternating with PEI reduced the pHRR by 40 to 50% with 2 to 5 BL. A synergistic effect was reported with SiO_2 particles (suppressing one of the two peaks of heat release rate observed for PUFs [216]), as well as with β-FeOOH nanorods.[217] Polydopamine-coated reduced GO (rGO)/PEI/PAA layer-by-layer achieved the same result with 3 TL.[218] 10 TL of CH/GO/Alg reduced pHRR by 60%,[219] but the best result was obtained with 3BL of PDADMAC/GO which completely prevented PUF combustion in cone calorimeter test and suppressed flame spread in a horizontal flame test.[220] In this last study, the GO-coated PUF was submitted to a burn-through test and the thermal gradient obtained was the same as an incombustible silica aerogel. All works report a delay and a slowdown in the emission of combustible gases, as well as a reduction in total smoke production.

One limitation in using GO is that it is less thermally stable than rGO for example, which is mentioned in a comparative study by Pan et al.[221] To enhance its activity and thermal stability, Chen et al functionalized GO nanosheets with Phenoxycycloposphazene and used them with PEI to coat a PVA sheet, showing HRR reduction at MCC test.[222]

Table 9. Passive composite layer-by-layer fire protective coatings with carbon-based nanoparticles.

Substrate	Material	System	Number of units	Result	Reference
Foam	PU	PAA/PEI-CNF	4	MLC: pHRR-40%; THR-21%	[210]
		PAA/PEI-MWCNT/PEI	4	MLC: pHRR-35%; THR-21%	[211]
		Pyrene-modified PEI/PAA-MWCNT	6	HFT, VFT: Self-extinguishment MLC: pHRR-68%; THR-3%; TSR-78%	[214]
		CH-CNT/MMT/Alginate	8	MLC: pHRR-69%; THR-3%	[215]
		PEI/alginate-GO/amino-modified SiO_2	5	MLC: pHRR-51%	[216]
		PEI/alginate-GO/β-FeOOH	5	MLC: pHRR-50%; THR+7%	[217]
		polydopamine-rGO/PAA/PEI	3	MLC: pHRR-49%; THR-5%; TSR-33%	[218]
		CH/GO/Alginate	10	MLC: pHRR-60%; THR-5%; TSR-31% Torch test : charring	[219]
		PDADMAC/GO	3	HFT: Self-extinguishment MLC: no ignition Burn-through torch test: temperature at the back maintained at 104°C	[220]
		PEI/alginate-GO	12	MLC: pHRR-72%; THR+18%; TSR-56%	[221]
		PEI/alginate-rGO		MLC: pHRR-65%; THR+7%; TSR-14%	
Polymer sheet	PVA	PEI/P,N functionalized GO	30	MCC: pHRR-60%; THR-67%	[222]
Textile	Barrier Fabric	PAA/PEI-CNF	4	MLC: Increased THR and pHRR	[211]
		PAA/PEI-MWCNT/PEI	4		

GO was also mentioned to be used in combination with β-FeOOH nanorods, which were also used in other systems for the fire protection of PUFs, either alone,[223] or in combination with MMT sheets.[224] In the first case, it was found to be more efficient in a trilayer coating with PEI and SA than in a bilayer coating with PEI only. It is believed to be due to an entangled network structure with whole coverage in the case of the trilayer coating, whereas only aggregate or island of nanorods were observed for the bilayer coating, failing to cover the foam.

This morphology caused the foam to retain its shape and the pHRR was reduced by 62% for 8 TL (15% for 8BL). The smoke production was delayed as well. MMT nanosheets were then added in the alginate solution to seek for a synergistic effect with the nanorods. Good coverage of the foams was obtained with either the FeOOH alone, MMT sheets alone, or both particles, with three cycles (cf Table 10). While MMT sheets alone already managed a 45% reduction on pHRR, the combination with the nanorods further enhanced the reduction in HRR and managed to prevent shrinkage, with impressive smoke suppression properties not observed with MMT.

Other metal-based nanoparticles were found quite efficient when used in layer-by-layer protective coatings for PUF, and showed good to excellent efficiency in reducing HRR and suppressing smoke. Nanosheets such as MnO_2, α-ZrP and MXene (Ti_3C_2) were found to show particularly good fire retardant properties. Metal oxide particles were also used, such as TiO_2 nanotubes, aluminum oxide, and one particularly efficient α-$Co(OH)_2$ nanosheets containing system, that reduced the pHRR by 59% with only one bilayer with sodium alginate. TiO_2 nanotubes were used in an 8TL coating with chitosan and alginate and reduced the flammability of the PUF substrate at cone calorimeter test, by reducing the pHRR by 70%, and the TSR by 41%. However, the THR was barely reduced, revealing that the emission of fuel was slowed down rather than impeded.[225] Similar performances in HRR were obtained with 6BL of PEI and PAA-stabilized Aluminum TriHydroxide (ATH) particles (pHRR reduced by 64% and no THR reduction, 85% residue), but without any smoke reduction.[226] A delayed and slowed down emission of fuel was also observed for nanosheets particle, starting with MnO_2 used with PEI/Alginate, where a 6TL coating reduced the pHRR by 47% but not the THR. Smoke and harmful gases emission were reduced.[227] The same performances were achieved with a 6TL CH/Alg/ZrP coating with high CH and Alg solution concentration, the pHRR being further reduced to 71% by an additional 3TL.[228] However, another study with MoS_2 nanosheets points out the role played by the chemistry of the particle. 8BL of CH/MoS_2 also reduced the pHRR by 71%, as well as smoke and harmful gases emission, yet, this time, a reduction of THR by 20% was observed.[229] Further reduction in THR was observed when switching MoS_2 with MXene (Ti_3C_2) nanosheets. A 66% reduction in THR and a 71% reduction in TSR were observed, despite a worse performance in term of pHRR (-57%).[230] 1BL of Alginate/α-$Co(OH)_2$ was enough to reduce the pHRR by 59% (65% for 2BL). It is attributed to the formation of a protective char thanks to the catalytic action of $Co(OH)_2$. However, increasing the number of bilayer and therefore the nanosheets' concentration led to a detrimental effect that further catalyzed the decomposition of the char, which was thus less protective.[231]

Table 10. Passive composite layer-by-layer fire protective coatings with metal-based nanoparticles.

Substrate	Material	System	Number of units	Result	Reference
Foam	PU	PEI/β-FeOOH/alginate	8	MLC: pHRR-62%; THR=; TSR-21%	[223]
		PEI/alginate-MMT/ β-FeOOH	3	MLC: pHRR-47%; THR-10%	[224]
		PEI/alginate-MMT		MLC: pHRR-45%; THR=	
		PEI/ β-FeOOH		MLC: pHRR-14%; THR=	
		CH/TiO2/Alginate	8	MLC: pHRR-70%; THR-13%; TSR-41%	[225]
		PEI/PAA-ATH	6	MLC: pHRR-70%; THR=; TSR+64% Torch test: self-extinguishment	[226]
		PEI/MnO_2/alginate	6	MLC: pHRR-47%; THR=	[227]
		CH/α-ZrP/alginate	9	MLC: pHRR-71%; THR=	[228]
		CH/MoS_2	8	MLC: pHRR-70%; THR-17%; TSR-33%	[229]
		CH/MXene(Ti_3C_2)	8	MLC: pHRR-57%; THR-66%; TSR-71%	[230]
		Alginate/$Co(OH)_2$	1	MLC: pHRR-59%; THR=	[231]

Other nanosheets were used in layer-by-layer coating to fire retard polyurethane foams (see Table 11). Graphene-like alginate-stabilized h-BN nanosheets, used in a 20BL layer-by-layer coating with BPEI applied on PUF, showed a reduction of pHRR and of the peak of CO production by about 50%, with increased charring effect, despite an increased smoke production.[232] More exotically, Lanthanum PhenylPhosphate nanosheets were reported to reduce the pHRR by 71% with 6BL with BPEI acting as mortar. It was also accompanied by a slight THR decrease (15%), because of slightly increased residue. This decrease in pHRR is suggested to be because of the delay in emission of volatile fuel as shown by the mass loss curve.[233] Layered Double Hydroxide (LDH) as clay-like nanosheets were also synthesized and used. MgAl-LDH and NiAl-LDH 12TL with CH and Alg reduced the pHRR by 65 and 75% respectively with a THR reduction of 25% due to enhanced charring (around 20% residue), with an enhanced catalytic carbonization effect brought by the presence of the Ni atom.[234] MgAl-LDH only decreased the pHRR by around 40% in a 5BL nanocoating, but completely suppressed the second HRR peak of PUF burning. With a residue of 20%, the THR was also slightly decreased.[235] However, this effect was enhanced with a 2TL coating. As the top of the sample burnt completely, the barrier created was protective enough to prevent the back of the sample from burning, reaching a residue of 71%.[236] All coatings were able to keep the open-cell structure of the exposed PUF, as well as the fiber structure of cotton fabric in one occurrence by Pan et al. They showed that an 20BL PEI/LDH coating could enhance the charring capacity of a cotton sample in a vertical fire test, and the pHRR and THR were reduced in a MCC test.[237]

Table 11. Passive composite layer-by-layer fire protective coatings with nanosheets.

Substrate	Material	System	Number of units	Result	Reference
Foam	PU	PEI/alginate-h-BN	10	MLC: pHRR-50%; THR=; TSR+107%	[232]
		Alginate-Lanthanum phenylphosphate/PEI	6	MLC: pHRR-70%; THR-15%; TSR-15%	[233]
		CH/alginate-MgAl LDH	12	MLC: pHRR-66%; THR-24%; TSR-74%	[234]
		CH/alginate-NiAl LDH		MLC: pHRR-75%; THR-27%; TSR-84%	
		PAA/BPEI-MgAl LDH	5	MLC: pHRR-40%; THR-14%	[235]
		PAA/MgAl LDH/PEI	2	MLC: pHRR-40%; THR-30%	[236]
Textile	Cotton	Alginate/MgAl LDH	20	VFT: cohesive residue MCC: pHRR-35%; THR-26%	[237]

Silicon-based nanoparticles were particularly studied. Some synergistic systems with clay or silica were already mentioned, and while some systems were proven more efficient, their ease of use, their availability and environmental-friendly nature make them a good and often favored compromise. First, the combination of anionic POSS with either cationic POSS or aminopropyl silsesquioxane oligomer reduced the intensity of flaming and increased the residue.[238] Silica used with BPEI and UV-cured PU allows PC sheets to self-extinguish in horizontal flame test.[239] Then, Si and P composite coatings were applied on Poly(acrylonitrile) (PAN) fabrics. If 6BL n-propylammonium chloride POSS/APP only reduced the pHRR by around 20%,[240] 10BL of Silica gel/phytic acid managed to reduce pHRR by 66% and THR by 73% thanks to an enhanced charring.[241] In the first study, the increase in CO production hinted at a barrier mechanism preventing oxygen heat and fuel transfer at the interface, while the second study combined the barrier effect from silica with charring enhancement from phytic acid. N-propylammonium chloride POSS was also used with sodium montmorillonite (MMT) clay platelets in the fire protection of PET fabric with a 5BL coating. In addition, with melt-dripping suppression and reduced burning rate, the combustion was slowed down, which was evidenced by the reduced HRR (reduction of 50% of the pHRR).[242] A few other systems using MMT have already been mentioned, and it is indeed clearly the most studied clay in layer-by-layer coating for fire protection. A 20BL starch/MMT coating did not prevent cotton fabric to be consumed, but the char layer was protective enough to preserve the fabric structure, slow down the burning rate in a vertical flame test, and attenuate the HRR in a low heat flux cone calorimeter test.[243] On Polyester, 4QL of CH/MMT/CH/TiO2 reduced the pHRR and THR by 48% and 36% respectively.[244] Batool et al. investigated epoxy-based composite MMT layer-by-layer coating combined with TriPhenylPhosphate, which induced a 25% reduction in pHRR.[245] The burning length of a

PI fabric was reduced with a 20BL Poly(N-benzyloxycarbonyl-3,4-dihydroxyphenylalanine)/MMT, even after washing,[246] but a 8TL PEI/MMT/PAA coating on a barrier fabric was found to be detrimental to the HRR.[211]

The same system on PUF only decreased the HRR by 17%, and while it might seem like an insignificant result, it was one of the first studies of a LbL MMT-based coating on PUF, and it had the advantage of highlighting the interest of the system by showing that with much less FR material, and with an environmental friendly method, results similar to those observed for commercial-used PUF fire retardant fillers were obtained.[211], [247].And indeed, it was possible to improve this behavior by adjusting the concentration of MMT in the solution, and to completely suppress the second HRR peak linked to polyol decomposition. While the pHRR was only reduced by 30%, the average HRR was reduced by 75%.[248] Even more impressive, an optimized coating (pHRR reduction of 42% in cone calorimetry) could reduce the pHRR by 53% in real scale mock-up test with only 5BL.[249] A 10BL thick CH/MMT led to similar results. The pHRR was reduced by 52%, and attenuated the HRR in general. The thick protective char layer is believed to be the cause for this delayed decomposition, which however only provoked longer burning with no THR loss, as everything was consumed.[250]

The use of other clays than MMT, not platelet-like but with other structures, should also be mentioned. Halloysite is a type of clay which rolls down on itself, creating Halloysite nanotubes (HAL) with negative charge on the outside and positive charge on the inside.[251] Also, sepiolite is a natural clay found under the form of needle. Both were used in layer-by-layer coatings and showed good efficiency in protecting PUF against fire. While the HAL-based coating reduced pHRR by 62% and TSR by 60%, it did not reduce THR as all PU was consumed.[252] But, the barrier formed by the sepiolite-based coating seems more effective as the pHRR was decreased by a further 14% and the THR was reduced, as it prevents the complete combustion of the sample. This study also provided some clues as to the smoke suppressing ability of clays, which seem to be releasing water when exposed to a temperature stress.[253] Other clay platelets were used to protect flammable substrates: Kaolin and Laponite were already mentioned, but among them, vermiculite (VMT) platelets might be more efficient, as evidenced in this study by Cain et al. With only 1 bilayer of PEI/VMT, pHRR was reduced by 54%, the foam structure was kept, and the THR was slightly decreased as the second HRR peak is suppressed. In the meantime, it took 4BL of PEI/MMT layer-by-layer coating to reach the same results.[254] There, it is suggested that VMT might act as a char catalyst. Other studies were conducted, one on Polystyrene plates, whose ignition from a butane torch was prevented by a thick 8BL CH/MMT or an 8BL CH/VMT nanocoating.[255] On PUF, 2BL of a VMT/Cellulose Nanofibrils was enough to prevent melt-dripping. The carbonaceous outer layer formed protected the sample from burning, and the highly stable char formed by the Cellulose Nanofibrils led to a better barrier than a 2BL CH/VMT coating.[256] It could also be linked to a thermal shielding effect, as proposed by the work of Carosio et al, where a self-standing film of Cellulose Nanofibrils/MMT could maintain the temperature at the back of the so-called paper under 260°C for 5 min while the front was subjected to a small butane torch. In this study they relate this to the charring of Cellulose Nanofibrils as well as to the delamination of the platelets.[257]

Table 12. Passive composite layer-by-layer fire protective coatings with Silicon-based nanoparticles.

Substrate	Material	System	Number of units	Result	Reference
Foam	PU	Poly(o-cresylglycidylether)-co-formaldehyde/NH_2-MMT/PEI-triphenylphosphate	12	MLC: pHRR-25%; increased TTI	[245]
		PEI/MMT/PAA	8	MLC: pHRR-17%; THR=	[244]
		PEI/MMT/PAA	3	MLC: pHRR-30%	[248]
		PAA-MMT/PEI	5	MLC: pHRR-42% Mock-up real scale test: pHRR-53%	[249]
		CH/MMT	10	Torch test: no melt-dripping MLC: pHRR-52%; THR-10%	[250]
		BPEI-HAL/PAA-HAL	5	Torch test: no melt-dripping MLC: pHRR-62%; THR=; TSR-60%	[252]
		PEI/alginate-Sepiolite	6	MLC: pHRR-76%; THR-27%; TSR-27%	[253]
		PEI/VMT	1	MLC: pHRR-54%; THR-13%; TSR-31% (needs 4BL CH/MMT to reach these results)	[254]
		Cellulose Nanofibrils/VMT	2	Torch test: no melt-dripping	[256]
Textile	Cotton	Starch/MMT	20	VFT: cohesive residue MLC: pHRR-21%; THR-15%; reduced TTI	[243]
		Cationic POSS/anionic POSS	20	VFT: cohesive residue MCC: pHRR-11%; THR-17% Pill test: smoldering, 7x53mm char	[238]
		Aminopropyl silsesquioxane/anionic POSS		VFT: cohesive residue MCC: pHRR-20%; THR-23% Pill test: smoldering, 7x20mm char	
	Acrylic	Cationic POSS/APP	6	VFT: no melt-dripping, limited burning LOI: 22% MLC: pHRR-23%; THR=	[240]
	PET	Cationic POSS/MMT	5	HFT: no melt-dripping, reduced burning rate MLC: pHRR-50%; THR=; TSR=; reduced TTI	[242]
		CH/MMT/CH/TiO_2	5	MLC: pHRR-48%; THR-36%; reduced TTI	[244]
	Barrier fabric	PEI/MMT/PAA	8	MLC: Increased pHRR and THR	[209]
	PI	Poly(benzyloxycarbonyl-3,4-dihydroxyphanylalanine)/MMT	20	VFT: reduced burning length	[246]
	PAN	Silica gel(APTES)/PA	10	MLC: pHRR-66%; THR-73% LOI: 33%	[241]
Bulk polymer	PC sheet	PEI/anionic SiO_2/cationic SiO_2/UV-curable aliphatic PU	5	HFT: Self-extinguishment, no melt-dripping	[239]
	PA6 sheet	PAH/MMT	20, 40	MLC: pHRR-60%; THR=; TSR-57%; increased TTI	[258], [259]
	PS plate	CH/VMT+amine salt treatment for increased thickness	2	Burn-through torch test: Self-extinguishment (8BL: no ignition)	[255]

iii. Thoughts on the mechanism

The mechanism of passive barrier coatings is not very clear, although some thoughts have been given to it in the literature. However, most point out a condensed phase mechanism. It appears that the composite nanocoatings are able to form a shell that maintains the substrate's shape. This shell, like an exoskeleton, acts as a physical barrier to delay and slow down the release of fuel into the flame, therefore effectively reducing the HRR during a cone calorimeter test (this has been verified through mass loss curves). In some cases, an increase of the time to ignition is observed. Apaydin et al. attributed this to the formation of a "high performance, stable, and flexible carbonaceous-silicate char barrier at the surface of the sample" which delay mass transfer of degradation products.[134] In some extreme occurrences, the protection formed prevents the ignition completely. In other cases, no effect on the time-to-ignition was observed, or the presence of the coating caused it to decrease. This might be due to several reasons. First, the barrier might not be thick or stable enough to delay the transfer of flammable products. Then, it can form cracks,[193] or be discontinuous, or the presence of particles can catalyze the degradation of the substrate.

This shell also prevents melt-dripping (in an open flame scenario) or pool burning (in a radiative scenario), therefore forcing the combustion (if any) of the polymer inside the exoskeleton. As a consequence, the stronger the barrier the better, and it should form early enough to be able to act efficiently (before substrate decomposition). This mechanism was investigated in the work by Apaydin et al., where they show how a PAH/MMT nanocoating could act to protect a PA6 sheet, by decreasing the pHRR by 60%.[258] They evidenced the early degradation of PAH, and that the MMT-reinforced char layer could act as a trap to combustion gases, which helped expanding the protective layer.[259] Indeed, the most efficient systems seem to be those producing a thermally stable, strong, and continuous char. It was suggested from Raman analyses that the more protective coatings gave residues with a high graphitization degree, which is attributed to a higher thermal stability of the char. The higher protective ability is ascribed to a better barrier effect because of a more compact residue. This has to do with the chemistry of the mortar and its inherent charring ability, or to the presence of catalytic sites favoring the formation of a graphitic char.[140], [154], [183], [218], [225], [231]–[233] This result may be surprising, because it was proven that an ordered char was more prone to cracks which was detrimental to fire properties.[260], [261] It is probable that the presence of particles maintains the char structure and improve the mechanical properties, but this point is not addressed in the mentioned papers.

The presence of phosphorus seems to help strengthen the char formed. This can be either by catalyzing its formation (therefore protecting the substrate before its decomposition), by promoting the decomposition pathways leading to the formation of aromatic carbon structures, by crosslinking, by formation of phosphorus-containing coating, or formation of inorganic glasses.[262] In the literature, it is also suggested that the presence of phosphorous can prevent the oxidation of the char at high temperature.[263], [264] It was also reported that chars containing phosphorous improve the capacity of the carbon layer to prevent volatile species and melting polymers from diffusing through it.[265] In addition, continuous coverage and higher thickness obviously allow to reach better performances. Consequently, better results are reached by adjusting the composition, pH and concentration of the deposition solutions to influence the physico-chemical phenomena driving the coating process (amine salt to increase thickness; polymers with higher molecular weight; higher concentrations of the solutions of nanoparticles etc.). Packing density of the particle is also important. The chemistry of the nanoparticle also seems to impact the effect of the nanocoating on the fire protection of the substrate. It seems that particles with believed catalytic ability such as metal nanoparticles or metal-rich clays are more efficient. It means that they can catalyze the formation of a compact and thermally stable char more easily. Less layers are thus required for good protection.

Usually inside the shell produced by the coating, the flammable substrate underneath is completely consumed, and therefore, the THR is not reduced. This is the reason why most composite coatings only slow down flame spread rather than stopping it, at least with textile or paper substrates. With foam substrates, however, the porous char layer formed on top is sometimes protective enough to prevent the combustion of the flammable material underneath, and less fuel means less heat produced. Smoke suppressing ability of some particles was pointed out, and it was suggested to be linked to either water release (in one occurrence with sepiolite clay), mesoporous nature of the particle, or catalytic activity of the particle, which in case of metal-based particles also led to less harmful gases being released. Finally, some works suggest that the protective effect of the films comes from a thermal barrier effect, although it was not proven in-situ.

IV. Exploring new opportunities part 1: alternatives to layer-by-layer thin coatings with similar mechanisms

1) One-pot nanocomposite coatings

To eliminate the inconvenience of depositing thin layer-by-layer coatings step-by-step, one-pot strategies have been explored. Polyelectrolyte complexes of intumescent systems have been deposited on different fabrics. Two polymers of opposite charge are mixed together in distilled water to form an insoluble complex which is adsorbed afterwards on the substrates by simple immersion for a definite soaking time. Polyethyleneimine and Poly(sodium Phosphate) were combined together on cotton fabric with different soaking times. Their action reduced the pHRR from 17% to 57%, as well as the THR (up to 77%) in MCC experiments (the reduction was improved by increasing weight gain). Self-extinguishment was obtained in vertical flame tests starting from 23% weight gain, while coherent charring was observed for lower complex quantities.[266] The soaking time required to reach this mass was reduced (from 10 min to 30 s) by increasing the complex concentration in the treating solution, and the performance and durability of the coating was improved with acid pH curing. This way, the reduction of pHRR with curing at pH 2 reached 81% while the THR was reduced by 88%. Again, it is accompanied by self-extinguishment in vertical flame testing.[267] Similar performances were obtained for a complex with poly(allylamine) instead of PEI (pHRR -78%, self-extinguishment), but they were more limited for synthetic fabrics (pHRR reduced by around 30% for Polyester-cotton blends and polyester).[137] Thanks to the high P quantities, a Poly Electrolyte Complex (PEC) of phytic acid and PEI on wool reduced pHRR by 39%, THR by 79% and smoke density of wool fabric samples, while increasing the LOI to 36.8%.[268] Bio-based resources were also used and chitosan and phosphorylated chitosan were deposited in a one pot process on PA6,6 fabrics, along with sodium polyacrylate for UV-crosslinking with an attempt of increasing durability. A 10 min impregnation increased LOI up to 22% and the suppression of dripping allowed reaching the V-1 level rating at UL94 test. In that case, however, the layer-by-layer coating was still more efficient than the one-pot process in a cone calorimetry test, as it did not reduce the flammability parameters.[151] While it did not rely on polyelectrolyte complex, another study took advantage of the precipitation of poly[1,4-diaminophenylene-tris(dimethylhydroxymethyl)phosphine] when para-phenylenediamine and tetrakis(hydroxymethyl)phosphonium chloride are mixed together. An aqueous solution of this specie was deposited on one side of a cotton sample by spray coating. Despite the fact that all faces were not covered, charring was observed in vertical flame testing, and self-extinguishment when exposed to a horizontal flame. MCC experiments revealed a reduction of 45% and 63% of pHRR and THR respectively.[269]

Composite dispersions were also deposited by dip-coating on several substrates to produce thin protections taking advantage of the physical protection offered by composite structures. For example, halloysite nanotubes were dispersed with aniline in water on cotton and acrylic fabrics, and aniline was further polymerized. This coating reduced the burning rate in vertical flame testing.[270] The same principle was applied by mixing PDMS precursor with MWCNT/ZnO complexes on paper filter and showed enhanced charring.[271] A mixture of a commercial polymeric binder, graphite, TiO_2 nanoparticles (for hydrophobicity) APP and N-[3-(trimethoxysilyl)propyl]-ethylene diamine stopped the flame spread thanks to the char layer and increased the LOI up to 24% when deposited on furniture fabric.[272] The same principle of mixing all the required ingredients to obtain a thin fire retardant film in a single pot and just impregnate the substrate by dip-coating was also applied on PU foams by Davis et al, who mixed sodium polyborate, starch and MMT by squeezing the substrates in an aqueous mixture of the three ingredients. This resulted in quite high weight gains, but also in reductions of 66% to 75% of the pHRR (no reduction in THR) in cone calorimetry tests depending on the formulation. What is interesting is that a real scale mock-up test of an armchair filled with treated PUF showed even better results, with similar reduction in pHRR depending on the furniture fabric, but also up to 71% reduction in THR, due to the protecting effect of starch and sodium polyborate slowing down the pyrolysis.[273]

However, the most interesting studies deal with the deposition of high filler content nanocomposite thin coatings. Some works propose making the composite before gluing it to the substrate by mean of an adhesive or by thermopressing.[274], [275] In a study by Carosio et al., a 70 µm film of cellulose nanofibrils and MMT prepared by vacuum filtration and hot-pressed on epoxy glass fibers composites sustained the flame of a butane/propane torch, while keeping the temperature at the back of the substrate below 100°C (whereas without coating the temperature was kept at 200°C with no flame penetration).[257]

Another study reached good results by immersing a PU foam in GO suspension before self-polymerizing dopamine in-situ. Kim et al. obtained a thin PDA/GO coating which brought self-extinguishment behavior and protected the samples inner core in a vertical flame test, and reduced the pHRR in cone calorimetry by 65%.[276] Researchers have taken inspiration from nacre, which has a hierarchical organized structure composed of 95% of aligned aragonite ($CaCO_3$) platelets linked together by proteins. The first goal of developing composites mimicking nacre was to make materials with interesting mechanical properties.[277] However, their high mineral content obviously raises an interest in using them for fire protection. While layer-by-layer is one of the methods to make nacre-like nanocomposites, one-pot strategies were developed to deposit thin coatings with high filler content mimicking nacre, that rely on mixing platelet-like nanoparticles with a polymer binder in concentrated slurries. Platelet-like nanoparticles tend to organize themselves by dip-coating, doctor-blading, painting, solution casting, vacuum-filtration processes…, allowing to obtain high scale organized nanocomposite with more than 50% of filler content. All techniques are not appropriate for coating substrates, but some such as dip-coating, doctor-blading and painting can be used easily, especially on textiles and polymer films or plates, although some one-pot self-assembly on foams have been reported.[278] GO and functionalized cellulose were mixed together and deposited on PU foam, wood bars and PP bars, with different GO content. Structured coatings were obtained, and while a single step was enough for PU foam to reach a significantly reduced flammability, several dip-coating steps were required to coat wood and PP bars efficiently. While it defeats the purpose of having a one pot coating, LOI values were increased, and a V-0 rating was obtained in a modified UL94 test with an alcohol lamp.[279] Xie et al. also mixed carboximethyl chitosan with MMT modified with epoxysilane, and deposited the mixture on PET films, cotton fabric and PUF, with several dipping repetitions on PET films. Self-extinguishment was observed in vertical flame testing with an alcohol lamp for PET and cotton fabrics. The flammability of PU foam under cone calorimetry was reduced as pHRR and THR decreased by more than 80%, and extensive residue was produced because of immediate extinction.[280] MMT as a natural platelet-like nanoparticle was extensively studied in high-filler nanocomposite one-pot coatings. Carosio et al coated CH/MMT complex on acrylic fabrics by several doctor-blading steps to coat both sides of the sample and reach the desired weight gain. The coating reduced pHRR, THR and TSR by 62%, 49% and 49% respectively in a cone calorimetry test, and increased the time to ignition. It also slowed down flame spread in horizontal flame test and suppressed dripping.[281] Walther et al. were pioneers in developing large scale one-pot nacre-mimicking structures, and they used either paper-making process, doctor-blading or simple painting. The shear-force of the last two systems was enough to align MMT platelets covered in PVA.[277] The same concept was developed to produce carboxymethylcellulose/MMT films from mixtures at 60/40 w/w proportions,[282] which were then applied on cotton fabrics by slowly dragging the fabrics through a 5wt% concentrated slurry. pHRR and THR were reduced by 37% and 44% respectively in cone calorimetry, and self-extinguishment and reduced burning rates were observed at vertical flame test. The cotton samples also resisted to a hand-held torch test and shrinkage was prevented.[283]

Flow-induced self-assembled coatings containing 70 wt% of MMT nanosheets with PVA were deposited on PU foams by dipping them in the mixture of both components with glutaraldehyde as cross-linking agent, and letting them to hang dry. The samples resisted a 10s hand-torch test.[284]

The use of cross-linked structures is usually carried out as a mean to increase the durability of the treatment on textile,[151] even if some studies on alginate and PEI/o-alginate cross-linked with phosphoric acid, or alginate coatings cross-linked with metal ions were more focused on the idea of taking advantage of the crosslinker as a potential active additive.[174], [285], [286] Crosslinking is known to enhance the thermal stability, and it could help enhancing the char forming ability of nanocomposite coatings. In this regard, the use of highly cross-linked structures such as hydrogels could be one way, once dried, to achieve such structures in order to improve the performance of nanocomposite thin coatings, while still keeping a one pot procedure.

In the next part, definition and use of hydrogel and dried hydrogel against fire are described.

2) Hydrogels and polymer networks for fire protection

a. Definition and application

A hydrogel is a three-dimensional cross-linked hydrophilic polymer network swollen in water. It is kept together and rendered insoluble by crosslinks (or tie-points, or junctions) which can be covalent bonds, ionic forces, hydrogen bonds, entanglements, crystallites, etc. They have the ability to absorb and retain a large quantity of water. In fact, the primary component of hydrogels is water, while the polymeric network constitutes a small part of the material. According to their method of crosslinking, they can be classified as chemically cross-linked (formation of the hydrogel via the establishment of covalent bonds between the polymer chains) or physically cross-linked (the network is maintained via physical forces such as ionic interactions, for example).[287] The latter is of particular interest because of the usually soft conditions in which they are formed. A broad variety of polymers can be used to form hydrogels, both synthetic and natural. Poly(2-hydroxyethyl methacrylate) (pHEMA) is one of the most well-known polymer and forms hydrogels via radical cross-linking. PVA and polysaccharides such as chitosan, carrageenan, agarose, collagen, gelatin or alginate are also used to form hydrogel materials through chemical or physical cross-linking. Most applications of hydrogels lie in the biomedical fields, and they are used for contact lenses, drug delivery systems, tissue engineering, wound-healing bio-adhesives, artificial skin etc.[288] They are also used in food and agricultural applications, as well as in soft robotic (conductive sensors for electronic devices, flexible displays…).[289] Last but not least, they also have applications in fire science.

b. The use of hydrogels against fire

First, hydrogels are largely used as fire extinguishments and prevention systems. They can be dispersed thanks to a traditional sprinkler system, for example. It is required that they have a high and rapid water uptake and high retention capacity. They are mostly thought of as fire resistant materials. In mines for example, they are used to extinguish coal combustion and prevent the spread of the fire by preventing coal oxidation. Overall, they are supposed to limit the temperature of the ignition source, reduce thermal radiation and reduce the amount of CO gas generated. Fire extinguishing gels are also designed to be able to cover the burning materials completely. Most gels are copolymers synthesized from at least an acrylamide or acrylamide-derived monomers,[290], [291] with eventual mineral fillers [292]–[294] and fire retardants.[295] Large scale use of hydrogel has been studied for wildland fires extinction with cellulose-derived/silica and fire retardant formulations,[296] while thermosensitive hydrogels (gel forming above a determined temperature) synthesized from N-isopropylacrylamide and hydrophilic monomers seem promising for this application.[297], [298]

As fire resistant materials, they are also used as active protection solutions for firefighting. For example, protective clothing or protective covers have been imagined using tough hydrogels as textile laminates. The idea behind this is that the hydrogel should keep the temperature low enough and absorb enough heat to be able to maneuver during a fire for a determined amount of time (until it is completely dehydrated). It requires a large amount of hydrogel to be able to keep the protection long enough.[299], [300] Protection of flammable materials for a short while during fire can also be obtained with hydrogels. For example, an electronic circuit with conductive hydrogels could work during a fire for a short moment.[301] Hydrogels casing for flammable oil transport can also be envisioned.[302] Very recently, a fire resistant robot skin made from a gelatin hydrogel filled with carbon nanotubes was developed.

It aims at manipulating and extracting objects from a fire scene.[303] Also very recently, a durable hydrogel fire resistant coating has been proposed for fireproof clothing, trees or structures. A 2 mm thick plate could prevent flame penetration for 40 s. Interestingly, the hydrogel was kept from drying thanks to high concentrations of a highly hydratable salt (LiCl).[304]

Hydrogels are therefore very promising for fire protection. Yet, despite the exciting perspective of having high quantities of water sealed away for fire retardant purposes, they are mostly used as active fire protective systems, although one study reports of a starch-g-poly(butyl acrylate)/mica hydrogel as a 3 mm thick fire protective coating on wood (the coating significantly increased the time to ignition without decreasing the pHRR too much in a MLC test).[305] The reason is that to be used as fire retardant materials, and *a fortiori* as fire retardant coatings, a drying step is necessary for practical purposes. Depending on the drying method, two types of materials can be obtained, namely aerogel or xerogel.

c. Aerogels

Aerogels are obtained by replacing water by air. Two methods can be employed. Freeze-drying consists in freezing water (usually at between -70°C and -80°C, but it depends on the sample), followed by the sublimation of the ice crystals by rising the temperature below 0°C. It creates porous structures whose morphologies depend on the formation of the water crystals during freezing. It can be used as a method of crosslinking for certain systems such as polyvinyl alcohol. However, the most thrilling approach is to obtain aerogels via supercritical drying. During this procedure, water is first replaced by alcohol, and then by supercritical CO_2. While expensive, it is an environmental friendly method which creates materials with unexpected properties, such as astonishingly low thermal conductivity. While the most known aerogels are made from silica network synthesized with a sol-gel procedure and dried with supercritical CO_2, they have poor mechanical properties. Even if there are some reports of good fire retardant graphene aerogel,[306] a large portion of the research on aerogel materials focuses on organic polymers, which are made through freeze-drying hydrogels or viscous aqueous solutions. Crosslinking often occurs during freeze-drying. As such, obtaining polymer aerogel with low flammability still requires the same strategies as their filled counterparts, but they easily reach LOI values higher than 30, and very low pHRR at MLC tests, even presenting non flaming combustion in some occurrences. First, they can be made from high performance polymers such as PI[307], [308] or PolyBenzoxazole (PBO).[309] Then, they can be formulated with fire retardant fillers. The advantage of hydrogels is that they allow reaching high filler content, for example with clays. Polysaccharides aerogels are often studied. For example, cellulose aerogels can char when they are subjected to the flame of a lighter,[310] and have quite low pHRR (around 120 kW/m² [311]) in MLC test, but still need the addition of magnesium hydroxide,[312] citric acid crosslinking [313] or LDH [311] to reduce their flammability. Wood fibers with palygorskite make aerogels with pHRR under 30 kW/m².[314] Cellulose NanoFibers (CelNF) are also largely used and combined with sodium carbonate,[315] graphene oxide mixed with ZrP [316] or sepiolite,[317] or in a mixture of carboxymethylcellulose, APP and MMT.[318] Sometimes an additional crosslinking step is performed, for example by heat treatment with the addition of N-methylol dimethylphosphonopropionamide (MDPA) and 1,2,3,4-butanetetracarboxylic acid (BTCA).[319] Also reported are the addition of Polyaniline and phosphoric acid,[320] PEI and 3-Glycidoxypropyltrimethoxysilane in a formulation of CelNF and hydroxyapatite,[321] or MMT and melamine formaldehyde resin with boric acid crosslinking (which reach a LOI superior to 85%).[322] The additional crosslinking usually decreases the flammability of the material further, which translates in a reduction of PHRR when compared to the system without cross-linkers.[323] Melamine formaldehyde is used quite frequently to improve the flammability of polymer aerogels, for example with pectin,[324] alginate,[325] or PVA.[326] PVA is quite well-known for forming cross-linked structures upon freeze-drying, and as such was extensively used in aerogel formulation. However, its flammability still requires additional flame retardants such as CelNF and APP,[327] laponite and fly ash,[328] Laponite, Halloysite nanotube, SiO_2,[329] APP and ZrP,[330] APP and MXene,[331] or APP and boron nitride nanosheets.[332] MMT is used quite a lot in PVA fire retardant aerogel, either alone [329] or in combination with CelNF,[333] gelatin,[334] or with APP, silica gel and K_2CO_3.[335] Again, an additional cross-linking step with chemical cross-linkers (borate,[336], borax, or glutaraldehyde [337]) or via a physical process (^{60}Co irradiation [338]), can further reduce the flammability of PVA/MMT aerogels. Other polysaccharides such as pectin,[339]–[341] chitosan,[342] xanthan gum and agar,[343] or gum Arabic,[344] were also used in combination with mineral fillers to yield fire retardant aerogels. Alginate, alone or with palygorskite,[345] magnesium or aluminum hydroxide, LDH, or Kaolin [346] also showed very good fire behavior with low pHRR at MLC and very high LOI. When combined with MMT and cross-linked with $CaCl_2$,[346] boron [347] or via pH change [348], they displayed even more impressive behaviors with very low pHRR or no ignition at all.

Interestingly, there is one report on alginate/MMT aerogel used on rigid PUF (RPUF) as fire retardant coating. Alginate/MMT suspension was cast on top of RPUF as 0.2 to 1.5 mm thick coating, and then freeze-dried. A coating made with a formulation of 7.5g of alginate and 7.5g of clay in 100 mL water reduced the pHRR by 30% with a 0.2 mm coating, and by 60% with a 1.5 mm coating. Therefore, aerogel coatings require high thickness to be efficient at protecting flammable substrates.

In addition, despite the low flammability of aerogels, their production requires special equipment and procedures which can be expensive. Therefore, drying of hydrogels at ambient condition to produce xerogels is sometimes favored, and for this reason, next part will focus on xerogels.

d. Xerogels

Xerogels are obtained by drying hydrogels at ambient conditions or elevated temperatures, so that water only evaporates. Although this method is not very common, it is still used to make films and materials from hydrogels. It forms smooth and compact structures. The only disadvantage is that it can cause severe shrinkage because of the collapse of the pores, but this phenomenon can be controlled. For example, cellulose/MMT plates were made from the hydrogel by hot pressing. LOI values went up to 29% by increasing MMT content.[349] Nanocomposites with high silica filler content (95%), in a biomimicry process mimicking nacre composition, were also prepared by air drying a poly(N,N-dimethylacrylamide) composite hydrogel. In this case, air drying was chosen to obtain compact structures and uniform shrinkage. It was introduced in delignified wood porous structure to produce composites, and LOI values over 75% as well as self-extinguishment after exposure to a flame show their high fire retardant potential.[350] As coatings, alginate and alginate/bentonite hydrogels formed via Ca^{2+} cross-linking and air dried also show potential for fire retardancy, although this approach has not been pursued further, to the best of our knowledge. It is reported that while a simple alginate coating could slightly delay the ignition of Masonite supports, gelation significantly increased the time to ignition. The same effect was obtained on balsa wood with the addition of bentonite.[351]

As a conclusion, it is possible to design nanocomposite coatings with high filler contents, just as LbL coatings, but in a one pot procedure thanks to nanoparticles self-assembly. Although it seems a convenient way to bring fire retardancy to flammable substrates, it is way less studied than layer-by-layer coatings. From the literature survey it can be noticed that a crosslinking step brings additional fire retardancy of materials and coatings. Uniformly cross-linked structures can be obtained by synthesizing hydrogels, which can easily incorporate large amount of fillers. Hydrogels have been explored as fire resistant materials for active protection in firefighting. Aerogels are promising fire retardant materials but aerogel fire retardant coatings are difficult to obtain. However, once dried in ambient conditions, hydrogels form thin, compact and smooth structures (xerogels) which are ideal for coating substrates, if the shrinkage is reasonable. Therefore, the combination of high-filler content one pot nanocomposite coatings and gels has great potential for the fire protection of flammable substrates, and could be a viable alternative to step-by-step layer-by-layer coatings. To the best of our knowledge, however, there is limited work exploring this topic. As a consequence, this pathway is explored in the chapter 3 of this PhD thesis.

V. Exploring new opportunities part 2: metallized surfaces as radiative heat barrier.

While pHRR is deemed the most important parameter to look at for improving the fire safety of polymers, one should not overlook the importance of the time to ignition. The short time to ignition of polymers is one of the main reasons they pose such a danger in case of a fire. Having a long time to ignition is a sure way to limit the flame spread and to give more time for people to evacuate the danger zone. Preventing ignition altogether completely suppresses the fire hazard. The ignitability of polymers when subjected to a heat source is enhanced by their low thermal conductivity. Moreover, it is a complex phenomenon which relies on a large number of parameters, one of the most important being heat absorption. In the following parts, it will be demonstrated how thin coatings can help reducing the heat absorption of polymers.

1) Heat transfer in fire

During a fire, or in presence of a hot object, heat is transmitted to the surroundings either by conduction, convection or thermal radiation, as the flame behaves as a hot object. The contribution of radiative heat transfer to the total heat flux can be quantified, and this has been the subject of several studies over time. It is acknowledged that in certain conditions, thermal radiations account for a large part of heat transfer in a fire, depending on the scale, fuel type, temperature, ambient oxygen concentration, flame chemistry/composition (notably the presence and type of soot and geometry), etc. It is caused by the absorption (and therefore the emission) of heat from soot. The emission spectrum follows Planck's law, with the addition of the emission of particular infrared wavelength due to the vibration of hot gases such as CO_2.[352] Radiative heat transfer account for a large part of total heat transfer in middle to large scale fires [353] (with a diameter of 0.2 m or more, while convection and conduction dominate at smaller scales).[354], [355]

2) Absorption of radiative heat by a material: an optical problem

When a light beam impacts the surface of a material, it will either be reflected or penetrate the object. The fraction of the incident light that is reflected is called reflectance (ρ). Once it penetrates the surface, it is either attenuated or not. In the first case, light is absorbed, in the other case it is transmitted. The fractions of incident energy that are absorbed and transmitted are respectively called absorbance (α) and transmittance (τ). Absorption of light occurs when the frequency of the incident ray matches the lattice vibration frequency (infrared), or the allowed electronic transitions (UV-visible and Near InfraRed (NIR)) of the material.[356] That is to say, absorption occurs when the material is able to raise its energy level in response to light external stimulation. This is followed by the relaxation of the material back to a more stable state (it lowers its energy level), with emission of a photon. As a consequence, an absorber is also an emitter, and the ratio of its emissive power (its exitance) to the emissive power of a perfect absorber (also called a black body) is the emissivity[1] of the surface. Per definition, it is always inferior to 1, since, theoretically, nothing can absorb and emit more light than a black body.

Additionally, Kirchhoff's law stipulates that, at thermal equilibrium, the power radiated from the surface of a material must be equal to the power absorbed.[357] It follows that the emissivity

---

[1] According to Modest in Radiative Heat Transfer, the terminology « -ance" is better suited for designating the rough and contaminated surface that this study is concerned about, whereas the terminology "-ivity" is dedicated to pure and smooth materials, as per NIST recommendation. However, as "emissivity" is more commonly used within the scientific community, when compared to "emittance", we will continue to use this term.

of a material is equal to its absorbance: $\varepsilon = \alpha$. For opaque materials, $\tau = 0$, and it follows that: $\varepsilon = 1 - \rho$. Therefore, the emissivity can be linked to the reflectance of a material. The lower the emissivity, the higher the reflectivity, and *vice-versa*. All these quantities are dependent of the wavelength of the incident light, the temperature and direction vector. The terms “spectral” and “directional” will therefore designate one quantity respectively at one distinctive wavelength and direction vector, and the terms total and hemispherical will designate the same quantity integrated over all wavelengths and over a half sphere on top of the surface.

A black body, or any hot object behaving as a black body (the sun, a heated resistance or a sooty fire for example), will absorb and emit all radiation according to Planck’s law, which describe the distribution of the intensity of radiation as a function of wavelength:

$$E_b(T,\lambda) = \frac{2\pi h {c_0}^2}{\lambda^5 [e^{(hc_0/k\lambda T)} - 1]}$$

Integration of this law over all wavelengths will produce the Stefan-Boltzmann law: $E_b(T) = \sigma.T^4$, where k is the Boltzmann constant ($k = 1.3805x10\text{-}23\ J.K^{-1}$), h is the Planck constant ($h = 6.6256x10^{-34}\ J.s$), σ is the Stefan-Boltzmann constant ($\sigma = 5.67x10^{-8}\ W.m^{-2}.K^{-4}$), c_0 [$m.s^{-1}$] is the speed of light in vacuum, and λ [m] is the emission wavelength. Per definition, for a real surface, $E(T,\lambda) = \varepsilon.E_b(T,\lambda)$.

When concerned with radiative heat transfer, the wavelengths of interest are comprised between 0.1 µm and 100 µm. They are called thermal radiation and are emitted by any object solely because of its temperature.[358] On the other hand, absorbing them will cause an object to heat up in response, because of induced vibrations. However, by considering a black body as the source of the radiations, for high temperature applications (between 1000 K and 2000 K), heat transfers are controlled by wavelength between 1 and 10 µm, [359] and are governed by the following equation:

$$\Phi = \varepsilon.S.\sigma.(T_2^4 - T_1^4)$$

Where Φ is the heat flux between a heat source at temperature T_1 and a surface S with an emissivity ε and a temperature T_2. As infrared radiation is converted into heat at the interface between the environment and the material, it can be considered first as a surface phenomenon.

From this dissertation it can be concluded that lowering the emissivity of the surface of a polymer in the infrared wavelengths can potentially lower its heat absorption and therefore have a huge impact on its ignitability, which has been confirmed recently by numerical simulations.[360]–[363]

3) On the use of thin coatings to limit radiative heat transfer

Since limiting heat absorption of polymers is a surface problem, it makes sense to use thin coatings to tackle it. The main applications where this concept has been put into use are the aerospace industry,[364], [365] the military field for infrared stealth,[366]–[368] and energy saving and user comfort in buildings.[369] While the systems can change from one work to another due to several constraints, the core principle remains the same. The coatings are composed of several layers of metals and dielectric. The metal plays the role of a reflector. The other layers either protect it, adjust the reflectivity range to cater for a particular application or promote the adhesion to the substrate.[370] The particularity of such coatings is that they are very thin, usually a few micrometers or even less than one micrometer.

Despite their obvious interest, they have been scarcely applied in fire protection. Paints or composite coatings with infrared reflective pigments [371], [372] have been developed as a first idea to improve flame retardancy of substrates, in order to improve the reflectivity of conventional white reflective paints in the infrared range. The pigments (aluminum flakes or coated mica flakes) were incorporated in a binder and reflected radiations from 1 to 10 µm specific of a wood fire. TiO_2 particles can also be incorporated but do not reflect the infrared radiation *per se*. They rather scatter the light and therefore must have a specific dimension and concentration.[371]–[373] Their effect was to delay the ignition of wood by a factor of two when exposed to a charcoal fire.[371] Paints containing infrared reflective pigments have been developed for infrared stealth or high temperature applications, but were not tested against any fire scenario.[374], [375] The inconvenience with those types of paints is that the binder can have strong infrared absorption and is usually flammable. An inherently flame retardant binder must therefore be used.[371], [372]

In a recent study, however, Sonnier et al. did develop composites films of polyethylene and aluminum flakes coated on polyethylene substrates. The samples were tested against a standard radiative fire scenario by mass loss cone calorimetry. They found that the time to ignition could be shifted for 80 s to 400 s against a 35 kW/m² heat flux.[376]

Applying the same concept of highly infrared reflective coatings as those used in energy savings or aerospace application has however not been pursued in fire protection before the study conducted by Schartel et al. They applied a three layers coating consisting of one chromium adhesive layer, one reflective copper layer, and one silica protective layer, which reached a thickness below 1 µm.[377] The time to ignition was shifted from 58 s to 537 s for a PA66 substrate, while a PC substrate ignited after 459 s of exposure instead of 82 s. This delay was enough to limit the flame spread and fire growth indices, lowering the MAHRE to levels that pass the EN 45545 standard.

Later on, Försth et al reported the use of spectrally selective surface and applied transparent conductive oxide on PMMA. Indium Tin Oxide, because of its electronic conductivity, has a low emissivity. A 0.1 µm coating decreased the absorptivity of PMMA by 30% and shifted its time to ignition from 101 to 257 s at mass loss cone test at 25 kW/m² and from 27 to 54 s at 50 kW/m². However, they observed a delamination between the substrate and the ITO coating and stated that the behavior could be improved, should the deposition conditions be optimized. They also coated a steel substrate with VO_2 by gluing the powder with a paint while it was still wet. VO_2 is a thermochromic material which shifts from insulating to conductive (reflective) at high temperature. They only observed a decrease of 5% in the absorptivity in the thermal range of a fire and at the time dismissed the possibility of VO_2 to be used in fire retardant applications.[352] However, in later research they found that by sputtering 50 to 100 nm layers of VO_2 on glass, the thermal radiation could be reduced by up to 30%. As they observed a strong absorption starting from 2.7µm, they concluded that it could not serve a fire retardant purpose by itself, but rather add a welcome side effect to thermochromic windows.[378]

The authors of these last four studies stated limitations and perspective ideas. First, they observed no effect on the pHRR and THR of the polymeric samples. Then, Sonnier et al. estimated that such coatings would only be effective in a radiative scenario. Against a small flame for example, their protective effect might be lost. Schartel et al. also proposed that "IR-mirror coatings present the possibility of combination with established flame retardancy approaches to yield the superposition of large effects, in particular combining the flame retardancy against radiation and a small flame".

Further studies on this concept have however not been conducted to the best of our knowledge. Low emissivity coatings present therefore a good opportunity for the development of fire protective coatings for flammable substrates. As a consequence, further work is developed in the Chapter 4 of this PhD thesis.

VI. Conclusion and strategy for new thin coatings for fire protection

In this section, different approaches for the development of thin coatings to fire protect various polymer substrates have been reviewed. Three strategies have been identified as particularly promising, each one being adapted to different kinds of substrates.

First of all, layer-by-layer coatings are an extensive part of research on thin coatings for fire protection. Passive composite barriers show promising applications, especially for porous substrates, and will be the object of the first part of this work. They have been extensively studied, but the reason for their high protective effect is still unclear and must be understood to gain fundamental insights for the development of novel systems.

Second, two barely explored strategies for fire protection have been identified as good opportunities for the development of innovative thin coating systems. The first one consists in casting one-pot composite coatings with high filler content to obtain the same properties as a layer-by-layer coating without the cumbersome step-by-step process. An idea to improve their performance was to coat a gel and let it dry. The cross-linked structure is expected to provide additional fire retardancy to the substrate. One-pot deposition techniques of high filler content are more adapted to textile substrates. Therefore, to validate the concept, they will be explored for supple substrates such as textiles.

From the literature survey, it seems that the protection of thick (3 mm) polymer plates, although not impossible, is trickier with thin coatings. Therefore, another approach was sought for this type of substrate. It appeared that one of the key hazards in polymers is their quick ignition, due to their high heat absorption. Changing this property should have a huge impact on their flammability by delaying the ignition. As a result, coatings with reflective properties have been studied. The use of copper or other conductive materials as coatings create low emissivity surfaces, and require low thickness. As the concept is still new and scarcely studied, it can be a good opportunity for innovation.

Chapter 2 . Layer-by-layer coatings for fire protection of porous substrates

The fire retardancy of porous substrates using a thin coating strategy is a bit tricky as it is difficult to find a way to coat every surface available. A coating remaining on the exterior surface of a foam would make it impracticable and limit its application. Moreover, the properties brought by the porosity of these materials should not be impacted by any fire retardant approach. As a result, in this chapter, layer-by-layer coatings were investigated as fire barrier for the protection of porous polymers, and in particular of polyurethane foams. Layer-by-layer coatings have very low thicknesses. The advantage is that they use as little material as possible, and their processing also allows them to coat all surface available of a substrate. Consequently, they will barely impact its properties, making them ideal to reduce the flammability of materials, especially porous substrates such as foams.

Thanks to their resiliency and strength, flexible polyurethane foams (PUF) are extensively used for furniture upholstery, acoustic and thermal insulation. However, as most polymers, they are extremely flammable and are therefore a major contributor during a fire. Their combustion is particularly quick and produce flaming drops and highly toxic gases. It is therefore compulsory to shield PUF against fire, with a system having as minimum an impact as possible on its overall properties, and as environmentally-friendly as possible. It is possible to match these requirements with layer-by-layer coatings, as these have thicknesses as low as a few dozens of nanometers, and are processed through an aqueous route.

In this chapter, the use of passive layer-by-layer nanocomposite coatings for the fire protection of PUF was investigated. While the literature is quite extensive on the use of LbL systems to reduce the flammability of PUF, and despite some attempts at investigating the reason for their efficiency (see chapter 1), their mechanism of action while applied on PUF remains unclear. Therefore, in this work, the mechanism of action of layer-by-layer coatings on polyurethane foam was investigated in detail. First, a chitosan (CH)/vermiculite (VMT) layer-by-layer coating applied on polyurethane foam was tested against a variety of thermal constraints, including high heat flux fire scenario. Fire behavior of these coated foams was evaluated and the mechanism of protection was investigated thoroughly. This section is based on an article published in ACS Applied Materials and Interfaces in 2018. It was made in collaboration with Dr Lazar and Prof Grunlan from Texas Agricultural and Mechanical University (TAMU). They developed the systems based on a previous study, deposited them on the substrates and made the screening fire tests. Prof Carosio from the Polytechnic Institute of Turin performed cone calorimetry. Our team performed the bench scale burn-through fire-test, as well as the mechanistic study on the behavior of the foam at high heat flux. In the second part, a single bilayer of PolyEthyleneImine (PEI) combined with another type of nanosheets, namely hexagonal Boron Nitride (h-BN), was investigated. Fire performances, mechanical properties and ageing resistance were considered. This part was made in association with Dr Lazar and Prof. Grunlan, who designed the system and carried out the fire tests and the characterizations. Our team performed the NMR analysis as well as data interpretation and paper writing. The part is based on a paper published in ACS Applied NanoMaterials in 2019.

The mechanism of action of both these systems was investigated to gain knowledge on how they work and the criteria to meet for them to be as effective.

I. Extreme Heat Shielding of Clay/Chitosan Nanobrick Wall on Flexible Foam

ACS Appl. Mater. Interfaces 2018, 10, 31686−31696

A renewable layer-by-layer coating composed of 8 bilayers of chitosan and vermiculite was deposited on flexible PUF. Chitosan acts as an organic binder to keep the sheets of vermiculite together and was chosen for its charring capacity, while vermiculite was chosen as a high aspect ratio fire resisting clay. The behavior of the coated PUF under different heat flux and fire scenario (hand-held butane torch, cone calorimeter and high heat flux butane torch) was established. More particularly, its excellent performance during a high heat flux bench scale burn-through fire test was investigated in an attempt to evaluate and understand its good heat shielding performance.

1) Characterizations before fire tests

After deposition, the polyurethane foam's is visually of homogeneous beige color due to the VMT platelets, adding 17.5 ± 0.5 wt % to the PUF with eight bilayers. A stiffening of the foam was also observed. The anionic vermiculite clay platelets are held together by cationic chitosan, that when deposited layer-by-layer on a silicon wafer, result in a linearly growing system, as measured by Quartz Crystal Microbalance (QCM). To deposit the same system on polyurethane foam, the sample was first primed with a PAA solution to induce a negative surface charge via hydrogen bonding.[254] Bilayers comprised of CH and VMT were then deposited on the PUF, with PEI substituting for chitosan in the first bilayer to improve adhesion.[379] Low-magnification SEM of the uncoated PUF shows the typical three-dimensional open-cell porosity that is characterized by a smooth, even morphology (Figure 4 c)).

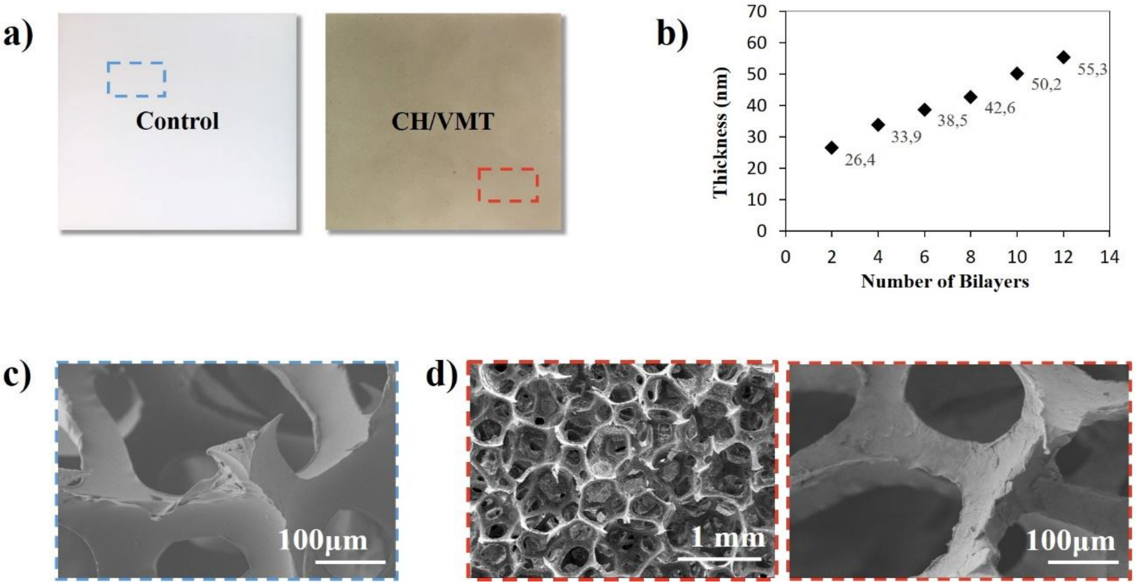

Figure 4. a) Digital photographs of uncoated and CH/VMT-coated foam. b) Growth profile of CH/VMT layer-by-layer nanocoating, recorded via QCM on polished Si wafers. c) SEM picture of uncoated PUF. d)SEM picture of CH/VMT-coated PUF, at two different magnifications.

This morphology is evidently changed after LbL deposition, in which the walls of the foam are conformally coated and possess some texture due to the presence of the clay-containing nanocoating. Despite some loss in porosity, the open-cell 3D structure of the foam is preserved. The surface appears rougher, with a crumpled appearance due to VMT platelets. It seems that the coating was subjected to some stripping during the deposition, as what is attributed to individual vermiculite platelet stick out at some places. Nevertheless, the pictures show that the coverage of the surface is good, even and homogeneous. (Figure 4d)) Electron probe microscopy, using aluminum X-ray mapping, provides a quantitative elemental analysis of aluminum that is characteristic of vermiculite found within the nanocoating. The aluminum X-ray mapping is found to be mainly in the blue/green region of the quantifiable scale, which confirms the homogeneous nature of the coating along a PUF strut compared to the uncoated PUF that lacks the presence of aluminum.

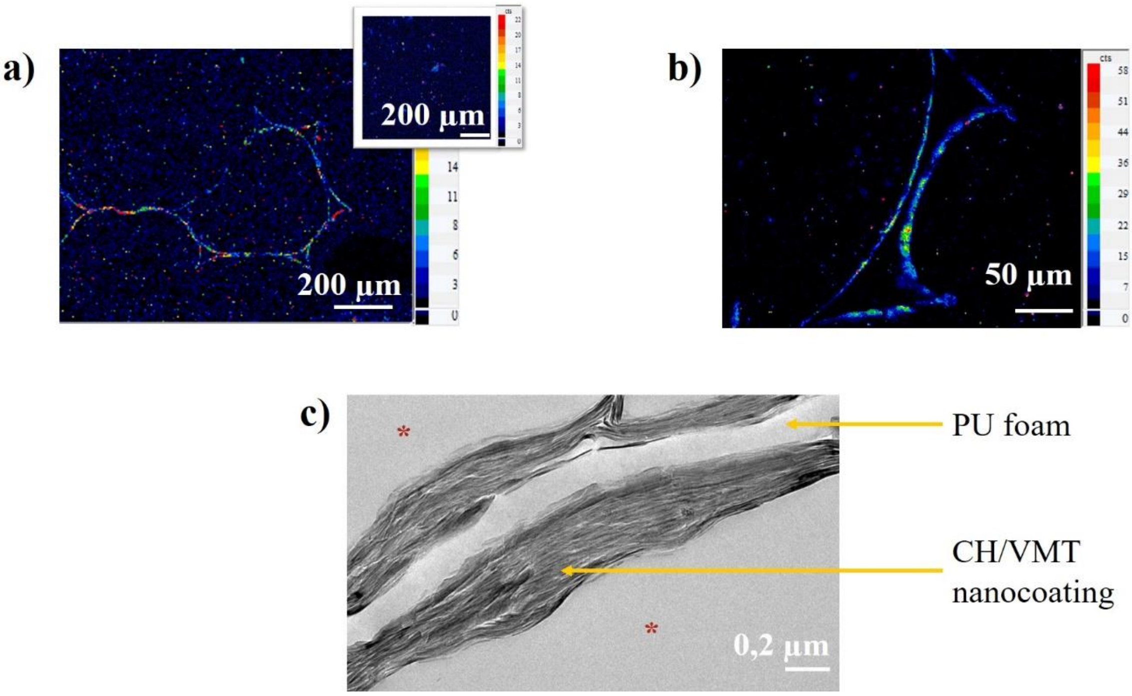

Figure 5. a) and b) represent EPMA Al X-Ray mappings of CH/VMT PUF. The insert in a) shows EPMA Al X-Ray mapping of uncoated PUF, highlighting the absence of Al atoms. c)TEM picture of the cross-section of CH/VMT PUF. (*) denote epoxy resin.

A cross-sectional TEM image reveals the multilayered structure of the deposited coating (Figure 5 c)). The darker lines of the micrograph represent the VMT nanoplatelets that are preferentially oriented parallel to the foam surface and are embedded within the CH matrix that appears lighter in color due to the difference in electron density. Although the thickness observed by TEM is not very accurate as a result of the sample preparation, it is representative of how the nanocoating deposits on PUF (i.e., three-dimensional porous substrate), which differs from how the system deposits on a silicon wafer. The coating of foam is not a “clean” process due to the rigorous rinsing and drying process that involves compressing the foam in water and thoroughly wringing out the foam after each deposited layer. Nonetheless, the micrograph clearly shows that or how the nanobrick wall coating follows the PUF’s complex three-dimensional structure by bending on the cell wall edges and conformally coating every surface available.

The thermal stability of the control and CH/VMT foam as well as the pyrolysis gases have been investigated by means of TGA under nitrogen atmosphere. The degradation of polyurethane occurs in two parts. The hard segments of polyurethane (urea and urethane groups coming from the diisocyanate) decompose during the first step, here at 286°C, while the overall solid mass melts. According to the literature, this decomposition yields different species such as carbon dioxide, amines, isocyanate and alcohol [380] and is a depolymerization process triggered by the decomposition of the C-NH bond, followed by decomposition phenomena.

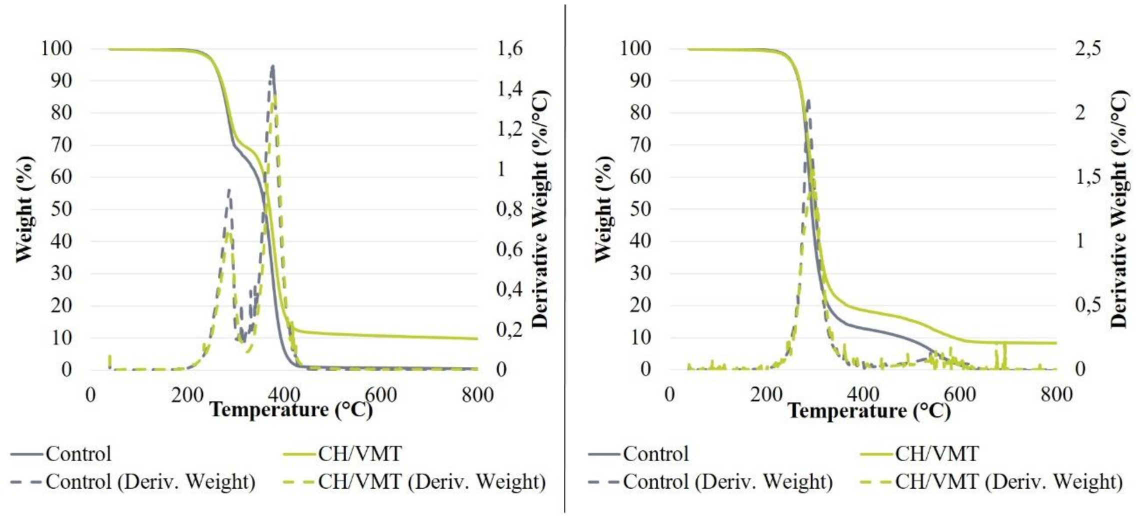

	$T_{95\%}$ [°C]	*1st step*		*2nd step*		Residue @800°C [%]
		T_{onset} [°C]	T_{max} [°C]	T_{onset} [°C]	T_{max} [°C]	
Control	256,0	263,2	286,3	356,0	375,8	0,39
CH/VMT	256,7	261,9	287,0	359,3	378,8	9,77

	$T_{95\%}$ [°C]	*1st step*		*2nd step*		Residue @800°C [%]
		T_{onset} [°C]	T_{max} [°C]	T_{onset} [°C]	T_{max} [°C]	
Control	255,8	270,5	286,8	516,4	552,5	0
CH/VMT	256,5	270,0	295,4	526,4	555,4	8,28

Figure 6. TGA of coated and uncoated PUF in N_2 (left) and air (right) atmosphere. $T_{95\%}$ represents the temperature at which 5% of the initial mass is lost. T_{onset} represent the temperature at the beginning of each degradation step, whereas T_{max} represents the temperature at which the mass loss rate is the highest.

The second step, here at 376°C, yields aldehydes, ether-containing species as well as CO_2 and H_2O (see Figure 6). The thermo-oxidation of PUF consists of two steps as well. The first step at 286°C corresponds to the breakdown of the PU molecule by depolymerization, followed by radical formation and chain scission of the soft segments.[380] It creates a stable char, which is further oxidized at 553°C. The addition of a CH/VMT nanocoating does not change these behaviors, as the same degradation steps are observed under inert and oxidative atmosphere. As it can be seen in Figure 6, under nitrogen atmosphere, the second degradation step occurs at 379°C instead of 376°C for CH/VMT and PU foam respectively, however, it is not a significant difference. Under air atmosphere, the first decomposition step is not delayed, as the onset temperature is similar between uncoated and coated foam (270°C). However, the thermo-oxidation is slowed down, as the temperature at which the maximum decomposition rate takes place is shifted by almost 10°C (287°C and 295°C for the control and CH/VMT foam respectively). As a consequence, the second decomposition step is delayed, with an onset temperature at 526°C for CH/VMT instead of 516°C for the uncoated foam. Whereas there is no residue left at 800°C for PUF, CH/VMT foam produce a residue between 8 and 10%. This corresponds to the mass of vermiculite, as it is the only element not degraded of the sample. As a conclusion, the nanocoating slightly improve the thermal stability of the PUF.

2) Flammability behavior at low and medium heat flux

a. Hand held torch test

The initial fire screening of the coated polyurethane foam was carried out using a 10 s butane torch test to evaluate the flame retardancy of the coated and uncoated PUF. When the torch test is carried out on uncoated foam, the flame entirely consumes the sample and melt dripping is observed.

When the 8BL CH/VMT-coated PUF is exposed to the same torch test for 10 s, the nanocoating shields the inner core of the PUF from the flame, allowing it to maintain its original shape and structure, losing only 25.2 ± 0.4 wt % of its initial mass (Figure 7 b)).

As seen in the cross-sectional image of the treated PUF, only the outer surface of the sample is charred, whereas the inner core is preserved (Figure 7 b)). Figure 7 c) and d) shows that the 3D porous structure observed from the charred area of the treated PUF has been hollowed, suggesting that the polyurethane substrate was consumed by the flame, leaving behind nothing but the nanocoating. The hollowed structure of the charred surface of the foam is further confirmed when discussing the mechanism for thermal shielding (see section 3).

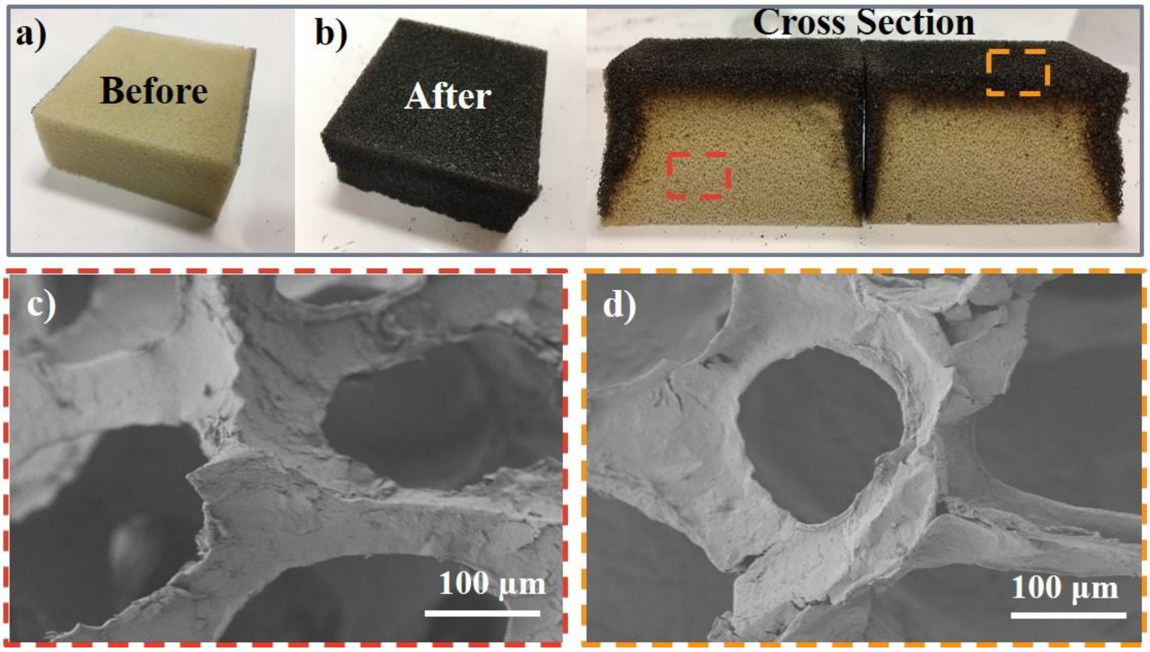

Figure 7. Digital images of 8BL CH/VMT PUF a) before and b) after 10 s torch test. The foam sample was cut through the middle to reveal the undamaged material inside (right). SEM images of c) core and d) char of 8BL CH/VMT PUF after torch test.

b. *Cone calorimetry*

Cone calorimetry was employed to evaluate the reaction of modified PUF to a radiant heat flux normally found in developing fires (35 kW/m^2).[381] Figure 8 shows heat release and smoke production data as well as the post combustion residue analysis performed with SEM. Table 13 summarizes the cone data. Upon exposure to the cone heat flux, the unmodified PUF quickly ignites and its structure starts collapsing, whereas the heat release rate sharply increases. The foam then completely melts, generating a pool of a low viscosity liquid that vigorously burns, achieving the maximum HRR (427 kW/m2). The flames almost completely consume the sample, leaving a residue that is just 3% of the initial mass. The presence of the CH/VMT coating completely changes the burning behavior of the foam. After ignition, no collapsing occurs, and the foam shows substantially reduced HRR values that peak at only 201 kW/m2 (Figure 8 a)).

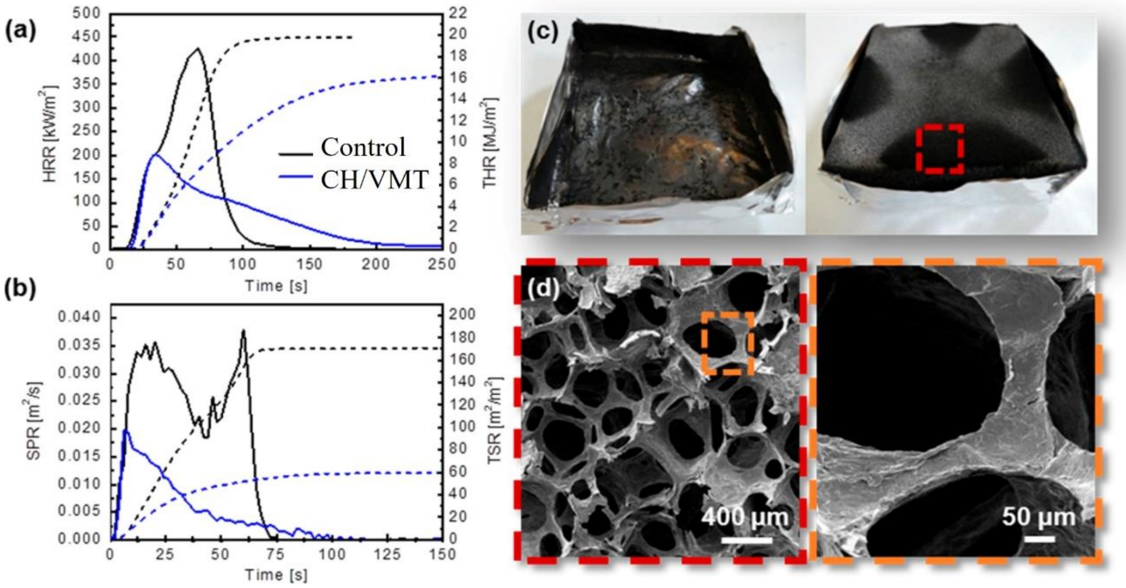

Figure 8. Heat release rate as a function of time, as measured by cone calorimetry and postcombustion residue morphology: (a) HRR and THR, (b) SPR and TSR, (c) digital images of postcombustion residues (left is neat PUF and right is CH/VMT-coated PUF), and (d) SEM micrographs of CH/VMT-coated PUF.

Table 13. Cone calorimetry results for coated and uncoated PUF

Sample	**TTI [s]**	**pHRR ± σ [kW/m²]** (reduction, %)	**THR ± σ [MJ/m²]** (reduction, %)	**TSR ± σ [m²/m²]** (reduction, %)	**Residue ± σ [%]**
Control	4 ± 1	427 ± 27	19.8 ± 0.2	171 ± 7	3 ± 1
CH/VMT	4 ± 1	201 ± 4 (53)	16.3 ± 0.4 (17)	64 ± 2 (63)	22 ± 1

This behavior is ascribed to the CH/VMT coating that can mechanically sustain the foam and produce a protective barrier. Indeed, upon heating, chitosan undergoes a char forming reaction that leads to the production of thermally stable aromatic char.[382] This carbon-based matrix holds together the VMT nanoplatelets and results in a protective coating that is capable of limiting mass and heat transfer from/to the flame, thereby reducing the heat release rate. Smoke generated is also dramatically reduced, as evidenced by a 63% reduction in total smoke released. This is an important result because reduced smoke production in the early stages of a fire will allow people to escape more easily (and without suffering from long-term health problems due to smoke inhalation).[383] The final residue of the 8BL-coated foam is increased to 22% indicating that the presence of the coating also improves the char forming ability of PUF. This additional reduction of the combustible volatile released is reflected in the THR values (see Table 13). This char was further confirmed by ATR spectroscopy (Figure 9), where the presence of a peak located at 1600 cm^{-1} can be ascribed to C=C stretching in conjugated aromatic carbonaceous structures.[384] The residue collected at the end of the test has been imaged by SEM microscopy (Figure 8 d)), revealing that the CH/VMT coating efficiently preserves the original PUF three-dimensional structure, similar to what was already observed in flame torch tests.

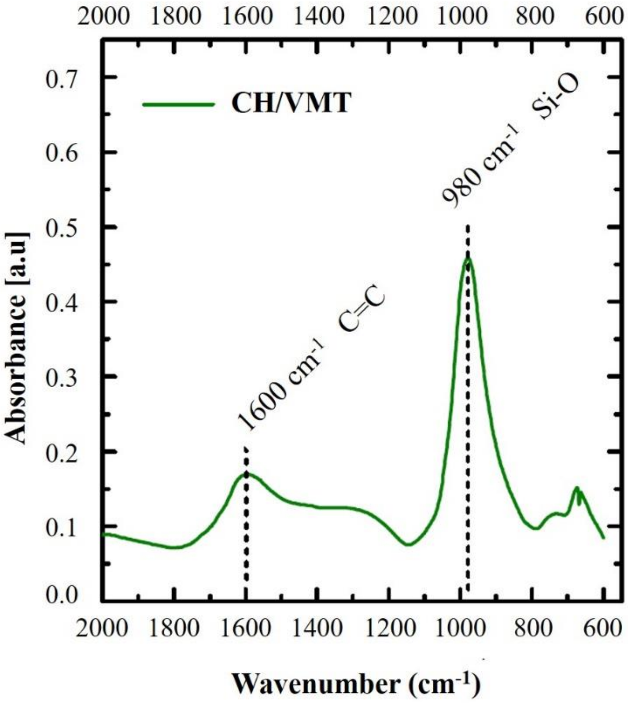

Figure 9. ATR FTIR spectrum of the CH/VMT foam residue collected after cone calorimetry.

3) Flammability behavior at high heat flux: burn-through fire test

Uncoated and coated foam were subjected to a burn- through fire test at high heat flux (116 kW/m^2) to assess the behavior of the samples in a fire scenario similar to those commonly used as an evaluation tool in industrial practice.[385] Thermocouples (T1−T4) were embedded in the foam at various distances to measure the temperature gradient across the sample (see Materials and Methods, Figure 96 d) and e)). Upon exposure, the uncoated polyurethane foam melts immediately and degrades completely under the flame in a matter of seconds. The 8BL

CH/VMT-coated PUF, however, withstands the high heat flux for more than 10 min. Figure 10 shows photographs taken at regular intervals during the burn-through fire test. No melt dripping is observed, but high amount of smoke is released during the first minute of the test. Moreover, as soon as the flame from the burner impinges the sample, it turns from blue to orange, suggesting the release of decomposition products from the foam stopped. This reaction occurs for the first minute of the test, before the smoking nearly stops and the flame turns blue again, suggesting the formation of soot created by the combustion of decomposing products of foam. The front side of the foam begins to glow red only after a few seconds of being exposed to the flame. This phenomenon is similar to that observed when a ceramic material is submitted to high temperatures, suggesting that the front side of the sample turned into a ceramic residue.

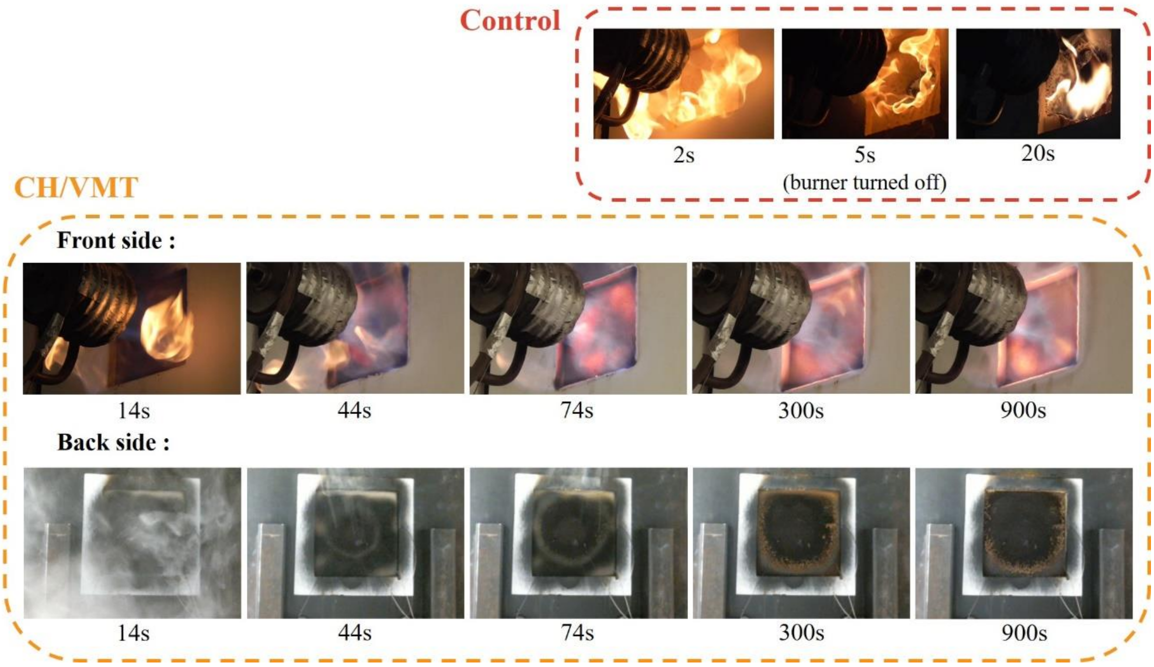

Figure 10. Digital images taken at several times during burn-through fire test for control and CH/VMT-coated foam.

The side exposed to the flame becomes brittle, light and powdery, with an ashy feel, and did not sustain even weak probing. In contrast, the backside of the sample turns into a black and rigid crust that grows during the test and is surrounded by yellowish particles, which is probably partially polymerized isocyanates and droplets of isocyanate.[386] Most importantly, it is possible to see that the open-cell structure of the foam is kept intact, and the foam does not collapse during the test. Weight measurements before and after testing show that the sample loses approximately 25 wt % of its mass in the case of the treated foam. The temperature registered by the thermocouples (Figure 11) shows that a steady-state regime is reached 3 min after exposure of the sample to the flame. The graph shows that the temperature difference between the thermocouples gradually increases from the front side of the foam to the back side (T1− T2 = 37 °C, T2−T3 = 87 °C, and T3−T4 = 121 °C). Moreover, a significant temperature variation of 245 °C between thermocouple 1 (T1 = 573 °C) and thermocouple 4 (T4 = 328 °C) is observed. This means that the CH/ VMT nanocoating exhibits thermal shielding behavior that may be of great interest for insulation.

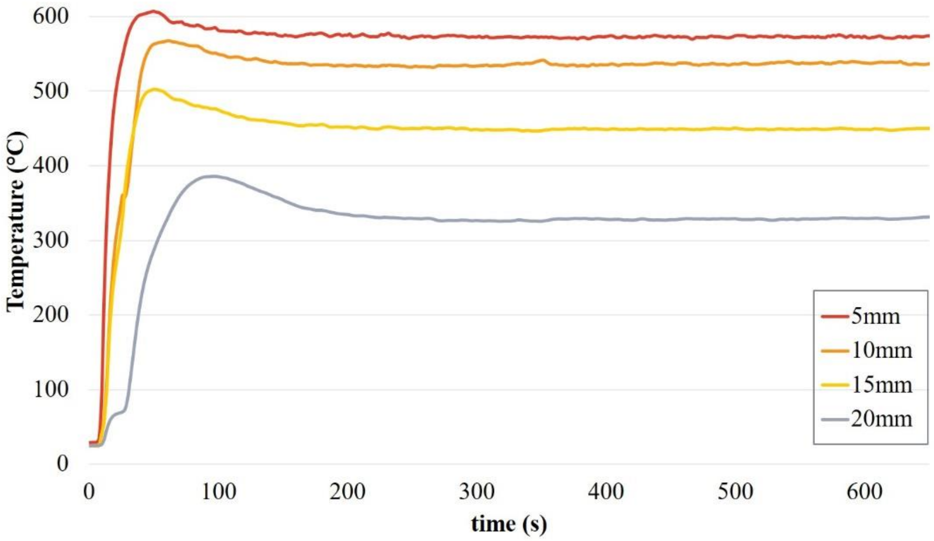

Figure 11. Temperature change within CH/VMT PUF during the burn-through fire test, as measured by thermocouples.

4) Investigation of the mode of action of CH/VMT coating at high heat flux: characterizations after burn-through fire test.

The morphology of the foam was analyzed after exposing the 8BL-coated foam sample to the burn-through fire test. Digital images of the front and backside of the coated foam provide a visual observation of the sample as a result of exposing it to the 900 s burn-through test (Figure 12 and Figure 13).

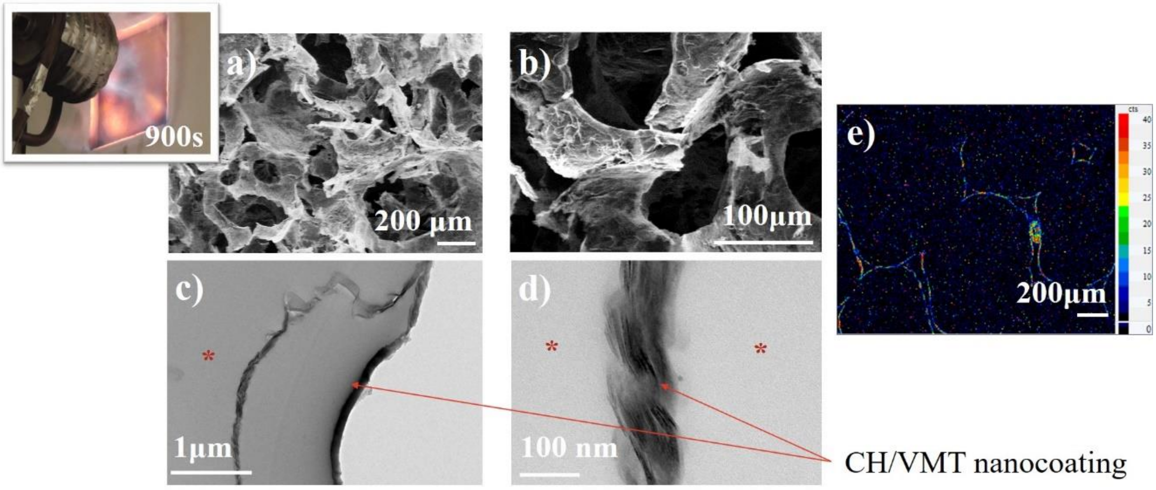

Figure 12. SEM images (a,b), TEM images (c,d) and EPMA Al X-Ray mapping (e) of the front side of CH/VMT PUF after burn-through fire test. The inset of a) shows a digital picture of the front side of CH/VMT foam after 900 s of test.

Cross-sectional X-ray mapping of aluminum in the coated foam residues (front side and backside) was obtained by EPMA (Figure 12 e) and Figure 13 e)). This confirms that the vermiculite within the coating is still present after burning, and that it maintains the open-cell structure. This is also confirmed by SEM micrographs of the front side of the residue (Figure 12 a) and b)), which was directly exposed to the flame. Similar to the charred surface of the PUF after torch testing, the polyurethane is completely consumed, leaving only a hollow porous skeleton behind. The open-cell structure of the foam is preserved, and vermiculite platelets are sticking out, as if they were ripped. This structure is very fragile and collapse easily, and the SEM images show extensive cracking of the exoskeleton. SEM of the sample closer to the backside (Figure 13 a) and b)) also shows the preserved foam structure, which is somewhat damaged (cracks and coarse surface) because of the fire test. However, it is clear that the extent of the damage is not as broad as what can be observed on the front-side, as the surface remains smooth in some places. There is also no extensive cracking, and the coarse surface looks like degraded polymer, which may be char. The insets in Figure 13 b) show some holes and round protuberances at the surface of the cell walls. This is likely the result of the release (or trapping) of combustion gases during the burn-through fire test, or the presence of char.

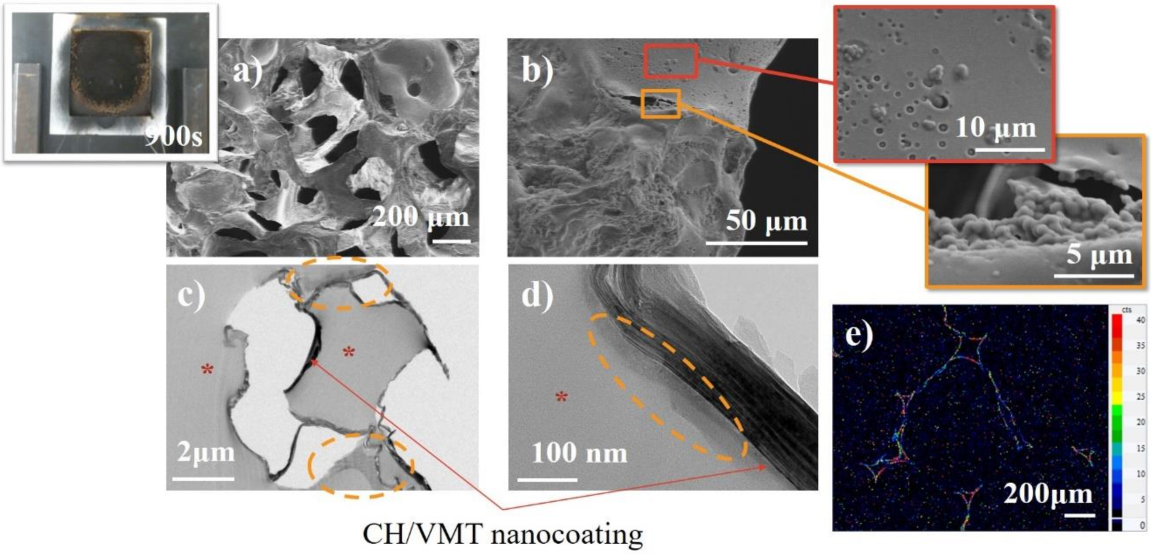

Figure 13. SEM images (a,b), TEM images (c,d) and EPMA Al X-Ray mapping (e) of the back side of CH/VMT PUF after burn-through fire test. The insets of b) are showing the apparition of small holes on the surface (red frame) and bubbly morphology (orange frame). The inset of a) shows a digital picture of the back side of CH/VMT foam after 900 s of test.

To examine any potential gas-phase action of the nanocoating, in situ gas-phase analysis was performed using a gas-picking system coupled with FTIR. It is observed that the gases emitted during the test are mainly carbon dioxide (CO_2), carbon monoxide (CO), nitric oxide (NO), water (H_2O), and propane (C_3H_8). No significant differences were observed between the neat PUF and 8BL-coated PUF (Figure 14). CO_2 and H_2O were emitted continuously throughout the test, along with CO and NO emissions. With regard to C_3H_8, quantities emitted seem higher for the coated PUF than for the neat PUF. These disparities can be explained by the different test durations, as the neat PUF test was stopped only seconds after it began to avoid damaging equipment from the significant flaming of the sample. When comparing the two samples on the same time scale, the level of C_3H_8 emitted by the 8BL-coated foam during the first few seconds of the test corresponds to the level emitted by the neat foam. This result suggests that the nanocoating does not have gas-phase action. Temperature measurements from the burn-through fire test as well as the evolution in the appearance of the residue through the thickness of the sample suggest a gradient in the composition of the residue depending on its distance from the flame.

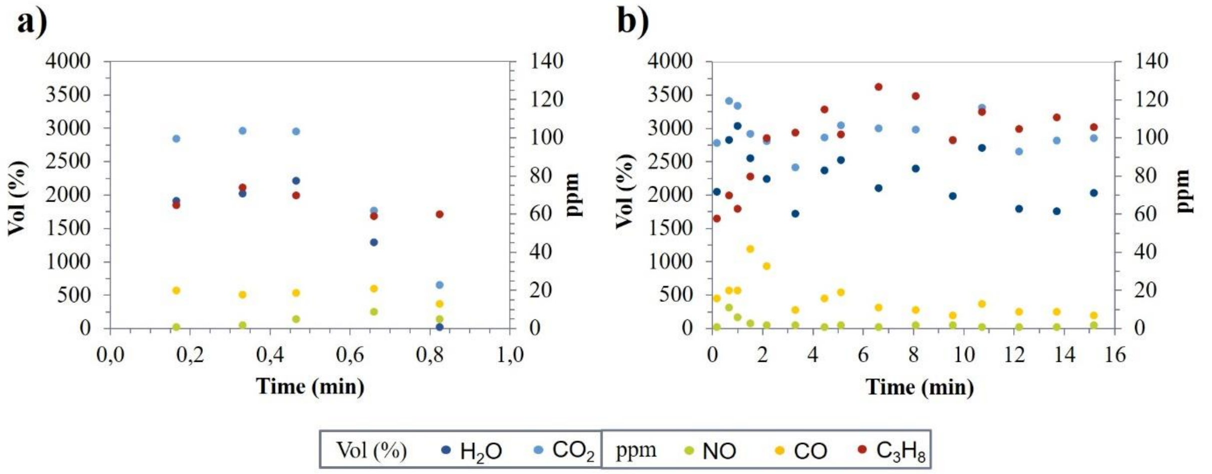

Figure 14. In situ FTIR analysis of the emitted gases from (a) uncoated PUF and (b) 8BL CH/VMT-coated PUF during the burn-through fire test.

Therefore, the char was divided into four parts, A−D, based on the position of the thermocouples in the burn- through fire test (Figure 15 a)). Thermogravimetric analysis was performed on these four portions of the residue to gain insight about its chemical composition and help elucidate the thermal protection mechanism. TGA of the four parts of the coated foam residue are compared to the uncoated and coated foam prior to the fire test (Figure 15 b)). Most residues exhibit degradation steps attributed to the degradation of residual organic matter. In other words, a charred residue was formed during the fire test, which further degrades during thermogravimetric analysis. Interestingly, this char proportion increases through the thickness of the sample, with position A (directly exposed to the flame) degrading only very slightly, meaning that no organic part remains at the end of the fire test, whereas position D (backside of the foam) loses more than 70 wt %.

Weight loss during the main degradation steps in TGA is attributed to the decomposition of the organic matter, suggesting an evolution in the organic/inorganic proportions of the residue as analysis is carried out further from the side of direct exposure to the flame. A more detailed analysis reveals that two degradation behaviors are observed in TGA. Initially, char A−C exhibit only one main degradation step between 500 and 600 °C, attributed to the degradation of a stable char formed by the exposure of polyurethane to high temperature during the fire test. The proportion of this char increases across the sample (4, 13, and 36% for char A, B, and C, respectively). FTIR analysis of the gases released were recorded during thermogravimetric testing to support the hypothesis of the degradation of residual organic matter. Figure 16 shows that the degradation consists mostly of carbon and nitrogen (emission of CO_2, CO, HCN, and

H_2O), whereas Table 14 provides the complete list of peak assignments. Finally, the mass loss not accounted for in the TGA graph (5, 3, and 2% for char A, B, and C, respectively) is attributed to dehydration of the mineral part (i.e., vermiculite).[387], [388]

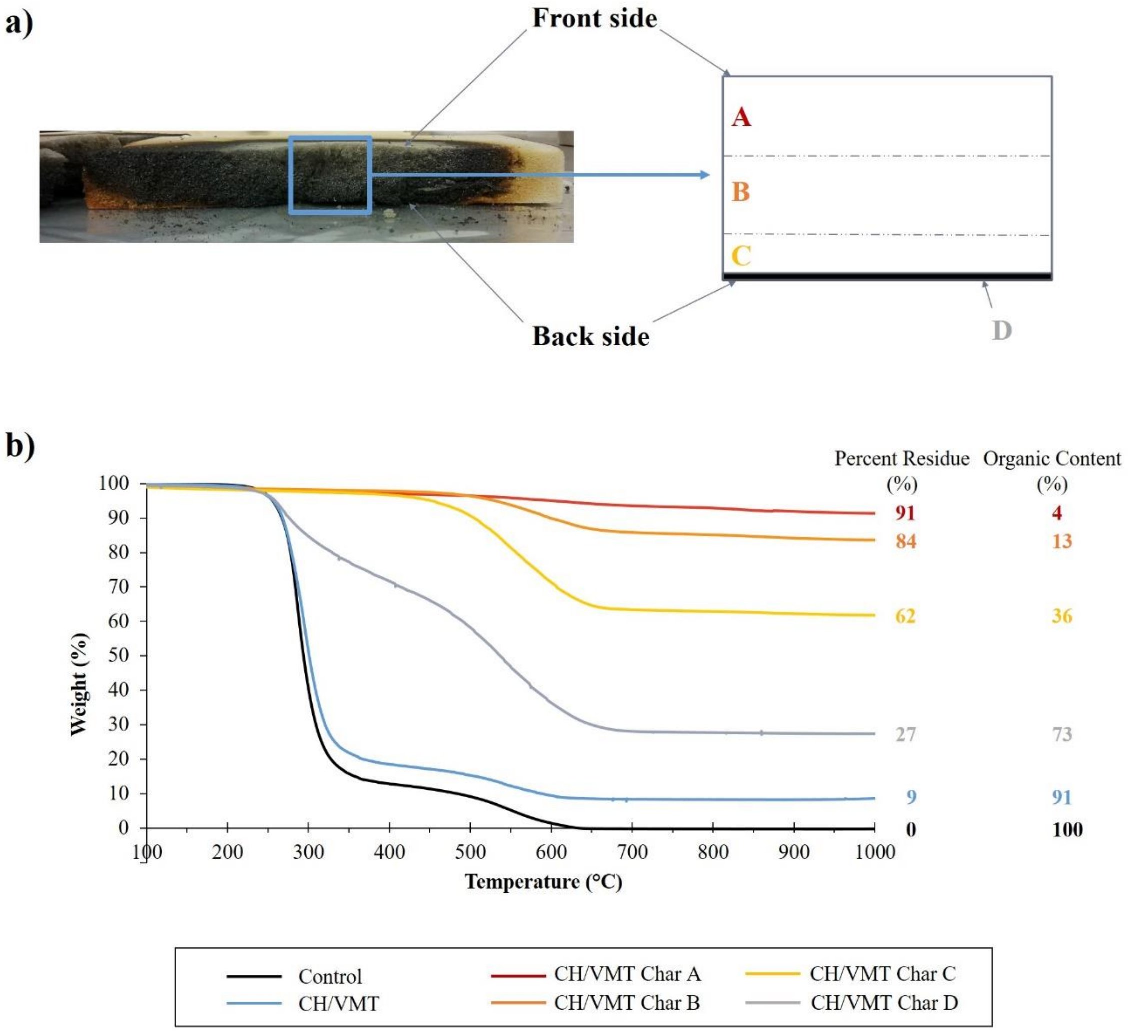

Figure 15. a) Cross-sectional image of the coated foam residue from the burn-through fire test, with schematic showing the position of the four parts (char A−D) collected for analysis. b) Thermogravimetric analysis of the residues from the burn-through fire test under air atmosphere, along with uncoated and 8BL CH/VMT-coated PUF prior to fire testing. Residual organic matter and residues are also indicated. The residual weight of char A−C is attributed to degradation of the organic part and dehydration, whereas the organic content was determined by the weight percentage degraded during the main degradation step. The residual weight and organic content of char D, coated, and uncoated PUF were determined by the weight percentage degraded during the two main decomposition steps of the TGA curve.

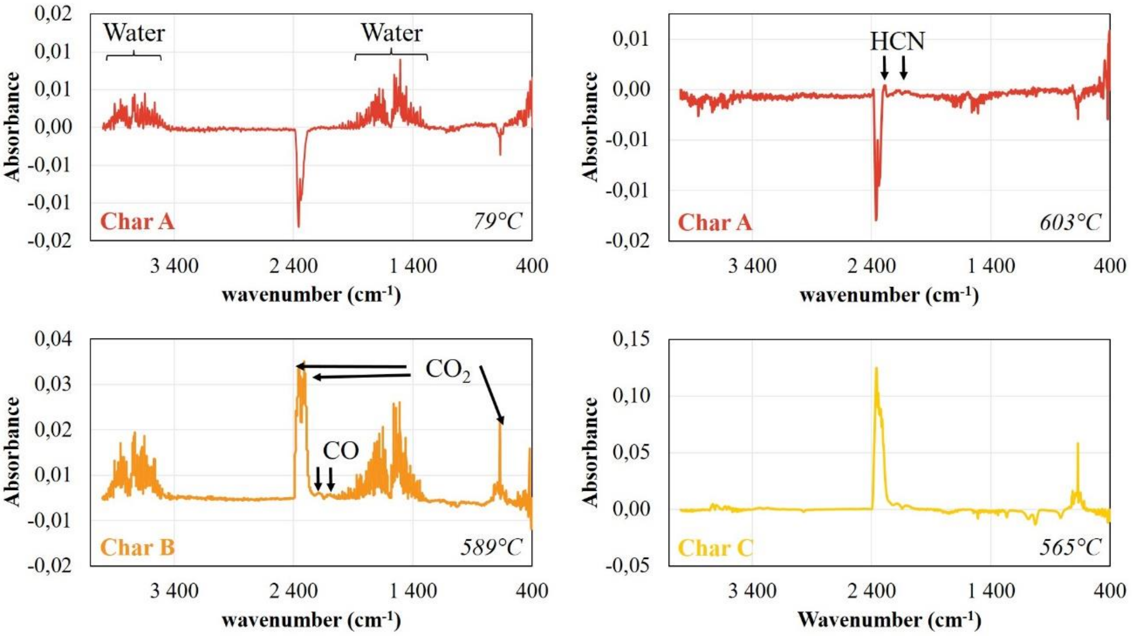

Figure 16. FTIR spectra of the emitted gases during TGA from the different positions (Char A-C) of the CH/VMT coated foam after burn-through fire test. Degradation temperatures recorded at half-height of inflection point from TGA curves.

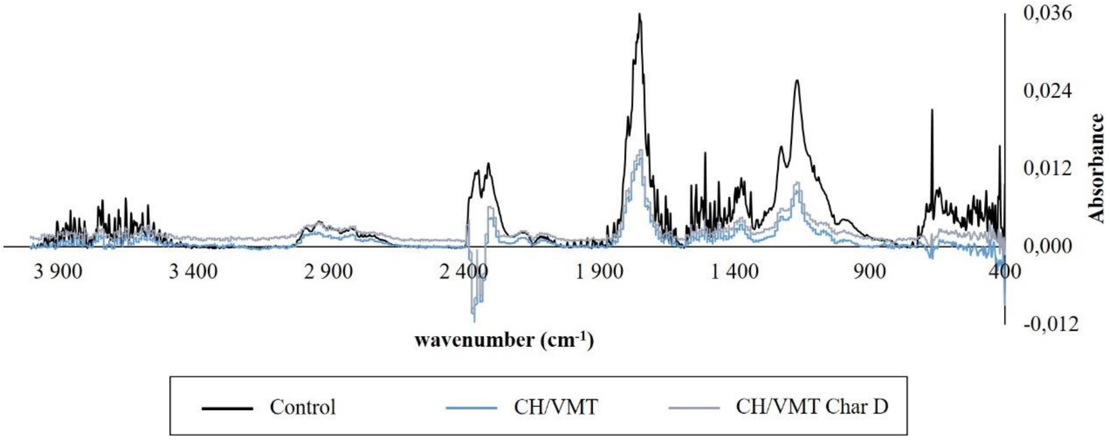

Figure 17. FTIR analysis of the emitted gases during thermogravimetric analysis. Comparison of unburnt coated and uncoated foam, and Char D of the residue from the burn-through fire test.

Char D, furthest from the flame, exhibits a different behavior, where two degradation steps are observed. The first one occurs between 200 and 300 °C, whereas the second one is between 450 and 500 °C. Both correspond to the degradation steps observed during the thermal degradation of unburnt polyurethane foam. FTIR analyses of the gases show that they are identical to the gases produced by thermal degradation of the unburnt coated foam (HCN, alkanes, ester and ether compounds, CO_2 and CO) (Figure 17). It seems reasonable to assume that neat polyurethane was preserved during the fire test despite the high heat flux.

Table 14. Peak assignments for FTIR spectra of the gases emitted during TGA/FTIR on the residues from the burn-through fire test.

	Wavenumber (cm^{-1})	Assignement
CH/VMT Char A	1256-2000, 3400-4000	Water
	669, 2358, 2339	CO_2
	2297, 2391	HCN
CH/VMT Char B	2308, 2348, 2380	HCN
	669,2320, 2330, 2358	CO_2
	2103, 2182	CO
	1256-2000, 3400-4000	Water
CH/VMT Char C	2308, 2348, 2380	HCN
	669, 2320, 2330, 2358	CO_2
	2103, 2182	CO
CH/VMT Char D	2305, 2348, 2382	HCN
	669, 2320, 2330, 2358	CO_2
	2250	Isocyanate
	2103, 2182	CO
	1700-1800	C=O
	1100-1280	C-O-C
	2700-3000	Aliphatic chains

The four portions of the residual foam were also analyzed by ^{13}C solid-state MAS NMR, as shown in Figure 18. Spectra for the uncoated and coated foam show peaks at 130 and 136 ppm, corresponding to aromatic carbons. The peak at 156 ppm is linked to the C=O bond from urethane and the peaks at 40 and 30 ppm correspond to aliphatic carbons from the diisocyanate monomer. The peaks at 75, 73, 71, and 69 ppm are linked to C−O bonds from the diol monomer, whereas the peak at 18 ppm is from the, $(CH_2)_n$, aliphatic region.[389] Regarding the residues (char A−C), no signal was recorded in ^{13}C solid-state MAS NMR with ^1H cross-polarization (CP). This finding suggests a lack of protons, due to the significant degradation. As a result, single-pulse experiments (direct observation) were carried out to observe their structure. A peak at 132 ppm is observed in the spectra of char B and C, suggesting that carbon is still present in aromatic form. It should be noted that the peak is asymmetric, which indicates oxidation of the aromatic carbon.[390] Regarding the spectrum of char A, no signal was detected. This result confirms that the part of the sample directly exposed to the flame is almost completely inorganic, due to the total degradation of the polymer.

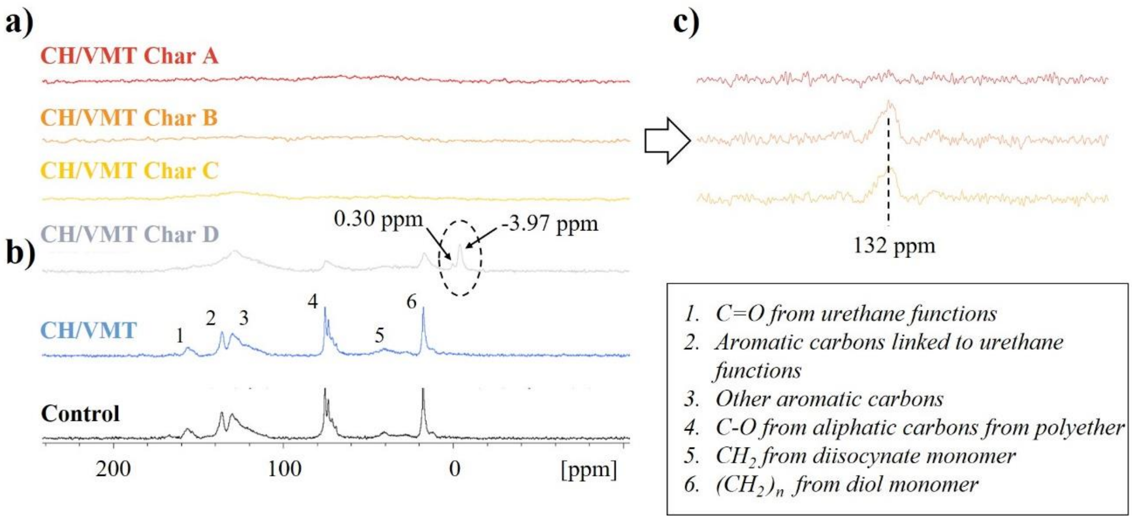

Figure 18. a) ^{13}C solid-state MAS NMR with ^{1}H cross-polarization of the residues (A−C) from the burn-through test. b) ^{13}C solid-state NMR with ^{1}H cross-polarization on char D from the burn-through test and on the unburnt coated and uncoated foam, with peak attributions. c) ^{13}C solid-state NMR (direct observation) on the residues (A−C) from the burn-through fire test.

On the contrary, the NMR spectrum of char D shows a broadening of the aromatic peak near 130 ppm, and a general loss of resolution, although the characteristic peaks of polyurethane remain. This implies that a good part of the organic moiety was preserved, though a little degraded. Two peaks appear at −0.30 and −3.97 ppm, which may correspond to the formation of a methyl−silica bond, resulting from a reaction between vermiculite and the organic part of the sample during burning.[391]–[393] This reaction is confirmed with single pulse ^{29}Si NMR analysis. CH/VMT Char D present a broad peak around -65.5 ppm which is characteristic of CH$_3$-Si bond, with Si linked to three oxygen atoms.[394]

Comparatively, char A-C and neat CH/VMT foam do not show this peak. ^{1}H cross-polarization ^{29}Si NMR analysis on char D confirms the presence of the peak at -65.5 ppm and reveals an additional peak around -19.2 ppm, less intense, which is also characteristic of CH$_3$-

Si bond, with Si linked to two oxygen atoms (Figure 19).[2][394] It is noteworthy the intensity of the band at -65.5ppm is higher with CP indicating the presence of ^{1}H in the close surrounding of ^{29}Si[3]. It is so consistent with the assignment to CH_3-Si. The formation of such adducts could be possible with the presence of methyl radicals within the organic portion of the material, which are reasonably found in chars formed upon thermal decomposition of polymers at the temperature recorded by the thermocouples.

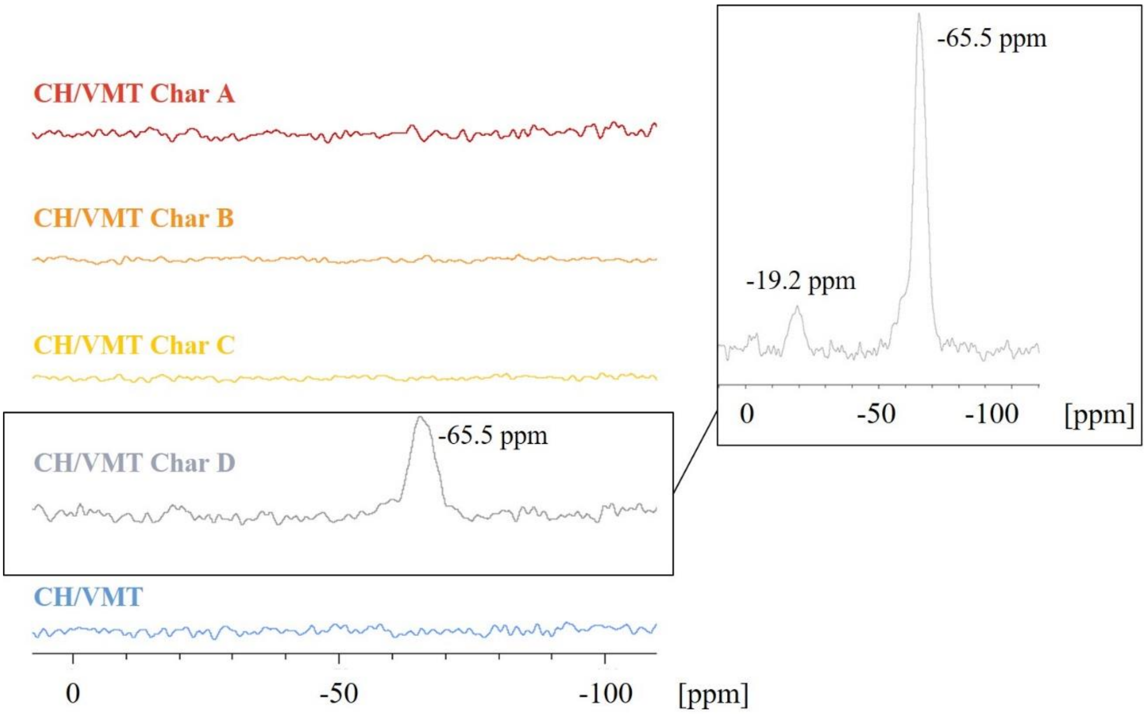

Figure 19. Single Pulse ^{29}Si MAS NMR solid-state NMR of the different part of the residue (char A-D) and of CH/VMT-coated foam. The insert shows the ^{29}Si solid-state MAS NMR spectra of CH/VMT char D with ^{1}H cross-polarization, showing the formation of organo-clay bonds.

---

[2] The presence of SiO_4 groups in vermiculite is usually shown on ^{29}Si NMR spectra with peaks between -70 and -114 ppm. Because of the presence of iron in relatively large quantity, those peaks can't be seen with the parameters used here for ^{29}Si analysis. They can be observed with another sequence and adequate parameters. For ^{29}Si spectra of vermiculite, the reader is referred to ref [449]

[3] It should be stressed out, however, that this is a qualitative observation, as the method used here cannot be used for quantification.

Indeed, it was proposed that methyl and benzene radicals in contact with clay surface form Si-C bonds, producing 5-fold coordinated silicon atoms. The bonding of the carbon-based radicals with Si is energetically favored over the bonding with the O atom in the siloxane network, because of the hypervalency of Si. This reaction can happen upon thermal heating and produce methyl-grafted organic-clay interface.[395]

^{27}Al MAS solid-state NMR was also carried out on the residual coated foam to provide more information on the eventual transformation of vermiculite during the burn-through fire test. Spectra of CH/ VMT-coated PUF, char D, and char C show two peaks at 57.4 and at −0.5 ppm, corresponding to the respective presence of tetrahedral (AlO_4) and octahedral sites (AlO_6) found in vermiculite clay (Figure 20). Spectra of char A and char B show only one peak at 57.4 ppm. These two pieces of information suggest that vermiculite is preserved during the fire test, although its structure is altered because of the high temperatures in char A and char B.

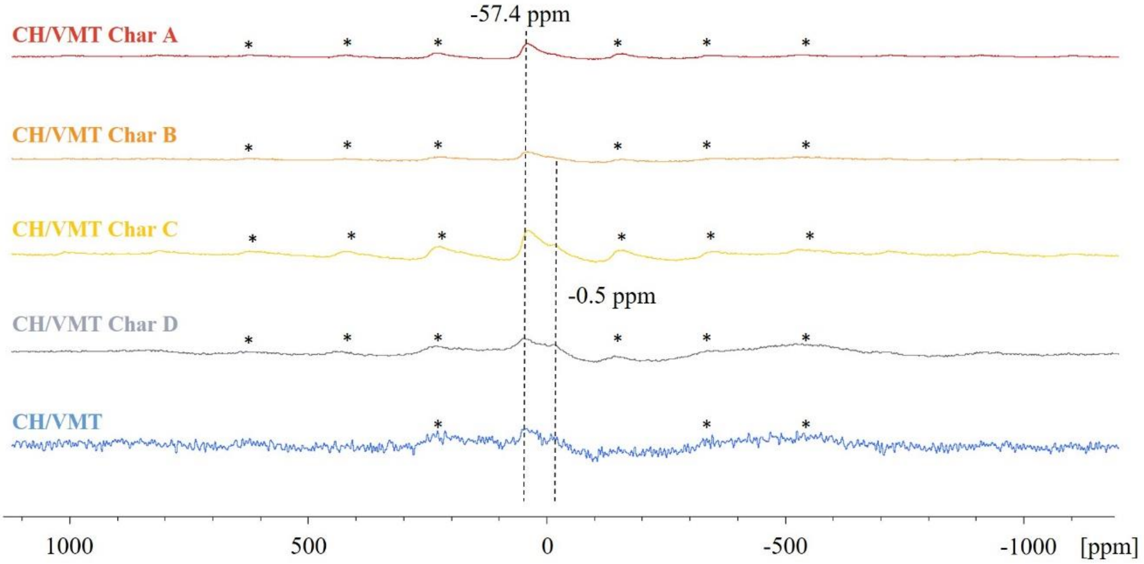

*Figure 20. ^{27}Al solid-state MAS NMR on CH/VMT coated PUF and on the residues from the burn-through fire test (Chars A-D). *Denotes spinning sidebands.*

Figure 12 a) and b) (front side) and Figure 13 a) and b) (back side) shows TEM micrographs used to compare the structure of the coating before and after the burn-though fire test. As previously shown in Figure 5, the nanocoating possesses a well-organized structure, with layers oriented parallel to the surface of the polyurethane foam. After the burn- through test, it can be seen that the highly organized nanostructure of the coating is preserved even after the application of a high heat flux. Clay nanoparticles are proposed to be the sole material staying intact during the test and remain organized on the walls of the foam, thus preserving their structure. Vermiculite sheets are clearly visible, even more than before the test, due to the degradation of the organic material. Moreover, closer to the backside, the coating retains the same morphology as observed prior to the burn-through fire test. Finally, the areas of the images circled in yellow, suggest that the charred residue concentrates in and around the coating, as observed by the analysis after cone calorimetry. The presence of vermiculite within a carbonaceous matrix prevents the sample from crumbling into ashes due to the fragility of the other parts of the residue.

5) Conclusion

An environmentally benign nanocoating, consisting of chitosan and vermiculite clay, was deposited on flexible polyurethane foam via layer-by-layer assembly. A nanobrick wall thin film was conformally deposited throughout the complex three-dimensional porous structure of the foam. This nanocoating was found to act only in the condensed phase by providing thermal shielding, in a variety of thermal constraints and heat flux. It provides an inorganic exoskeleton that maintains the structure of the foam, through nano-organization of the vermiculite platelets. At the surface of the foam, only inorganic matter is observed following fire testing, which serves to reduce the temperature deeper within the foam. The resulting temperature gradient promotes char formation and a stable residue. Chemical analyses reveal that the char is primarily aromatic. This mechanism takes place across the sample from the front side to the backside and demonstrates the protection of polyurethane, which is shown to degrade only partially at the backside of the sample after being exposed to an 1100 °C flame. This tremendous heat shielding behavior, from such a thin and conformal coating, is promising for improving the fire safety of polyurethane foam, especially in insulating application.

However, as it was mentioned beforehand, the technological lock in the industrial application of layer-by-layer coating for the fire safety of PUF is the high number of processing steps. While research has been developed to accelerate the process to industrially accepting times, or to design machines towards its automation, one of the most promising approach consists in reducing the number of processing steps drastically. Some papers have shown that a single bilayer could be enough to act as a very effective fire retardant coating for polyurethane foams, by using high performance nanosheets. In the case of vermiculite, it is indeed possible to reduce the number of layers. Indeed, it was found that vermiculite, when used with PEI or with another clay, could reduce the flammability of PUF with a single bilayer.[128], [254] The advantage of VMT is that it is relatively cheap and environmentally benign. It has some disadvantages though, the first one being that it stiffens the foam considerably, and that the resulting coating is brittle. Therefore, it is necessary to investigate in other high performance 2D materials that could have similar performance. h-BN nanosheets, as environmental-friendly nanoparticles with previously shown fire retardant properties, have attracted a lot of interest in this direction. In the next part, single bilayer PEI/h-BN layer-by-layer coatings were deposited on PUF and compared with PEI/VMT single bilayer nanocoating. The fire performance was evaluated using a torch test and mass loss cone calorimetry, and the mechanism of action of PEI/h-BN was investigated.

II. Hexagonal Boron Nitride Platelet-Based Nanocoating for Fire Protection

(ACS Appl. Nano Mater. 2019, 2, 9, 5450-5459)

Hexagonal boron nitride nanosheets are prospective high performance 2D nanoparticles. Their potential as fire retardant have been recently discovered and as such, aqueous dispersion of h-BN in water were prepared in order to use them in layer-by-layer fire retardant nanocoating. In this section, a single bilayer of h-BN and PEI was applied on flexible PUF to evaluate its behavior against different fire scenario. Its performance was compared to a well-known PEI/VMT nanocoating. Structural properties of the resulting materials such as tensile strength and weathering resistance were also tested. The mechanism of action of the h-BN/PEI nanocoating was investigated to gain understanding on its good fire performance.

1) Exfoliation and Assembly of h-BN Nanosheets.

Hexagonal boron nitride is composed of nanosheets held together in a graphitic structure via weak van der Waals interactions. The boron and nitrogen atoms present in these nanosheets are covalently linked together and arranged in a honeycomb-like structure (similar to graphene), resulting in stacked nanosheets that form a hexagonal crystalline structure.[396], [397] Exfoliation can be easily achieved through sonication in solvents that match its surface energy, such as isopropyl alcohol and DMF,[398] but the hydrophobicity of h-BN makes exfoliation in water difficult, resulting in low concentration and fast reaggregation.

To overcome this problem, Lin et al. demonstrated that these nanosheets can be successfully dispersed in water by using sonication-assisted hydrolysis, which reduces the size of the nanosheets and introduces hydroxyl groups on the edges after prolonged sonication (see Materials and methods I.2)).[399] Figure 21 compares the FTIR spectra of h-BN, before and after 8 h of exfoliation. The absorptions at 1327 and 760 cm^{-1} correspond to the B−N stretching and B−N−B bending for pristine h-BN, respectively.[400] After exfoliation, a broad absorption around 3330 cm^{-1} is observed due to the hydroxyl edge functionalization, while the two absorptions characteristic of h-BN broaden and shift toward a lower frequency due to hydrogen-bonding interactions.

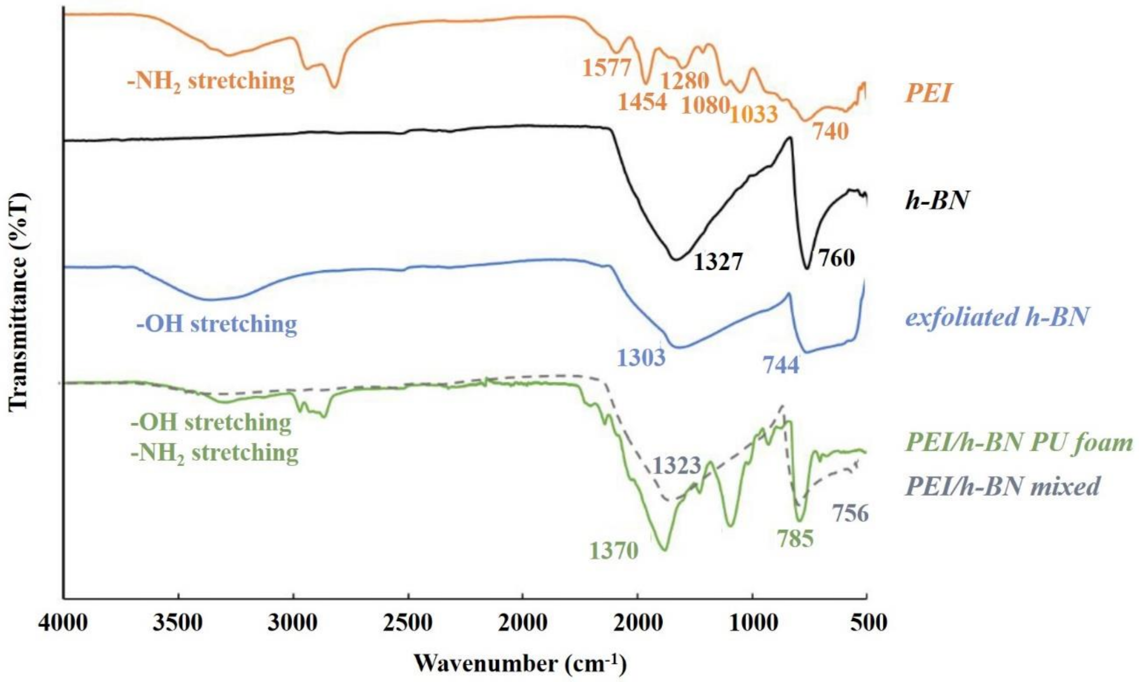

Figure 21. FTIR spectra of PEI, h-BN powder, exfoliated h-BN, and PEI/h-BN-coated PUF.

This aqueous dispersion of exfoliated nanosheets was used for deposition on polyurethane foam, which was first coated with a thin layer of PAA through hydrogen bonding. A layer of h-BN nanosheets was then deposited by means of an intermediate PEI layer, also held together by hydrogen bonds between PAA and exfoliated h-BN, as well as Lewis adducts formed between the lone pair boron acceptors and electron-rich amine functionalities of PEI.[401]–[403] The same process was used to deposit a single bilayer of PEI/VMT for comparison. From an aesthetic point of view, the PEI/h-BN system did not change the color of the white polyurethane foam (Figure 22 a)), whereas a homogeneous beige coloration was observed after the deposition of the PEI/VMT bilayer.

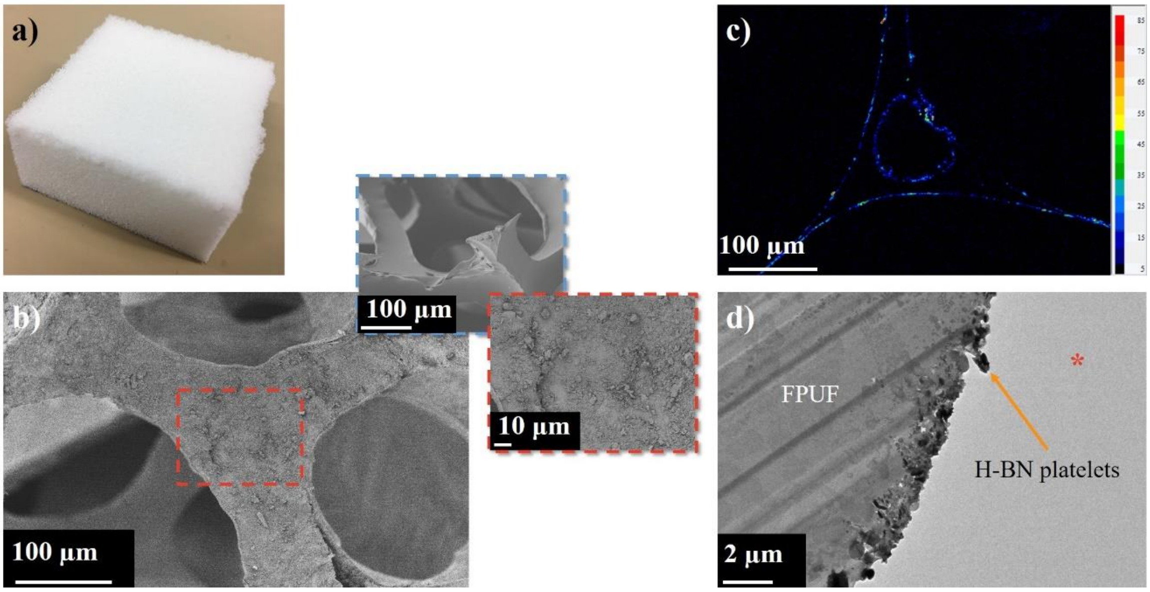

Figure 22. a) Digital image of PEI/h-BN PUF. b) SEM image of PEI/h-BN PUF; the blue-framed inset is neat PUF, while the red-framed inset is a close-up of b) showing the coarse surface of the coated foam. c) EPMA B X-ray mapping and d) TEM image of PEI/h-BN PUF.

Both systems resulted in very little weight gain, but the PEI/h- BN bilayer is thicker than PEI/VMT (11.1 ± 0.2 vs 2.3 ± 0.2 wt % added, respectively). Electron probe microscopy, with boron X-ray mapping, demonstrates the homogeneous and conformal deposition of PEI/h-BN (Figure 22 c)). Boron distribution is quantified on a color scale ranging from dark blue (low concentration of boron atoms) to bright red (high concentration of boron atoms). Signals corresponding to the presence of boron are found to be homogeneously distributed in the dark blue range of the scale, tracing an outline of the foam's cellular structure. Significant quantities of boron atoms were detected and are localized on the cell walls of the three-dimensional PUF structure. SEM images confirm this observation, as shown in Figure 22 b), which displays the typical open-cell morphology of the foam. The textured surface of the cell walls, in contrast with the smooth morphology of the uncoated foam, shows that the coating is deposited conformally throughout the cells, with no change in the porosity. A TEM cross-sectional image depicts the two- dimensional h-BN platelets as round shaped, appearing slightly darker than the polymeric material (Figure 22 d)). The platelets appear to be embedded in the PEI matrix that follows the PUF structure with no preferential spatial arrangement, contrary to systems constituted of clay nanoplatelets.

2) Thermal Stability.

The thermal stability of the PEI/h-BN system was investigated by using thermogravimetric analysis, under air and nitrogen atmospheres, as shown in Figure 23. Under nitrogen, the uncoated foam exhibits two clear degradation steps that are attributed to the decomposition of hard segments of polyurethane, followed by the decomposition of soft segments.[380] This can be seen around 270 and 370 °C (maximum degradation rate) for both the control and PEI/h-BN-coated foam, respectively. Under air, the uncoated foam also undergoes two degradation steps. Almost all the polyurethane is consumed during the first step (93% mass loss), occurring at ~260 °C, resulting in a stable residue that further degrades at around 550 °C. The presence of the nanocoating slightly delays oxidation, with the maximum degradation rate temperature being 282 °C, but the apparent degradation pathway is unchanged. Although h-BN has high intrinsic thermal conductivity, the coating is likely too thin to accelerate heat transfer and alter the degradation of the polyurethane. In both nitrogen and air, a residual mass around 8% is observed for the coated samples, while there is no residue left behind from the control foam at 800 °C. The presence of the nanocoating slightly delays the foam pyrolysis or its oxidation, but it does not change its decomposition behavior. It can be postulated that only h-BN platelets remain at the end of the TGA experiment, with all organic matter having been degraded.

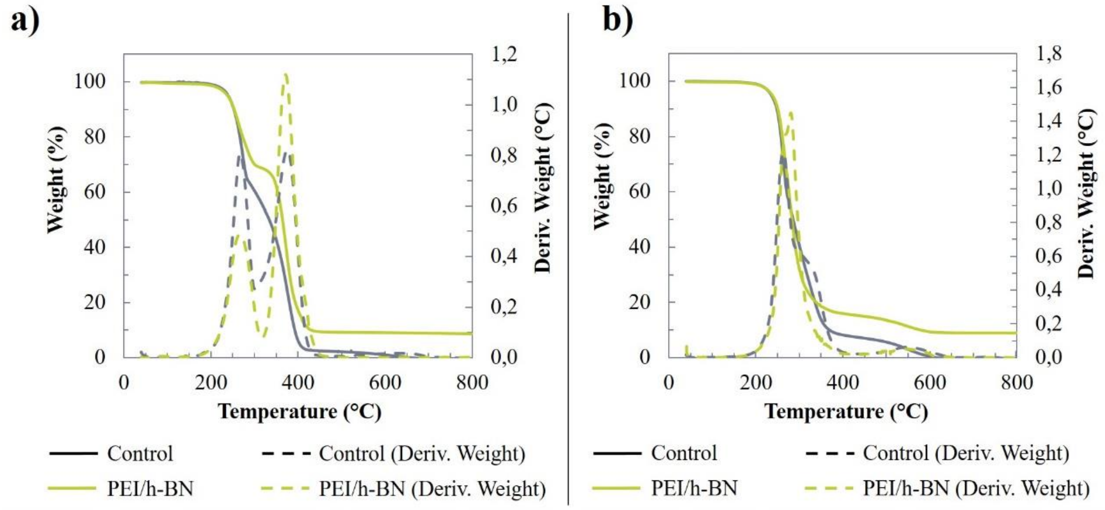

	$T_{95\%}$ [°C]	*1st step*		*2nd step*		Residue @800°C [%]
		T_{onset} [°C]	T_{max} [°C]	T_{onset} [°C]	T_{max} [°C]	
Control	238	246	271	347	374	0
PEI/h-BN	238	246	273	353	375	8,71

	$T_{95\%}$ [°C]	*1st step*		*2nd step*		Residue @800°C [%]
		T_{onset} [°C]	T_{max} [°C]	T_{onset} [°C]	T_{max} [°C]	
Control	237	248	260	518	560	0
PEI/h-BN	237	248	282	516	560	8,91

Figure 23. Thermogravimetric analysis of PEI/h-BN and neat PUF in a) nitrogen atmosphere and b) air atmosphere.

3) Fire Behavior.

The flame retardancy of foam was evaluated by exposing samples to a butane torch test for 10 s (the heat flux then is relatively low), which provides essentially the same information as the UL-94 test that is commonly used to test dense, nonporous bars or plaques. This test serves as a quick comparison of the PEI/h-BN system with the PEI/VMT coating. Upon exposure to the flame, the uncoated control foam completely degrades, and melt dripping is observed. The addition of a PEI/h-BN bilayer is enough to completely suppress this phenomenon, similar to what is observed with PEI/VMT. Both coated foam samples retain their macroscopic open-cell structure with little shrinkage. The h-BN coating is comparable to the clay coating, with a slightly higher mass loss of 48.9 ± 1.1% (PEI/VMT is 42.1 ± 1.1%). An image of the cross section of the residue of the PEI/h-BN treated foam shows that only the outer layer of the sample was charred (Figure 24 a)), as indicated by its black color. The color then turns from dark brown to a faded yellow and then white for the inner core. This implies a degradation gradient within the sample.

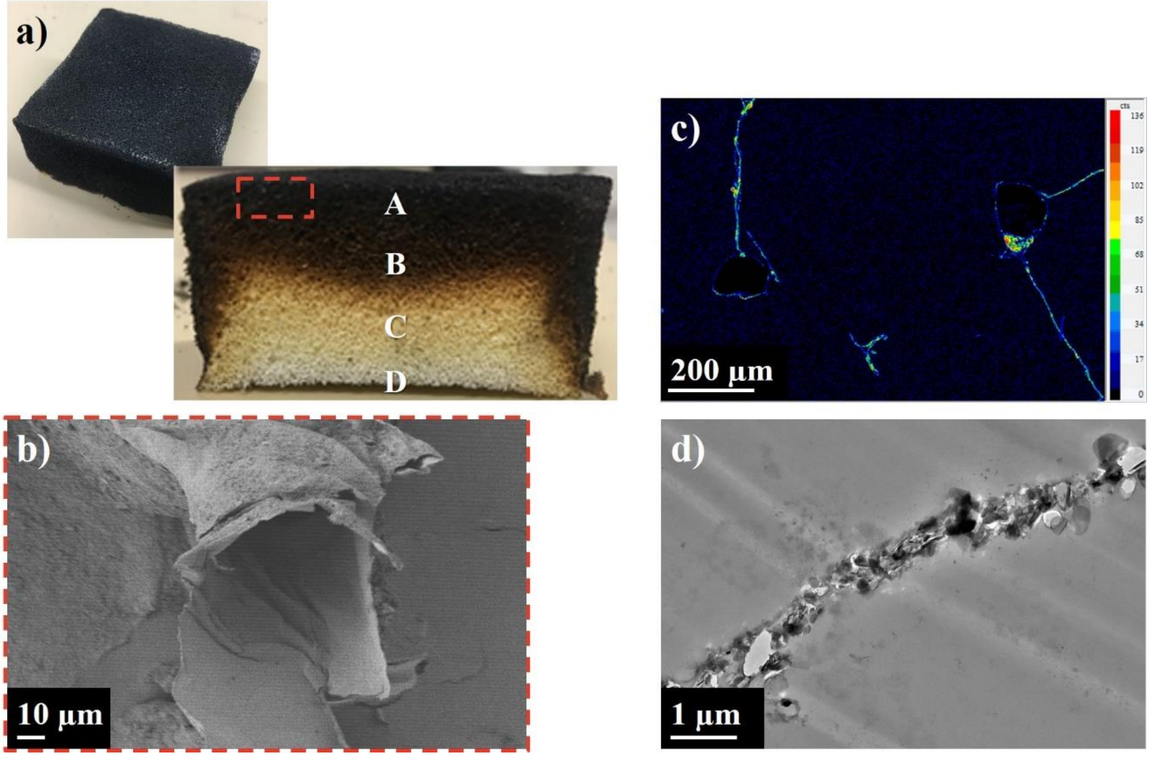

Figure 24. a) Digital image b) SEM image c) EPMA B X-ray mapping and d) TEM image of PEI/h-BN PUF. of PEI/h-BN PUF after 10s torch test.

To quantify this observation, the residue was divided into four parts (A−D), with each part analyzed by thermogravimetric analysis to measure the residual organic content (Table 15).

Because h-BN nanoplatelets do not degrade during the test, the mass loss observed can be attributed to residual organic matter. The TGA of parts C and D in Figure 25 almost perfectly fit the curve of the unburnt PEI/h-BN treated foam, suggesting that the polyurethane foam was protected by the upper layers and did not degrade during the torch test. The only indication of some damage to the polymer is the faded yellow coloration of part C, which implies that it begins to slightly oxidize because of the heat. Parts A and B in Figure 25 exhibit different degradation behavior upon torch exposure. Part B degrades in two steps: the first one being at the same temperature as the unburnt polyurethane and the second one corresponding to the decomposition of the stable char. This suggests that some of the neat polymer did not degrade during the torch test. Polyurethane in part A was completely degraded and turned into a stable char during the torch test, which is shown by the absence of degradation around 300 °C and by the decomposition step around 500 °C in Figure 25. The increasing residue at 800 °C shows the evolution of the mineral/organic ratio of the char. The organic content is minimal in part A but increases to the level of the unburnt treated foam in parts C and D.

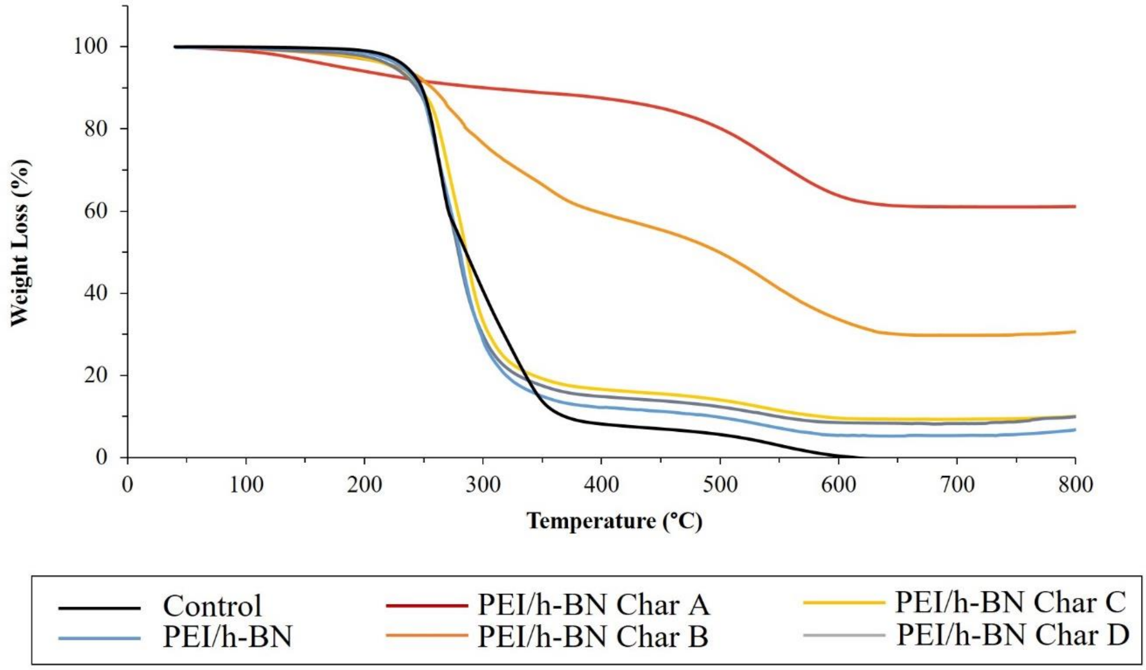

Figure 25. Thermogravimetric analysis of the residues from the 10s fire test under air atmosphere, along with uncoated and PEI/h-BN-coated PUF prior to fire testing.

Table 15. Organic content and residue at 800°C of the different parts of the residue of PEI/h-BN PUF after 10s torch test, with PEI/h-BN PUF and neat PUF before fire test. The organic content in each sample was calculated by substracting the residue with the total, assuming that all organic content is degraded and that all mass loss is due to organic content degrading.

Sample	Residue	Organic Content
PEI/h-BN Char A	61.1 %	38.9 %
PEI/h-BN Char B	30.6 %	70.1 %
PEI/h-BN Char C	10.1 %	90.6 %
PEI/h-BN Char D	9.9 %	91.7 %
PEI/h-BN	6.8 %	94.6 %
Control	0 %	100 %

The morphology of the char was investigated by using electron microscopy. The PEI/h-BN-coated PUF retains its open-cell structure as can be seen in the boron X-ray mapping of the cross section of the char by using EPMA (Figure 24 c)). The boron within the nanoplatelets trace the boundaries of the structure of the foam even after torch testing. The SEM image in Figure 24 b) confirms this observation, since the residue is composed of an empty shell, in which the boundaries are defined by the coating and remain in place during the test. This means the undegraded coating remains on the cell walls during the torch test, while the polymer decomposes, leaving a hollow mineral shell that forms a skeleton with an open cell structure. Additionally, the nanocoating provides a support for the polymer to char on, preventing the sample from collapsing and crumbling, all while shielding the inner part of the sample. The stability of the platelets nanostructure during the torch test was investigated to determine whether they experienced any physical or chemical modifications. As can be seen in Figure 24 d), exposure to a torch flame did not change the organization of the nanocoating. Moreover, there is no difference between the nanostructure of the unburnt and burnt coating, which shows impressive thermal stability of the nanoparticles.

The stability of these nanoparticles is also confirmed by ^{11}B solid-state NMR analysis (Figure 26). Boron is an atom that has a 3/2 spin, meaning quadrupolar interactions within the sample during NMR analysis generate wide and asymmetric peaks. Raising the magnetic field to 800 MHz cancels weak quadrupolar interactions (of tetracoordinated atomic structures), but in the case of trigonally coordinated boron, the quadrupolar constant is too high to cancel and the resonance band exhibits the “wavy” line shape shown in the spectra. The simulation of the spectra of pristine h-BN platelets shows a single peak around 30 ppm, which is characteristic of trigonally coordinated boron and corresponds to BN_3 sites.[404]–[406] The spectra of the coated h-BN foam is very similar to that of the h-BN powder. Moreover, no difference can be seen with the burnt residue, which means the h-BN did not degrade during the test. The absence of other peaks in the simulated spectra suggests that the nanoparticles did not react nor interact with their surrounding matrix during the fire test.

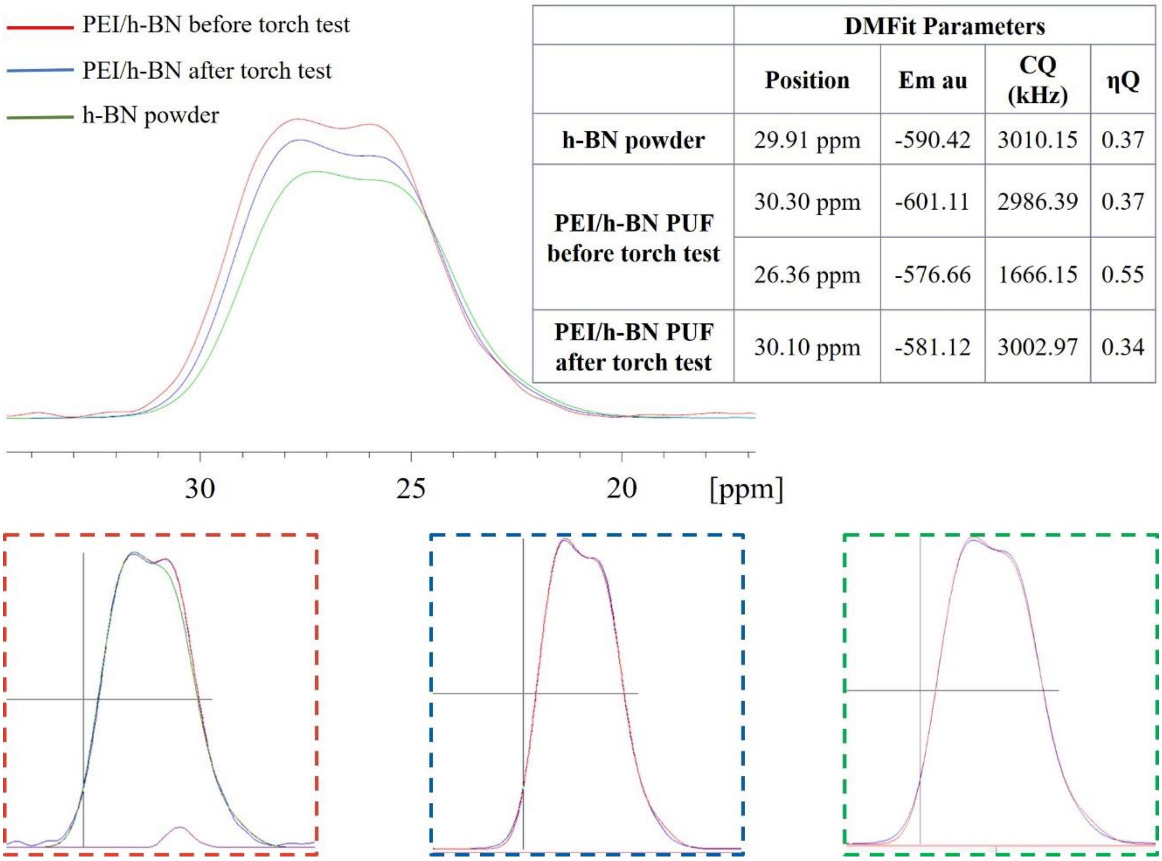

	DMFit Parameters			
	Position	Em au	CQ (kHz)	ηQ
h-BN powder	29.91 ppm	-590.42	3010.15	0.37
PEI/h-BN PUF before torch test	30.30 ppm	-601.11	2986.39	0.37
	26.36 ppm	-576.66	1666.15	0.55
PEI/h-BN PUF after torch test	30.10 ppm	-581.12	3002.97	0.34

Figure 26. ^{11}B solid-state NMR spectra of PEI/h-BN-coated PUF before and after torch testing compared with pristine h-BN platelets. The insets show the Simulation of ^{11}B solid state NMR spectra using DMFit. The blue line is the experimental spectrum and the red line is the simulated spectrum. The simulation parameters are presented in the inserted table. CQ is the quadrupolar constant, ηQ is the asymmetry factor.

4) Cone Calorimetry.

Uncoated, PEI/VMT-coated, and PEI/h-BN-coated PUF were evaluated by cone calorimetry. All three samples caught fire immediately when exposed to the 35 kW/m^2 heat flux. The entire uncoated sample was consumed quickly, whereas a foam-like residue remained for both coated samples. Both systems maintain ~20% of the initial mass, despite the differences in appearance (Figure 27 c)). After cone calorimetry, the PEI/VMT sample’s surface is gray, while the PEI/h-BN sample’s surface is black with disparate white spots. These coated foam samples greatly improve the stability of the PUF, reducing the pHRR by more than 50% (51% for PEI/ VMT and 54% for PEI/h-BN). These two values are within a 10% error range, meaning both systems have a very similar effect on the pHRR. It should be noted that the time to pHRR is shortened, from approximately 40 to 20 s, for both the coated systems (Figure 27 a)). Figure 27 b) shows that both samples have a reduced total heat release compared to the neat foam. The only difference between the two coatings is the slight reduction of THR brought about by the PEI/VMT system, which is not seen with the boron-containing coating (Table 16).

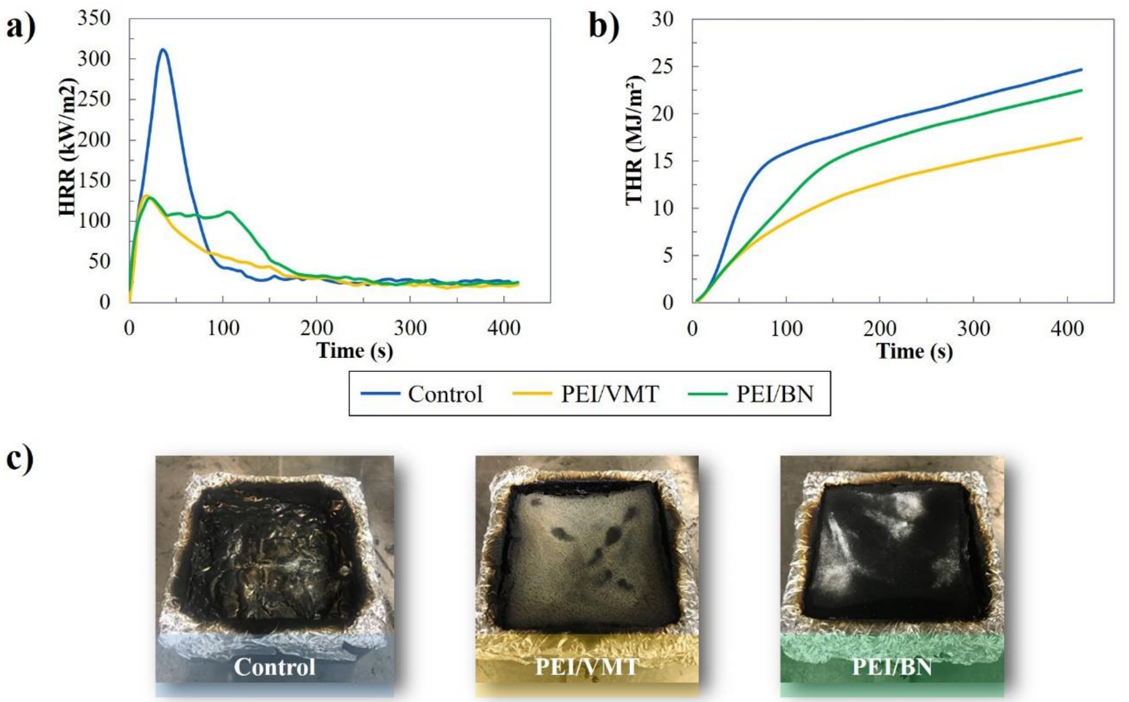

Figure 27. a) Heat release rate and b) total heat release as a function of testing time, as well as c) digital images of the foam residue after cone calorimetry for uncoated, PEI/h-BN-coated, and PEI/VMT-coated PUF.

Table 16. Cone calorimetry results for neat, PEI/VMT and PEI/h-BN PUF.

Sample	**Weight Gain ± σ [%]**	**TTI [s]**	**pHRR ± σ [kW/m²] (reduction, %)**	**THR ± σ [MJ/m²] (reduction, %)**	**Residue ± σ [%]**
Control	-	1	291 ± 32	23.3 ± 0.1	3 ± 0.9
PEI/VMT	2.3 ± 0.2	1	144 ± 14 (51)	20.5 ± 1.3 (12)	20 ± 0.7
PEI/h-BN	11.1 ± 0.2	1	132 ± 3 (54)	23.2 ± 1.4 (0)	21 ± 0.6

To gain a better understanding of the PEI/h-BN coating's mode of action, the gases released during cone testing were quantified by in situ FTIR analysis. Water (H_2O), carbon dioxide

(CO_2), nitric oxide (NO), and carbon monoxide (CO) are released during the combustion of the uncoated PUF (Figure 28). Traces of HCN and methane are also detected, however not in significant quantities. Regarding HCN, it means that the temperature is high enough that it oxidized to form NO.[407] The evolution of all four major gases follows almost exactly the HRR curve during the flaming stage, although the evolution of CO differs after flame-out. In regard to H_2O, CO_2, and NO, the treated foam samples both release the same gases as the uncoated control, but in much lower quantities. The peak of gas released during the combustion is reduced by more than 50% for both coated systems. It should be pointed out that this behavior occurs faster than what is observed for the control foam. The release of water, carbon dioxide, and nitric oxide during combustion follows the curve of heat release rate and is negligible after flame-out.

For these gases, the PEI/VMT-treated foam is a little more advantageous than the h-BN-coated one. Even so, the boron-containing foam releases far less CO than the PEI/ VMT system, suggesting that h-BN may provide a better thermal barrier (due to thicker coating) that suppresses the transfer of decomposed volatiles, more so than the VMT platelets.[408] Surprisingly, for both treated foams, a large peak can be observed just after flame-out. This phenomenon, which is not seen in the control foam, is very pronounced in the case of the PEI/VMT-coated foam, which can be attributed to an incandescence phenomenon. Indeed, a peak at 190 ppm at 200 s is observed, whereas for the PEI/h-BN-coated foam, the curve peaks at 140 ppm at 150 s. In this case, the h-BN coating has a clear advantage, since lower quantities of CO are released initially compared to the clay-containing system. In a radiative fire scenario, LbL-treated foam reduces the pHRR by more than 50%, while also reducing the THR and the quantities of water, carbon dioxide, and nitric oxide released. Both coatings have similar performance, but larger quantities of carbon monoxide evolve compared to the control because of incandescence. This undesirable release of gas is attenuated in the PEI/h-BN system. Additionally, the coating provides structural integrity to the material, preserving the open-cellular structure of the foam. The increased mass residue demonstrates the improved char-forming ability of the material due to its structural integrity, a phenomenon which is mentioned in section C.

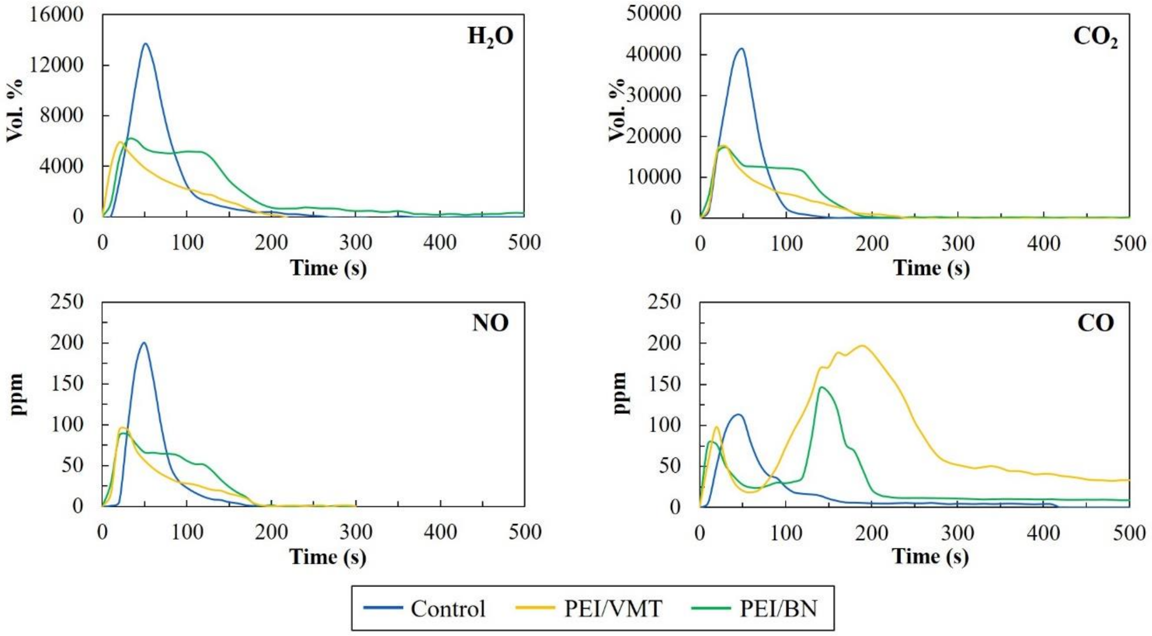

Figure 28. Quantitative in situ FTIR analyses of the gases released during cone calorimetry.

5) Mechanical Properties.

The foam stress−strain behavior was evaluated to determine the change in mechanical properties brought on by the deposited coatings when compared to the uncoated control (**Erreur ! Source du renvoi introuvable.**). Samples were run in triplicate, and their average elongations at break are reported in Table 17. The curves shown in **Erreur ! Source du renvoi introuvable.** are representative examples of each type of foam. The h-BN- treated foam is only modestly stiffer than the control, with the elongation at break decreasing by 22.5%.

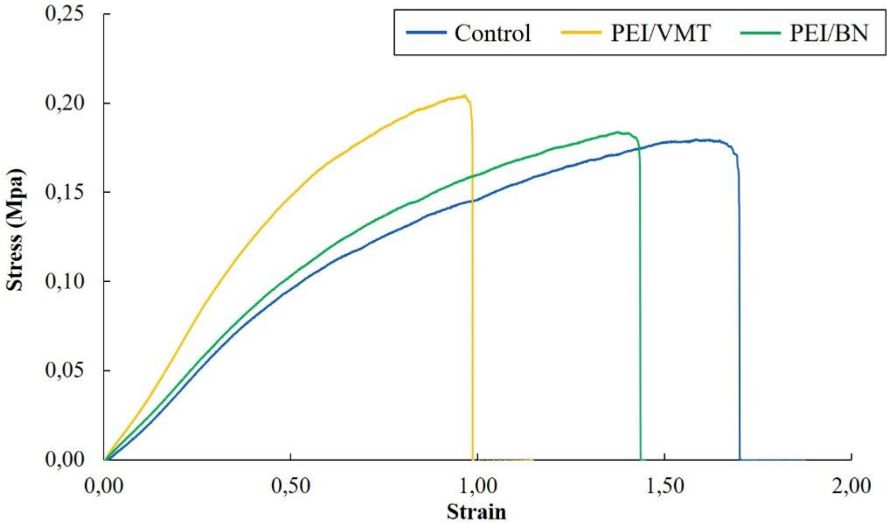

Figure 29. Stress as a function of strain for uncoated, PEI/VMT- coated, and PEI/h-BN-coated PUF.

This is desirable since protective coatings should have as little impact as possible on the functional properties of the material at hand. Flexible foam is typically used as cushioning in upholstered furniture. The VMT-based nanocoating has a much greater impact on the stiffness and elongation at break (−42.7%) of the foam. The stiffening of both treated foam samples can be attributed to the presence of the nanocoating. It is speculated that the stiffness enhancement of the PEI/VMT-coated foam is due to the highly organized platelets within the polymer−clay system. It has been shown that this organization maximizes the interaction between the polymer and the clay platelets, which constrains the polymer chains and enhances the load transfer between the two components of the coating.[409], [410] The counter effect of this improvement of tensile strength is that the nanocomposite is more stiff. As shown in Figure 22 d), the h-BN nanocoating lacks this high level of organization, which explains why the stiffening is less pronounced for the PEI/h- BN-coated foam.

Table 17. Mechanical properties of untreated and treated PUF samples.

Sample	**Elongation at break**			
	Trial 1	*Trial 2*	*Trial 3*	*Average ± σ*
Control	1.97	1.70	1.52	1.73 ± 0.23
PEI/VMT	1.01	0.99	0.98	0.99 ± 0.02
PEI/h-BN	1.21	1.43	1.39	1.34 ± 0.12

6) Aging.

Natural aging tests were conducted on neat, PEI/h-BN-coated, and PEI/VMT-coated PUF to evaluate weathering resistance. Flexible polyurethane foam is generally used for indoor purposes, so samples were placed on a ledge behind a closed window, while the curtains remained open, allowing adequate exposure to sunlight. After 7 days, the color of the foam changes from white to yellow, whereas the PEI/h- BN-coated foam remains white (Figure 30). As previously mentioned, the PEI/VMT coating imparts a beige color to the foam from the natural coloring of the clay. This color darkens when exposed to the environment, meaning that there is no significant improvement compared to the control. An artificial accelerated aging test under UV light was conducted on the control and PEI/h-BN foam to further evaluate UV resistance.

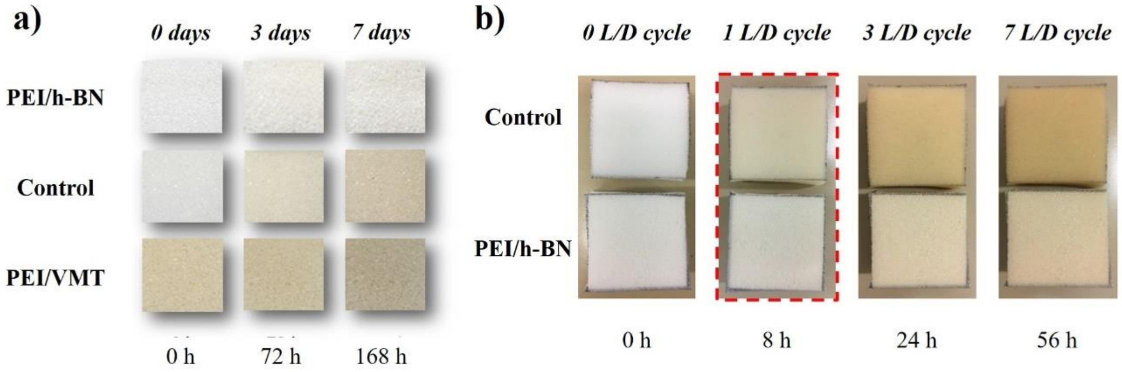

Figure 30. Aging results from (a) the natural environment and (b) UV light, in terms of discoloration. Notation: 4 h light (L); 4 h dark (D).

Figure 30 b) shows images of foam samples before and after testing. After only one cycle, the uncoated foam begins to turn a yellowish color, characteristic of degradation of the polymer chains, which create chromophore units.[411] The change in color intensifies as the number of testing cycles increases. The change in color is much less dramatic for the PEI/h-BN-coated foam. Yellowing of the foam is not visible until after three cycles, which means that the polymer is protected from degradation for a longer period of time. Additionally, the change in color is not as dramatic, remaining lighter compared to the control foam. This UV protective behavior may be attributed to the high surface-to-volume ratio (i.e., thicker coating/larger weight gain) of the deposited boron nanosheets compared to vermiculite clay, as the shielding would be greater.[412] It should be noted that PEI by itself yellows over time and is not contributing to the anti-yellowing behavior observed here.

7) Conclusion

In this work, h-BN platelets were successfully exfoliated to enable aqueous processing and utilization in layer-by-layer assembly on flexible polyurethane foam for fire protection purposes. The nanoparticles were conformally deposited on the cell walls of the foam with polyethylenimine in a single ~82 nm thick bilayer. Against a butane torch, the PEI/h-BN coating is found to act as an inflammable shield that protects the inner parts of the sample, resulting in a degradation gradient through the foam's thickness. In a cone calorimeter, the coating is found to reduce the pHRR by 54% and the THR by 20%, while also demonstrating the ability to reduce the amount of gas emitted. This behavior is believed to be due to char formation enhancement of the h-BN, thereby reducing the amount of gaseous products emitted. This is an advantage that is not observed when comparing gas emissions to a well-known PEI/VMT coating. Additionally, the PEI/h-BN coating protects the polyurethane foam from weathering and only modestly alters the foam's mechanical properties. When considering practical applications, the preservation of foam flexibility is very important. The ability to achieve this level of protection using a single bilayer deposited from water makes this a scalable system that could be used commercially.

III. Discussion and perspectives

The results from the two studies described in this chapter show that the protective action of passive layer-by-layer coating passes by the formation of a highly protective composite barrier. First, it prevents melt-dripping or pool fire by preventing the molten polymer to flow away and forcing it to combust inside the exoskeleton. Then, the structure and integrity of this barrier is very important. Indeed, it was found that at high heat flux the thin layer is primarily not enough to protect the polymer directly exposed to the heat source. Most of the polymer is decomposed on the surface, with little to no char left, as the structure of the coating is severely degraded and wide cracks appear. Still, the presence of the refractory particle creates a ceramic shell which maintains the 3D porous structure of the foam, showing how important it is that the particle remains stable at high temperature. This porous exoskeleton acts as a barrier, shielding the material underneath from the worst of the constraint. Conductive and convective heat transfer are limited, bringing the temperature at a level at which a charred structure would not completely degrade. As a result, some char is able to form, which will slow down mass transfer and insulate the rest of the material. As the proportion of the char increases, the protection becomes more efficient, to the point where some of the original material is preserved. As the heat flux decreases (for example during a hand-held torch test), more char is able to form on the first layers and the integrity of the coating is preserved. As a result, the protective effect is more efficient, and the core material will be preserved by the open cell carbonaceous thick layer. Therefore, the formation of a char from the surface of the material will allow a better protection.

The barrier created by the hybrid carbonaceous open-cell structured residue slows down the release of flammable compounds. It also shields the rest of the material against heat, which enhances char formation. These two mechanisms are responsible for the reduced pHRR during cone calorimetry. An efficient barrier will bring self-extinguishment behavior and suppress the second HRR peak observed during PUF pool fire (as observed with the vermiculite containing LbL coatings, or as extensively reported in the literature). This will lead to incomplete combustion, lower the THR a little, and increase CO emission levels. A porous barrier will only slow down volatile emission (no reduction in THR), but will keep CO emission levels low (as observed with the PEI/h-BN PUF). Based on the results of this study and on the literature, as long as the coating maintains its integrity (no cracks, no collapse of the structure, cohesive residue…), it is expected to bring sufficient protection against a radiative fire scenario.

To sum up, the ability to form a thermally stable, compact and coherent residue seems to be the key parameter for the application of passive barrier layer-by-layer coating. First, failing to have perfect coverage of the substrate by the filler will result in porous residues and the protection will be less efficient. The organic mortar might have the ability of forming a thermally stable char in itself, but the presence of phosphate might enhance its formation and stability. Then, the chemistry of the nanoparticle should not be overlooked, as they can catalyze char formation (caution must be taken as to not catalyze char decomposition). Therefore, research on polymer and nanoparticle interaction should be an important work to pursue. This has already been investigated in the case of clay polymer composite, and it was found that the acid sites on clay surface catalyzed char forming degradation pathways and stable radical formation.[413] But to our knowledge, this was not investigated in the particular case of layer-by-layer coating with higher loadings and probably confinement effects. It is likely that beneficial properties could be reached with a variety of other two-dimensional nanomaterials (e.g., MoS_2), which could be the topic of future studies. A more fundamental understanding of the bonding/adhesion between these nanomaterials and various polymers is another important topic to be addressed in future work.

Additionally, it was found here that the conservation of the porous structure of the PUF substrate was also a big advantage and a significant element in the thermal shielding mechanism. This might give a clue as to why it might be more difficult to protect low surface volume ratio substrates such as textile or polymer plate with passive composite nanocoating. The protection of such substrates requires either a high number of bilayer (30,40) or special formulations to increase the thickness with less number of layers (by the use of amine salts for example, as it was shown by Guin et al.[255]), at the condition that the coating's integrity is maintained during the test. Considering this, as well as the results obtained during this work, high temperature stability, low porosity, and mechanical integrity of the nanocomposite carbonaceous char should be the desired result of the nanocomposite design.

Finally, as it was highlighted in the second study, the fire retardancy of a polymer is usually a necessity and a requirement for the final material, but not necessarily its primary function. Therefore, it is sometimes required that the fire retardant treatment should have as little impact as possible on the polymer, or that it brings it a constant improvement. Regardless of its fire protection property, it was found that the h-BN-based nanocoating had little impact on the aesthetic and mechanical properties of the foam, but also brought UV protection. Therefore, the development of fire retardant treatments having multifunctional abilities (conductive, antimicrobial etc.) should be privileged.

Chapter 3 . One-pot high-filler content coatings for fire protection of textiles.

As it was pointed out in the previous chapters, passive composite layer-by-layer coatings act by forming a highly stable compact charred barrier, with a high proportion of refractory nanoparticles and good coverage. This type of coating acts as a physical barrier against mass transfer that forms before the degradation of the substrate. It maintains its shape and limits the combustion of the material.

In this chapter, our understanding of the protection mechanisms was applied to design new coating systems. In addition, the main inconvenience of layer-by-layer coatings, which is their long and tedious processing, was overcome. In the first part of this chapter, clay/polymer dispersions were made so that they could be casted in a one-pot process. The proportion of clay and polymer was adjusted so that it was similar to what is typically found in layer-by-layer coatings (that is approximately 70/30 wt%/wt% when dried). While in the previous chapter the technology of layer-by-layer was studied on porous substrates, as it was particularly adapted, here the concept was tested on flexible textile substrates. Indeed, they are more suitable for one-pot deposition techniques such as doctor-blading, painting, dip-coating etc. Another advantage of using fabrics to prove this concept is that layer-by-layer passive composite coatings are less efficient on these substrates, unless they are very thick, which is tedious to achieve with this technology (high number of layers, special treatment) but easy with one-pot processes. Indeed, even if the flammability of layer-by-layer treated textiles is improved in a radiative fire scenario, the coating does not prevent the substrate to burn underneath. As a result, they often fail in a small scale fire scenario such as UL94. Consequently, the efficiency of the developed system when compared to layer-by-layer will be easily determined.

Thanks to its high mechanical properties, its large operating temperature range, chemical resistance and aesthetics, PA66 is a common engineering polymer used in various technical applications, going from the car industry to household appliances and sports equipment. Textiles made from PA66 fibers are particularly common for clothing, flooring (carpets…) and industrial applications. However, it is highly flammable and its quick combustion is accompanied by melt-dripping which increases its hazard. It was therefore chosen as the substrate material for this study.

In a second part, the coatings were subjected to a crosslinking step in order to obtain hydrogel composite coatings. They were dried in ambient condition to obtain thermally stable and highly compact structures (high filler content composite xerogel), in order to try and improve the performance of passive barrier coating.

I. One-pot clay nanocomposite (NC) coatings

1) Alginate/VMT coating

3 wt% of alginate was added to a 7 wt% VMT dispersion in order to have a 30:70 ratio of alginate/vermiculite. With these quantities, the solution was viscous enough to produce a uniform coating on the PA66 textile. In order to improve the wettability of PA66 samples, they were first pre-treated with a primer of PAA and PEI. They were then immersed in the alginate/VMT dispersion and the excess was removed by a padding step. Afterwards, the alginate composite dispersion was casted on both sides of the fabric samples using a paint brush in order to control the added weight. With a 600 wt% wet pick-up, the dry add-on was 68 %, which corresponds to a density of 6 mg/cm^2. The coated fabrics were dried horizontally to prevent inhomogeneities. The fabric feels a bit rough to the touch and is less flexible, but the coating is even, conformal, and resists hand manipulation.

Figure 31 a) and b) show SEM observations of cross-sections of PA66 coated with Alginate/VMT (abbreviated by PA66 VMT_NC in the following). The coating is dense and uniform with VMT platelets that are roughly aligned (see inserts in Figure 31 b)), and does not permeate the fibers. Energy dispersive X-Ray mappings allow to distinguish between the different elements composing the coating. Indeed, Si, Al, Mg and K atoms are characteristics of VMT platelets, whereas C atoms are characteristics of alginate. As such, X-ray mappings of cross-sections presented in Figure 31 b$_1$) to b$_6$) show that the coating is mainly composed of VMT platelets. Indeed, Si, Al, Mg and K atoms are detected in large concentrations on the surface of the PA66 fibers. On the contrary, the C atoms of alginate are detected at low concentration in the coating.

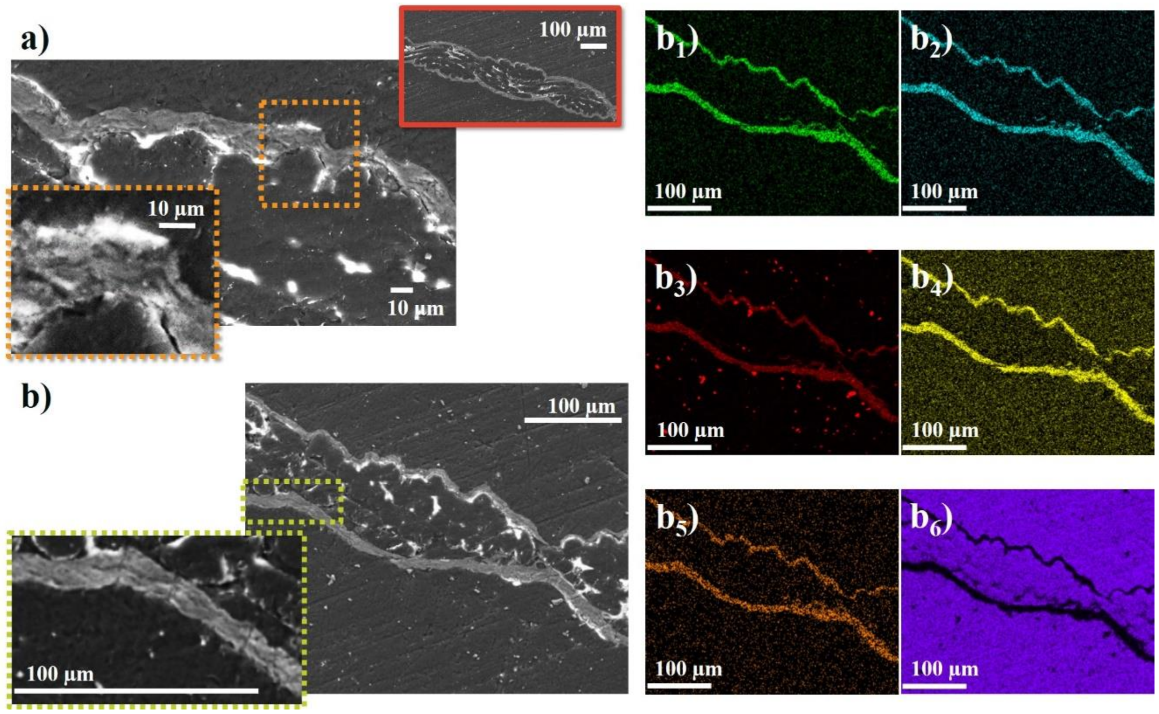

Figure 31. a) and b) shows SEM observations of a cross section of PA66 VMT_NC. Inserts in orange and green show close-ups that display the roughly aligned VMT platelets. b_1) to b_6) are energy dispersive X-ray mappings of b_1) Mg, b_2) Al, b_3) Si, b_4) O, b_5) K and b_6) C atoms.

The thermal stability of PA66 VMT_NC was evaluated by TGA. As illustrated in Figure 32, PA66 fibers present a single degradation step at 434 °C with no residue at 800°C (see Table 18). It is linked to the breakdown of the polymer chain, with the emission of NH_3, H_2O, CO, CO_2, cyclopentanone and hydrocarbons.[414] As alginate is a hydrophilic polymer, it absorbs ambient water. This is the cause of the weight loss observed before 200°C. The first main degradation step (243°C) corresponds to the degradation of alginate molecules, and more specifically, the destruction of the glycosidic bonds.[415] This produces a carbonaceous material that further decomposes at 760°C. The residue at 1000°C is of 14%, which highlights the charring capacity of alginate. The first degradation step is slightly delayed for Alg/VMT, but the decomposition pathway of alginate is not disturbed otherwise. As a result, there is a 72% final residue, composed of the remaining vermiculite and the charred alginate. This corresponds to the residue that is expected of alginate and VMT decomposing independently of each other. It can be concluded that there is no interaction between alginate and VMT. PA66 VMT_NC presents two main decomposition steps at 247 °C and 391 °C. The first one corresponds to the decomposition of the alginate contained in the coating, which occurs at the same point as the alginate/VMT blend but on a larger thermal range. The second main decomposition step is the highest in term of mass loss, and corresponds to the decomposition of PA66 fibers. It is noteworthy that this degradation occurs significantly earlier than that of uncoated PA66, which is likely due to an interaction between the decomposing coating and the substrate. The mass loss rate slows down at the end of this decomposition step, which is shown by the presence of a shoulder on the curve. All in all, it occurs on a larger thermal range than PA66 and therefore ends at the same point than the textile fibers. The residue corresponds to around 24% of the initial mass. It matches the residue of the alginate/VMT coating, composed of charred alginate and VMT, which means that all PA66 has decomposed during the test.

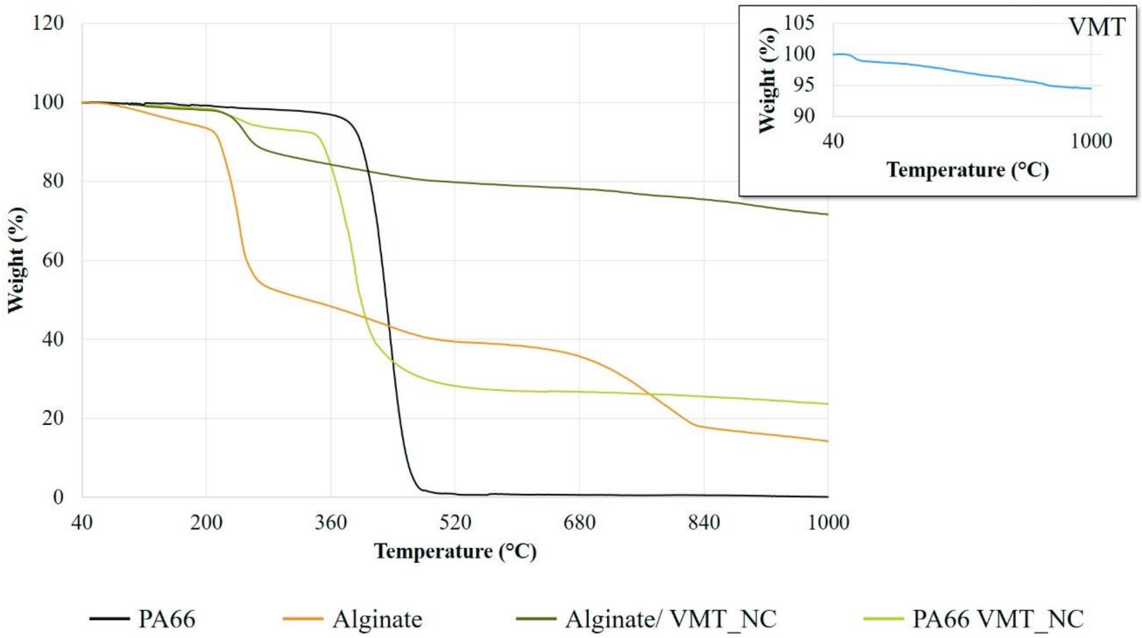

Figure 32. TGA of uncoated PA66 and PA66 coated with an alginate/VMT coating under N_2 atmosphere. The insert in the top right corner show the thermal decomposition of vermiculite clay.

Table 18. TGA results of alginate/VMT-coated and uncoated PA66.

	$T_{95\%}$ (°C)	Main step 1		Main Step 2		Residue@ 1000°C (%)
		T_{onset} (°C)	T_{max} (°C)	T_{onset} (°C)	T_{max} (°C)	
PA66	383	406	434	/	/	0
Alginate	169	223	243	688	768	14
Alginate/VMT_NC	239	231	248	725	*	72
PA66 VMT_NC	250	213	247	364	391	24

To conclude, the coating does not enhance the charring capacity of PA66 which decomposes completely. But the TGA shows an interaction with the substrate, as it also lowers the thermal stability of the fibers that degrade earlier than the uncoated sample. It is likely that the coating catalyzes the degradation of PA66. It may be due to several mechanisms. First, the presence of acid sites on the clay surface (Bronsted acid sites due to the presence of hydroxyl and silanol groups, and Lewis acid sites due for example to the presence of multivalent metal atoms such as Fe) triggers the early decomposition of polymers. Second, the presence of water favors hydrolysis reactions.[416]–[419] Another element on the TGA curves is that the coating starts to decompose ahead of PA66. It is expected that this will benefit PA66 flammability, because of the formation of the stable ceramic/char composite barrier before the beginning of its decomposition.

The flammability behavior of PA66 VMT_NC was investigated at UL94 test. Upon flame application, the ignition of uncoated PA66 is followed by melt-dripping. This phenomenon can be beneficial, as it takes the heat away from the burning polymer. However, it can also cause a large fire threat as it contributes to spreading the fire if the temperature of the drops is too high. This is evaluated by a piece of cotton underneath the sample. Here, the flaming drops caused the ignition of the cotton, highlighting the high flammability of PA66. After two flame applications of 10 s, the polymer was completely consumed, and is therefore not classified according to the UL94 rating. The addition of the PAA/PEI primer did not improve its flammability, and even slightly increased its combustion rate. The polymer was completely consumed after the first flame application.

Adding an alginate/vermiculite nanocomposite coating drastically improved the flammability behavior of PA66. On the first flame application, the coating cracked on the edge where the burner was applied, and any flaming was limited to this spot (Figure 33). It is due to the pressure caused by the evolution of the decomposition gases as the substrate decomposes. However, the sample exhibited self-extinguishing behavior and extinguished in less than 1 s in average without afterglow. Moreover, the melt-dripping was completely suppressed. No flame nor afterglow were observed on the second flame application. All these elements give the sample a V-0 rating according to the UL94 classification. Interestingly, the addition of the coating also reduced the combustion rate. All test results are presented in Table 19.

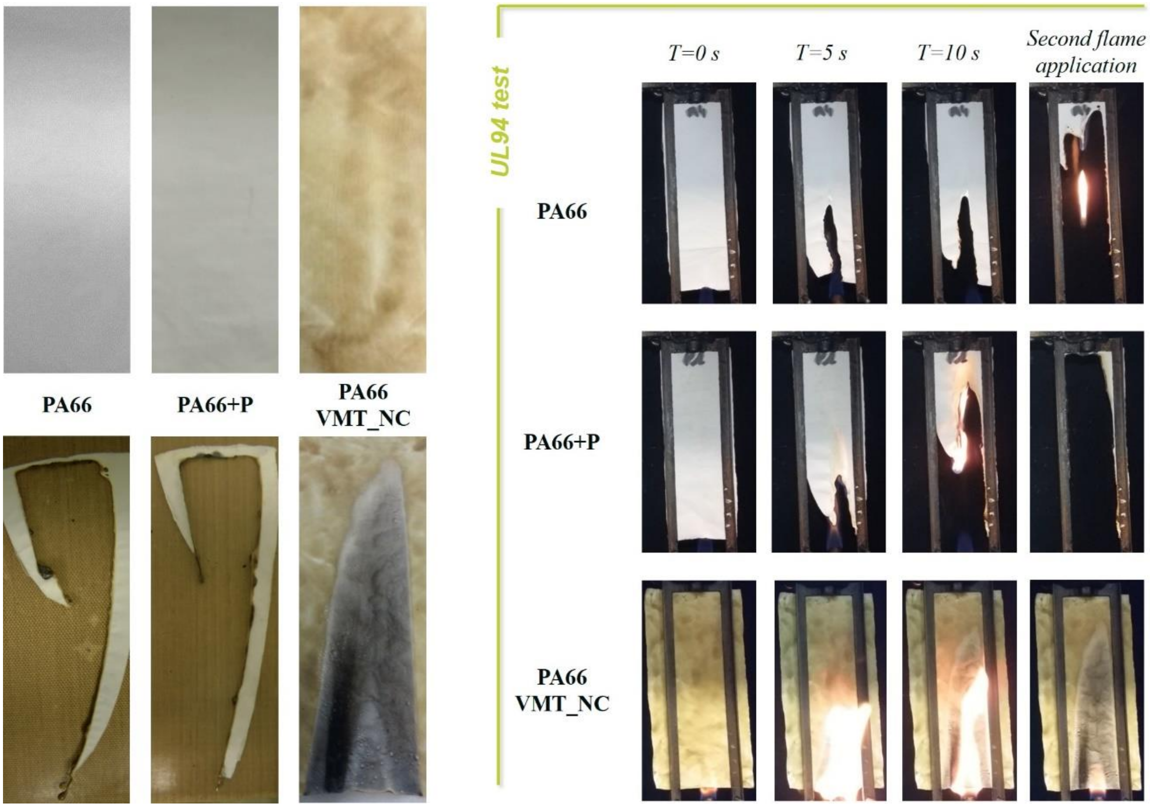

Figure 33. Left hand-side: digital images of the samples before(top) and after (bottom) UL94 test. Right hand-side: digital images of PA66, PA66 coated with the primer and PA66 VMT_NC taken during UL94 test at t=0, t=5 s t= 10 s and during the second flame application.

The only observed shortcoming is the intensive flaming when compared to an uncoated PA66 fabric. As the coating starts to degrade, it provides a support for the melted PA66, forcing it to combust within the confines of the coating, which explains both the suppression of melt-dripping and the intense flaming. The substrate was completely consumed, and the residue was composed of the degraded coating.

Table 19. UL94 results of PA66 and PA66 VMT_NC. N.R = non rated. The combustion spread was calculated on a 5 cm decomposed length.

	Weight gain [%] ± σ	**Weight loss [%] ± σ**	**Residual combustion time [s] ± σ**	**Complete combustion**	**UL rating**	**Combustion spread [cm/s] ± σ**
PA66	/	37.4 ± 10	16.0 ± 12	Yes	N.R.	1.83 ± 0.09
PA66 VMT_NC	67.9 ± 4	12.4 ± 3	0.4 ± 0.6	No	V-0	1.37 ± 0.09

SEM images of cross sections on different parts of the residue clarify the combustion behavior. First of all, they show very distinctively the aligned VMT platelets which remain un-degraded at the end of the test, as illustrated in Figure 34. Second, it is observed that the degraded coating has considerably delaminated, due to the trapping of decomposition gases (probably from alginate decomposition), which shows its barrier effect. This is also seen by macroscopic observation of the residue which presents bubbling on its surface, as well as the emission of large amount of soot.

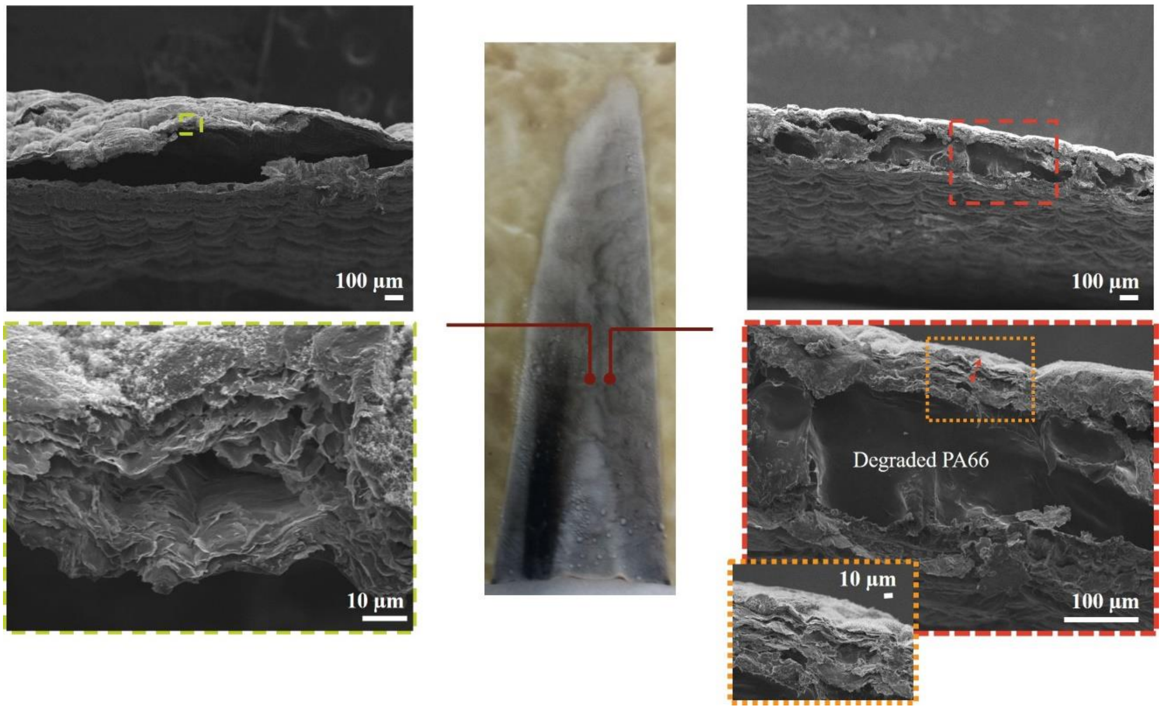

Figure 34. SEM images of the cross-section of residue of PA66 VMT_NC. The samples for analysis were extracted in the middle of the decomposed area, in the center and on the side, as indicated on the scheme.

The central part of the residue is only composed of the hollowed shell of the coating, which has kept the shape of the textile fiber. Aside of the central degraded area, the molten PA66 fibers are clearly seen between the two coatings walls, showing the incomplete combustion process. There is no delamination between the coating and the melted polymer, however, the space between the vermiculite platelets has increased.

FTIR analysis of the residue gives more information on the combustion behavior. PA66 VMT_NC before fire test presents the specific peaks of alginate at 1604 cm^{-1} and 1415 cm^{-1}, which corresponds to C=O stretching of the carboxylic moieties, at 3370 cm^{-1} corresponding to

OH function and at 2927 cm^{-1} corresponding to C-H bonds. The peak at 950 cm^{-1} corresponds to Si-O bonds of vermiculite clays. In Figure 35 the residues are noted PA66 VMT_NC_UL1 to 3 depending on their position with regards to the flame (far to close).

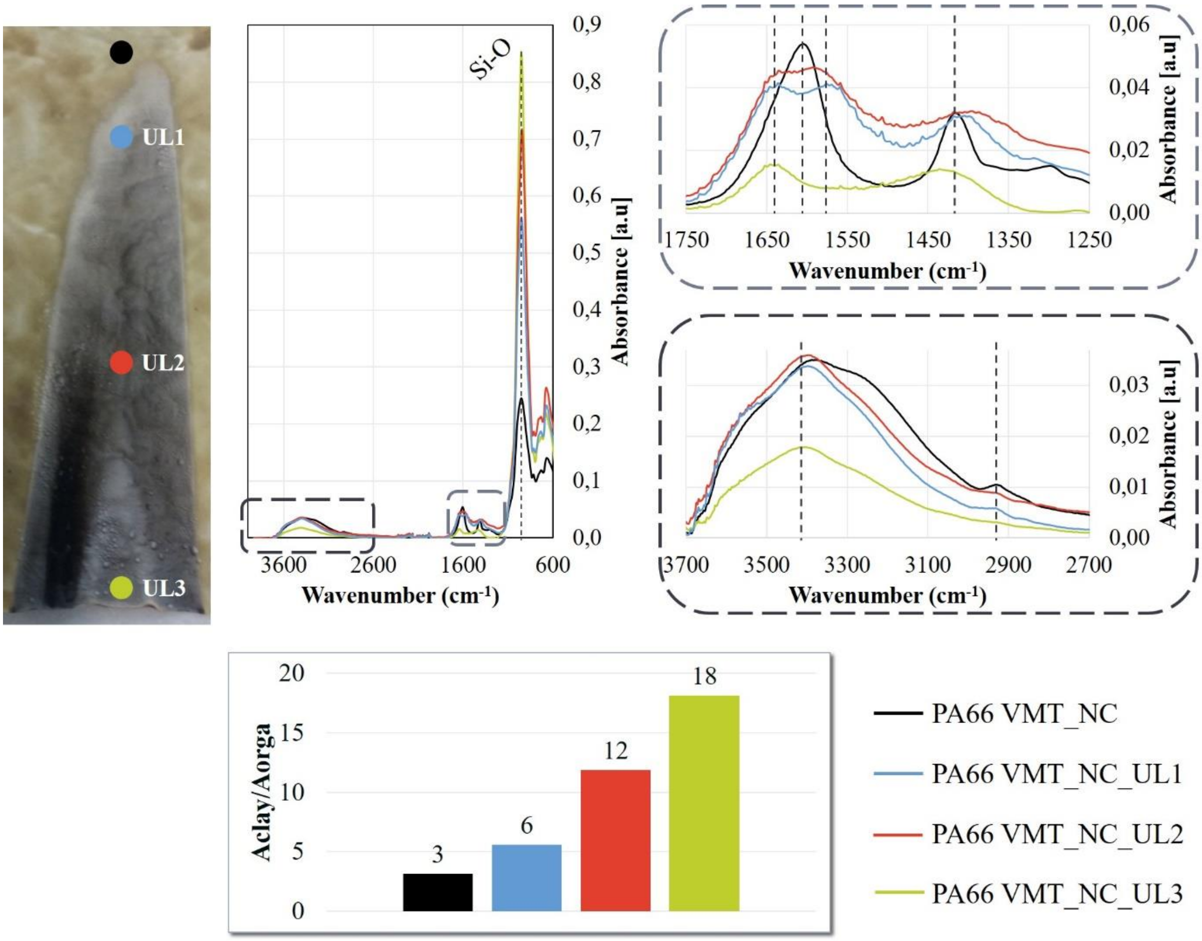

Figure 35. FTIR analysis of the residue of PA66 VMT_NC. The observations were done at different point on the surface, as indicated on the scheme. The diagram on the bottom show the evolution of the ratio of the 950 cm-1 peak area(A_{clay}) and the area of the peaks characteristics of organic matter (A_{orga}).

The organic matter of the residues is characterized by the peaks around 1640 cm^{-1} and 1580 cm^{-1} corresponding to C=C bonds of char. The residues PA66 VMT_NC_UL1 and 2 also present peaks around 2930 cm^{-1} due to C-H bonds, which have disappeared in PA66 VMT_NC_UL3. Also, for PA66 VMT_NC_UL3, the peak at 1580 cm^{-1} is also absent, which shows an advanced stage of decomposition of the organic matter. The ratio of the 950 cm^{-1} peak area (A_{clay}, characteristic of VMT) against the area under the characteristic peaks of organic matter (A_{orga}, either alginate or char, between 1800 and 1150 cm^{-1}) was calculated for each spectrum. As they were acquired on the same day and rigorously in the same conditions, this ratio gives a semi-quantitative idea of the clay/organic ratio within the residue. It appears that it increases from PA66 VMT_NC to PA66 VMT_NC_UL3 where it is the highest. (see Figure 35). It means that the residue closer to the flame is mainly composed of remaining VMT whereas the proportion in organic matter increases with the distance to the flame.

This difference in residue composition and morphology is due to the difference in temperature from the bottom to the top of the sample during FTIR analysis, and shows the different decomposition stages of the coating. This can be explained thanks to infrared imaging during the test, using an infrared camera equipped with a filter eliminating the specific wavelengths emitted by the flame, allowing to see through it. Figure 36 shows screenshots of the film taken at different times. Because the emissivity is not known, it is not possible to quantify exactly the temperature at the surface of the sample. But, the color gradient still shows the difference between high temperatures (yellow-white) and low temperatures (violet-blue), and can give a qualitative idea of what is happening when a flame is applied. When the burner comes close to the sample, the images show the apparition of a conical shape which is yellow at the bottom and blue on top. This corresponds to the decomposing area and the difference in color indicates that a temperature gradient appears during the test. As a result, there is a progressive decomposition of the coating, as the temperatures on top of the decomposed area are lower than those on the bottom.

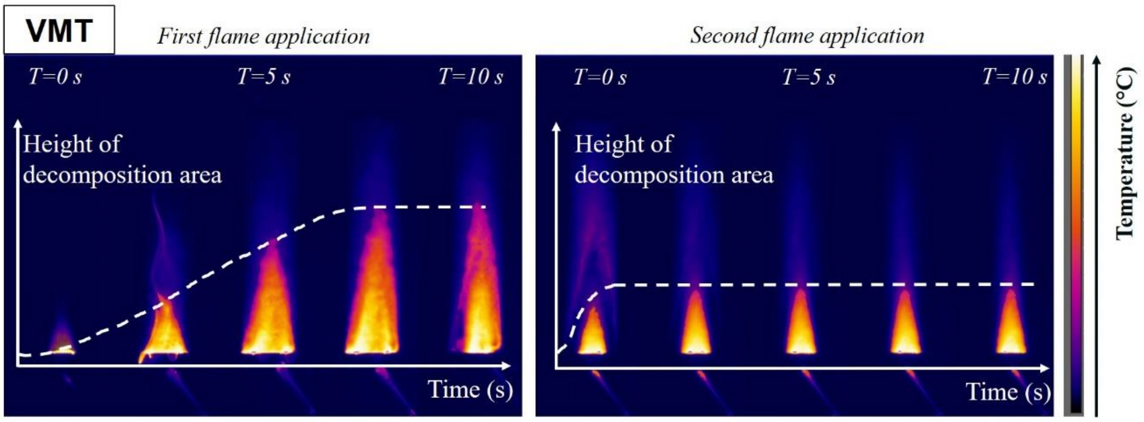

Figure 36. Temperature measurement by infrared imaging at the surface of PA66 VMT_NC during UL94 test.

In addition, this conical shape increases in size and height until it reaches a maximum and stops propagating. It means that the propagation of heat is limited at one point during the test.

Moreover, during the second flame application, the conical shape is reduced in size and the yellow area corresponding to the high temperature is restricted to the location of the flame from the burner. It does not change for the 10 s during which the flame is applied. It can be concluded that the residue formed during the test blocks the heat from the flame and limits heat propagation.

To conclude, two elements could explain the self-extinguishing behavior of the sample. First, the coating acts as a mass barrier which traps decomposition gases and prevents the flame spread. Second, the residue does not conduct heat very well. Therefore, once the coating has decomposed and the PA66 fibers have combusted, the heat from the flame is blocked and a thermal gradient takes place along the surface, which favors the formation of a stable residue, until the temperature is low enough that PA66 does not degrade.

2) Combination of clays

The action of other clays on the fire protection of PA66 was evaluated. First, sepiolite (SEP) was used, then vermiculite, sepiolite and halloysite (HAL) were combined to reach better performances. The interest of selecting SEP and HAL is because both clays have different morphologies than VMT. While VMT is found in the form of platelets, SEP particles are needles and HAL particles have nanotube shapes. 5 systems were studied: VMT, SEP, VMT-SEP, VMT-HAL and VMT-SEP-HAL (the coated fabrics are thereafter called PA66 VMT_NC, PA66 SEP_NC, PA66 VMT-HAL_NC and PA66 VMT-SEP-HAL_NC respectively). The system with halloysite alone was not tested because of the poor mechanical properties and high shrinkage of the dried coating, causing cracks and delamination and preventing any handling. All systems were dispersed in water with 30 wt% alginate and 70 wt% of clay. When clay were combined, they were each added in equal proportion (see the Materials and Methods sections, part II.2)).

Cross-section SEM observations of the samples (Figure 37) show the deposition of a conformal and dense coating, that does not permeate the inner fibers of the PA66 fabrics. While it is not possible to observe a particular organization in PA66 SEP_NC and PA66 VMT-HAL_NC, PA66 VMT-SEP_NC and PA66 VMT-SEP-HAL_NC show aligned VMT platelets. The coatings are mostly composed of clays, as can be seen on the energy dispersive X-Ray mappings in Annex 3-1 p.131.

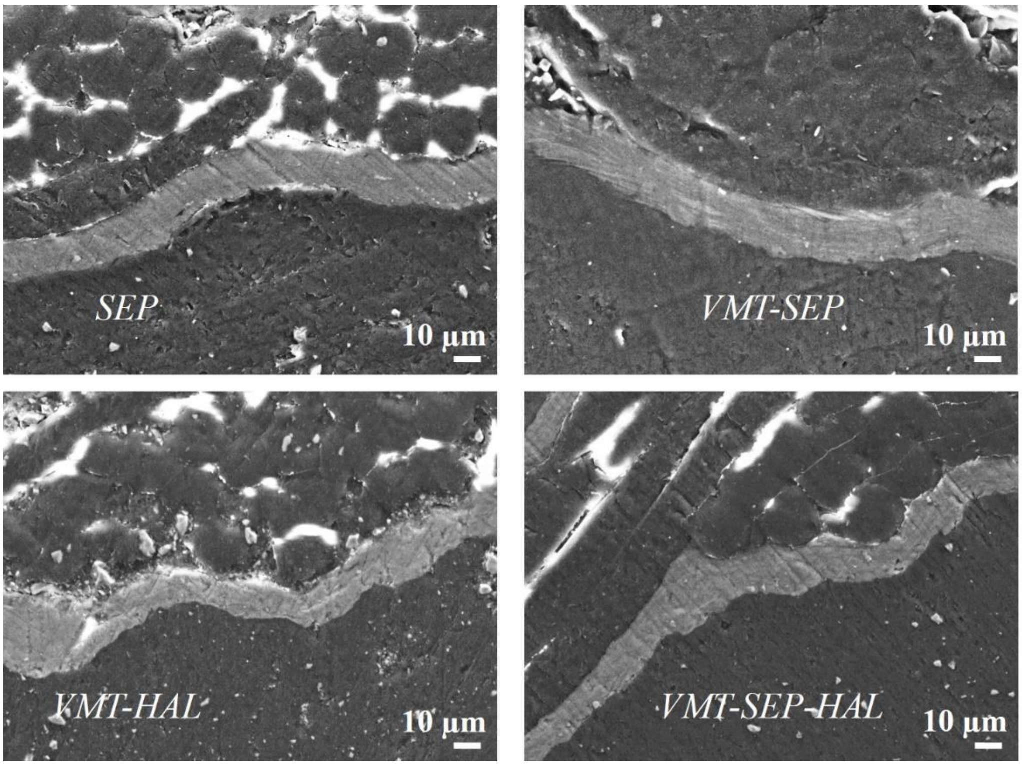

Figure 37. SEM images of cross-sections of PA66 SEP_NC, PA66 VMT-SEP_NC, PA66 VMT-HAL_NC and PA66 VMT-SEP-HAL_NC.

When submitted to TGA, VMT presents three mass loss steps due to (from low to high temperature): loss of superficial water, loss of interstitial water and loss of hydroxyl groups (inducing phase change). SEP presents also three mass loss steps due to two consecutive losses of coordinated water and loss of hydroxyl groups (inducing phase change). HAL shows the lowest residue because of the loss of superficial water and the loss of hydroxyl groups (inducing phase change). PA66 Clay_NC samples all present the same steps observed with PA66 VMT_NC, corresponding respectively to the decomposition of alginate and PA66.

Table 20. Thermal Gravimetric Analysis results of PA66 Clay_NC samples

	$T_{95\%}$ (°C)	**Main step 1**		**Main Step 2**		**Residue@ 1000°C (%)**
		T_{onset} (°C)	T_{max} (°C)	T_{onset} (°C)	T_{max} (°C)	
PA66	383	406	434	/	/	0
Alginate	169	223	243	688	768	14
Alg/VMT_NC	239	231	248	/	/	72
Alg/SEP_NC	226	225	245	/	/	71
Alg/VMT-SEP_NC	233	231	245	/	/	67
Alg/VMT-HAL_NC	237	229	248	377	420	69
Alg/VMT-SEP-HAL_NC	237	226	247	386	406	71
PA66 VMT_NC	250	213	247	345	391	24
PA66 SEP_NC	267	236	248	347	404	22
PA66 VMT-SEP_NC	284	228	235	356	403	28
PA66 VMT-HAL_NC	301	222	243	349	403	26
PA66 VMT-SEP-HAL_NC	237	227	236	345	404	28

However, several differences can be noted. First, while the decomposition of alginate is delayed in the case of PA66 VMT_NC and PA66 SEP_NC, it is unchanged for PA66 VMT-HAL_NC and even anticipated in the case of PA66 VMT-SEP_NC and PA66 VMT-SEP-HAL_NC. Then, the decomposition of PA66 occurs for all coated samples earlier than for the uncoated material. However, it is much more anticipated in the case of PA66_VMT NC (391°C) than for all other systems, for which it occurs around 403°C. Interestingly, the decomposition step ends at the same time for all samples, which means that they differ by the thermal range on which it takes place (from large to narrow: VMT-SEP-HAL> VMT > SEP > VMT-HAL > VMT-SEP). The residues are in between 22 and 28 %, which corresponds to the residues from the coatings. By comparing with the residues from Alg/Clay films, the difference is linked to the difference in clay composition that induces more or less mass loss. TGA curves are presented in Figure 38.

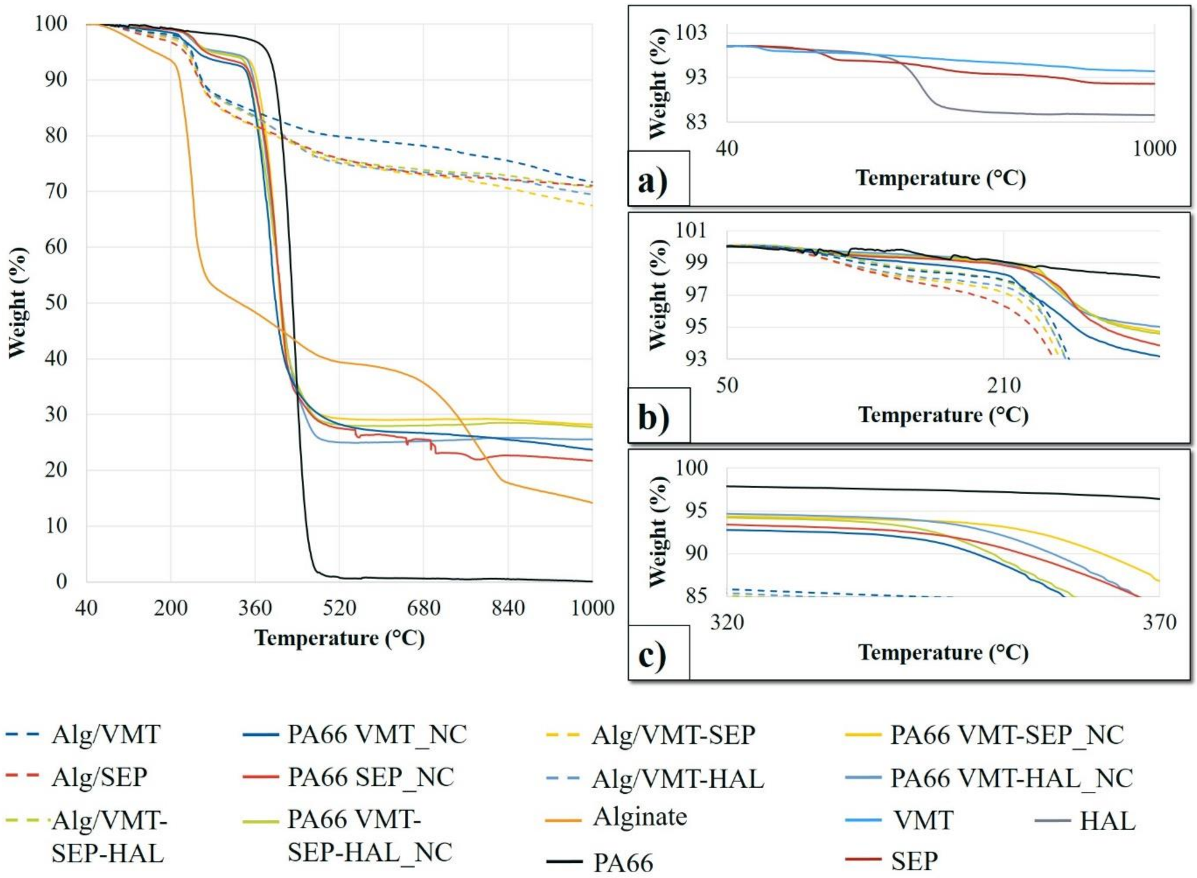

Figure 38. Thermogravimetric analysis of PA66 Clay_NC samples under N_2 atmosphere. a) thermal decomposition of the three different clay used in this study. b) and c) are close-ups of the onset of the two main decomposition steps.

At UL94 fire test (Figure 39), all samples presented no melt-dripping, and all but PA66 SEP_NC showed a self-extinguishing behavior. PA66 VMT-SEP_NC, PA66 VMT-HAL_NC and PA66 VMT-SEP-HAL_NC behaved similarly as PA66 VMT_NC.

Indeed, the coating cracked open on the edge where the burner is applied, and the flame sprouted from this place only, without spreading. PA66 SEP_NC, on the other hand, burnt intensively, and the flame spread along the sample all the way to the top, which prevented the system from being rated in the test. This poor result is due to the fact that the coating cracked during the test, cancelling its protective effect. While SEP alone does not improve the fire behavior of PA66, in combination with VMT it slows down the combustion rate a little, which is not the case of HAL. The combination of VMT and SEP, and of the three clays, however, showed the most promising behavior, in that the combustion rate, mass loss and residual combustion time are the lowest.

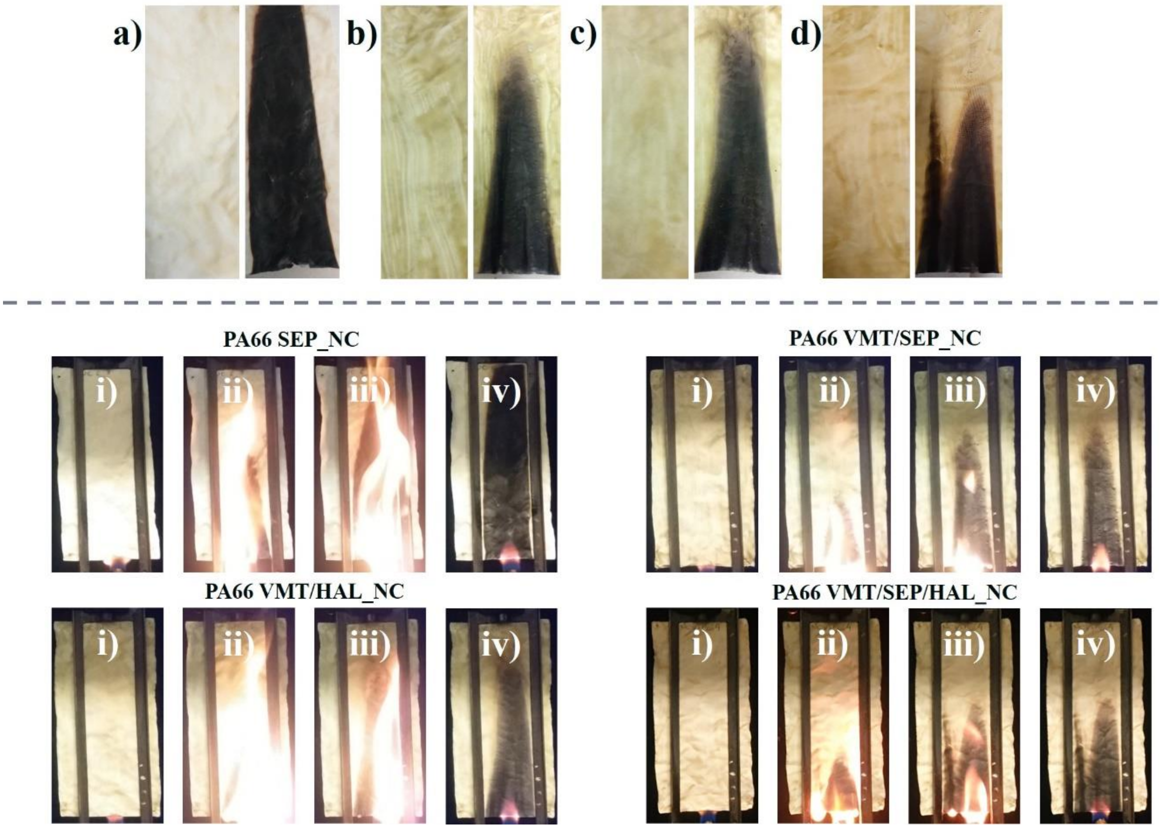

Figure 39. Digital images of a) PA66 SEP_NC, b) PA66 VMT-SEP_NC, c) PA66 VMT-HAL_NC and d) PA66 VMT-SEP-HAL_NC samples before and after UL94 test. Sequences of pictures underneath were taken during UL94 test at i) t=0 s, ii) t=5 s, iii) t= 10 s and iv) during second flame application.

Table 21. UL94 results for PA66 Clay_NC textiles. N.R = Non Rated

	Weight gain [%] ± σ	**Weight loss [%] ± σ**	**Residual combustion time [s] ± σ**	**Complete combustion**	**UL rating**	**Combustion spread [cm/s] ± σ**
PA66 VMT_NC	67.9 ± 4	12.4 ± 3	0.4 ± 0.6	No	V-0	1.37 ± 0.09
PA66 SEP_NC	67.2 ± 4	26.2 ± 7	7.3 ± 2.9	Yes	N.R.	1.17 ± 0.07
PA66 VMT-SEP_NC	69.3 ± 2	8.4 ± 2	1.0 ± 0.8	No	V-0	1.14 ± 0.08
PA66 VMT-HAL_NC	62.2 ± 3	12.3 ± 2	1.2 ± 1.0	No	V-0	1.31 ± 0.14
PA66 VMT-SEP-HAL_NC	70.8 ± 3	9.6 ± 1	0.6 ± 0.2	No	V-0	1.11 ± 0.10

SEM observations gathered in Figure 40 show the retention of the clay organization upon burning, but also how the coating serves as support for the combustion of PA66. The SEM images were taken as described in Figure 34, that is to say in two points in the middle of the degraded area, first in the center and then a little aside.

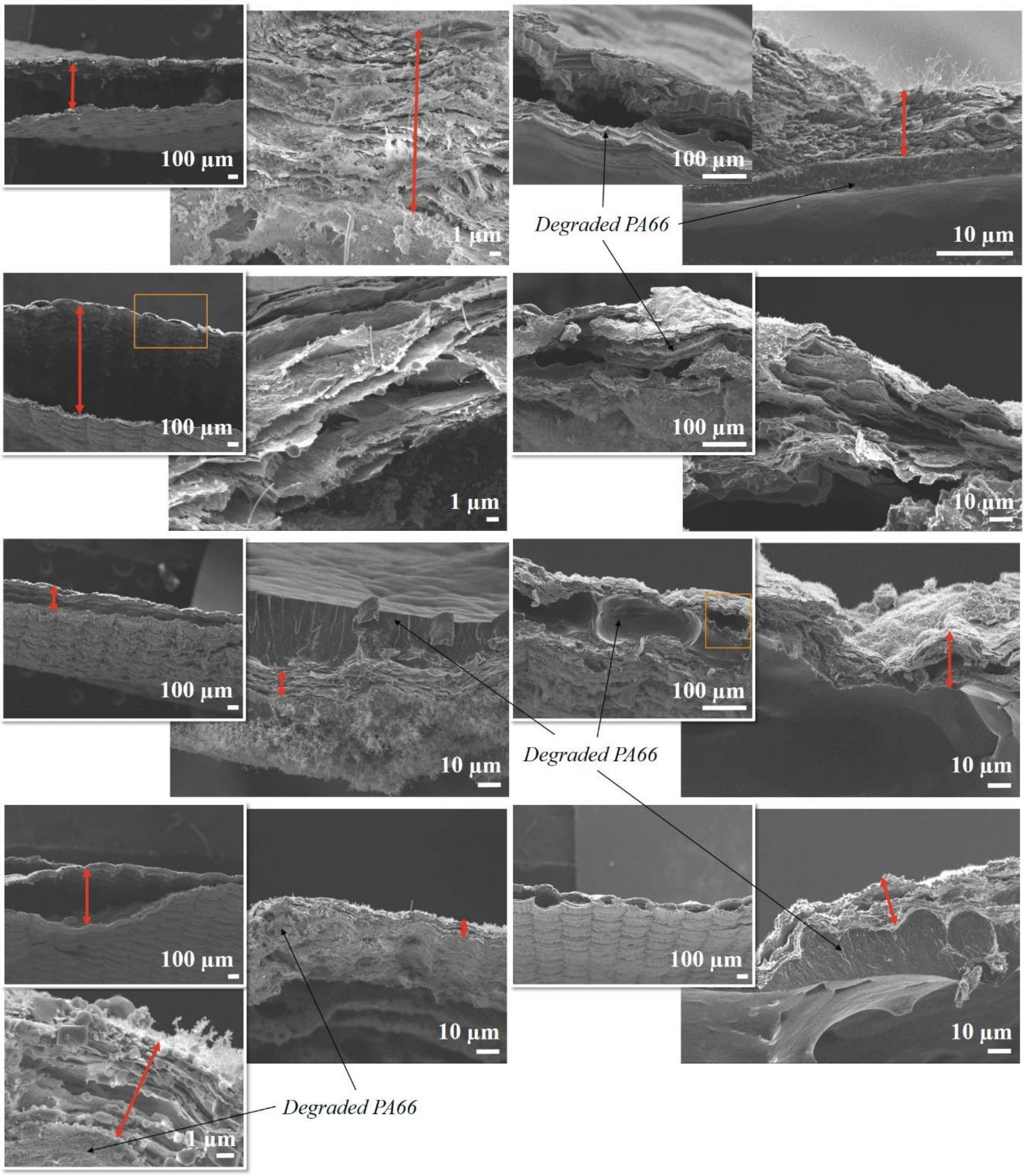

Figure 40. SEM images of residues from PA66 SEP_NC (first row at the top), PA66 VMT-SEP_NC (second row), PA66 VMT-HAL_NC (third row) and PA66 VMT-SEP-HAL_NC (last row at the bottom). Left column: taken in the middle of the decomposed area at the center and right column: taken in the middle of the decomposed area, on the side, as presented in Figure 34.

First, it is seen that the nanoparticles in all coatings are organized. SEP needles are organized in large domains oriented in the same manner, and in systems containing VMT, the platelets are parallel to one another. In the case of the systems combining VMT and SEP, SEP nanoparticles are observed on the surface of VMT platelets. Second, they clearly show the expansion of the coatings containing VMT platelets because of the delamination between the particles, attributed to a gas trapping effect. This is probably caused by the morphology of the VMT particles as well as their organization which creates a tortuous path hindering gas flow.[221], [250], [254], [258] PA66 SEP_NC does not present this characteristic, but the SEP particles seems to be glued together in foil-like layers, probably alginate charred residue, forming a compact structure. This could explain the reduced combustion rate observed for this sample, the poor behavior during UL94 being solely due to the poor mechanical resistance of the coating, as discussed later.

Lastly, the SEM images provide more elements to describe PA66 combustion behavior with the coating. The central area is the most degraded (left column on Figure 40). PA66 is consumed from the core to the interface with the coating. Indeed, most of the polymer is gone, leaving the hollow shell of the coating that has kept the shape of the fibers. However, melted PA66 can still be seen just underneath the coating, which is shown as a smooth layer in SEM. On the side of the central degraded area, the degradation is not as advanced, as larger quantities of degraded PA66 are observed.

FTIR spectra of PA66 Clay_NC (presented in Figure 41) are similar, in that they show the peak characteristic of Si-O bonds in clay at 950 cm^{-1}, and the peaks characteristic of alginate as described in the previous section. FTIR spectra of chars were acquired in the same manner as described in Figure 35. Differences can be distinguished between the systems. First, the part directly exposed to the flame during the test (PA66_Clay_NC_UL3) is different between the samples and present various stages of degradation. The spectrum of PA66 SEP_NC_UL3 shows the peaks characteristic of SEP but no peak indicates the presence of char or organic matter; consequently, it was completely consumed during the test. While PA66 VMT-SEP_NC_UL3 presents a single peak at 1650 cm^{-1}, its low intensity when compared the Si-O peak shows that the char is highly degraded. On the opposite, the char in PA66 VMT-HAL_NC_UL3 still presents OH groups, and PA66 VMT-SEP-HAL_UL3 has remaining C-H bonds (peaks around 2950 cm^{-1} and presence of a shoulder at 1400 cm^{-1}) indicating a lesser degree of degradation of the organic matter. In conclusion, even in direct contact to the flame, the clay/alginate system can produce a stable and protective residue, at least when with VMT platelets.

Parts UL1 and UL2 of the residue show lesser level of decomposition, and their spectra are similar with what was observed with PA66 VMT_NC. The only exception is PA66 SEP_NC where the organic matter is in a more decomposed state. In addition, as was observed with PA66 VMT_NC, the ratio clay/organic increases from UL1 to UL3. This is indicated by the increasing ratio of the 950 cm^{-1} peak area with the area under the peaks characteristic of alginate and char (from approximately 1150 to 1800 cm^{-1}, see Figure 41).

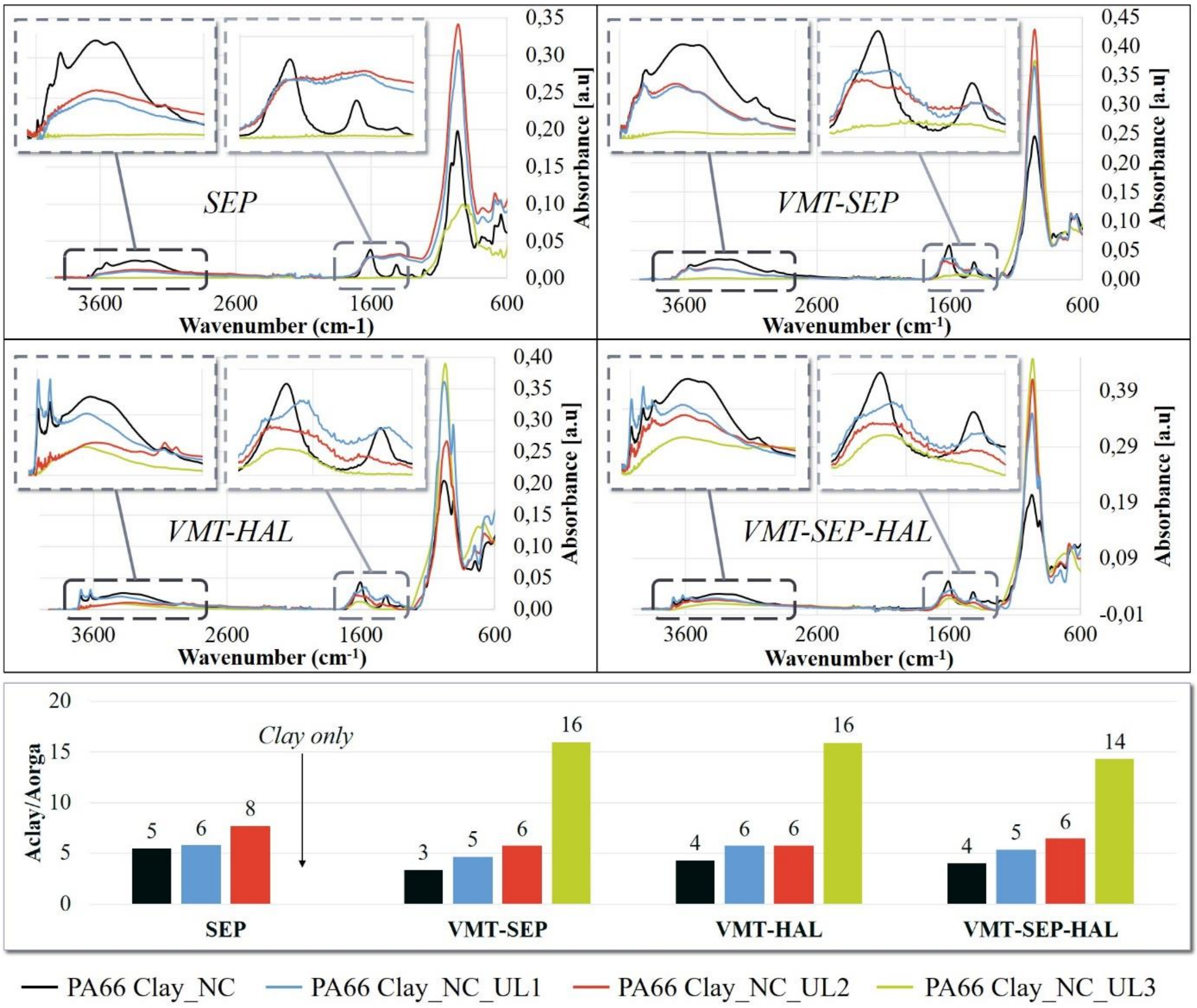

Figure 41. FTIR spectra of PA66 Clay_NC and corresponding residue taken at different places on the burnt textile, as indicated in Figure 35. The diagram on the bottom show the evolution of the ratio of the 950 cm-1 peak (A_{clay}) and the area of the peaks characteristics of organic matter (A_{orga}).

As discussed in the previous section, the temperature at the surface of the sample during the UL94 test was monitored thanks to an IR camera.

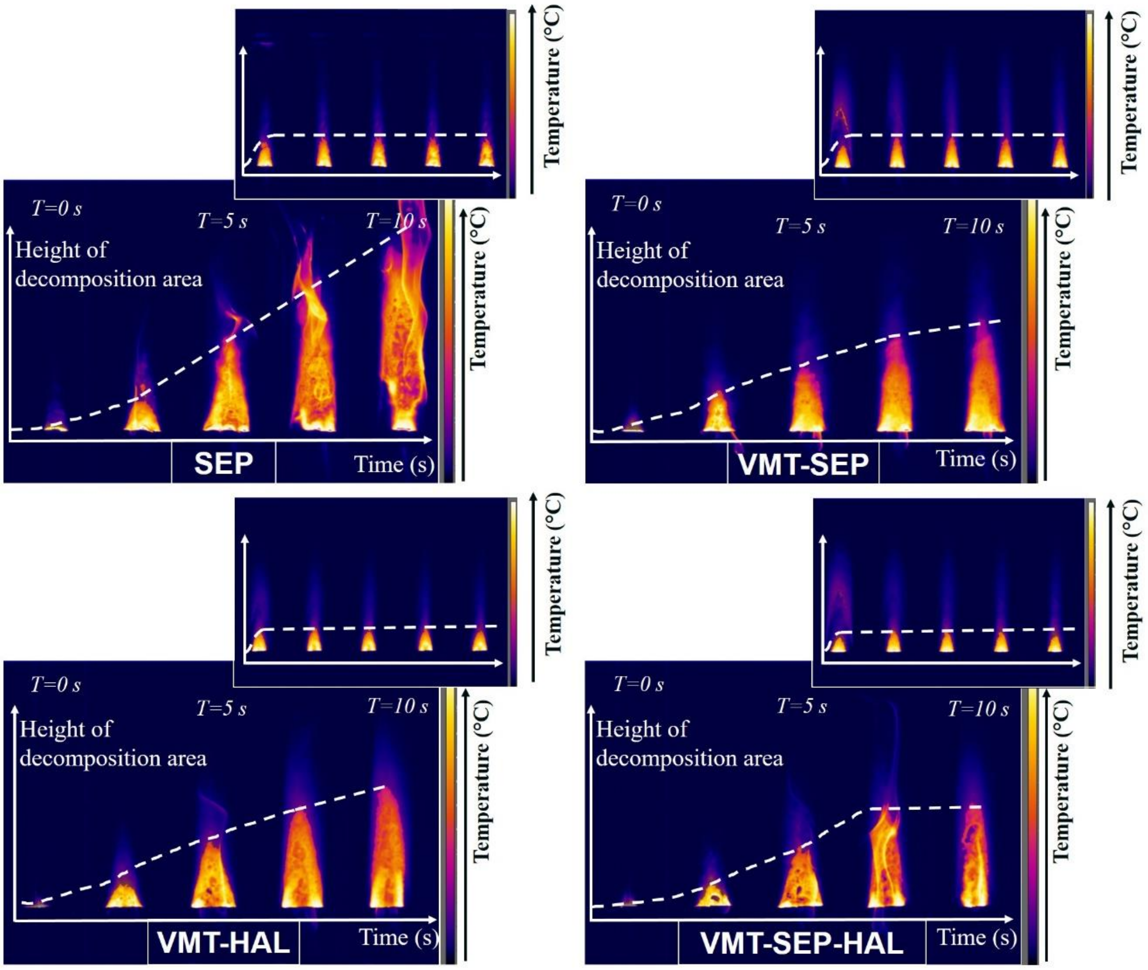

Figure 42. Temperature measurement by infrared imaging at the surface of PA66 Clay_NC during UL94 test.

The difference from high to low temperature is represented by a color gradient from yellow to blue. First, it shows that, except for PA66 SEP_NC, there is no significant difference between the different PA66 Clay_NC samples. As the burner is applied at the bottom of the sample, the temperature starts to rise and the substrate combusts, as shown by the appearance of a yellow-to-orange cone on the infrared images. It continues to rise along the sample causing further degradation of PA66, leaving only the coating as residue. At some point, the degradation stops, which is materialized by the fact that the height of the decomposition zone stops rising. Indeed, as the coating residue does not conduct heat efficiently (see the gradient during second flame application in Figure 42), and as the flame does not propagate along the sample, there is a thermal gradient from the top to the bottom of the sample. Therefore, the degradation front reaches a point where the temperature is lower than the temperature of degradation of PA66. This, combined with the gas barrier effect of the VMT containing coatings (that stops the flame from propagating in the first place) explains the self-extinguishment of the samples. However, if the flame propagates along the sample, as it is the case for PA66 SEP_NC, the degradation progresses until it reaches the top of the fabric, despite the fact that the residue does not conduct heat either.

3) Heat Release during flame spread

As it was mentioned before, the fact that the alginate/clay coatings suppressed the melt-dripping caused intense flaming instead. To gain further insights on this fire behavior, a small scale version of EN 50399 standard, that quantifies heat release and flame spread, was used. The test consists in submitting the sample to the flame of a methane burner for 60 s, and measuring the oxygen consumed during the test. Incidentally, the exposure time is higher than that for UL94. As illustrated in Figure 43, all PA66 Clay_NC samples have higher heat release than PA66 alone. Indeed, as PA66 melts away it stops burning almost immediately. On the opposite, as the coatings provide support for the combustion of PA66, preventing melt-dripping, the fuel is concentrated in the same place and is consumed at the same time, resulting in higher heat release rates. Out of all systems, PA66 VMT_NC has the lowest pHRR, followed by PA66 VMT-HAL_NC and PA66 VMT-SEP-HAL_NC. However, THR was constant for all samples.

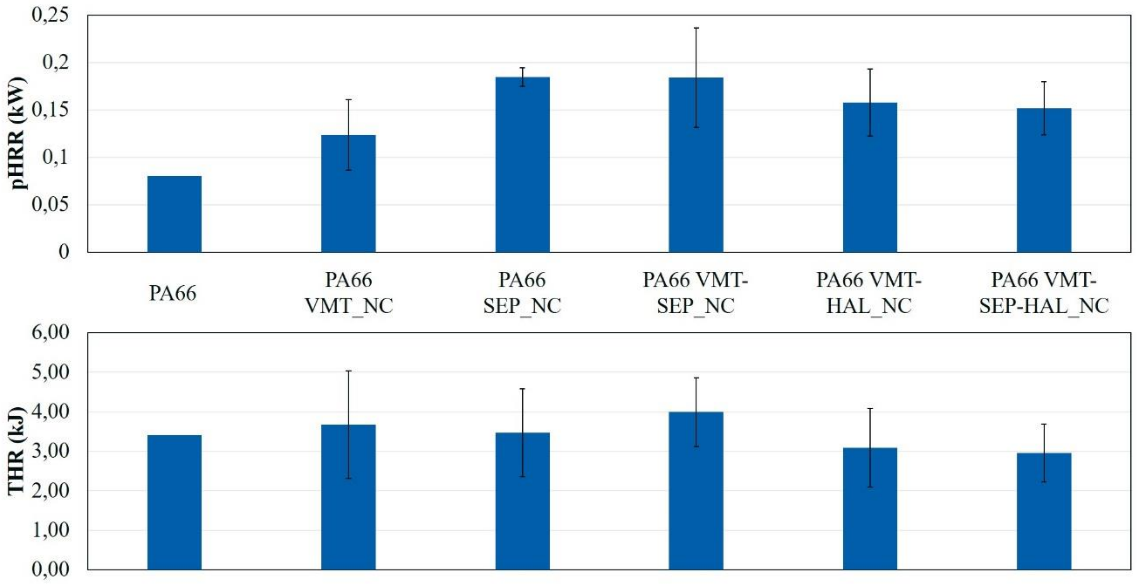

Figure 43. pHRR and THR results of PA66 Clay_NC samples during EN 50399 flame spread test.

As PA66 was consumed, the only residue left was the degraded coating. Due to the set-up, the stress on this part of the sample was quite high. As a result, some of the tested samples failed as they cracked due to the fragility of the residue (they were not taken into account for the calculation of the pHRR, as they presented uncharacteristic behavior). This served to evaluate the robustness of the coating after it was exposed to a flame. Out of all the samples tested, 25% of PA66 VMT_NC cracked during the test, 40% of the PA66 SEP_NC samples, and none of PA66 VMT-SEP_NC, PA66 VMT-HAL_NC and PA66 VMT-SEP-HAL_NC, which shows that combining clays could help improving the mechanical properties of the coating. In Figure 44, all the parameters are gathered in radar diagrams, which shows that PA66 VMT-SEP_NC, PA66 VMT-HAL_NC and PA66 VMT-SEP-HAL_NC allow to have the best performances (represented by a smaller area on the diagram), although PA66 VMT _NC is fairly close.

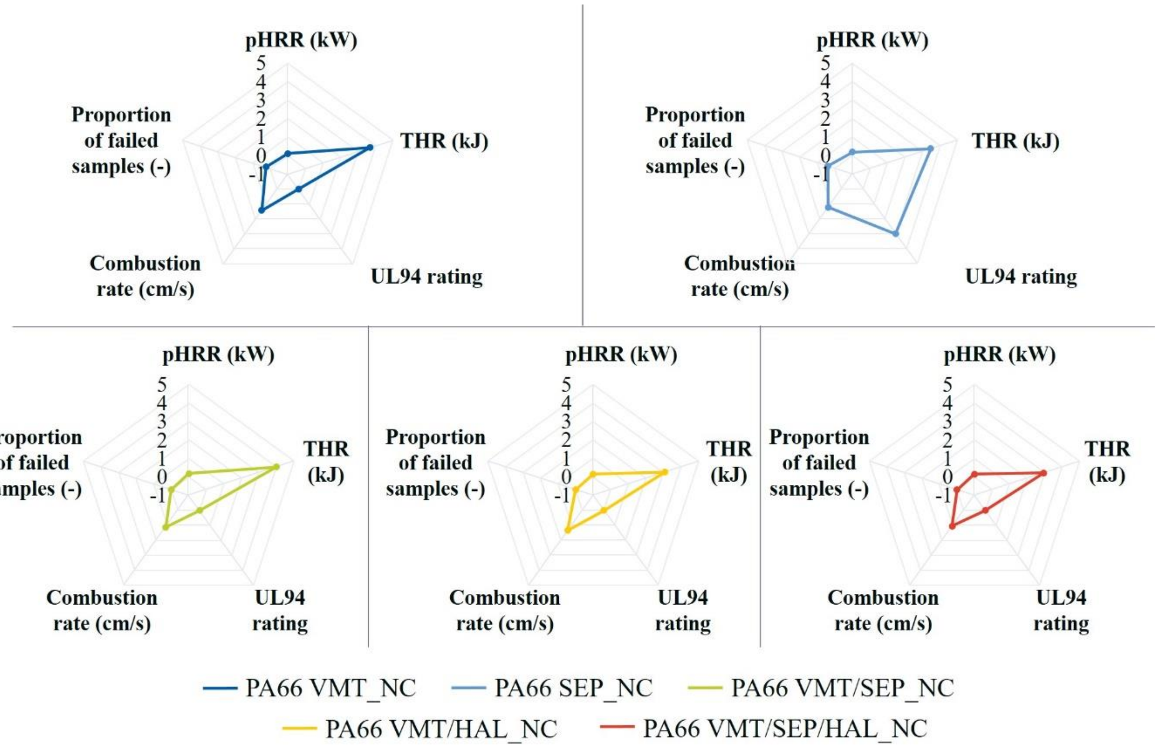

Figure 44. Radar diagrams summing up the relevant parameters obtained during UL94 and EN 50399 fire tests for PA66 Clay_NC. UL94 ratings was adapted as follows: V-0 = 0, V-1 = 1, V-2 = 2, and non rated = 3. The proportion of failed samples was calculated as follows: number of fails/number of samples tested. It is a number between 0 and 1.

4) Discussion and conclusion

To conclude, depositing alginate/clay dispersions on PA66 fabrics produces high filler content coatings that improve the fire behavior of the polymer in a small flame fire scenario. The protection mechanism is a physical process, attributed to several concurrent effects, that create a beneficial scenario allowing the samples to be rated V-0 at UL94 test.

First, in vermiculite-containing systems, the alignment of VMT and their platelet-like morphology traps decomposition gases. The residue is therefore composed of char and delaminated vermiculite. For PA66 SEP_NC this is not observed, but the residue is composed of SEP particles glued together tightly in charred foils, helping create compact composite structures. Both are stable even against the flame and are believed to slow down mass transfer, limiting and slowing down the release of combustible gases. Indeed, the combustion rate is slower, especially with SEP particles. However, for PA66 SEP_NC, these structures are very fragile and crack upon burning, which cancel their protective effect. Then, the composite char acts as a support for the decomposing fibers, suppressing the melt-dripping phenomenon. Finally, as shown by infrared imaging, the charred composite layer does not conduct heat. As a result, there is a thermal gradient from the top to the bottom of the sample, which means that the temperature is kept at levels where PA66 does not decompose, or not entirely. As a result, the samples exhibit self-extinguishment.

A great part of the efficiency of the systems rely on the fact that the alginate/clay coatings decompose ahead of the substrate, as shown by TGA. As alginate starts to decompose, it forms a charred composite structure. As it is exposed to high temperature the organic part further decomposes until it reaches a final stable state, but otherwise there is no major transformation. This evolution can be seen with the FTIR analysis, that shows the different stages of decomposition (lower temperatures for shorter exposure times). To conclude, the coating forms a protective charred residue that blocks the heat and the flame in the early stage of the test, before PA66 decomposition.

On the other hand, the fact that (1) the residue does not conduct heat, (2) the heat from PA66 burning is not evacuated by melted drops, and (3) the decomposition gases are released on a single point create intense flaming. Indeed, the heat accumulates, creating a hot spot, and the volatile products are highly concentrated. Consequently, the heat release during flame spread is higher, as observed in the EN 50399 test. Combining VMT with other type of clay does not change the combustion mechanism, but slightly improves the fire behavior of PA66 VMT_NC, as the combustion rate in UL94 was further lowered, especially with the presence of SEP particles in the coating. It is believed that this comes from the combination of the two barrier effects from VMT and SEP as described above. The results also showed the importance of mechanical resistance of the coating during combustion. Indeed, the physical barrier effect of the coating implies that combustible volatile products accumulate underneath, which increases pressure by accumulating between the decomposing substrate and the coating, creating cracks where combustion gases can escape. Combining VMT with other clay particles seemed to improve this, as the number of failures during the EN 50399 test was reduced.

II. Using nanocomposite hydrogel for improving the fire behavior of PA66 textiles

In this part, alginate/clay dispersions were casted on PA66 fabrics as described in the previous section. In order to improve the performance of PA66 Clay_NC systems, especially by limiting the intense flaming observed, the coatings were cross-linked in order to form hydrogels, before drying.

1) Choice of cross-linking system

Alginate is a polysaccharide which easily forms a hydrogel when in contact with Ca^{2+} ions in water. Four C=O functions in the G-unit (guluronate unit) of alginate forms ionic complexes with one Ca^{2+} ion, forming what is typically called an “egg-box” structure.[420] The most classical and simple way to form a Ca-alginate hydrogel is to drop a solution of alginate into a $CaCl_2$ aqueous solution and letting it sit long enough for the Ca^{2+} ions to diffuse into the polymer matrix. The addition of clays in the alginate solution does not disturb the gelation process. The problem with this method is that unfortunately, the hydrogels are very stiff, and retracts a lot upon drying, which causes the apparition of cracks. Pérez-Madrigal et al showed that alginate can also be cross-linked by polycarboxylic acids, including citric acid.[421] While citric acid-cross-linked alginate was mechanically too weak to form a coating on PA66, the combination of Ca^{2+} ions and citric acid did form a tough, flexible and coherent coating, that also showed minimal retraction upon drying.

2) Alginate/VMT dried hydrogel coating on PA66

An alginate/VMT dispersion was first casted on PA66 samples with a paint brush in order to have a 600 wt% wet add-on. Then, the samples were immersed in a solution of $CaCl_2$ and citric acid for cross-linking overnight. The resulting hydrogel coated PA66 was then dried in ambient conditions in a horizontal position, and the final sample was called PA66 VMT_HG. Because of the permeation of Ca^{2+} ions (proved by Ca energy dispersive X-ray mapping, see Figure 45) and citric acid (detected by FTIR, see Figure 49), the dry add-on was higher than PA66 VMT_NC, reaching about 109 %.

SEM images of the cross section presented in Figure 45 a) and b) show the deposition of a conformal and organized coating. Indeed, the VMT platelets are parallel to each other and to the surface of the fibers. Therefore, the cross-linking step did not disturb their organization. X-Ray mappings show that the coating is composed mostly of VMT platelets with C atoms detected in low concentration when compared to the Si, Al and Mg atoms characteristic of clays.

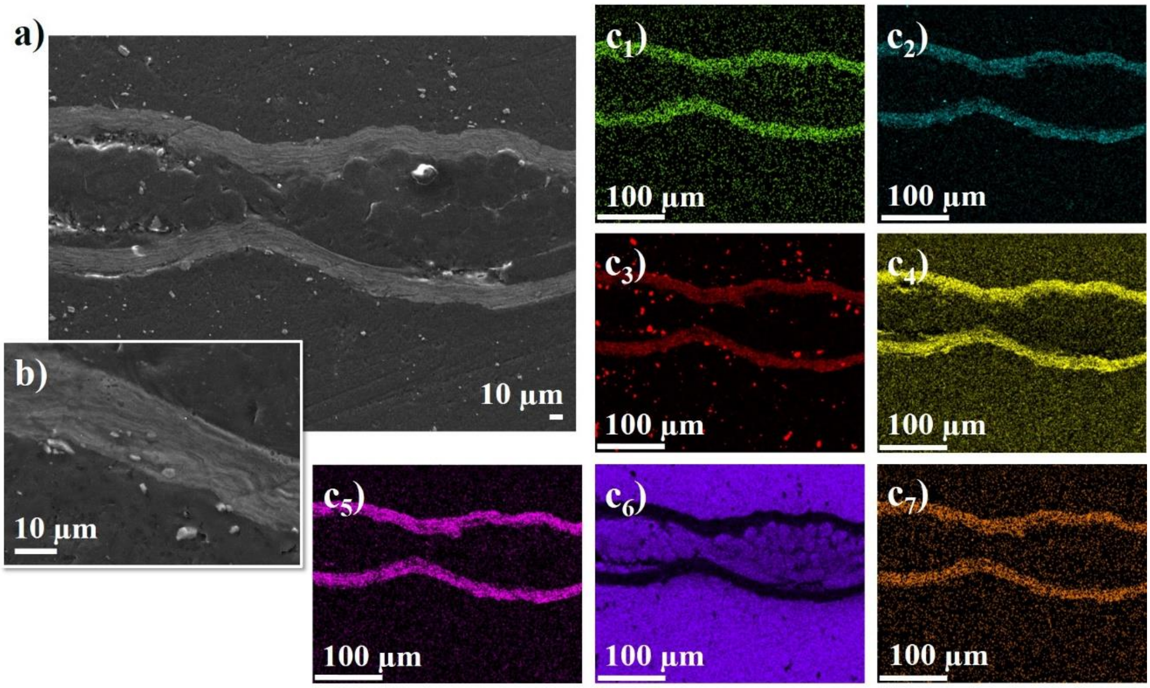

Figure 45. a) and b) SEM observations of a cross section of PA66 VMT_HG. c_1) to c_7) energy dispersive X-ray mappings of c_1) Ca, c_2) Al, c_3) Si, c_4) O, c_5) Mg c_6) C and c_7) K atoms.

The consequence of cross-linking alginate with Ca^{2+} ions and citric acid is that the degradation of alginate is strongly anticipated. Indeed, an alginate xerogel degrades at 205°C versus 243°C for alginate. However, the weight loss rate is reduced as the degradation is slowed down and dragged out on a larger thermal range. The thermal stability of the xerogel residue is still improved, as the second degradation step is significantly smaller, to the point of being barely discernible. As a result, and due the presence of calcium in the sample, the residue at the end is higher than alginate (24% vs 14%) (see Figure 46 and Table 22).

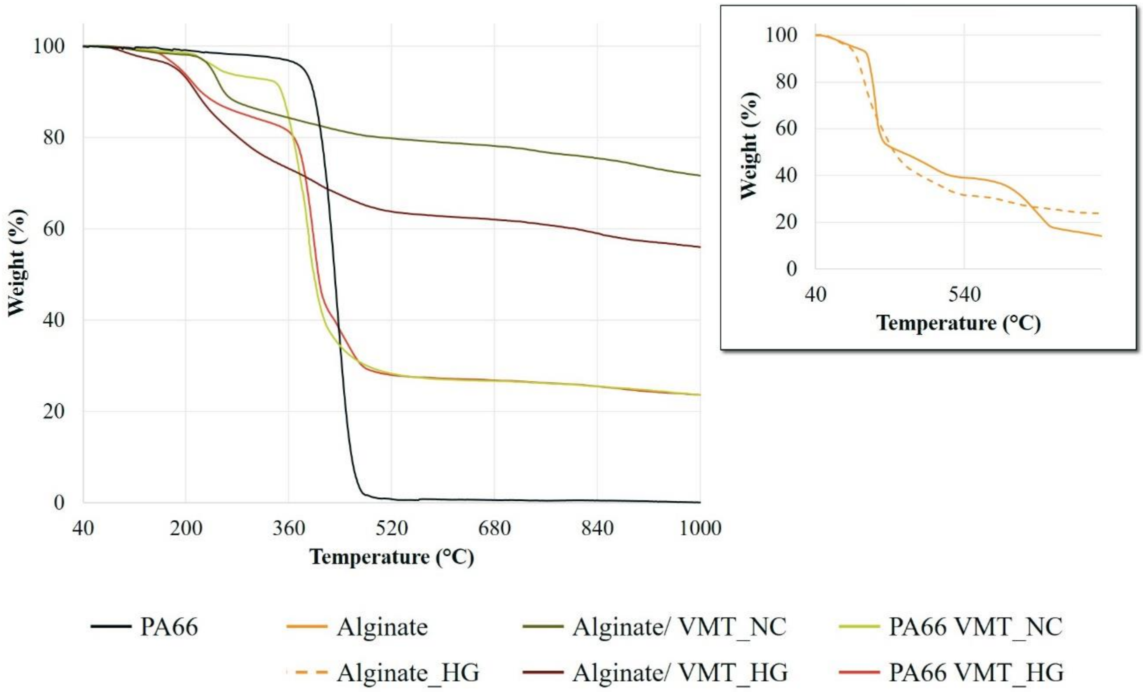

Figure 46. TGA of uncoated PA66 and PA66 coated with an alginate/VMT xerogel coating in nitrogen atmosphere. The insert in the top right corner show the thermal decomposition of alginate and alginate cross-linked with Ca^{2+} ions and citric acid.

The degradation of alginate/VMT_HG follows the outline of the degradation of alginate HG. It is noteworthy that the residue of Alginate/VMT_HG is way smaller than the residue of Alginate/VMT_NC. It is explained by the fact that the mass fraction of alginate xerogel in alginate/VMT_HG is higher than that of alginate in alginate/VMT_NC due to the permeation of citric acid and Ca^{2+}. As a result, the proportion of alginate hydrogel in the coating is a little less than 60%. Regarding PA66 VMT_HG, the degradation of alginate in the coating occurs at the same temperature than an alginate xerogel, which should be beneficial as the protective effect of the coating will be quicker. The decomposition of PA66, however, occurs earlier than uncoated PA66 (398°C instead of 434°C). At the end, the residues of PA66 VMT_HG and PA66 VMT_NC are similar, as all PA66 is consumed and only the coatings residue remains.

Table 22. TGA results for PA66 and PA66 VMT_HG

	$T_{95\%}$ (°C)	Main step 1		Main Step 2		Residue@ 1000°C (%)
		T_{onset} (°C)	T_{max} (°C)	T_{onset} (°C)	T_{max} (°C)	
PA66	383	406	434	/	/	0
Alginate	169	223	243	688	768	14
Alginate HG	151	176	205	646	684	24
Alginate/VMT_NC	239	231	248	/	/	72
Alginate/VMT_HG	185	189	216	/	/	56
PA66 VMT_NC	250	213	247	364	391	24
PA66 VMT_HG	191	174	207	379	398	24

The flammability of PA66 VMT_HG was evaluated by UL94 and compared to PA66 VMT_NC. In terms of performance during the test, PA66 VMT_HG is rated V-0, and behaves in the same manner as PA66 VMT_NC. However, some improvements can be noticed. First, the ignition of the sample is slightly delayed. The degraded area at the end of the test is also smaller, resulting in a smaller weight loss. Nevertheless, the sample burns longer, although it still extinguishes fast enough to be rated V-0 in the test. An interesting characteristic is the delamination of the coating in some points, where bubbles appear due to the release of combustion gases. It means that the combustion gases remain trapped between the coating and the substrate, causing the delamination, instead of escaping from the bottom of the sample as it is the case for PA66 VMT_NC. As a result, they do not contribute to the flame. Finally, the combustion rate is lower, and the flaming of the sample is less intense than PA66 VMT_NC. This last part was quantified via HRR measurements during flame spread in a small scale EN 50399 test, and it was observed that the HRR of PA66 VMT_HG is slightly smaller than that of PA66 VMT_NC (see Figure 47 f)). A significant decrease in THR was also measured, which shows that there was less fuel released during the test, and is consistent with the reduced weight loss at UL94 test when compared to PA66 VMT_NC. All these elements (longer burning time, reduced combustion rate, lower pHRR and THR) imply that the barrier effect of the coating is better than PA66 VMT_NC.

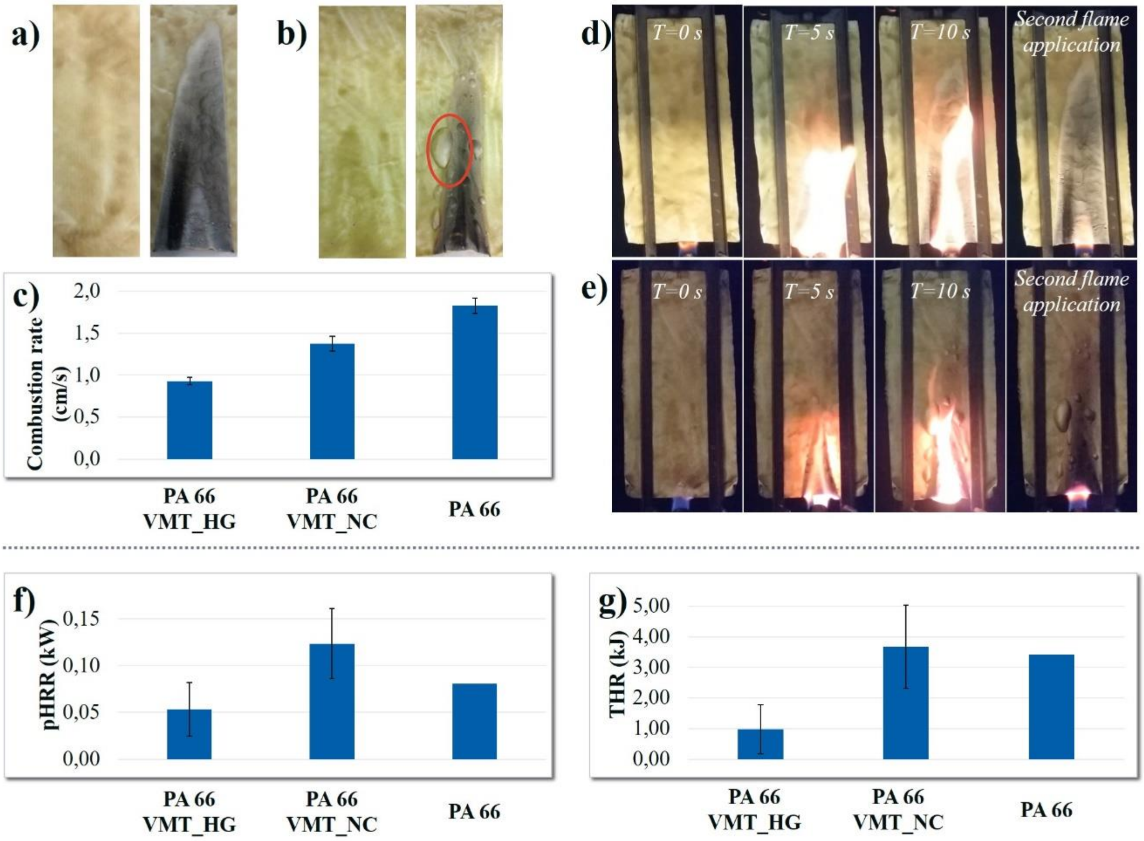

Figure 47. Digital images of a) PA66 VMT_NC and b) PA66 VMT_HG before and after test. The red circle in b) shows the formation of bubbles during the test. c) Combustion rate of PA66 VMT_HG, compared with PA66 VMT_NC and PA66. Digital images taken during UL94 test of d) Pa66 VMT_NC and e) PA66 VMT_HG. f) pHRR and g) THR results of PA66 VMT_HG compared with PA66 VMT_NC and PA66 during EN 50399 flame spread test.

Table 23. UL94 results of PA66, PA66 VMT_NC and PA66 VMT_HG

	Weight gain [%] ± σ	Weight loss [%] ± σ	Residual combustion time [s] ± σ	Complete combustion	UL rating	Combustion spread [cm/s] ± σ
PA66	/	37.4 ± 10	16.0 ± 12.2	Yes	N.C	1.83 ± 0.09
PA66 VMT_NC	67.9 ± 4	12.4 ± 3	0.4 ± 0.6	No	V-0	1.37 ± 0.09
PA66 VMT_HG	109.4 ± 6	7.3 ± 2	3.0 ± 1.1	No	V-0	0.93 ± 0.04

The only downside is the stiffening of the system because of the highly cross-linked structure, which was seen during this test. Indeed, whereas only 25% of PA66 VMT_NC cracked because of the strain induced by the set-up, this proportion increased to 60% for PA66

VMT_HG (cracked samples were not taken into account for the calculation of the pHRR and THR).

Cross section SEM images taken in the middle of the degraded area (Figure 48) show elements that were already observed for PA66 VMT_NC. That is to say, the presence of degraded melted PA66 underneath the coating and the delamination of the VMT platelets. However, the decomposition seems to be less advanced than that of PA66 VMT_NC, as PA66 is also observed in the central part of the decomposed area.

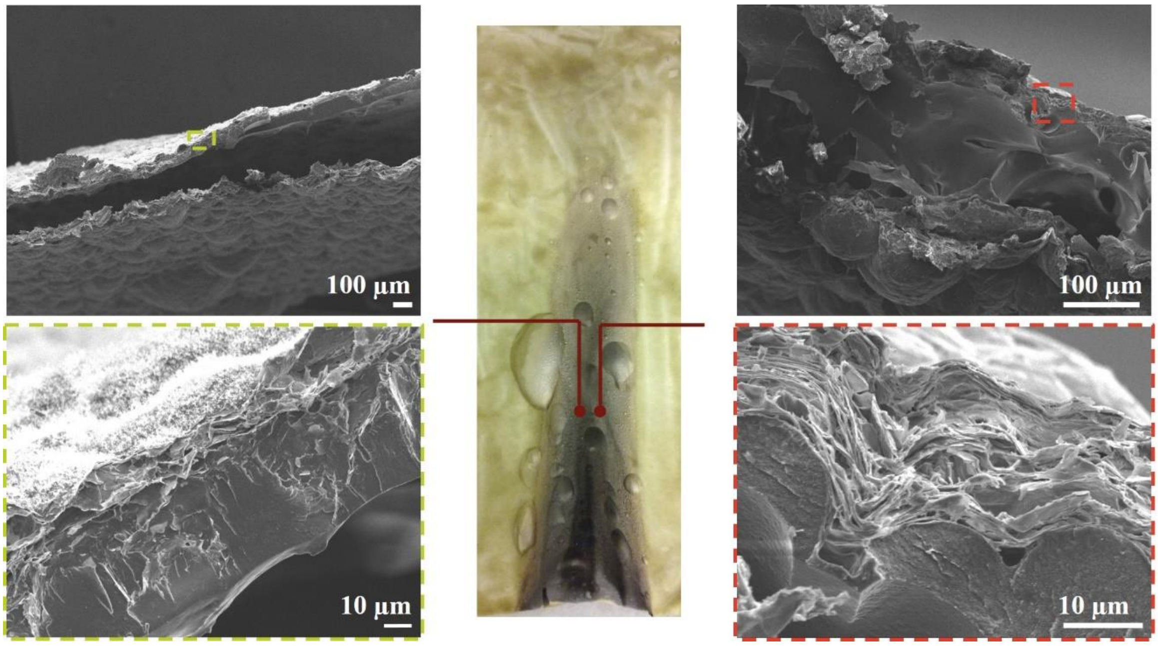

Figure 48. SEM images of the cross-section of residue of PA66 VMT_HG. The samples for analysis were extracted in the middle of the decomposed area, in the center and on the side, as indicated on the scheme.

FTIR spectrum of PA66 VMT_HG shows the same peaks characteristics of alginate and vermiculite, with the exception of additional peaks at 1235 cm^{-1} and 1714 cm^{-1} and a shoulder to the peak at 1415 cm^{-1} which corresponds to the presence of citric acid in the coating (see insert in Figure 49). The FTIR spectra of the residues of PA66 VMT_HG show that the coating is thermally stable, as there are still some remnants of organic matter even in PA66 VMT_HG_UL1 (shown by peaks around 2900 cm^{-1} characteristics of C-H bonds), which is the part of the sample directly exposed to the flame. The peak at 1624 cm^{-1} is characteristic of the presence of char. Interestingly, PA66 VMT_HG_UL1 also exhibits peaks that are characteristics of $CaCO_3$ at 1409 cm^{-1} and 876 cm^{-1}. Its presence could explain the preservation of the char when compared to PA66 VMT_NC_UL1. Indeed, it also shows remnants of carboxylic moieties from alginate evidenced by the peak at 1415 cm^{-1} (see Figure 49). As a consequence, PA66 VMT_HG_UL2 and UL3 will be systematically more preserved than PA66 VMT_NC_UL2 and UL3. The absence of peaks characteristics of $CaCO_3$ shows that the temperature was below that of calcite formation.

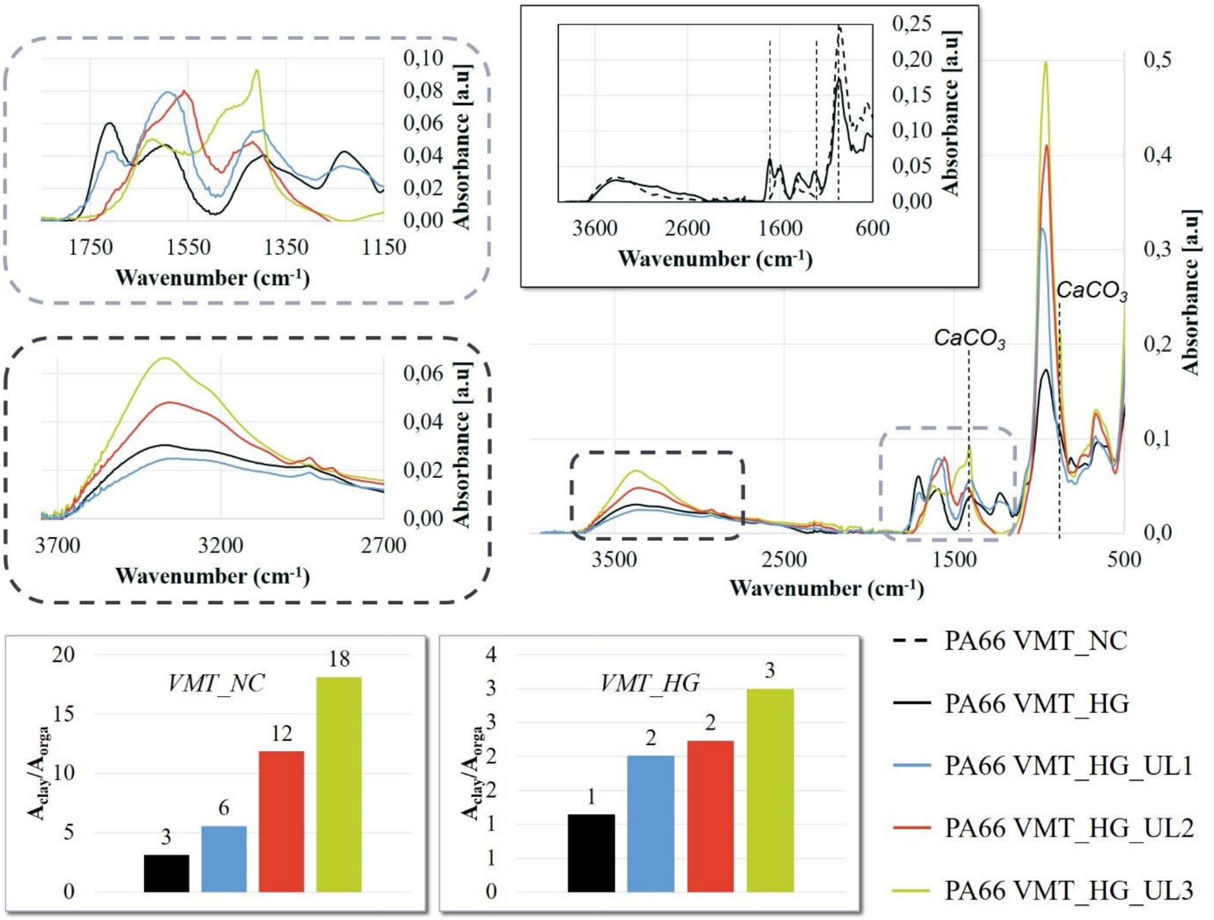

Figure 49. FTIR analysis of the residue of PA66 VMT_HG. The observations were done at different point on the surface, as indicated in Figure 35. The insert on the right compares the FTIR of PA66 VMT_NC and PA66 VMT_HG before test. The diagram on the bottom show the evolution of the ratio of the 950 cm-1 peak (A_{clay}) and the area of the peaks characteristics of organic matter (A_{orga}).

Finally, it can be observed that the decomposition of PA66 VMT_HG_UL3 is very limited as not even the peaks characteristics of char are detected. Instead, the outline of the FTIR spectra follows that of PA66 VMT_HG. The only sign of decomposition is the increase of the A_{clay}/A_{orga} ratio which shows an increase in clay proportion when compared to organic matter. As previously observed, the clay/organic ratio increases from PA66 VMT_HG to PA66 VMT_HG_UL3. However, this increase is less pronounced than for PA66 VMT_NC, which gives another clue in favor of a higher thermal stability of the cross-linked system (see Figure 49).

As can be seen on the images taken by infrared camera in Figure 50, PA66 VMT_HG conducts heat in a similar manner as PA66 VMT_NC. The decomposing area (materialized by a yellow-to-blue conical shape) increases in size before stabilizing at a certain height without reaching the top of the sample. The color gradient from the top to the bottom of the sample indicates that a temperature gradient appears. This explains the difference in composition between PA66 VMT_HG_UL3 and PA66 VMT_HG_UL1. However, the difference in flammability with PA66 VMT_NC is attributed to a better protection and thermal stability of the cross-linked coating, rather than to lower temperatures on the surface of the sample. Indeed, the thermal gradient is similar to PA66 VMT_NC. The images taken during the second flame application show that otherwise, the same protection mechanisms are taking place. Indeed, the residue formed during the test does not conduct heat, as the yellow area does not increase in size during the 10 s duration of burner application.

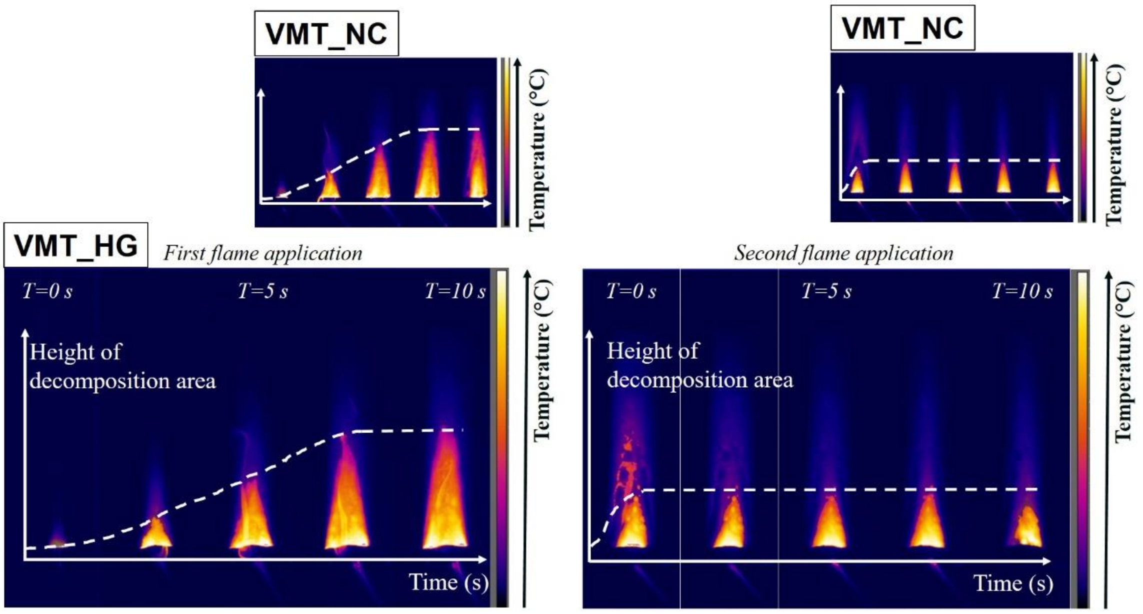

Figure 50. Temperature measurement by infrared imaging at the surface of PA66 VMT_HG during UL94 test, compared with PA66 VMT_NC

3) Combination of clays

As previously, the combination of different kinds of clay on the fire performance of alginate/clay xerogel coatings on PA66 fabrics was evaluated, and the results are presented in Figure 51 and Table 24.

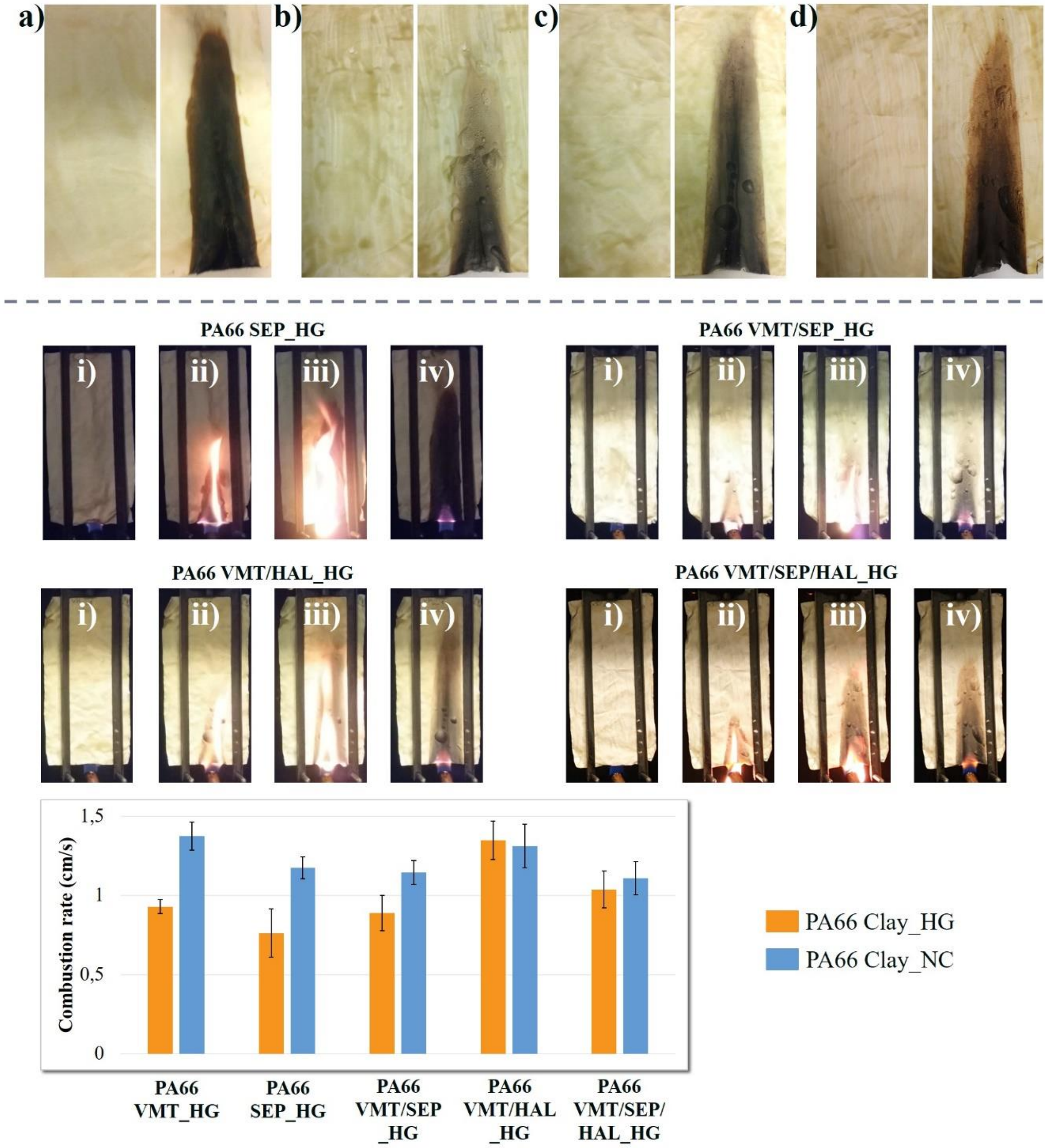

Figure 51. Digital images of a) PA66 SEP_HG, b) PA66 VMT-SEP_HG, c) PA66 VMT-HAL_HG and d) PA66 VMT-SEP-HAL_HG samples before and after UL94 test. Sequences of pictures underneath were taken during UL94 test at i) t=0 s, ii) t=5 s, iii) t= 10 s and iv) during second flame application. The diagram shows the combustion rate of all PA66 Clay_HG samples compared with PA66 Clay_NC.

Table 24. UL94 results for PA66 Clay_HG

	Weight gain [%] ± σ	Weight loss [%] ± σ	Residual combustion time [s] ± σ	Complete combustion	UL rating	Combustion spread [cm/s] ± σ
PA66 VMT_HG	109.4 ± 6	7.3 ± 2	3.0 ± 1	No	V-0	0.93 ± 0.04
PA66 SEP_HG	104.2 ± 3	7.5 ± 3	2.7 ± 1	No	V-0	0,76 ± 0.15
PA66 VMT-SEP_HG	105.1 ± 6	6.6 ± 2	1.0 ± 1	No	V-0	0.89 ± 0.11
PA66 VMT-HAL_HG	96.0 ± 7	8.6 ± 2	1.9 ± 1	No	V-0	1.35 ± 0.12
PA66 VMT-SEP-HAL_HG	108.4 ± 1	5.5 ± 1	2.2 ± 2	No	V-0	1.04 ± 0.12

Like PA66 VMT_HG, using dried hydrogel coatings improved the flammability of PA66 fabrics when compared to uncross-linked coatings. This is particularly true for PA66 SEP_HG which is rated V-0 when PA66 SEP_NC was not classified. The mass loss is smaller for all samples, the ignition is slightly delayed, and interestingly, the combustion rate was further reduced when compared to PA66 Clay_NC samples for VMT, SEP and VMT-SEP-coated fabrics. However, there was no improvement for PA66 VMT-HAL_HG and PA66 VMT-SEP-HAL_HG.

The beginning of an explanation to this improvement can be found by TGA. As illustrated in Figure 52, PA66 Clay_HG samples present two main mass loss steps, corresponding to the decomposition of alginate and PA66, with little significant difference between the different systems. What is interesting is that the decomposition of alginate is strongly anticipated in PA66 Clay_HG systems when compared to PA66 Clay_NC, whereas the degradation of PA66 is less impacted (although the onset temperature is higher, as seen in Table 25). As a result, the temperature gap between the two decomposition steps is higher in the case of PA66 Clay_HG than it is for PA66 Clay_NC. Consequently, the xerogel coatings start to protect the substrate earlier than the composite coating, which may be one element of explanation for its superior behavior.

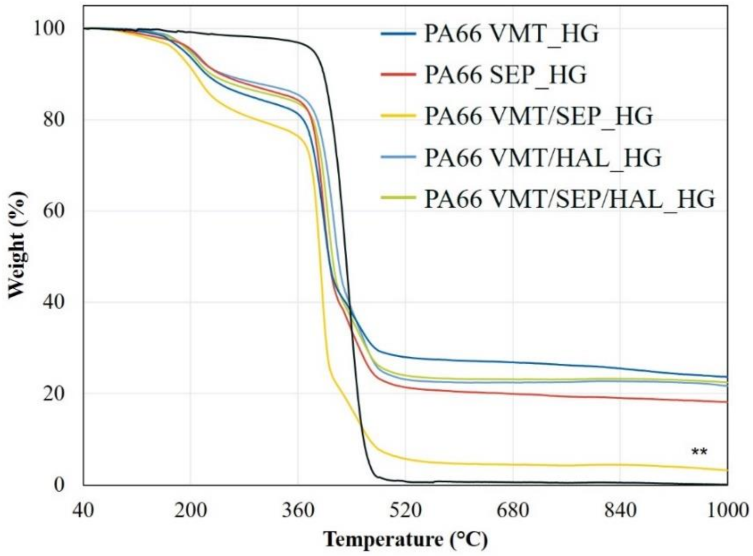

Figure 52. Thermogravimetric analysis of PA66 Clay_HG samples in nitrogen atmosphere. The curve marked with (**) presents abnormal weight loss, due to an experimental problem, but the observed decomposition temperatures are dependable.

Table 25. Thermal Gravimetric Analysis results of PA66 Clay_HG samples

	$T_{95\%}$ (°C)	Main step 1		Main Step 2		Residue@ 1000°C (%)
		T_{onset} (°C)	T_{max} (°C)	T_{onset} (°C)	T_{max} (°C)	
PA66	383	406	434	/	/	0
Alginate HG	151	176	205	646	684	24
Alg/VMT_HG	185	189	216	/	/	56
Alg/SEP_HG	156	191	220	/	/	45*
Alg/VMT-SEP_HG	187	197	221	/	/	55
Alg/VMT-HAL_HG	184	187	210	/	/	53
Alg/VMT-SEP-HAL_HG	180	194	219	/	/	54
PA66 VMT_HG	191	174	207	379	398	24
PA66 SEP_HG	204	196	216	383	397	18
PA66 VMT-SEP_HG	180	181	214	381	395	**
PA66 VMT-HAL_HG	202	178	207	391	414	22
PA66 VMT-SEP-HAL_HG	198	183	208	388	404	22

Before UL94, cross section SEM images of the samples show the deposition of a conformal dense coating (Figure 53).

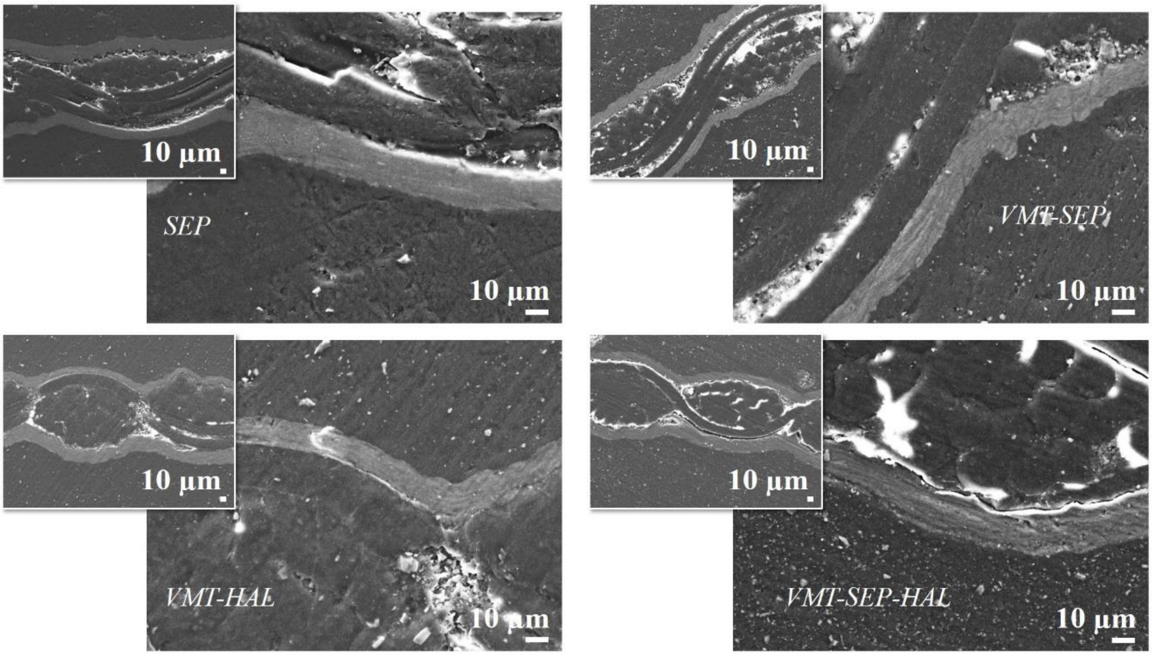

Figure 53. SEM images of cross sections of PA66 SEP_HG, PA66 VMT-SEP_HG, PA66 VMT-HAL_HG and PA66 VMT-SEP-HAL_HG.

All systems containing VMT particles show a preferential orientation of the platelets parallel to each other and to the surface of PA66 fibers. No organization can be seen for PA66 SEP_HG as the coating is very compact, but it is likely that the SEP particles are also oriented. Indeed, after UL 94 test, the cross section SEM images of the residue display SEP needles oriented in the same direction (Figure 54). The coating shows delamination that has not been observed for PA66 SEP_NC, with large bubbles forming on the surface. PA66 was partially preserved, and the remaining decomposed polymer is supported by the residual coating (no lack of adhesion between the substrate and the charred alginate/SEP system). The SEP needles are embedded in foils of char oriented parallel to each other. All the other coatings show delamination between the VMT particles (that otherwise keep their pre-test organization), and decomposed PA66 polymer underneath. Those containing SEP also present needles embedded in char between the VMT platelets. Interestingly, the residue presents a lower decomposition degree when compared to PA66 Clay_NC, showing the better protection offered by the cross-linked system. Indeed, the amount of remaining PA66 is higher, especially on the side of the residue, where the sample maintained its integrity.

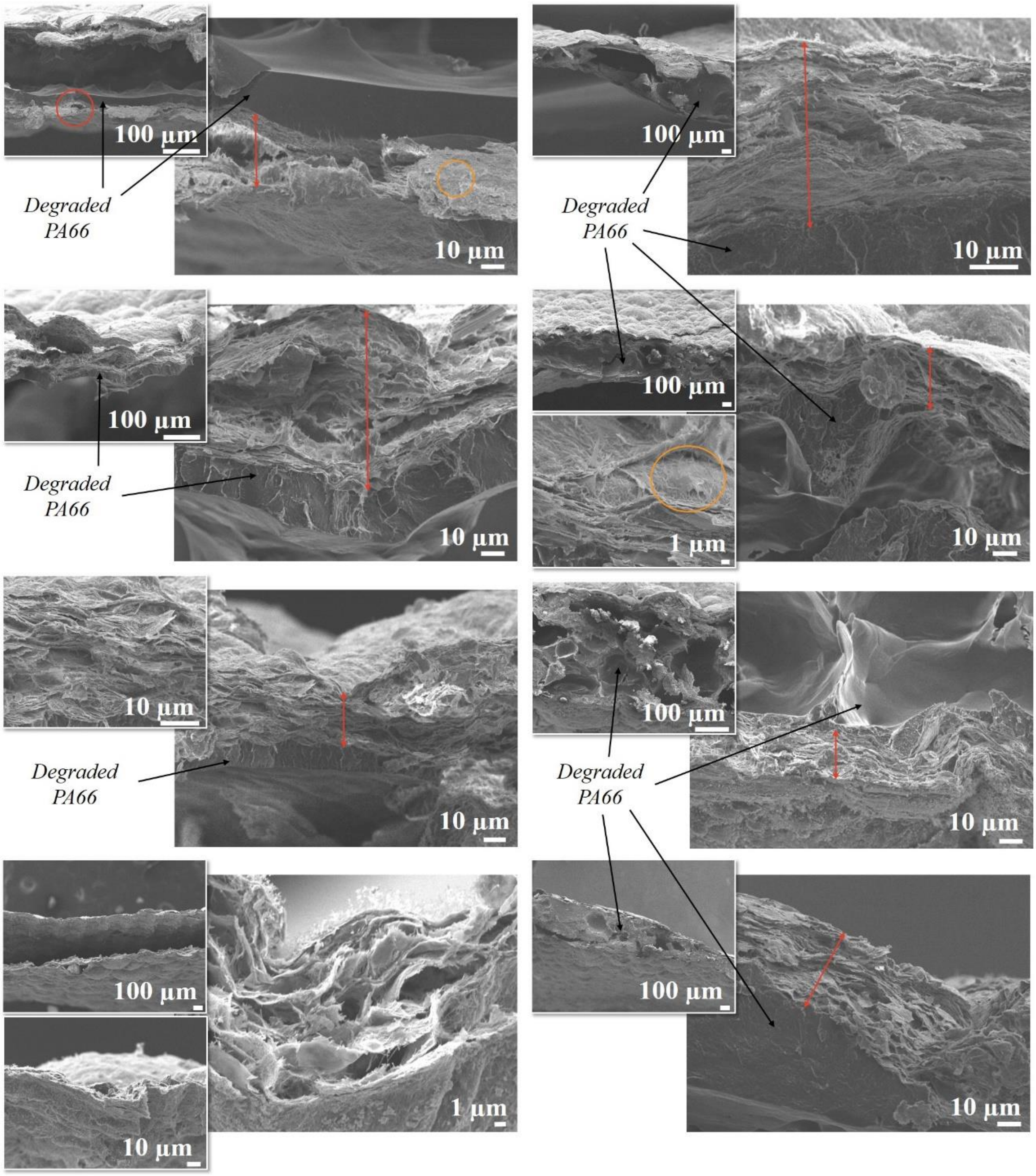

Figure 54. SEM images of residues from PA66 SEP_HG (first row at the top), PA66 VMT-SEP_HG (second row), PA66 VMT-HAL_HG (third row) and PA66 VMT-SEP-HAL_HG (last row at the bottom). Left column: taken in the middle of the decomposed area at the center and right column: taken in the middle of the decomposed area, on the side, as presented in Figure 34.

The high thermal stability of the coating is illustrated by the FTIR spectra of the residues, taken at different points compared to the flame (Figure 55). First, the spectrum of PA66 Clay_HG before test is the same as PA66 VMT_HG, as both display the peaks characteristics of alginate, citric acid and their respective clays.

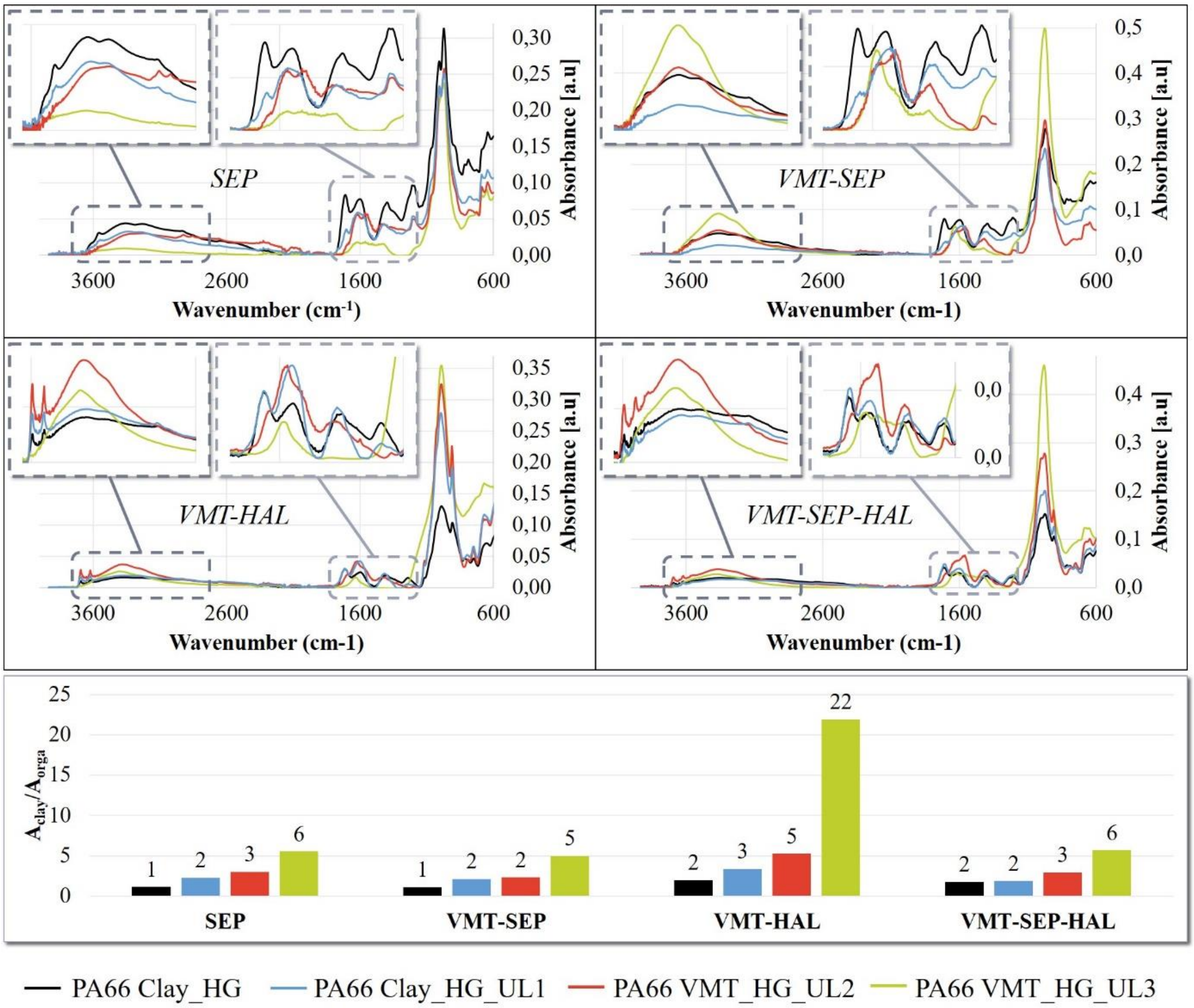

Figure 55. FTIR analysis of the residue of PA66 Clay_HG. The observations were done at different point on the surface, as indicated in Figure 35. The diagram on the bottom show the evolution of the ratio of the 950 cm^{-1} peak (A_{clay}) and the area of the peaks characteristics of organic matter (A_{orga}).

Interestingly, the residue directly exposed to the flame does not show the presence of $CaCO_3$ as it was the case for PA66 VMT_HG_UL3. It could be due to the decomposition of $CaCO_3$ to CaO. This would indicate that the decomposition was more advanced than the PA66 VMT_HG, indicating a better thermal stability of the latter. Otherwise, all of them show the presence of peaks at 1640 cm^{-1} and 1546 cm^{-1} characteristics of char, as well as the peak around 1415 cm^{-1} corresponding to carboxylic function. The only exception is PA66 VMT-HAL_UL3 which is in the most advanced decomposition state, as illustrated by the presence of a single peak around 1640 cm^{-1}. They all lose the peaks corresponding to citric acid, showing that it is the first component to degrade. Then, all PA66 Clay_HG_UL2 FTIR spectra display the peaks of citric acid, and PA66 Clay_HG_UL3 FTIR spectra are all very similar to unburnt PA66 Clay_HG, proving the high thermal stability of the coating. The FTIR spectrum of PA66 VMT-SEP-HAL_HG_UL3 follows the outline of the FTIR spectrum of PA66 VMT-SEP-HAL_HG almost perfectly. The only hint of decomposition in PA66 SEP_HG_UL3 and PA66_VMT-SEP_HG_UL3 is the fading of the peak characteristic of the C=O bond in citric acid. As illustrated in Figure 55, the ratio clay/organic increases from PA66 Clay_HG to PA66_Clay_UL3. This increase is not very pronounced when compared to PA66 Clay_NC. Interestingly, it is more pronounced for PA66 VMT-HAL_HG, which confirms the previous observation that its decomposition stage was more advanced.

As was shown for PA66 VMT_HG, this is attributed to a better thermal stability of the coating rather than a higher thermal gradient than PA66 Clay_NC during the test, as illustrated by IR images in Figure 56.

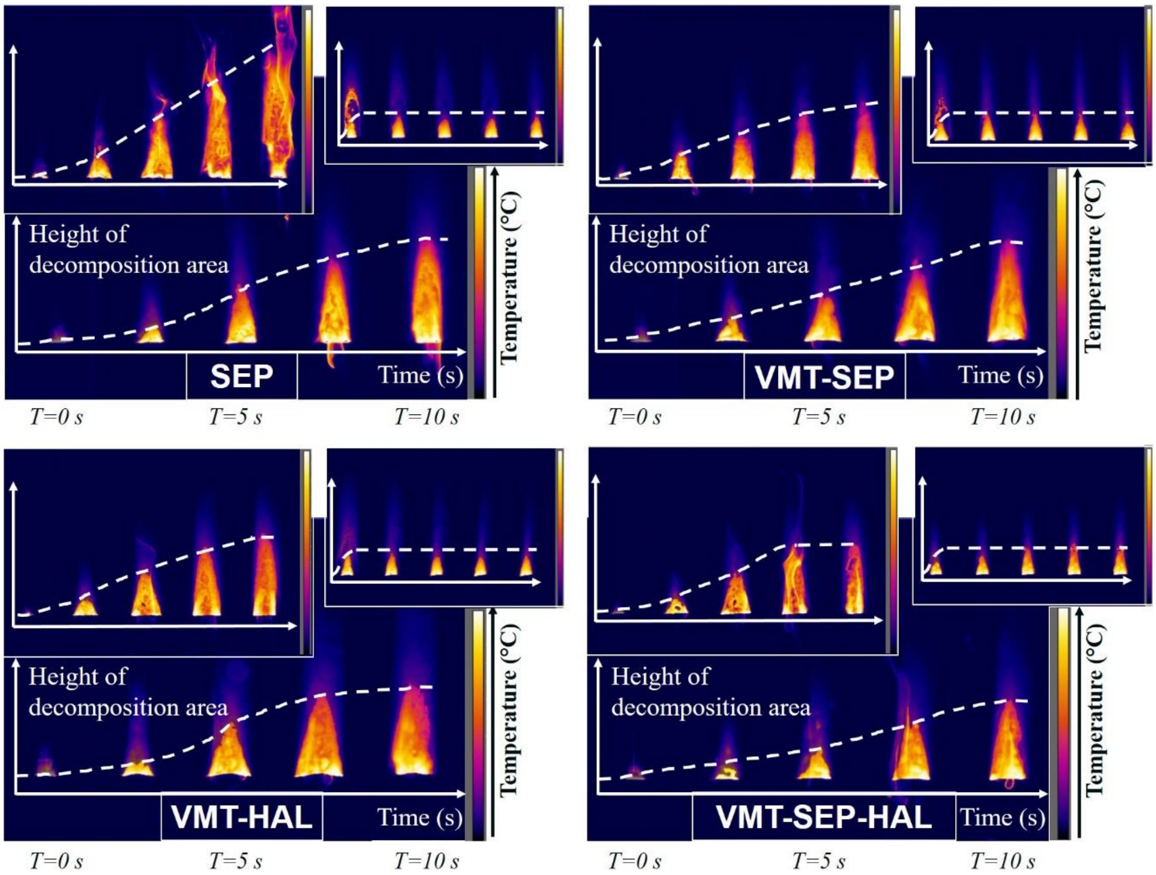

Figure 56. Temperature measurement by infrared imaging at the surface of PA66 Clay_HG during UL94 test. Each image was taken at 2.5 s intervals, from t=0 s to 10s. Inserts on the right show the second flame application. Inserts on the left show the same experiment on PA66 Clay_NC samples, as a reminder.

Indeed, as it was explained in the previous section, the temperature gradient (indicated by the color gradient from yellow to blue) is the same for all PA66 Clay_HG samples. What can be observed is that the decomposition area increases in size, before reaching a maximum height. Afterwards it does not change further. During the second flame application, it can be seen that all residues formed during the test do not conduct heat, as the colored area does not change in size for 10 s.

PA66 Clay samples were also tested on a EN 50399 test to measure the HRR during flame spread. Interestingly, the pHRR and THR of all PA66 Clay_HG samples are lower than those of PA66 Clay_NC (see insert in Figure 57).

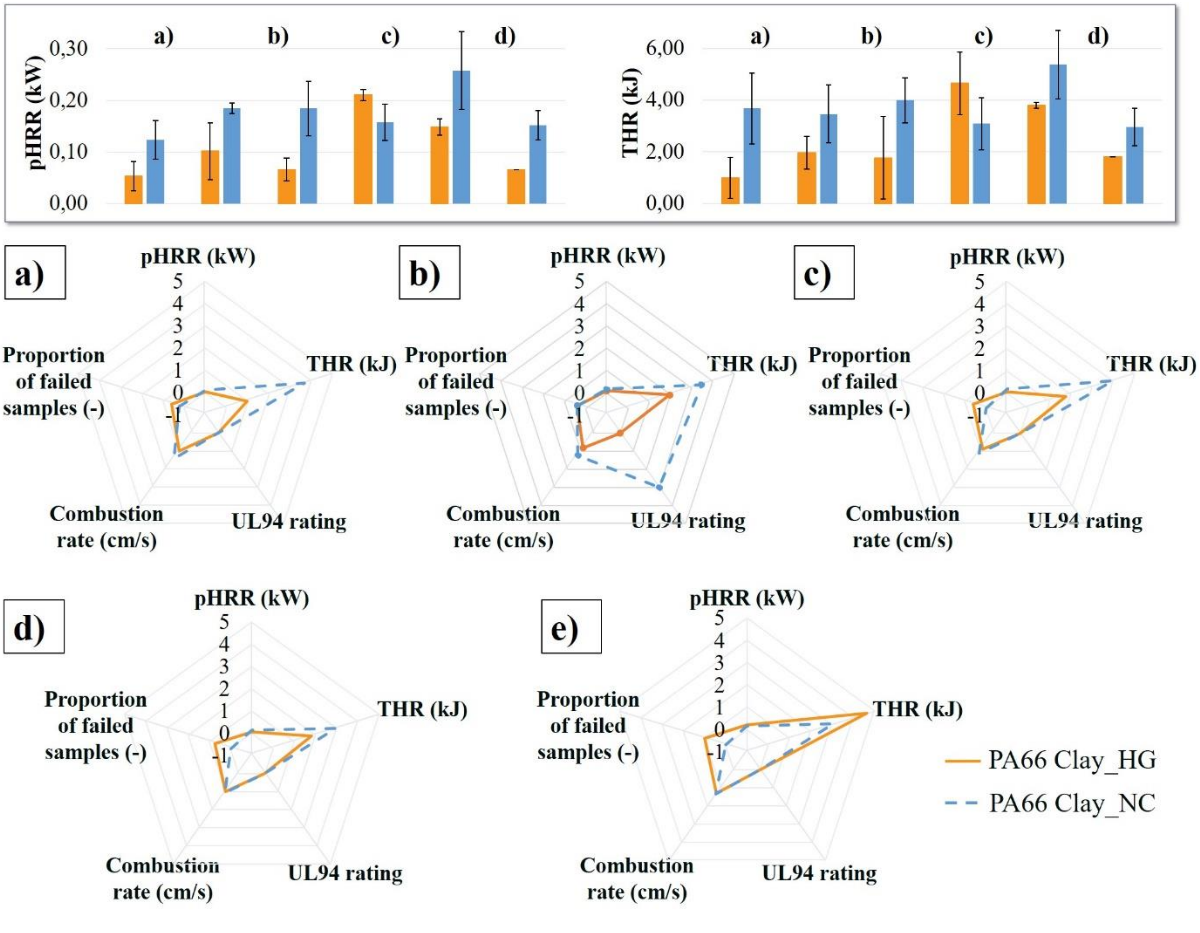

Figure 57. Top: pHRR and THR results obtained during the EN 50399 flame spread test for a) PA66 VMT, b) PA66 SEP, c) PA66 VMT-SEP and d) PA66 VMT-SEP-HAL_HG, compared with PA66 Clay_NC. The high variation observed in the result is due to the experimental set-up inducing edge effects (side burning). Bottom: radar diagrams for a) PA66 VMT, b) PA66 SEP, c) PA66 VMT-SEP, d) PA66 VMT-SEP-HAL and e) PA66 VMT-HAL, comparing relevant results obtained during UL94 and EN 50399 fire tests for NC and HG samples. UL94 ratings was adapted as follows: V-0 = 0, V-1 = 1, V-2 = 2, and non rated = 3. The proportion of failed samples was calculated as followed: number of fails/number of samples tested. It is a number between 0 and 1.

However, none of the systems improved the stiffening of the sample, and they all presented a proportion of failure going from 40 to 75 % (the failed samples were not taken into account for the calculation of pHRR and THR). The case of PA66 VMT-HAL is even more extreme as none of the samples sustained the stress during the test. Still, when the relevant parameters in all tests are compared, it appears that cross-linked coatings further improve the flammability of PA66 when compared to un-cross-linked composite coatings, for all composition except PA66 VMT-HAL_HG because of the fragile nature of the film. This shows that even if xerogel samples improve the flammability of PA66 when compared to composite, it is necessary to improve their mechanical properties.

4) Conclusion and discussion

The results show that adding a crosslinking step to form hydrogels before drying the composite clay coatings can improve the flammability of PA66 fabrics when compared to uncross-linked composite clay coatings (this is particularly remarkable with PA66 SEP_HG). Indeed, at UL94 test, all samples are rated V-0, the combustion rate is decreased and the ignition is delayed. The burning is also less intense, which was shown by the decrease of pHRR values calculated obtained during heat release measurements. The thermal stability was found to be higher than composite coatings as the decomposition of the system was less severe. Finally, the lower mass loss and reduced THR show that there was less decomposition. These elements point out towards the establishment of a better physical barrier. First, the coating can trap the combustible decomposition gases between the coating and the substrate, but also has the capacity to accommodate the stress due to the increase in pressure. This was observed as huge bubbles formed during the test. Finally, it was observed that the cross-linked coating decomposed earlier than the uncross-linked systems. This can also explain their better behavior, as the protective effect of the coating is put sooner into place.

In this study, a cross-linking system was designed to obtain a conformal coating with little retraction. While the interest of the concept for the fire retardancy of PA66 fabrics was proven, it is true that the stiffening of the coating is a disadvantage, which could be easily overcome by optimizing the crosslinking, for example.[422]

From the results obtained it seems that the systems with VMT platelets or VMT in combination with SEP needles can help achieving the best results (in term of UL94, combustion rate, pHRR, THR and resistance) for cross-linked systems, and *a fortiori* for this whole study. While the sample coated with VMT-HAL achieved good results at UL94, the improvement when compared to PA66 VMT-HAL_NC was not especially significant. In the end, they were found to have a worse behavior than PA66 VMT-HAL_NC because of their fragility. This can be explained by the fact that alginate when mixed with HAL nanotubes interacts with their inner surface, which is positively charged. Therefore, alginate chains are confined within the HAL nanotubes. As a result, they do not participate to load discharge within the coating and there is less interaction between them and the particles outer surface. Combined with the stiffening of the matrix due to cross-linking, this can explain the excessive weakening of the system.[423]

III. Conclusion

As a conclusion, composite coatings from alginate/clay dispersion with a high filler content were deposited on PA66 fabrics in a facile one pot process. The flammability of the sample was improved to the point of being rated V-0 at UL94 test. It was found that the protection mechanism of these coatings was similar to that observed in layer-by-layer systems. In other words, the protection mechanism was attributed to:

- a physical barrier effect (it slows down combustion rate, contributes to self-extinguishment). VMT and SEP particles were found to contribute to this effect in two different manners. The platelet-like morphology and the piling of VMT particles slow down the release of combustion gases, probably thanks to the high tortuosity of this architecture. This causes a swelling of the coating as the particles delaminate. SEP particles act in a different manner: the high concentration of SEP creates a compact composite charred structure where the needles are tightly glued together in alginate char. This last phenomenon was the most efficient in reducing the combustion rate. Both mechanisms can be combined to have a complementary effect.
- The early decomposition of the coating. This condition is needed so that the protective structure can form ahead of the PA66 fibers decomposition. It forms a composite structure of char and clay at a lower temperature than PA66 degradation. Afterwards, the char further decomposes until a stable final state, as suggested by FTIR, but there is no major transformation. Therefore, the char/clay residue constitutes a protective structure that blocks the heat and the flame and protects the substrate as well as the rest of the sample in the early stage of the test.
- The thermal stability of the coating and its residue.

- The robustness of the coating, that remains in place during the test as it keeps the substrate shape.
- The insulation brought by the coating. As it does not conduct heat, the heat transfer from the flame is blocked and a thermal gradient takes place along the sample. This limits the decomposition and increases the char/clay proportion of the residue as the temperature decreases.
- The support brought to the melting PA66, as the coating remains in place during the test. This phenomenon allows to suppress the hazardous melt-dripping.

The downside of these systems was however the intense flaming which increased the heat release during the fire test.

Afterwards, a new concept was explored and it was found that forming an alginate composite hydrogel matrix before drying the coatings had a beneficial effect on reducing the flammability of PA66. The protective structure is indeed formed earlier, and the physical barrier and thermal stability of the systems were improved by Ca^{2+} and citric acid cross-linking. As a result, the combustion rate and mass loss of the samples were decreased. Moreover, the heat release and the total heat release were decreased, which is an improvement compared to PA66 Clay_NC samples. The downside here was the stiffening of the samples as well as the high weight gain, and the weakening of the coating and residue because of the crosslinking, which caused an increased number of failures. It should be possible to improve this point, either by optimizing the cross-linking, by combining covalent and non covalent cross-linking, as well as engineering the interaction between the matrix and the particles.

Finally, the feel and flexibility of the original fabrics were lost upon coating, and the systems should therefore be improved accordingly. Moreover, the adhesion was satisfying enough for this study, but it should also be improved to envision a concrete application for these systems.

Based on the part of this work related to hydrogels, they were also used as hydrated phases to fill 3D printed innovative multimaterials developed within the framework of the Firebar Project by Laura Geoffroy. Exceptional fire retardancy was obtained, and the results were published in Polymer Degradation and Stability in 2020.[424] This highlights the potential of such materials in the field of fire protection.

IV. Annex 3-1: Energy X-Ray mappings of PA66 Clay_NC

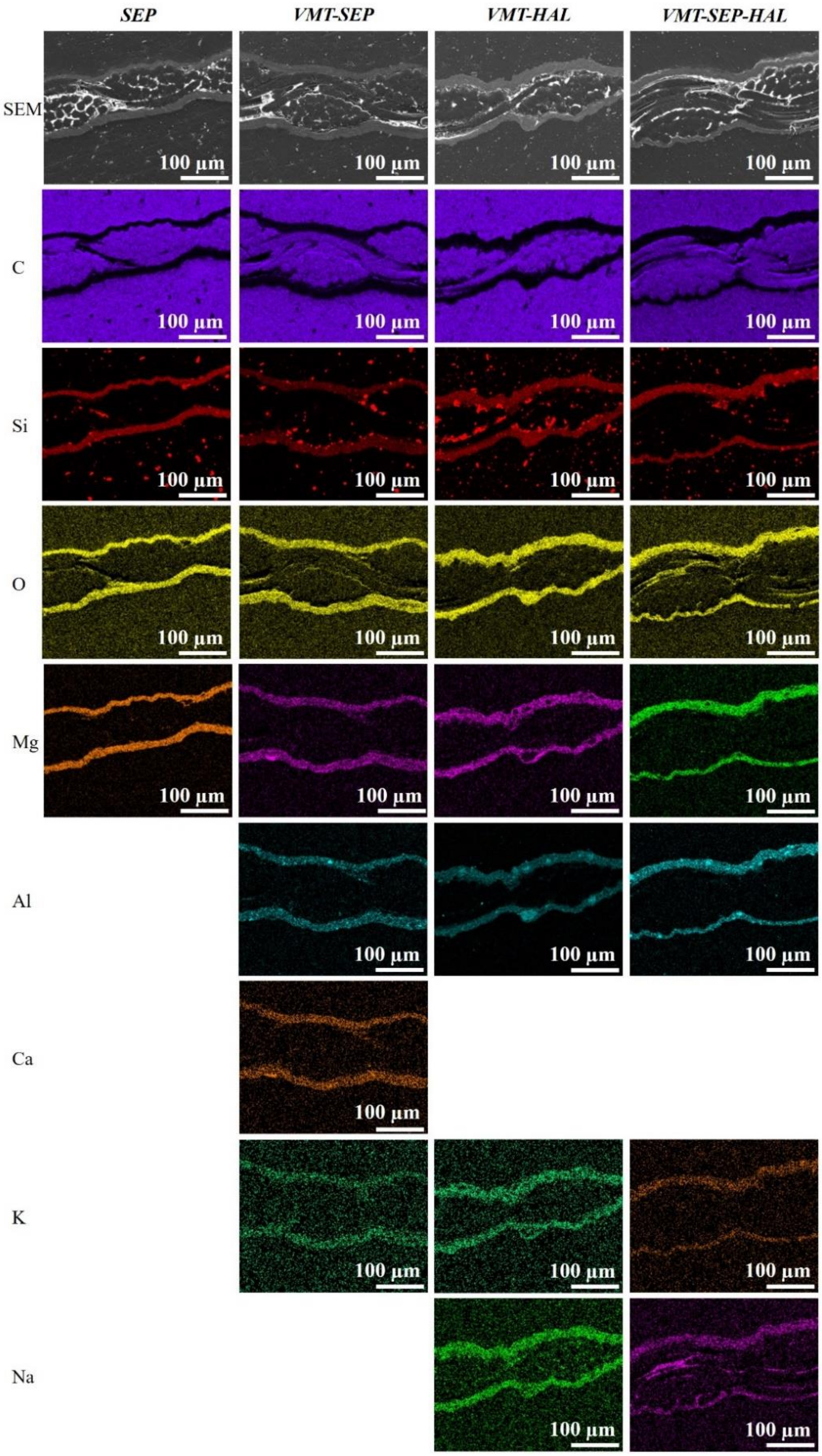

V. Annex 3-2: Energy X-Ray mappings of PA66 Clay_HG

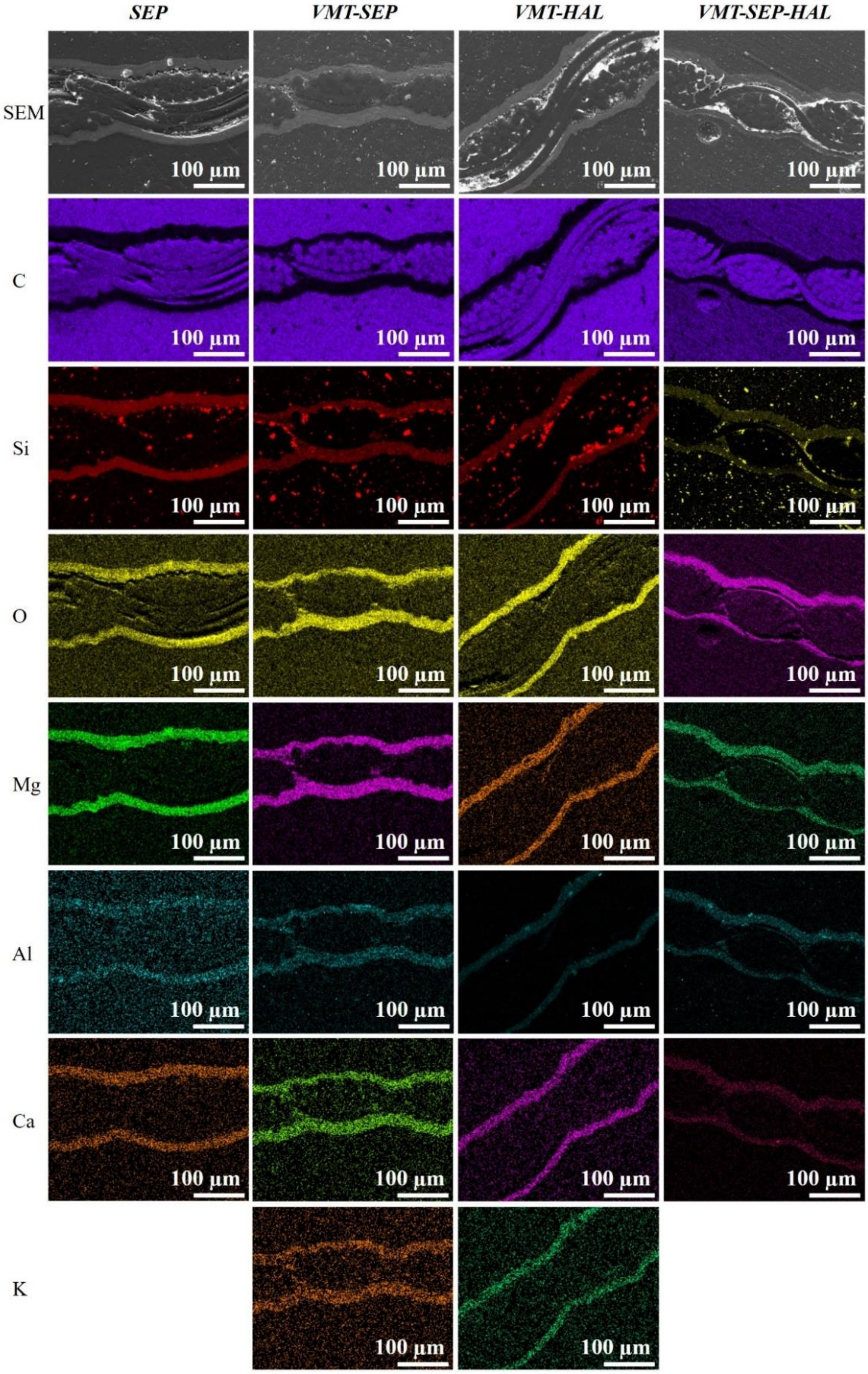

Chapter 4 . Low-emissivity coatings for the fire protection of raw and formulated polymer substrates

The fire risk of polymers is partly linked to their short time to ignition. Increasing this parameter through a surface treatment (for example) would be a sure way to limit the flame spread and increase people safety's in case of a fire. As reported in chapter 1, a nanocomposite barrier made by LbL could effectively increase the time to ignition by several seconds in some cases, which was attributed to mass transfer delaying due to a physical barrier effect. However, the increase in time to ignition is not long enough to have a significant impact on the flammability.

In the present chapter, the use of a thermal barrier was considered to significantly increase the time to ignition of polymers. More specifically, the ability of certain materials to reflect thermal radiation was used to design a coating aiming at limiting heat absorption by the material. Indeed, the ease of ignitability of polymers is mainly due to their high absorption of infrared radiation.[4] Considering that radiative heat transfer is dominant in middle to large scale fires, it is relevant to lower the heat absorptivity of polymers. Since it is a surface property, the strategy chosen here is to increase the reflectivity of the surface by using thin coatings with a low emissivity in the infrared range. Altering this property was shown to have a huge impact on the flammability of materials. As the emissivity of materials is partly linked to the surface aspect of a given material, this strategy is particularly adapted for the protection of flat polymer substrates such as sheets and plates, whose fire protection using thin coatings is trickier than foams and textiles. In this part, PA6 was chosen as the substrate. It is indeed a common polymer extensively used for various technical applications and its behavior in case of a fire is well known and has been extensively studied. First, the choice of the materials and of the coating design are explained. Then, the deposition of low emissivity coatings on PA6 is described, and

---

[4] It is also partly linked to their low thermal conductivity, creating hot spots on the surface.

their effect against a radiative fire scenario is evaluated. Finally, the combination of this surface treatment with fire-retardant fillers incorporated in the bulk of the polymer was investigated.

This part was made in collaboration with Prof. Frédéric Sanchette (LASMIS, Université de Technologie de Troyes) who performed the deposition of the low emissivity coatings. Some of the results presented in this part are published in ACS Applied Polymer Materials (2020).

I. Design of metal-dielectric coating

1) Deposition and characterizations

Metals such as Au, Ag, Pt, Cu or Al are near perfect reflectors in a large range of the UV-visible and infrared area of the electromagnetic spectrum. This is due to their high density of free electrons that screen the electromagnetic field within a very small thickness. Therefore, they are materials of choice for the conception of thin low emissivity coatings. However, they are prone to lose their reflective properties by environmental or high temperature corrosion. It is thus necessary to protect them against external aggression, without impacting their optical properties. Thin layers of passive transparent refractory dielectrics are usually used to this end. Dielectrics are however strong absorbers in the infrared and hence, this layer should be as thin as possible so as not to impact the emissivity of the metallic layer.[425] Moreover, it should be compatible with the chosen metal.

As it was mentioned before, thermal radiations are infrared rays with wavelengths between 1 and 10 µm. Therefore, SiO_2 and Al_2O_3 would be good materials to consider since they can sustain high temperatures and have a large transparency range (from 0.16 µm to 4 µm and from 0.19 µm to 5 µm respectively).[426] Here, we chose to use Al_2O_3-protected aluminum as metal-dielectric thin coating. Aluminum may not be the most reflective metal but it has the broadest reflectivity range and is more resistant to environmental aggressions. Al_2O_3 has the broadest transparency range and is highly compatible with aluminum. Afterwards, to study the influence of the metal on the performance of the coating, copper was used instead of aluminum. Au, Pt or Ag were not considered at first because of their high cost.

Metal-dielectric coatings were deposited on PA6 plates by pulsed DC magnetron sputtering. This is a low pressure and low temperature technique, which ensured that the polymer would not degrade during the deposition. It also guaranteed a good control of the thickness of the deposit. First, the substrate was cleaned by argon plasma treatment, in order to enhance the adhesion of the metal to the polymer. Then, a thin layer of metal (aluminum or copper) was deposited by sputtering a target made out of the corresponding element. Once a thin film was obtained, oxygen was introduced in the chamber and reacted with sputtered aluminum to form Al_2O_3. The process is schemed in Figure 58.

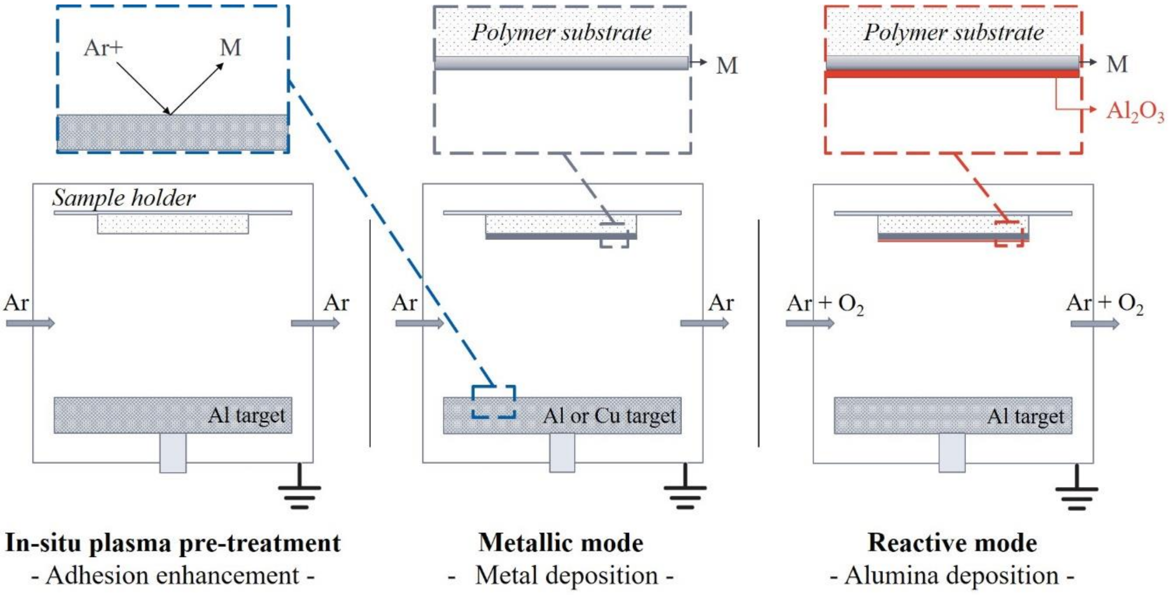

Figure 58. Scheme of the Physical Vapor Deposition process: pulsed DC magnetron sputtering, for the deposition of metal/dielectric films on polymer substrates.

Surface of the coated plates appear smooth and metallic, with the respective grey and orange color of aluminum and copper, dulled out by the presence of Al_2O_3 (Figure 59 a)). Tape peel tests were performed to have a qualitative feeling of the adhesion of the coating on the PA6 plates. It was found that the plasma pre-treatment allows to have a good adhesion, as a limited amount of metal/dielectric was peeled off (see Figure 59 a)). A visual assessment of the surface rates the adhesion to 5B for both aluminum and copper, which is the best classification.

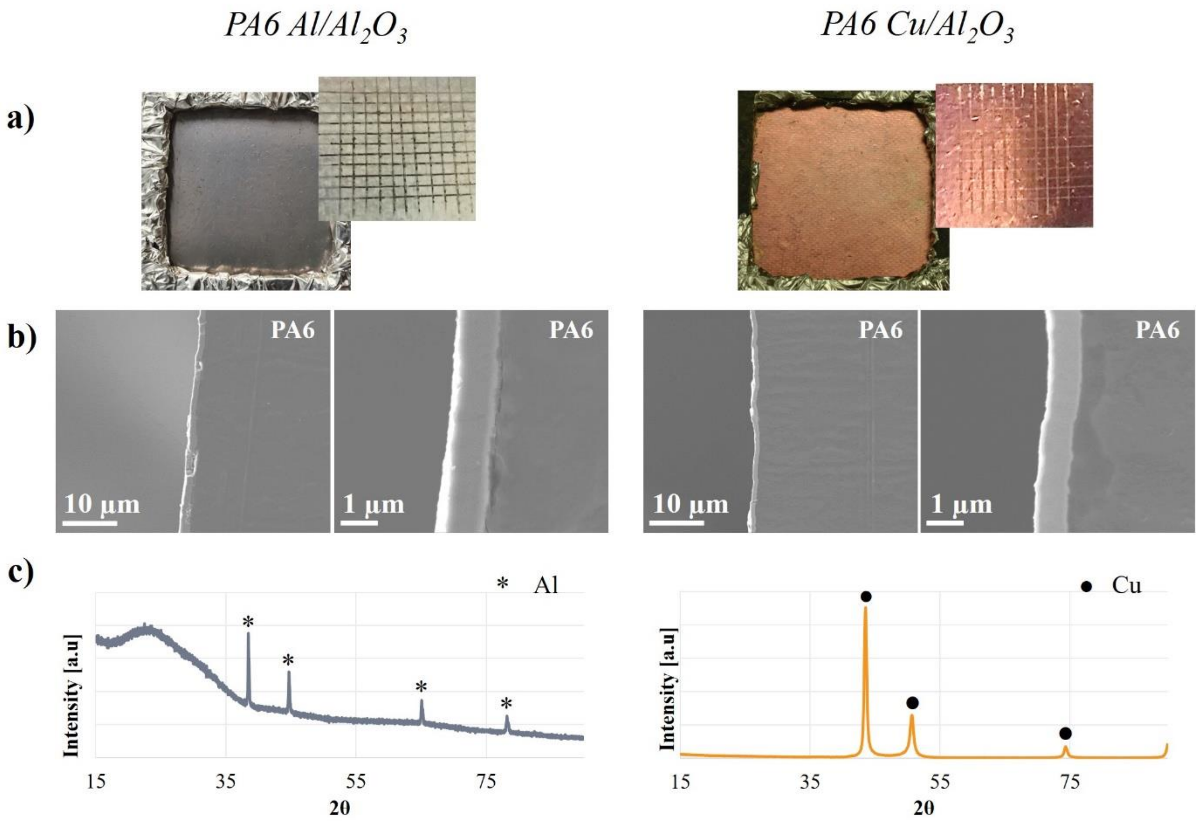

*Figure 59. a) digital images showing the surface of PA6 Al/Al_2O_3 and PA6 Cu/Al_2O_3. Inserts show the results of the tape peel test. b) SEM pictures of cross-sections of PA6 Al/Al_2O_3 and PA6 Cu/Al_2O_3 at different magnifications. c) XRD of Al/Al_2O_3 and Cu/Al_2O_3 on glass substrates. * shows the distinctive peaks of Al, while ● notes the peaks of Cu.*

SEM observations (Figure 59 b)) and Al and Cu Energy Dispersive X-Ray mappings were performed on coated PA6 cross-sections (Figure 60 a) and b) respectively). They show the deposition of thin and dense aluminum and copper based coatings. The coatings are continuous and as a result, in both cases, the Al_2O_3 top layer cannot be distinguished from the metallic layer. This problem was overcome by oxygen X-Ray mapping and indeed, a high concentration of oxygen atom is seen, which can be attributed to Al_2O_3. The thickness of both systems was measured and can be found in Figure 60 c). It should be stressed out that the Cu layer (0.61µm) is thinner than the Al layer (0.94 µm). The reason for that is that in order to ensure adhesion between Cu and the substrate, the deposition time needed to be shortened when compared to Al to prevent delamination. Therefore, the total thickness of Al/Al_2O_3 was found to be at 1.02 ± 0.03 µm while Cu/Al_2O_3 has a thickness of 0.690 ± 0.04 µm, as determined by SEM observation of the cross-sections. The layer of Al_2O_3 was found to be around 0.082 µm thick. According to XRD analysis, it also seems that this layer is amorphous. Indeed, whereas the diffractograms

(Figure 59 c) show the characteristic peaks of Al and Cu respectively, the specific peaks of crystalline phases of Al_2O_3 are not visible.[5]

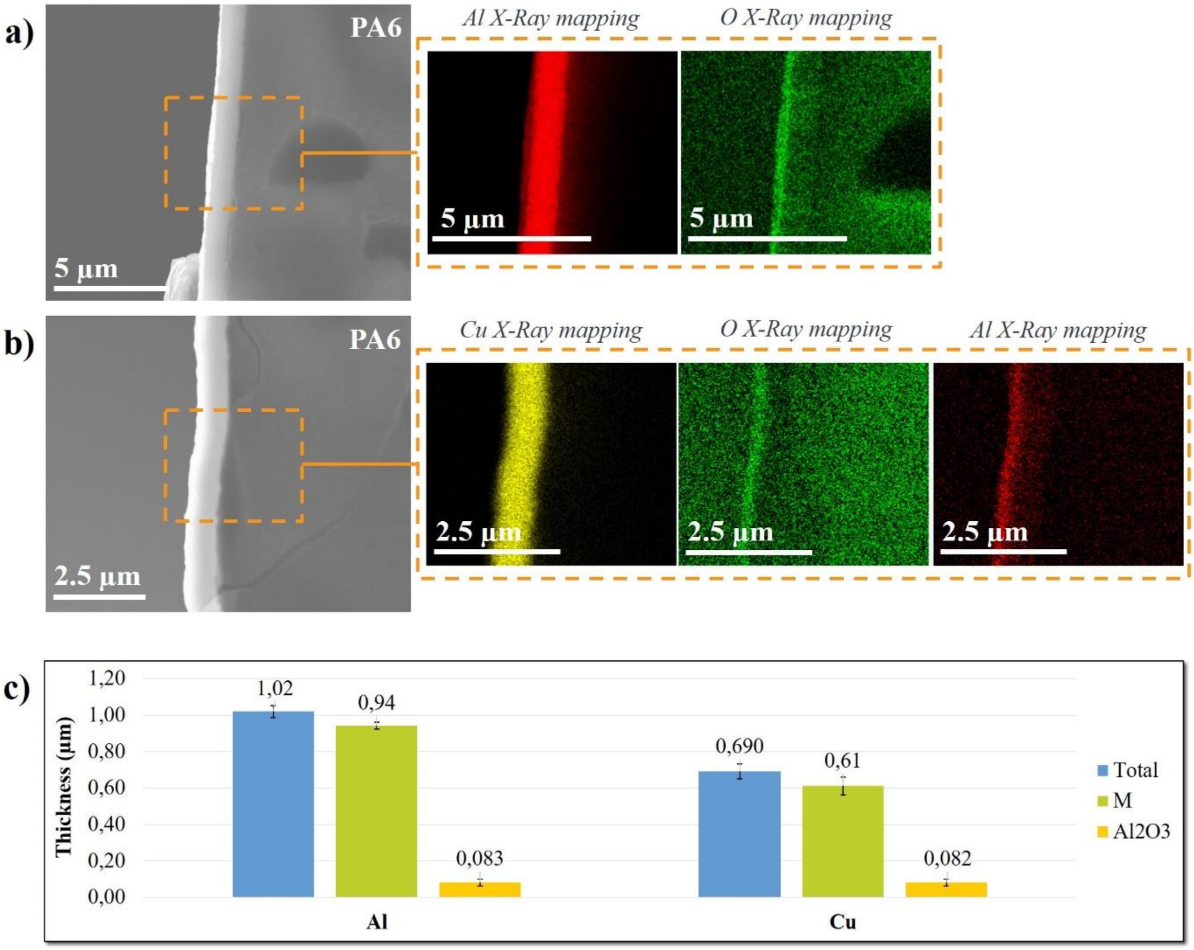

Figure 60. a) SEM, Al X-Ray mapping and O X-ray mappings of a cross-section of PA6 Al/Al_2O_3. b) SEM, Cu X-Ray mapping, O X-Ray mapping and Al X-Ray mapping of a cross-section of PA6 Cu/Al_2O_3. c) Thickness measurements.

Total hemispherical emissivity of the coated surfaces was measured at 20°C by infrared diffuse reflectance measurements through an integrating sphere. The surface of uncoated PA6

---

[5] It should be stressed out that the large hump shape between 15° and 35° on the Al/Al2O3 XRD diffractogram is due to the glass supports. This is not shown on the Cu/Al2O3 diffractogram, as the method was changed in order to observe the diffraction peaks of Cu (see the Materials and Methods section, part III).

has an emissivity of 0.95, which shows its limited reflectance. With the deposition of an Al/Al_2O_3 thin coating this value drops down to 0.15, which is consistent with the values found in the literature for oxidized aluminum.[359] The emissivity of Cu/Al_2O_3-coated PA6 is quite similar, although slightly higher (0.24) (see Figure 61). The high emissivity when compared to a pure metal (between 0.01 and 0.05 usually) is due to the presence of the Al_2O_3 layer.

As a conclusion, decreasing the emissivity of a substrate is possible with the addition of protected metal thin layers, which means that most of infrared rays responsible for radiative heat transfer will be reflected.

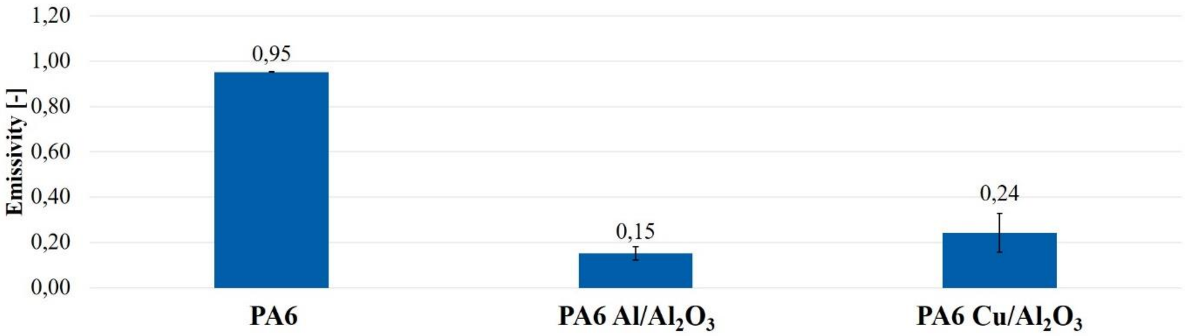

Figure 61. Total hemispherical emissivity of PA6, PA6 Al/Al_2O_3 and PA6 Cu/Al_2O_3 as calculated by infrared diffuse reflectance measurement at room temperature.

2) Behavior against a radiative thermal constraint: mass loss cone calorimetry.

In order to simulate a radiative thermal constraint, the samples were tested with a cone calorimeter test under a 50 kW/m² heat flux. It corresponds to the late stage of a developing fire.[381] The barrier effect of the coating was checked by monitoring the temperature at the back of the sample. To this means, a thermocouple was put in contact with the polymer and maintained in place with a calcium silicate board so that it does not pierce the deposit during the test (Figure 62). To prevent early decomposition from the sides of the sample and improve repeatability, non-flammable glue was deposited along the edges of the sample and of the calcium silicate plate to hold them together.

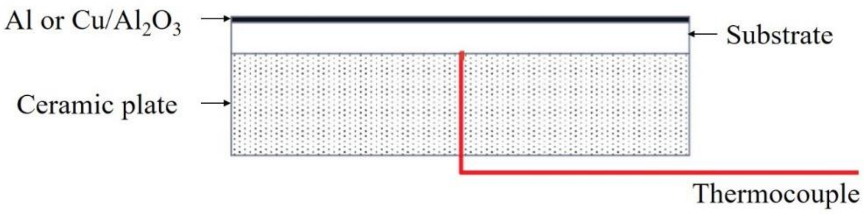

Figure 62. Scheme of the experimental set-up for MLC test.

A polyamide plate submitted to a radiative heat flux heats up quickly. Bubbles appear on the surface while a large amount of smoke is produced as it starts to decompose, before it ignites after 73 s. The HRR curve of PA6 exhibits a typical shape of a thermally intermediate thick non charring material.[381]

When a thin low emissivity metal/dielectric coating is deposited on its surface, the ignition behavior of PA6 is remarkably impacted. Both aluminum and copper coated samples behaved similarly. At first, no evolution of the aspect of the surface was observed for a long time, which means that the degradation temperature was not reached. Then, the substrate started to degrade and swell on one edge, resulting in the failure of the coating and the release of degradation products through the cracks. No delamination was observed at this point, however, showing the good adhesion between the substrate and the metallic film. Moreover, the coating remained glossy, and it is safe to say that both aluminum and copper were successfully protected by the Al_2O_3 layer.

Just before ignition, the behavior of the sample was complex. Even as the coating was cracked, ignition did not occur immediately. Indeed, degradation gases were temporarily held underneath the swollen surface, before they were released in a burst as the surface deflated. At this point, the coating looked like a crumpled cracked metal sheet, while the polymer underneath had a black, viscous appearance. This phenomenon occurred several times before the gas flux became critical and the fuel caught fire. It might hint at the fact that the coating also acts as a mass transfer barrier initially, by delaying and slowing down the release of gases, until the failure becomes critical. The degradation then progressed until the sample caught fire. Ignition was however remarkably delayed, and the samples ignited after 16 min and 16 min 40 s for Al/Al_2O_3 and Cu/Al_2O_3 respectively. Once ignition occurred, PA6 burnt with the deposit remaining on top of the boiling pool of fuel, until it was completely consumed, leaving no residue except for the degraded coating.

HRR curves vs time of PA6 Al/Al_2O_3 and PA6 Cu/Al_2O_3 are shown in Figure 63 a). The HRR curve of PA6 Al/Al_2O_3 presents an initial shoulder. This corresponds to a step where the combustion only happens through the cracks in the coating (see Figure 64).

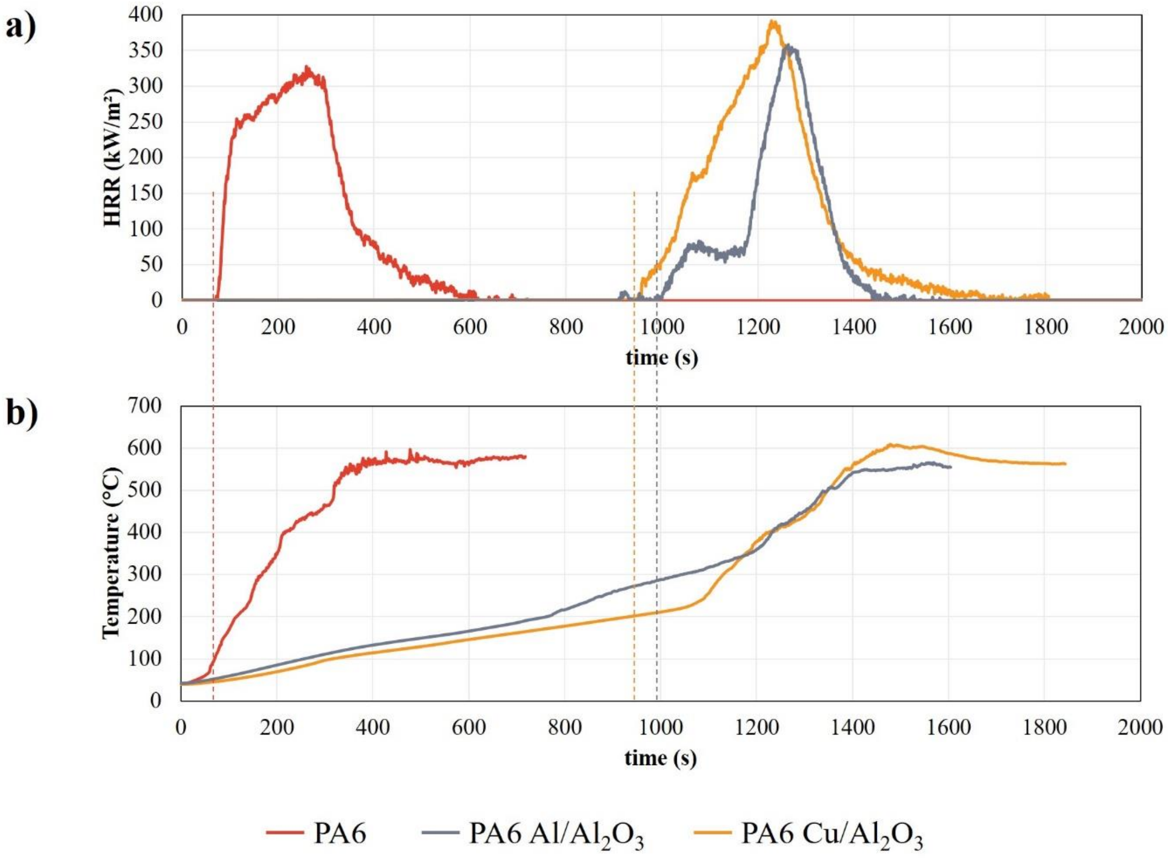

Figure 63. MLC test results of PA6, PA6 Al/Al_2O_3 and PA Cu/Al_2O_3 (heat flux: 50 kW/m² and distance to heater: 35 mm). a) HRR curve vs time and b) temperature at the back of the sample plate vs time.

After some time, the failure of the metallic film reaches a critical point and the combustion accelerates and reaches the pHRR very quickly, before stopping once the fuel is depleted. The second peak of the HRR curve is sharp, meaning that most of the fuel is consumed at the same time. As a result, the pHRR is slightly increased (+16%), but the THR decreased by 26%. Only fragments of the deposit and flakes remain after the test, with the appearance of crumpled oxidized aluminum (see Figure 64).

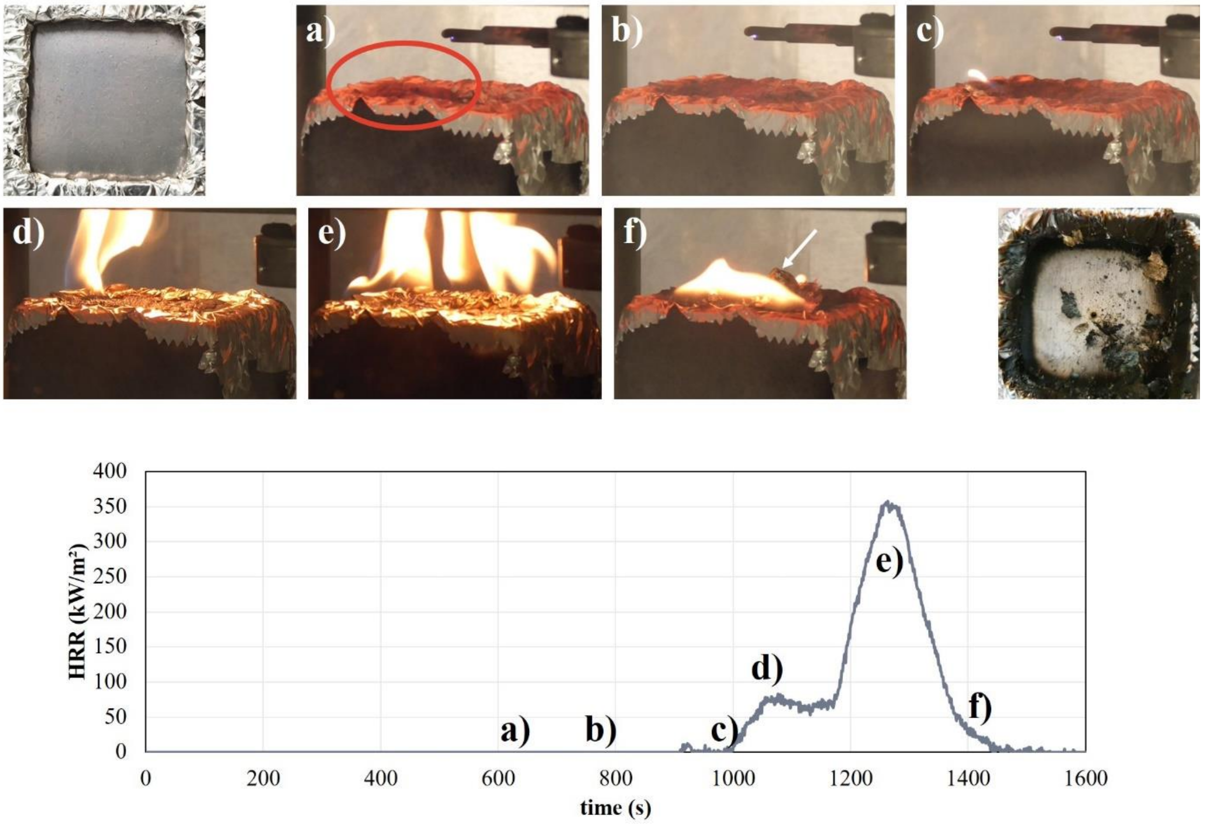

Figure 64. Digital images of the combustion process of PA6 Al/Al_2O_3 during MLC test (heat flux: 50 kW/m² and distance to heater: 35 mm). The approximate time where each image was taken is indicated on the HRR curve below.
a) The degradation starts from the edges: the substrate starts to swell and boil, and the coating cracks as a result. The red circle shows the degraded part.
b) The degradation has progressed on the whole surface.
c) Ignition.
d)Combustion through cracks.
e) The failure of the coating reaches a critical level, pHRR.
f) Flame-out. The white arrow shows the degraded coating.
The pictures at the beginning and at the end of the combustion timeline show the sample before and after test.

The HRR curve of PA6 Cu/Al_2O_3 also presents an initial shoulder, however it is less defined as the coating fails critically much more quickly. Therefore, the pHRR and THR are not impacted, and the substrate burns similarly to raw PA6. What remains is a fragment of the deposit, which has taken a grey color during the test, suggesting that copper oxidized. (see Figure 65)

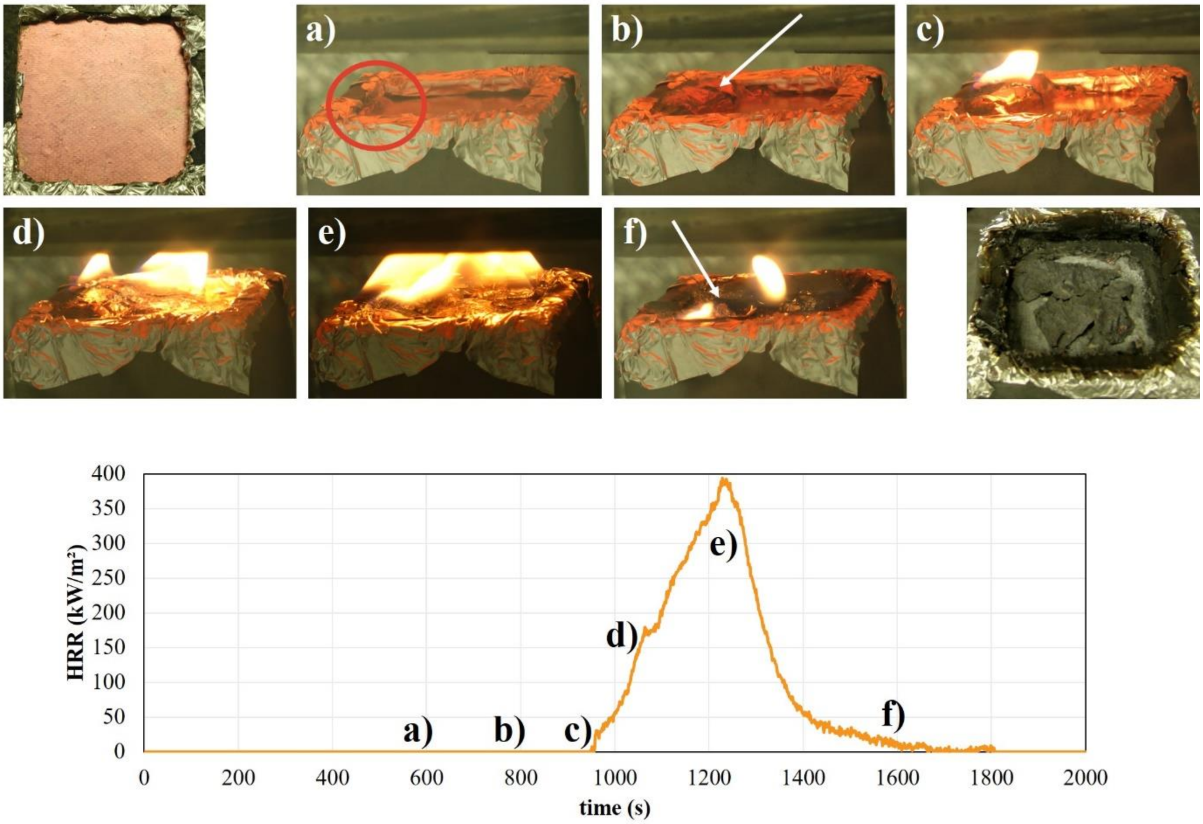

Figure 65. Digital images of the combustion process of PA6 Cu/Al_2O_3 during MLC test (heat flux: 50 kW/m² and distance to heater: 35 mm). The approximate time where each image was taken is indicated on the HRR curve below.
a) The degradation starts from the edges: the substrate starts to swell and boil, and the coating cracks as a result. The red circle shows the degraded part.
b) The degradation has progressed; the white arrow shows the cracks appearing in the coating due to the stress.
c) Ignition.
d)Combustion through cracks.
e) The failure of the coating reaches a critical level, pHRR.
f) Flame-out. The white arrow shows the degraded coating.
The pictures at the beginning and at the end of the combustion timeline show the sample before and after test.

The increased time to ignition is due to the low emissivity of the surfaces, which reduced the heat absorption of the substrate, as shown by the temperature measurements in Figure 63 b). It is clear that the rise in temperature at the back of the sample was considerably slowed down compared to the control thanks to the metal/dielectric coatings. As a result, high temperatures are reached much later than the control sample. It is noteworthy that the temperature at the back of PA6 Cu/Al_2O_3 is a bit lower than that at the back of PA6 Al/Al_2O_3. Especially, the copper-based coating keeps the temperature at the back of the PA6 plate under 200°C for more than 17 min, against 13 min for the aluminum-based deposit, because of a sudden temperature rise. Nevertheless, the time to ignition of both samples is similar.

Table 26. MLC result for PA6 Al/Al_2O_3 and PA6 Cu/Al_2O_3.

	TTI ± σ [s] (variation, %)	PkHRR ± σ [kW/m²] (variation, %)	THR ± σ [MJ/m²] (variation ,%)
PA6	73 ± 11	313,0 ± 35,9	82,6 ± 9,5
PA6 Al/Al_2O_3	964 ± 76 (+1200%)	363,1 ± 60,3 (+16%)	61,5 ± 4,6 (-26%)
PA6 Cu/Al_2O_3	999 ± 178 (+1300%)	338,1 ± 51,3 (+8,0%)	88,3 ± 5,8 (+7,0%)

3) Emissivity of PA6 Al/Al_2O_3 and PA6 Cu/Al_2O_3 as a function of temperature

The total normal emissivities of both PA6 Al/Al_2O_3 and PA6 Cu/Al_2O_3 have been measured as a function of temperature to try and gain more insights on their behavior during the test. For PA6, the emissivity does not change from 60 to 200°C, temperature at which it starts to degrade in air. For coated samples, the same evolution is observed as shown in Figure 66.

The emissivity for both systems at 60°C is lower (around 0.07 and 0.06 for PA6 Al/Al_2O_3 and PA6 Cu/Al_2O_3 respectively) than the hemispherical emissivity obtained at room temperature through the integrating sphere. It is assumed that this decrease is due to surface effect and interactions between the substrate and the coating. Indeed, it was proven that the roughness of a surface has a strong effect on emissivity, especially in the optical range this study is concerned about.[427] It is assumed that the roughness of the samples is due to the apparition of constraints during the cooling step of the PVD deposition process. Indeed, the sputtering increases the temperature of the substrate while the metal and then the dielectric are deposited. The hypothesis made here is that the increase in temperature smooths the surface of the substrate during deposition.[428] After the deposition is over, the mismatch in thermal expansion between the metal and the polymer creates constraints[429] that roughen the surface.[430], [431] As the temperature increases, the substrate and coating go back to the state they were during deposition. The resulting relaxation lessens the constraints and smooths the surface, causing a decrease in emissivity.

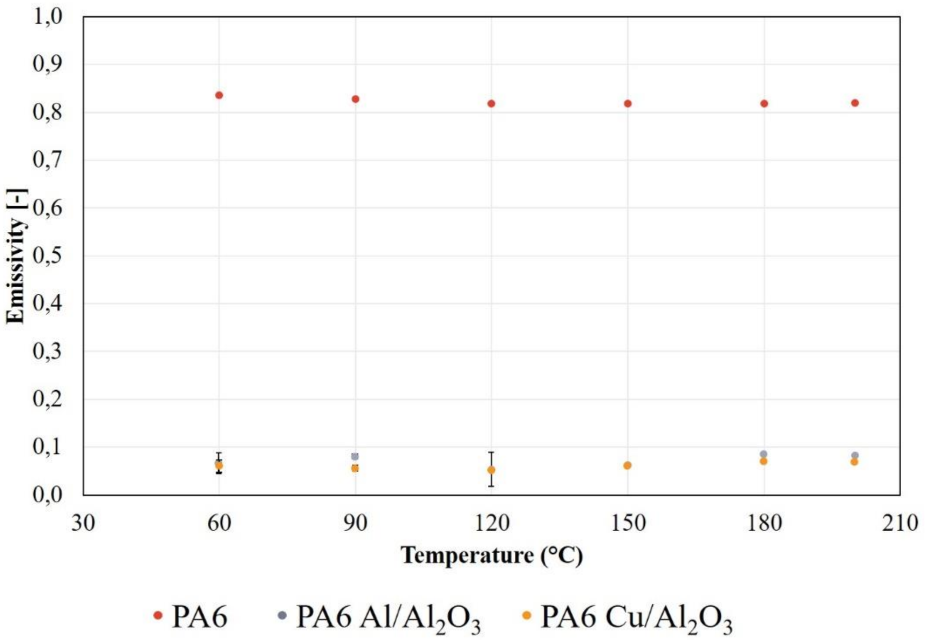

Figure 66. Total normal emissivity of PA6, PA6 Al/Al_2O_3 and PA6 Cu/Al_2O_3 as a function of temperature.

Afterwards, the emissivity is constant even as the temperature increases from 60°C to 200°C, which is coherent with this hypothesis.

As a result, the low emissivity of the coating is preserved until the substrate starts to degrade. It is therefore likely that there is no change in the optical properties of the coating until it starts to lose its protective effect because of substrate degradation and the appearance of cracks, which shows its thermal stability.

4) Discussion and conclusion

Metal/Al_2O_3 films can be considered as protected mirrors for heat shielding and have been studied on plain PA6 substrates. Temperature measurements have shown how these low-emissivity surfaces reduce the radiative heat absorption and delay the ignition, thanks to the reflection of infrared radiation. Whether with Al or Cu, the performance of the low emissivity coatings on PA6 is similar. However, Cu/Al_2O_3 is slightly more performant, be it in term of time to ignition or temperature reached at the back of the sample during the test. Al/Al_2O_3 provides however better results in terms of THR. Since the emissivities of both systems are close, it may be because of the better thermal stability of copper. Which is why it is actually surprising that the time to ignition of PA6 Cu/Al_2O_3 is not even better. When looking at the temperature curves, PA6 Cu/Al_2O_3 ignites at a much lower temperature than PA6 Al/Al_2O_3. In fact, it ignites even as the degradation of the surface is not complete and limited to one side of the sample (see Figure 65). It implies that the possible influence of other parameters such as the mechanical properties of the film, for example, have an important influence on the performance of the coatings. It is possible that PA6 Cu/Al_2O_3 does not adjust the stretch caused by the swelling of the substrate well. Thus it presents critical failure as soon as the substrate starts to degrade. On the other hand, even if the heat shield effect of PA6 Al/Al_2O_3 is less efficient than PA6 Cu/Al_2O_3, it keeps the substrate from igniting even as the whole surface has degraded, maybe because it can better adjust to the mechanical constraints. To summarize, the mechanical behavior of the coating is significant for the fire properties of the sample. This is also linked to the limitation of the mass transfers by the film, and how long it keeps this barrier effect during the test. The results of PA6 Al/Al_2O_3 hint that this aspect could be better than PA6 Cu/Al_2O_3, which can explain why their behavior is similar, despite the fact that PA6 Cu/Al_2O_3 is better at limiting the temperature rise of the sample.

To conclude, low-emissivity metal/dielectric coatings are very promising in providing fire protection to polymer substrates. They act by reflecting infrared radiation, which lower the heat absorption of polymers and increase the time to ignition by several order of magnitude as a result. With times to ignition higher than 10 min, both aluminum and copper coatings protected by Al_2O_3 brought practical incombustibility to PA6 plates, even with a thickness equal to or lower than 1 µm. On the downside, this concept has several limitations. One is that the presence of defects in the coating will compromise its protective effect and cause early degradation of the sample. Situations where soot or dust deposit on the sample may also alter its reflective properties,[432] lowering its performance in case of a fire. Moreover, once ignited, the intensity of the fire in term of pHRR and THR is similar to the uncoated plate. Finally, in theory, metal/dielectric coatings are only effective in a limited number of fire scenarios, where radiative heat transfers are dominant. It is likely that they will fail to protect the polymer effectively in situations where conductive or convective heat transfers prevail. As a conclusion, low emissivity coatings provide an interesting yet incomplete fire protection to neat polymers. It is therefore necessary to combine them with other fire retardant strategies in order to overcome these shortcomings, especially to reduce the pHRR and THR when the substrate ignites.

In the next part, the combination of low emissivity coatings with bulk fire retardant was explored. Al/Al_2O_3 coatings were deposited on fire retardant PA6 plates. The reason for choosing aluminum instead of copper here stems from practical reason. Its deposition on PA6 is easier, it is more environmentally resistant and it is cheaper. Moreover, it is more compatible with Al_2O_3.

II. Combination of low-emissivity coatings with bulk fire retardant fillers

Flame retardants for PA6 are already available and have proven to be very efficient in reducing the pHRR and THR in a mass loss cone calorimeter. More often than not, however, they tend to lower the time to ignition, which is a cause for concern. Combining their action with low emissivity coatings could overcome the shortcomings of both mechanisms. The reasoning is the following: the metal/dielectric coating would act first, as a radiative heat barrier, by reflecting infrared radiation. As it was shown previously, this will limit the heat absorbed by the formulated PA6 and slow down the rise in temperature. As a consequence, the temperature will be kept below the activation level of the fire retardant filler for several minutes, delaying its action. This would significantly increase the time to ignition of the FR-PA6 plate. Once the coating fails, the fire retardants would take over to limit the intensity of the fire according to its specific mechanism (gas or condensed phase action). Here, three systems were investigated in order to test this concept.

1) Description and mode of action of selected fire retardants

OP1311 is a fire retardant mixture composed of aluminum diethylphosphate (DEPAL) and melamine polyphosphate (MPP), commercialized by Clariant under the name Exolit OP1311©. Its mode of action is chemical intumescence, and its positive action for PA6 flammability was investigated by several groups.[433]–[436] It was found that a 23 wt% infill could reduce pHRR and THR thanks to a gas and condensed phase mechanism. The reaction between PA6 and DEPAL leads to the formation of a protective layer of aluminophosphate ($AlPO_4$) and the release of phosphinic acid, which acts in the gas phase. The reaction of polyphosphate with PA6 leads to both condensation and vaporization of melamine. The condensation of melamine produces melon and cyameluric polymers which reinforce the protective effect of the ceramic layer. It dilutes the flame by releasing NH_3 gas. Finally, the system is cooled down by the vaporization of melamine and its decomposition in the flame, since these are endothermic phenomena.[433] Uncoated formulated PA6 plates and coated formulated PA6 plates containing 23 wt% of OP1311 will be named PA6 OP and PA6 OP Al/Al_2O_3 thereafter.

Afterwards, organically-modified cloisite (o-Cloisite) was added with OP1311 at 5 wt% and 18 wt% infill respectively. The organically-modified clay acts as a synergist with the mixture of DEPAL and MPP. Clay particles act as support for the nucleation of small and well-distributed bubbles during the decomposition, accumulate on the surface and complement the protective layer.[434] However, it does not expand like OP1311, because of the rigidity of the resulting surface. This system was chosen because it could be beneficial as it won't deform the thin reflective coating. Uncoated formulated PA6 plates and coated formulated PA6 plates will be named PA6 OPC and PA6 OPC Al/Al_2O_3 thereafter.

Finally, a vinylsilane-coated magnesium dihydroxide (MDH) (H5A) was tested at 50 wt% infill. This high filler content makes matrix dilution one of the first mechanisms of action of MDH. Then, its decomposition between 310°C and 459°C [437] cools the material as it is endothermic and releases water. As a consequence, the time to ignition is already increased a bit. The reaction also produces magnesium oxide which forms a protective superficial layer, reinforced by the surface treatment of MDH, that helps reducing pHRR and THR.[437] Here, it would be interesting to see if the presence of MDH can enhance the action of the low emissivity coating as well as reduce pHRR and THR. Also, it does not have an intumescent mechanism, meaning the undesirable swelling of the surface should be avoided. Uncoated formulated PA6 plates and coated formulated PA6 plates will be named PA6 MDH and PA6 MDH Al/Al_2O_3 thereafter.

The filler content and mechanism of all systems studied are gathered in Table 27, whereas the combustion behavior of all PA6 FR plates at mass loss cone calorimeter is summarized in Figure 67. All systems studied have a decomposition temperature around 300°C or higher. According to the results obtained in Section I of this chapter, the Al/Al_2O_3 coating keeps the temperature at the back of the sample under 300°C for more than 16 min in average. Therefore, the radiative barrier effect of the low emissivity coating should be enough to delay the activation of the fire retardant fillers by reducing the heat absorption of the sample.

Table 27. Fire retardant systems and their mode of action.

System	Infill	Decomposition temperature	Mechanism
OP1311	23 wt%	>300°C	Chemical intumescence Formation of a protective layer Gas phase mechanism
OP1311 o-Cloisite	18 wt% 5 wt%		Formation of a reinforced protective layer Gas phase mechanism
H5A	50 wt%	310°C and 459°C	Matrix dilution Cooling effect: H_2O emission and endothermic decomposition Formation of a protective layer

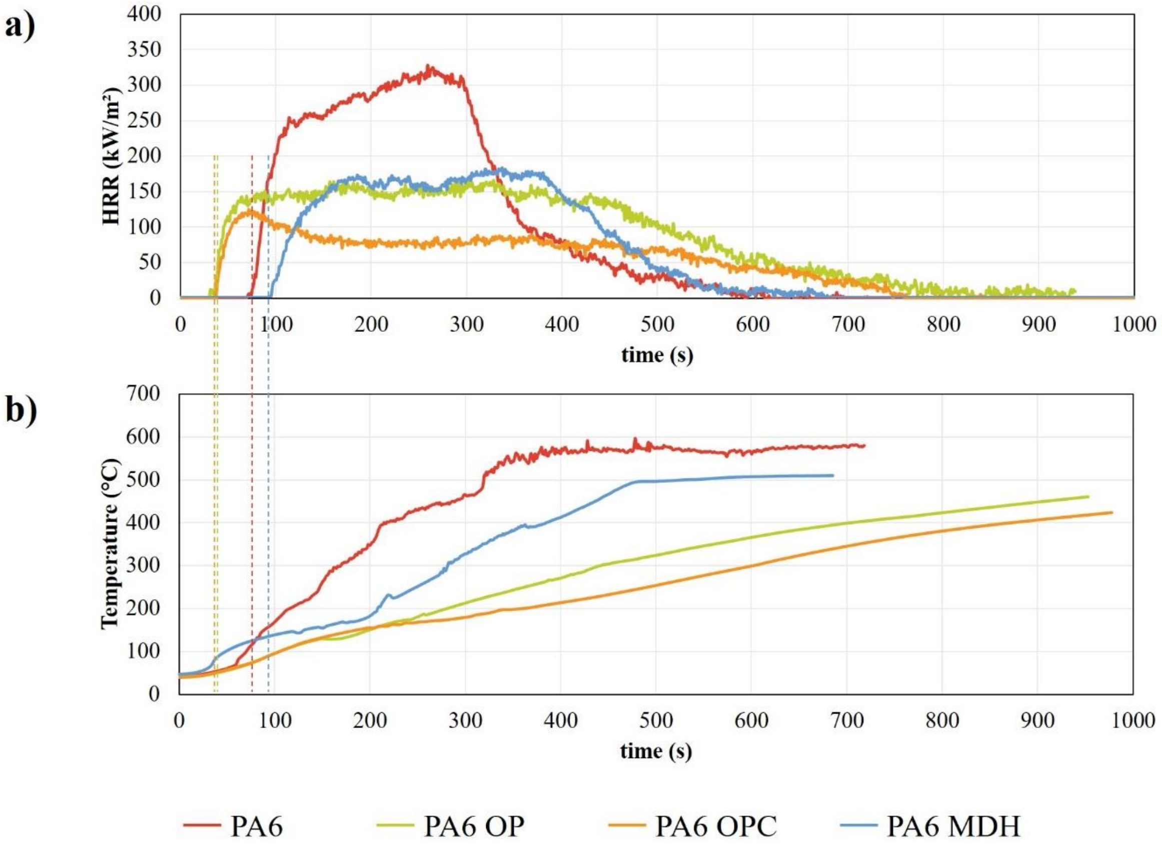

Figure 67. MLC test results of PA6 formulated with 23 wt% of OP1311 (PA6 OP), 18 wt% of OP1311 and 5 wt% of o-Cloisite (PA6 OPC), and 50 wt% of MDH (PA6 MDH), compared with PA6 (heat flux: 50 kW/m² and distance to heater: 35 mm). a) HRR curve vs time and b) temperature at the back of the sample plate vs time.

2) Emissivity measurements

Emissivity measurements via diffuse infrared reflectance through an integrating sphere show first that the addition of FR fillers in the PA6 matrix does not influence on the emissivity of the surface (as expected), as all uncoated surfaces have an emissivity of 0.95-0.96 (see Figure 68). As such, their absorbance is high in the infrared. The addition of the Al/Al_2O_3 coating reduces this value to around 0.2 (respectively 0.18, 0.23 and 0.17 for PA6 OP Al/Al_2O_3, PA6 OPC Al/Al_2O_3 and PA6 MDH Al/Al_2O_3). It shows that not only is the infrared reflection enhanced when compared to the uncoated substrates, but the value is around the same than PA6 Al/Al_2O_3.

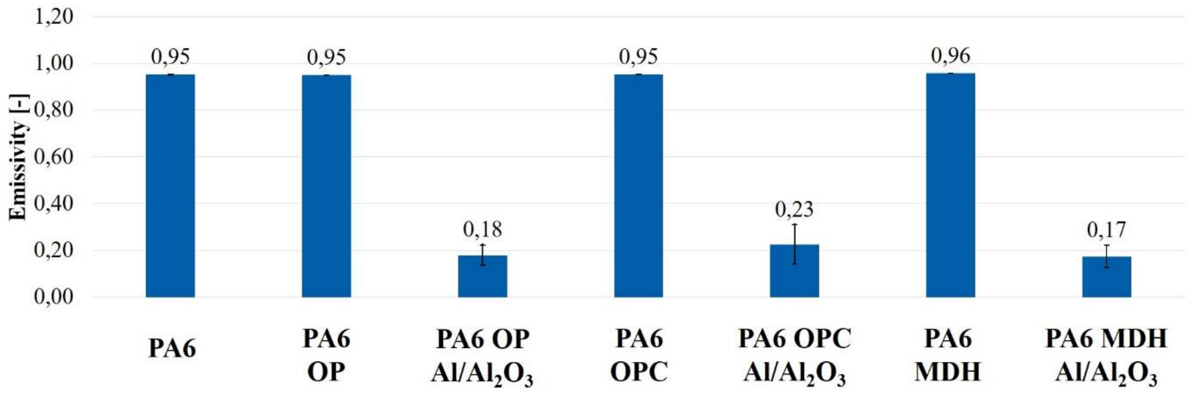

Figure 68. Emissivity of coated and uncoated FR PA6 compared with PA6, calculated at room temperature by infrared diffuse reflectance measurements.

3) Fire test: mass loss cone calorimetry

a. PA6 OP Al/Al_2O_3

As it was explained before, OP1311 acts by chemical intumescence. When exposed to a 50 kW/m² heat flux, large smoke emissions are observed very quickly, while the surface turns from white to black as it starts to char and swell. Combustion occurs through cracks formed in this layer around 47 s which is 26 s earlier than PA6. Afterwards, the sample continues to swell as it burns, leaving an expanded black residue. Figure 69 a) presents the variation of HRR against time of PA6 OP. The HRR rises quickly before reaching a plateau. It decreases slowly as the fuel begins to deplete before flame out. This curve is characteristic of a thick charring material, which is consistent with what is known of this system. It reaches a pHRR of around 160 kW/m², which corresponds to a decrease of 49% when compared to a plain PA6 plate. It indicates that the combustion is slowed down. However, the THR is not impacted (75.9 MJ/m², i.e an 8% decrease compared to PA6), which shows that all fuel is consumed, but its consumption is spread out over a longer time.

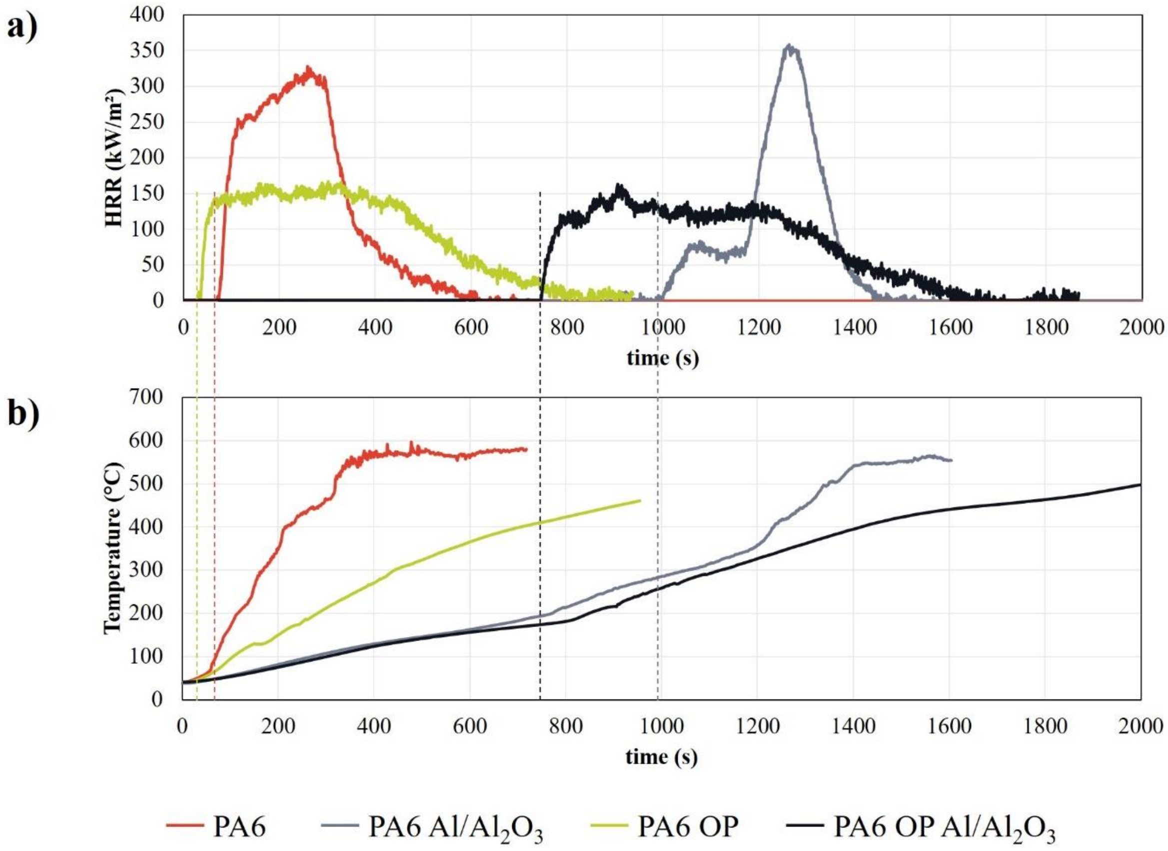

Figure 69. MLC test results of PA6 formulated with 23wt% of OP1311 without (PA6 OP) and with (PA6 OP Al/Al$_2$O$_3$) Al/Al$_2$O$_3$ coating, compared with PA6 and PA6 Al/Al$_2$O$_3$ (heat flux: 50 kW/m² and distance to heater: 35 mm). a) HRR curve vs time and b) temperature at the back of the sample plate vs time.

Exactly the same behavior is observed for PA6 OP Al/Al$_2$O$_3$, except that the TTI is now 14 min, which is 18 times and 12 times more than PA6 OP (47 s) and PA6 (73 s) respectively. The coating starts to swell on one edge as an extensive amount of smoke is released. Since the coating is not elastic enough to accommodate for this type of stress, cracks appear all along the degraded surface. The substrate appears black underneath as the protective layer forms. Just as PA6 OP, combustion occurs through the cracks until the fuel is completely depleted. As a result, both HRR, pHRR and THR evolutions were completely similar to the uncoated FR sample. Therefore, as soon as the coating reaches a critical failure, the substrate underneath behaves independently. Two reasons can explain the fact that the TTI of PA6 OP Al/Al$_2$O$_3$ is slightly shorter than the one of PA6 Al/Al_2O_3. The main one is the extensive swelling which causes premature cracking of the coating and the early loss of its protective effect. The second is that the decomposition and reaction of OP1311 with the PA6 matrix is what drives the behavior of the sample, which lowers the degradation temperature. At the end, the surface of the residue is cohesive and shows the soot-covered degraded Al/Al_2O_3 deposit (Figure 70).

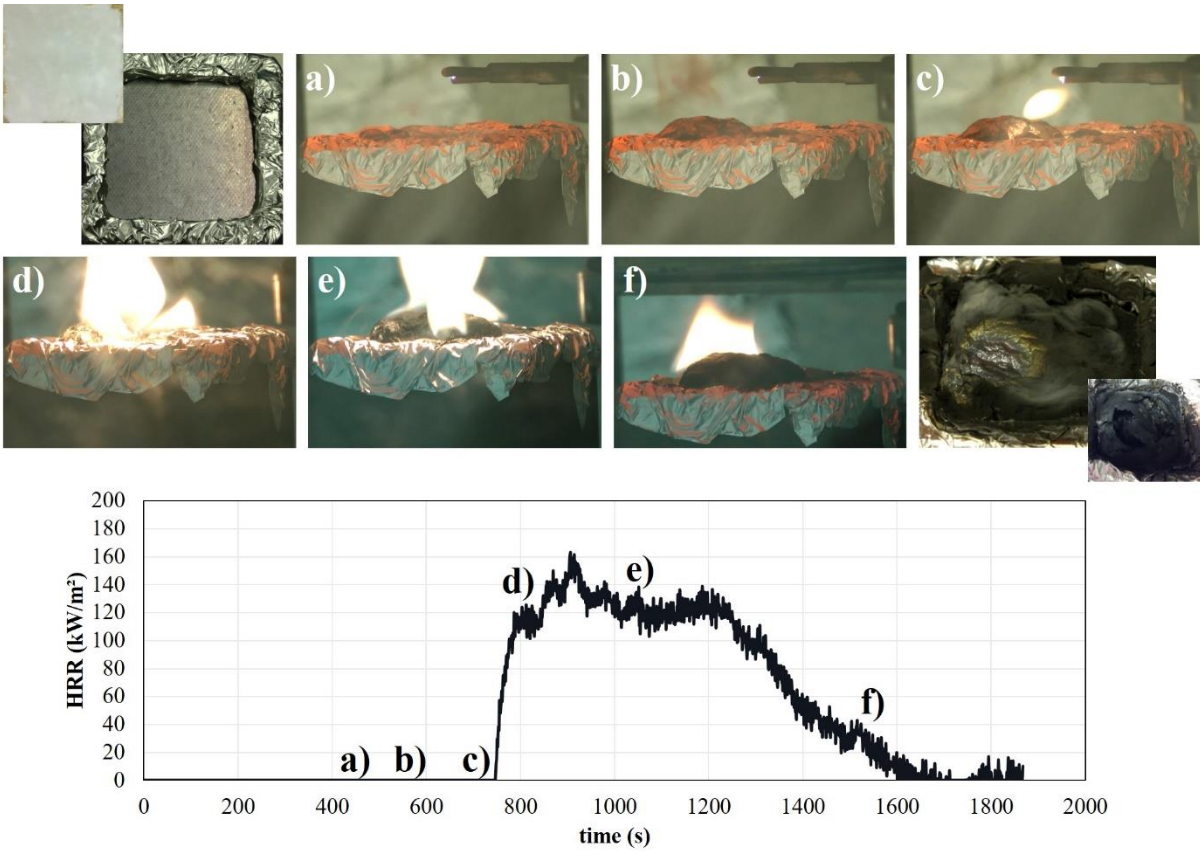

Figure 70. Digital images of the combustion process of PA6 OP Al/Al_2O_3 during MLC test (heat flux: 50 kW/m² and distance to heater: 35 mm). The approximate time where each image was taken is indicated on the HRR curve below.
a) The degradation starts from the edges: the substrate starts to swell and boil, and the coating cracks as a result.
b) The degradation has progressed and extensive swelling takes place.
c) Ignition.
d)Combustion through cracks.
e) The protective barrier has finished forming.
f) Flame-out.
The pictures at the beginning and at the end of the combustion timeline show the sample before and after test. Inserts show the FR plate before and after test.

Before ignition, OP1311 did not slow down the rise in temperature at the back of the sample. However, the reaction of the fire retardant with the matrix and the resulting chemical intumescent phenomena further insulated the material. Consequently, the temperature was kept under 500°C for the whole duration of the test, as shown in Figure 69 b). The addition of the low-emissivity coating and the limitation of radiative heat absorption slowed down the rise in temperature. The curve follows that of a coated PA6 plate for the first 10 min of the test. Afterwards, the insulation brought by the intumescent phenomenon and the formation of the protective layer limited the temperature levels further and the curve was kept below that of PA6 Al/Al_2O_3 for the rest of the test, to reach 500°C after 33 min, that is 5 min after the end of test.

Table 28. MLC result for PA6 OP and PA6 OP Al/Al_2O_3, compared with PA6.

	TTI ± σ [s] (variation, %)	**PkHRR ± σ [kW/m²] (variation, %)**	**THR ± σ [MJ/m²] (variation, %)**
PA6	73 ± 11	313,0 ± 35,9	82,6 ± 9,5
PA6 OP	47 ± 18 (-35%)	159,8,1 ± 10,3 (-49%)	75,9 ± 5,7 (-8%)
PA6 OP Al/Al_2O_3	862 ± 100 (+1086%)	160,1 ± 33,2 (-49%)	71,8 ± 4,7 (-13%)

b. PA6 OPC Al/Al_2O_3

Adding 5 wt% of organically modified cloisite to 18 wt% of OP1311 slightly modified the behavior of PA6 OPC when compared to PA6 OP. First, because of the action of clay, ignition occurs sooner, before the sample starts to swell. A black char layer forms, which cracks before the surface swells uniformly. At ignition the HRR rises and reaches the pHRR quickly. This step corresponds to the formation of the char layer (see Figure 71). Once it is established, the HRR decreases due to its protective effect, showing the distinctive curve of a thick charring material. The residue is a cracked and hollow black material with a smooth surface (Figure 72). Crevices are present all along the edges because of the stress between the material and the sample holder, from where the flames sprout out in the last stage of the combustion.

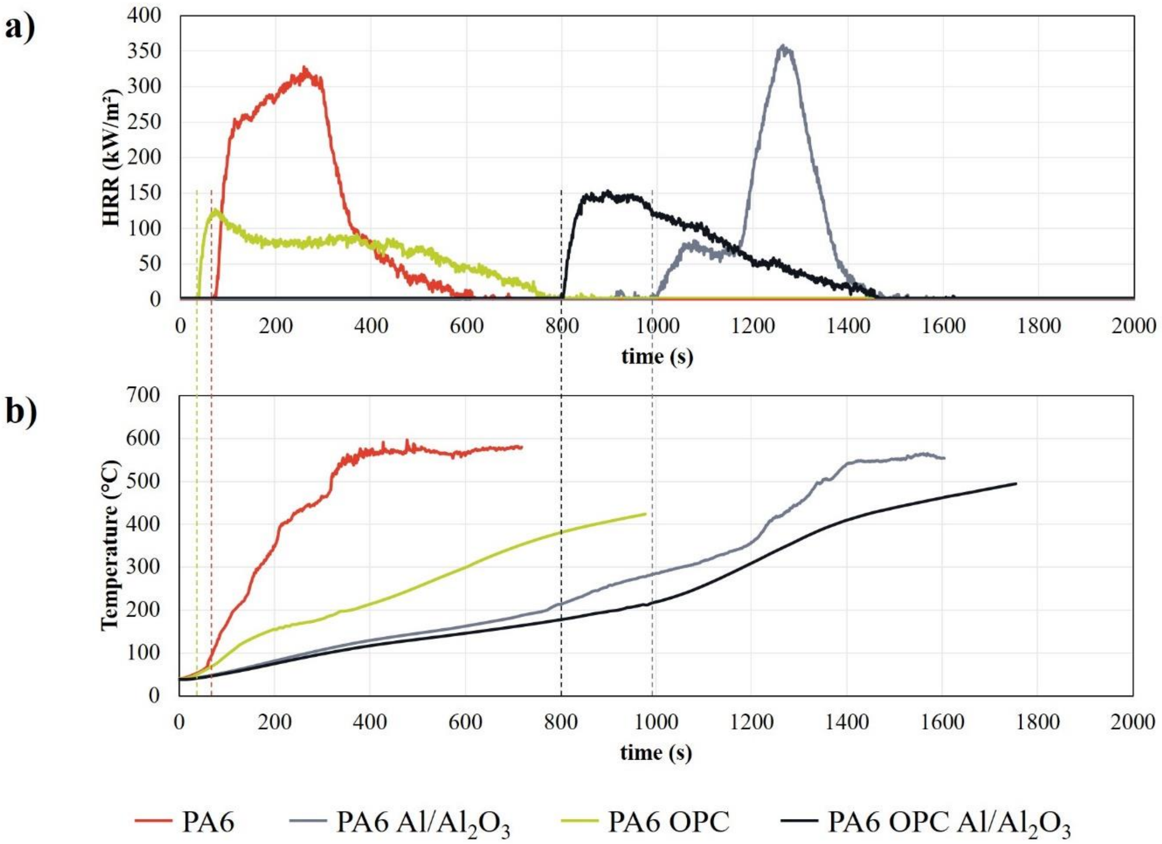

Figure 71. MLC test results of PA6 formulated with 18 wt% of OP1311 and 5 wt% of o-Cloisite, without (PA6 OP) and with (PA6 OP Al/Al_2O_3) Al/Al_2O_3 coating, compared with PA6 and PA6 Al/Al_2O_3 (heat flux: 50 kW/m² and distance to heater: 35 mm). a) HRR curve vs time and b) temperature at the back of the sample plate vs time.

PA6 OPC Al/Al_2O_3 ignites after nearly 12 min, which is almost 10 times more than PA6 and 20 times more than PA6 OPC, but less than PA6 OP Al/Al_2O_3 and *a fortiori* less than PA6 Al/Al_2O_3. As all coated samples, it started to swell from the edge, damaging the protective coating because of numerous small regular bubbles. Once the degradation reached a critical level, the sample ignited at once, and expanded further. This resulted in a pHRR slightly higher than PA6 OPC (+22%), but still 51% lower than PA6. The coating remained on top of the sample as the char layer formed underneath, slowing down the heat release until flame out. As a consequence, the HRR curve is similar to PA6 OP in terms of shape and THR. At the end, numerous small cracks were observed on the surface of the white residue, but the coating and top layer cracked mainly at the edges. The residue was composed of a rigid aluminum coated carbonaceous layer, but the sample underneath was consumed and charred just like PA6 OPC.

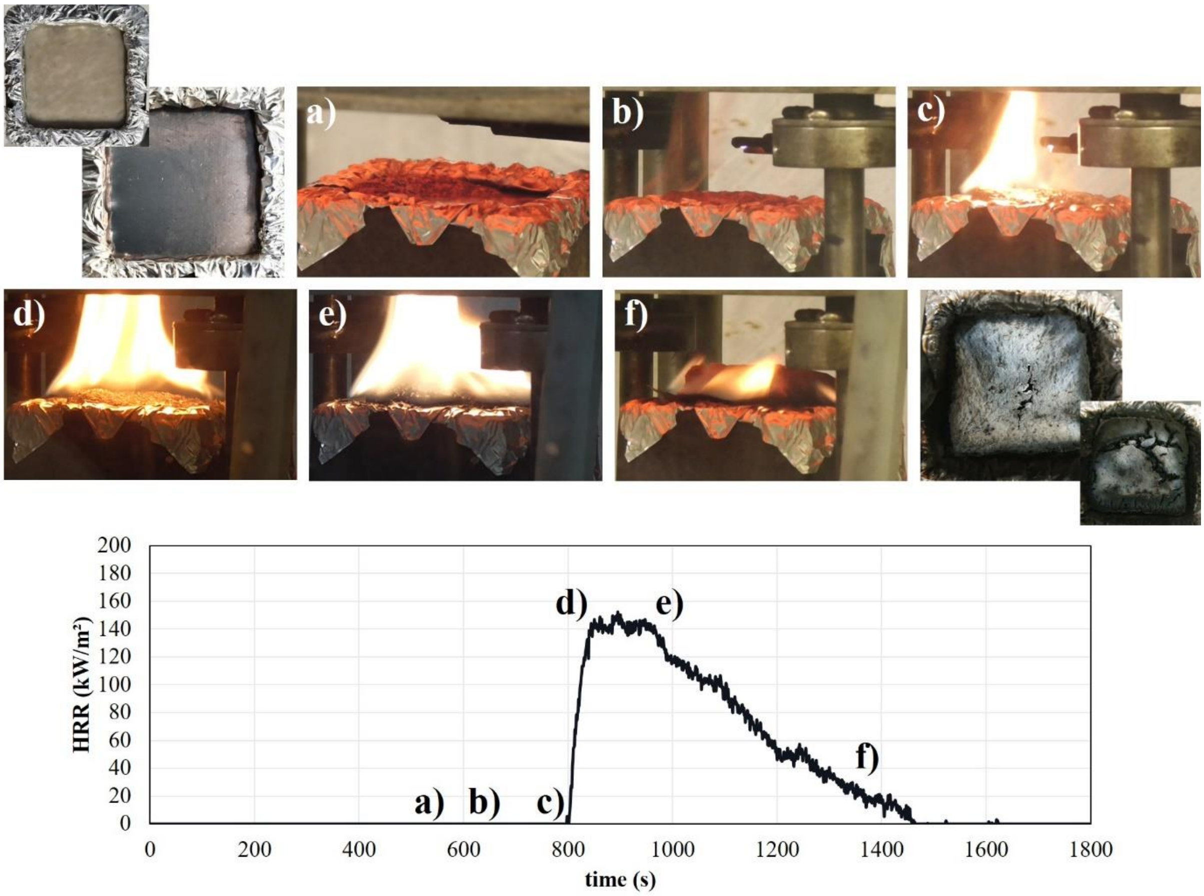

Figure 72. Digital images of the combustion process of PA6 OPC Al/Al_2O_3 during MLC test (heat flux: 50 kW/m² and distance to heater: 35 mm). The approximate time where each image was taken is indicated on the HRR curve below.
a) The degradation starts from the edges: the substrate starts to swell and boil, and the coating cracks as a result.
b) The degradation has progressed and extensive swelling takes place.
c) Ignition.
d)The combustion is fast and reach pHRR soon after ignition.
e) The protective barrier has finished forming.
f) Flame-out.
The pictures at the beginning and at the end of the combustion timeline show the sample before and after test. Inserts show the FR plate before and after test.

The mixture of OP1311 and clay did not limit heat absorption at the beginning of the test, as seen in Figure 71 b). However, after ignition, the intumescent phenomena helped insulating the core of the sample, keeping the backside temperature of the sample below 500°C for the whole duration of the test, and even slightly improving the performance of PA6 OP at the end of the test. By reflecting infrared radiation, the low emissivity Al/Al_2O_3 coating helped lowering the heat absorption at the beginning of the test before the loss of its protective effect. The fire retardant fillers take over afterwards, and the added insulating effect further limits the temperature rise when compared to PA6 Al/Al_2O_3.

Table 29. MLC result for PA6 OPC and PA6 OPC Al/Al_2O_3, compared with PA6.

	TTI ± σ [s] (variation, %)	**PkHRR ± σ [kW/m²] (variation, %)**	**THR ± σ [MJ/m²] (variation, %)**
PA6	73 ± 11	313,0 ± 35,9	82,6 ± 9,5
PA6 OPC	35 ± 2 (-53%)	124,4 ± 2,6 (-60%)	48,8 ± 0,8 (-41%)
PA6 OPC Al/Al_2O_3	712 ± 144 (+880%)	152,1 ± 2,4 (-51%)	52,2 ± 1,7 (-37%)

c. PA6 MDH Al/Al_2O_3

When submitted to a 50 kW/m² radiative flux, MDH-containing PA6 starts to swell and releases large quantities of smoke. It bubbles vigorously while a protective layer forms on the surface, which disrupts the release of fuel. This, as well as the cooling action of MDH, increases the time to ignition of PA6 by 27 s. The residue is hollow, with a rigid black superficial layer. Closed cells form within this layer, which implies that the ceramic layer acts as a fuel barrier. According to Michaux et al.,[437] it is composed of a ceramic residue from the dehydration of MDH and of a hybrid silicon-carbon residue formed after the degradation of the surface treatment of MDH. Its formation leads to the formation of a plateau on the HRR curve (Figure 73) with a pHRR lower than PA6 by 42%, and a THR reduced by 30%.

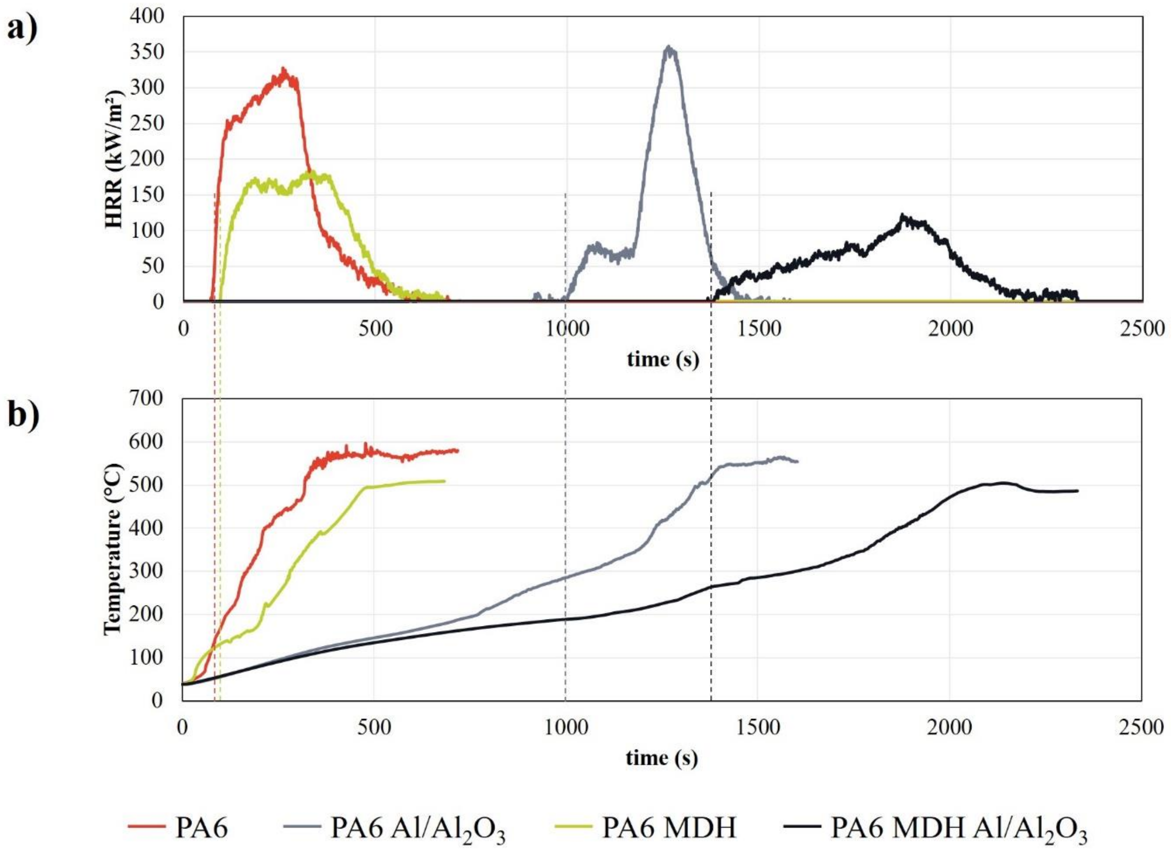

Figure 73. MLC test results of PA6 formulated with 50 wt% of MDH, without (PA6 OP) and with (PA6 OP Al/Al_2O_3) Al/Al_2O_3 coating, compared with PA6 and PA6 Al/Al_2O_3 (heat flux: 50 kW/m² and distance to heater: 35 mm). a) HRR curve vs time and b) temperature at the back of the sample plate vs time.

With the addition of the low emissivity coating, the substrate begins to bubble vigorously with the coating remaining on top. The combination of MDH and low emissivity coatings presents a beneficial chain of events that ultimately improves the performance of both separate systems. At first, Al/Al_2O_3 acts as a radiative heat barrier and keeps the temperature of the system below the decomposition temperature of MDH for at least 10 min. Once MDH starts to decompose, the endothermic formation of MgO and release of H_2O helps limiting the increase in temperature further. As a result, the time to ignition of PA6 MDH Al/Al_2O_3 was improved with respect to PA6 Al/Al_2O_3 and reached in average around 22 min. In addition, once the composite MgO protective layer has formed, it acts as an effective gas barrier (reinforced by the Al/Al_2O_3 coating), trapping the volatile decomposition products underneath. As a result, the substrate swelled extensively, to the point of touching the electric arc before ignition (the ignition time might be underestimated because of this phenomenon). There were numerous cracks in the coating on the edges because of this stress, through which fuel was released preferentially. Once the sample ignited, small flames sprouted from the major defects in the coating, but did not propagate on the whole surface. The formation of the MgO barrier before ignition as well as its resistance explains the low pHRR and THR, which were reduced by 67% and 46 % respectively when compared to PA6 (they were even reduced by 43% and 23% respectively when compared to PA6 MDH). The residue at the end of the test looked like PA6 MDH, but with the addition of the degraded Al/Al_2O_3 on top (see Figure 74).

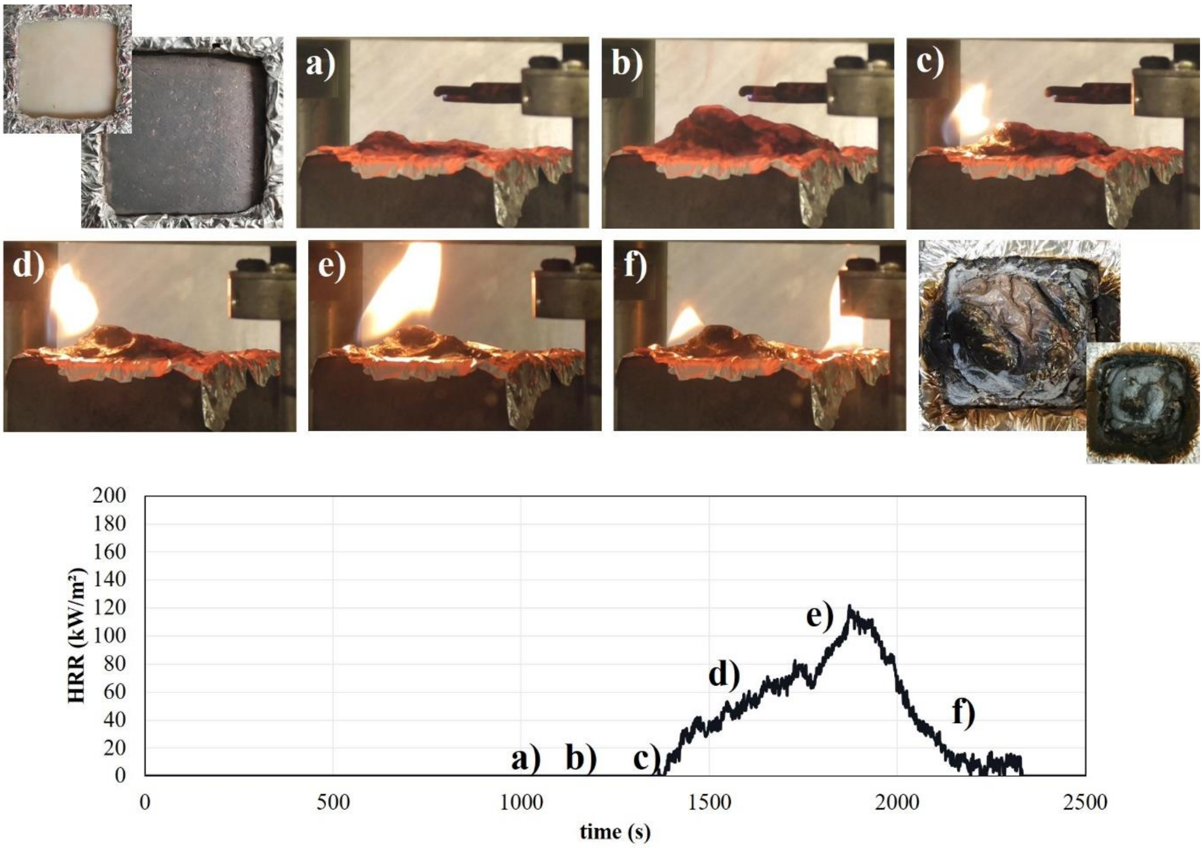

Figure 74. Digital images of the combustion process of PA6 MDH Al/Al_2O_3 during MLC test (heat flux: 50 kW/m² and distance to heater: 35 mm). The approximate time where each image was taken is indicated on the HRR curve below.
a) The degradation starts from the edges: the substrate starts to swell and boil, and the coating cracks as a result.
b) The degradation has progressed and the image shows the extreme swelling of the sample.
c) Ignition.
d)The combustion progressed but very slowly.
e) pHRR.
f) Flame-out.
The pictures at the beginning and at the end of the combustion timeline show the sample before and after test. Inserts show the FR plate before and after test.

As seen in Figure 73 b), the temperature at the back of PA6 MDH rises very quickly at the beginning of the test as MDH increases the conductivity of the sample, before the fire retardant takes effect to insulate the sample. With the low emissivity coating, this phenomenon is suppressed as the reflection of infrared rays slows the temperature rise down and smooths the beginning of the curve, which is then similar to PA6 Al/Al_2O_3. The temperature at the back of PA6 MDH Al/Al_2O_3 was also kept under 200°C for a longer time, almost 17 min in average, which shows the efficiency of the system.

Table 30. MLC result for PA6 MDH and PA6 MDH Al/Al_2O_3, compared with PA6.

	TTI ± σ [s] (variation, %)	**PkHRR ± σ [kW/m²] (variation, %)**	**THR ± σ [MJ/m²] (variation, %)**
PA6	73 ± 11	313,0 ± 35,9	82,6 ± 9,5
PA6 MDH	100 ± 9 (+37%)	182,8 ± 0,5 (-42%)	57,6 ± 0,6 (-30%)
PA6 MDH Al/Al_2O_3	1307 ± 86 (1698%)	103,7 ± 26,0 (-67%)	44,5 ± 3,7 (-46%)

4) Discussion and conclusion

The emissivities of PA6 OP, PA6 OPC and PA6 MDH are constant around 0.85 between 60°C and 200°C. The emissivity of the coated plates is constant around 0.1 for all systems between 60°C and 200°C, as shown in Figure 75. These observations are consistent with what was observed for PA6 Al/Al_2O_3 and shows that the emissivity does not depend on the substrate but only on the surface treatment. The slight differences between the plates are probably not significant, and only attest of experimental imprecisions and likely small variations in the coatings between the plates because of the process. The fact that the emissivity of PA6 FR Al/Al_2O_3 is similar to that of PA6 Al/Al_2O_3 explains that the variations of temperature at the back of the samples are similar between PA6 FR Al/Al_2O_3 and PA6 Al/Al_2O_3 at the beginning of the test. This shows that for the first 5 to 10 min, the effect of the coating is predominant on the behavior of the sample, regardless of the FR system studied. As a result, it is clear that the low emissivity metal/dielectric film does indeed delay the activation of the FR fillers by reducing heat absorption through the reflection of infrared rays. This significantly increases the time to ignition of the FR plate, effectively counterbalancing the short time to ignition observed notably with PA6 OP and PA6 OPC.

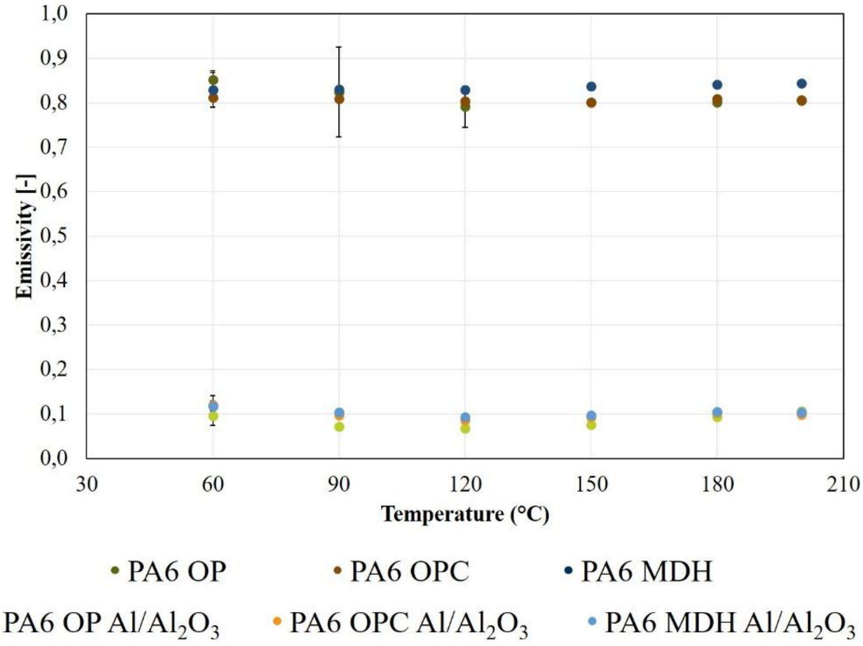

Figure 75. Emissivity of coated and uncoated PA6 OP, PA6 OPC and PA6 MDH as a function of temperature.

Once the degradation of the substrate progresses, the FR fillers activate according to their respective mechanisms. The formation of a protective insulating layer further limits the rise in temperature at the back of the plate. The gas trapping effect of the coating is further evidenced as all FR coated samples present a severe swelling before ignition, more than what is observed with uncoated FR plates. The metal/dielectric film acts as a barrier that reinforces the carbonaceous layer that forms via the reaction of the PA6 matrix with the FR fillers.

This is especially true for PA6 OPC Al/Al$_2$O$_3$ and PA6 MDH Al/Al$_2$O$_3$. Once the degradation reaches a critical point, the coating starts to fail and the sample ignites as its protective effect is lost. At this point, the action of the FR fillers is predominant as they activate and take over to limit the intensity of the combustion and the pHRR and the THR.

As a result, once ignited, the combustion behavior of the coated FR samples is the same as their uncoated counterparts. Which is why it is not surprising that the TTI of PA6 OP Al/Al$_2$O$_3$ and PA6 OPC Al/Al$_2$O$_3$ is smaller than that of PA6 Al/Al$_2$O$_3$, as the same catalyzing effect of

OP1311 and OP1311+Cloisite on the degradation of PA6 is observed. This, combined with the gas trapping effect and the consecutive severe swelling leads to an earlier loss of the coating protection and therefore an earlier ignition (which is still reasonable as it is higher than 10 min).

To conclude, the low emissivity coating on FR plates does not inhibit the action of the fillers on the sample's combustion behavior. Once the coating fails, they act as if without one. The only exception is PA6 MDH, where the presence of the coating further improves the behavior of the system, thanks to a sequence of beneficial events. Indeed, the coating prevents MDH from decomposing for a long time. Afterwards, the endothermic decomposition of MDH and release of H_2O helps improving the time to ignition by slowing down the increase in temperature, even as the coating starts to fail. Then, the formation of a strong protective ceramic-carbonaceous layer and its combination with the Al/Al_2O_3 films is very effective at trapping the degradation gases, as proved by the extensive swelling. Once the ignition occurs, this strong barrier lowers the pHRR and THR even with respects to PA6 MDH. Therefore, the performance of PA6 MDH Al/Al_2O_3 was better than the two mechanisms separated (longer TTI when compared to PA6 Al/Al_2O_3, and lower pHRR and THR than PA6 MDH).

The combustion behavior of all PA FR Al/Al_2O_3 samples is summarized in Figure 76.

In the literature, it was found that PA6 OP and PA6 OPC both have a V0 rating at UL94 test, and respective LOI of 29% and 31%.[433] V0 rating of a PA6 filled with 55% of vinylsilane treated MDH was reported, and the behavior of PA6 with 50% of MDH should be close.[438] As mentioned previously, it is expected that the low emissivity coating must be less effective against fire scenario where convective and conductive heat transfer are dominant. As a result, the coated FR samples are efficient against all scenarios: the low emissivity coating will be very protective against radiative constraints, supported by the bulk mechanism, whereas the FR systems will be efficient against other thermal constraints, supported by the barrier effect of the coating.

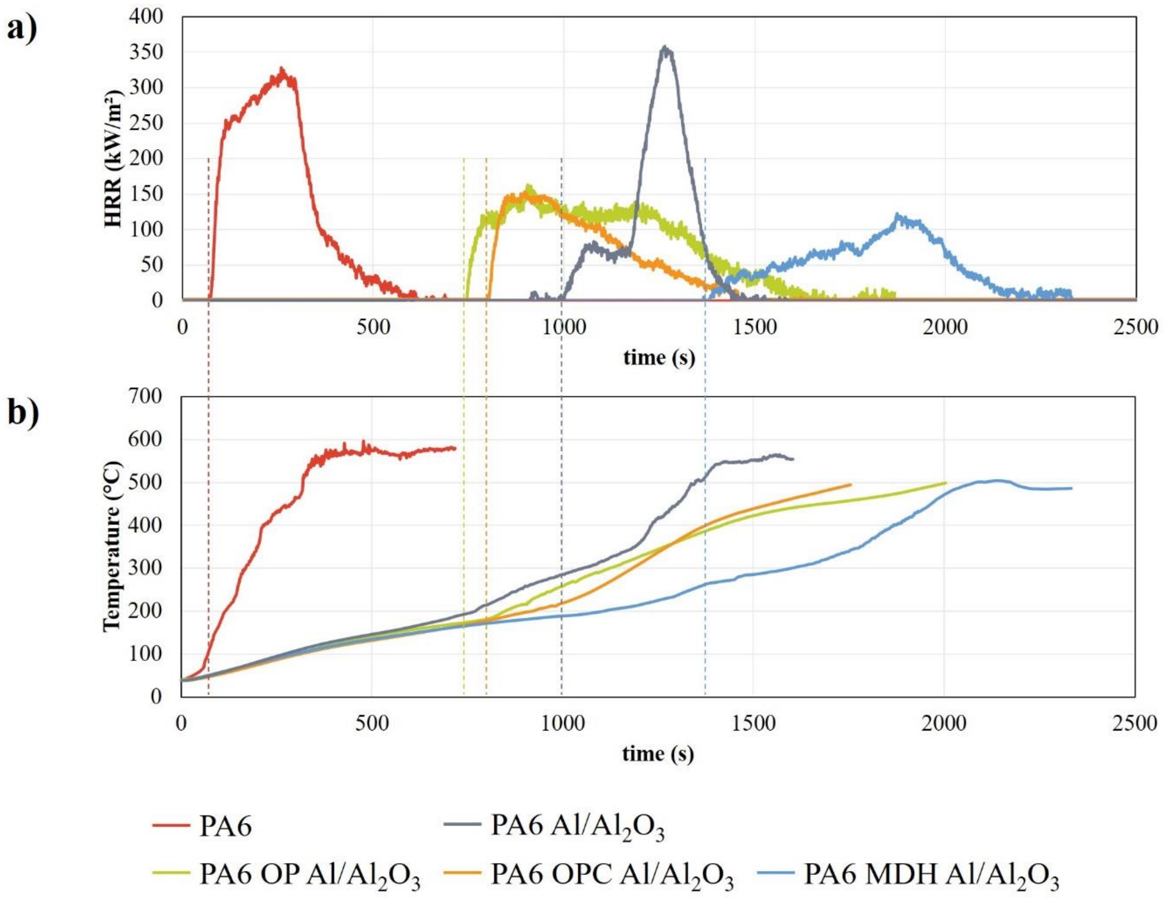

Figure 76. MLC test results of Al/Al$_2$O$_3$-coated PA6 formulated with 23 wt% of OP1311 (PA6 OP), 18 wt% of OP1311 and 5 wt% of o-Cloisite (PA6 OPC), and 50 wt% of MDH (PA6 MDH), compared with PA6 (heat flux: 50 kW/m² and distance to heater: 35 mm). a) HRR curve vs time and b) temperature at the back of the sample plate vs time.

III. *Influence of Al$_2$O$_3$ deposition time*

1) Characterizations

As previously stated, according to the literature, the dielectric layer in a low emissivity thin coating should be as thin as possible so that it is transparent in the infrared. To observe and confirm whether the thickness of the dielectric layer has an impact on the fire performance of the system, two deposition times were studied. In a first system, called C1, alumina was deposited for 60 min (PA6 C1), and in a second, called C2, alumina was deposited for 210 min (PA6 C2). Whereas PA6 C1 has the grey and shiny color of aluminum, PA6 C2 surface goes from blue to pink and slightly yellow on one edge (Figure 77 a) and b)).

The apparition of these colors depends on the angle of view. It is due to the apparition of thin film interferences caused by the stack of Al/Al_2O_3, and because of the thickness of the alumina layer, and therefore it is probable that there are very slight inhomogeneities in thickness across the sample's surface (a few nanometers).[439] Tape peel tests (Figure 77 a) and b)) show that the adhesion of C2 is satisfactory, but not as good as C1, as some parts of the coating went off when the tape was stripped of the surface (reaching a 3B rate instead of 5B for C1).

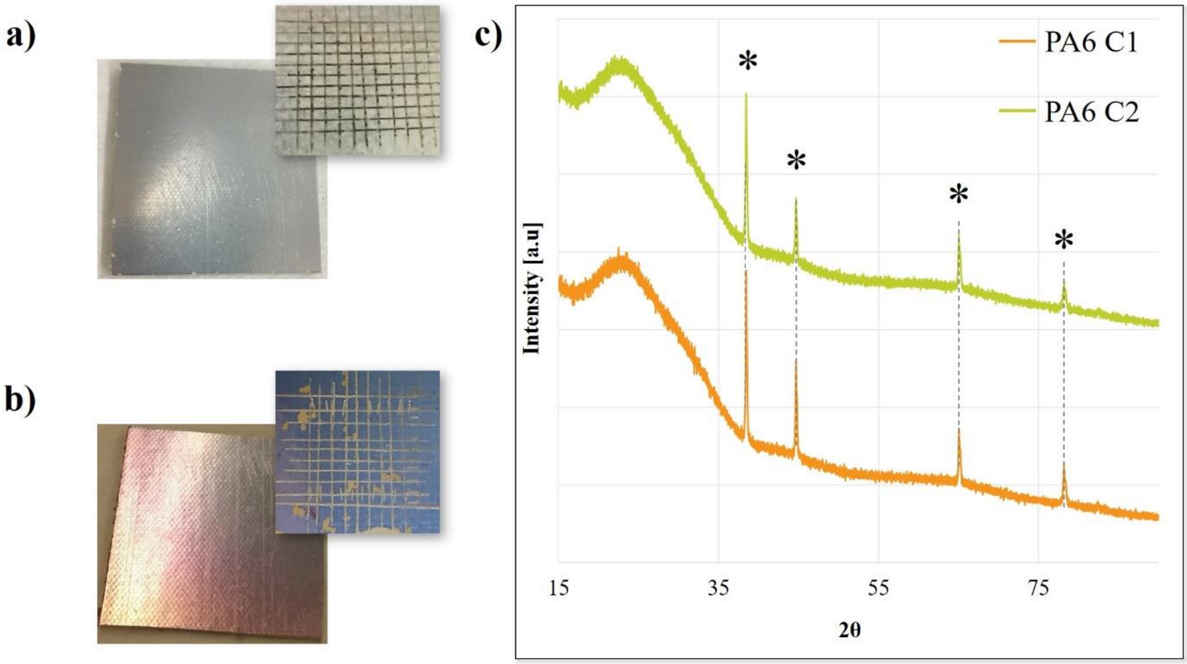

*Figure 77. Digital images of a) PA6 C1 and b) PA6 C2. Inserts show the results of the tape peel test. c) XRD of PA6 C1 and PA6 C2 on glass substrates. * shows the distinctive peaks of Al.*

SEM observations combined with energy dispersive X-ray mappings were made on cross-sections of PA6 C1 and PA6 C2 and are presented in Figure 78 a) and b) respectively. In both cases, a dense aluminum based coating is obtained. The Al_2O_3 layer is observed and its thickness calculated by O X-ray mapping (Figure 78 c)). While C1 on PA6 is 1.02 ± 0.03 µm thick, C2 is 1.37 ± 0.03 µm thick, because of a slightly thicker Al_2O_3 layer (0.08 ± 0.02 µm for C1, versus 0.30 ± 0.03 µm for C2). XRD in Figure 77 c) shows no difference between the two coatings, and as a result it is likely that Al_2O_3 is amorphous in both cases.

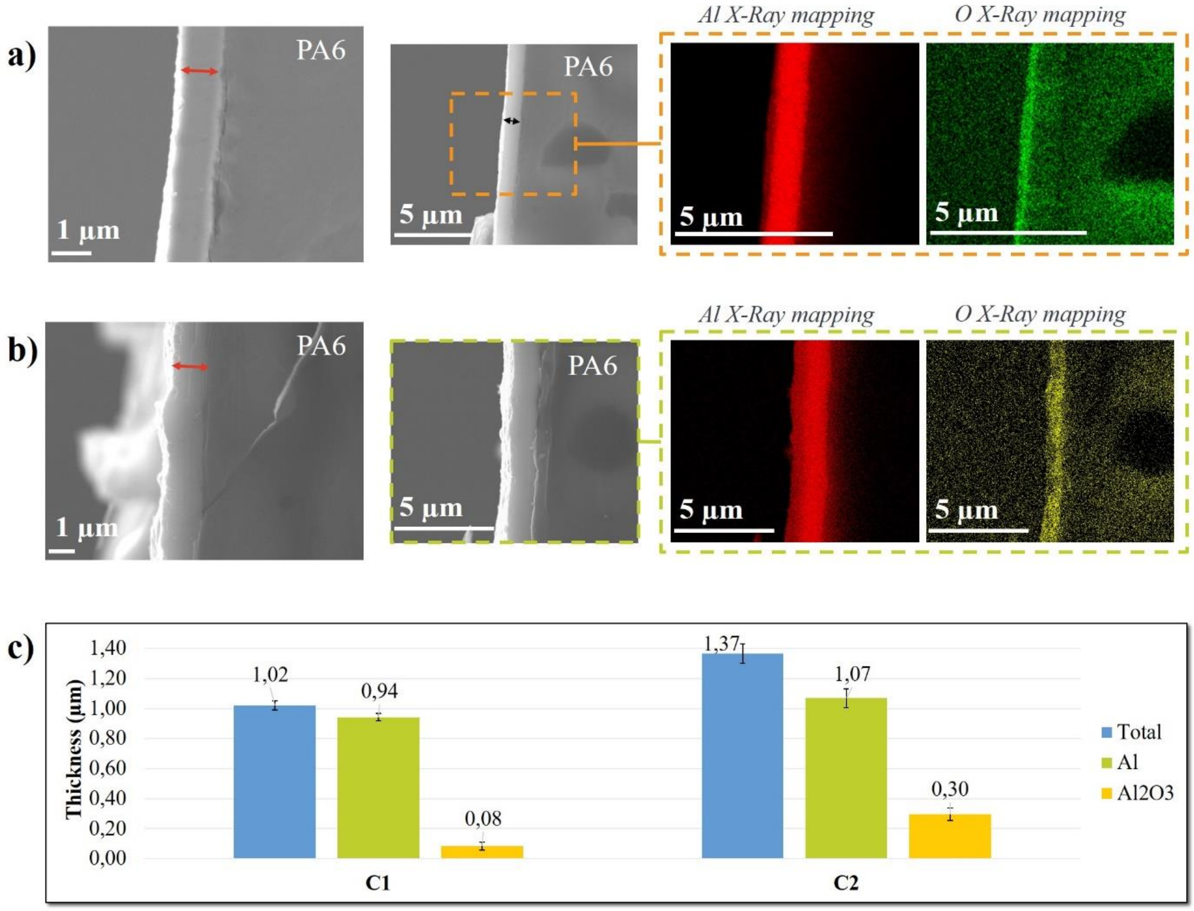

Figure 78. a) SEM, Al X-Ray mapping and O X-ray mappings of a cross-section of a) PA6 C1 and b) PA6 C2. c) Thickness measurements.

Emissivity measurements by infrared diffuse reflectance through an integrating sphere also show no difference in emissivity between PA6 C1 and PA6 C2 (0.23 for both, see Figure 79), but evidence the increase in infrared reflectivity when compared to PA6.

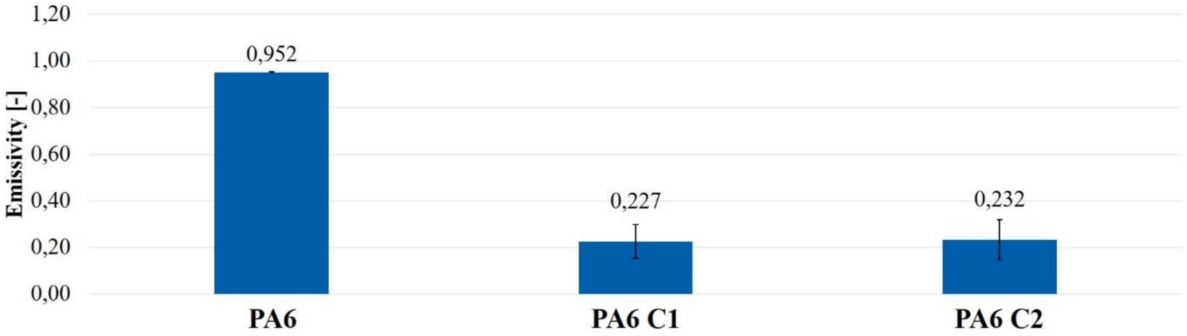

Figure 79. Emissivity of PA6, PA6 C1 and PA6 C2, as calculated by infrared diffuse reflectance measurement through an integrating sphere at room temperature.

2) Fire test: mass loss cone calorimetry

As previously, PA6 C1 and PA6 C2 were tested with a 50 kW/m² heat flux with the same set up.

Remark: In the previous paragraph, the sides of the samples were coated with a non flammable glue in order to prevent an eventual combustion from the sides. The idea was to force the combustion on the exposed surface only, and to improve the repeatability, especially for FR filled plates. As a consequence, the heat accumulation inside the sample was high when compared to a situation where the sides of the samples are bare. In this part, however, the sides of the sample were left bare to have an idea of its behavior in proper mass loss cone conditions.

The change of the boundary conditions had quite an influence on the behavior of PA6 C1. When the edges are isolated, the sample ignites after approximately 16 min (see section I of this chapter). Here, without non flammable glue on the edges, the Al/Al_2O_3 film completely prevented ignition for more than 50 min., as shown in Figure 80. This can be explained by the change in experimental boundary conditions which are no longer insulative. There is no longer accumulation of heat and hence, there is heat dissipation that lengthens the TTI.[440]

When exposed to the cone heater, and after several dozen minutes, the coating warped and then cracked, probably because of mechanical constraints when PA6 transitioned from solid to viscous liquid. However, the release of gases was not observed, which is most likely due to the fact that the decomposition temperature was not reached yet. Afterwards, the substrate swelled critically, starting from the edges, which caused the failure of the protective effect of the coating, and the release of combustible gases in enough quantities to spark ignition after a bit more than one hour. Then, the fuel was consumed and formed a boiling pool underneath the coating. The burning behavior was not modified, with the exception of a slight decrease in pHRR and THR (approximately 25% and 24% respectively, cf Table 31). Only some metallic flakes from the deposit remained as residue after the tests. The coating remained glossy before ignition, and it is safe to say that aluminum was successfully protected by the alumina layer. Additionally, no delamination was observed, which evidences the good adhesion between the metal/dielectric layer and the substrate.

However, PA6-C2 did not ignite, despite the presence of cracks that are visible in Figure 80. The substrate became brownish, which evidenced some level of degradation, and the Al/Al_2O_3 coating was crumpled and remained glossy and slightly pink, with the aspect of oxidized aluminum.

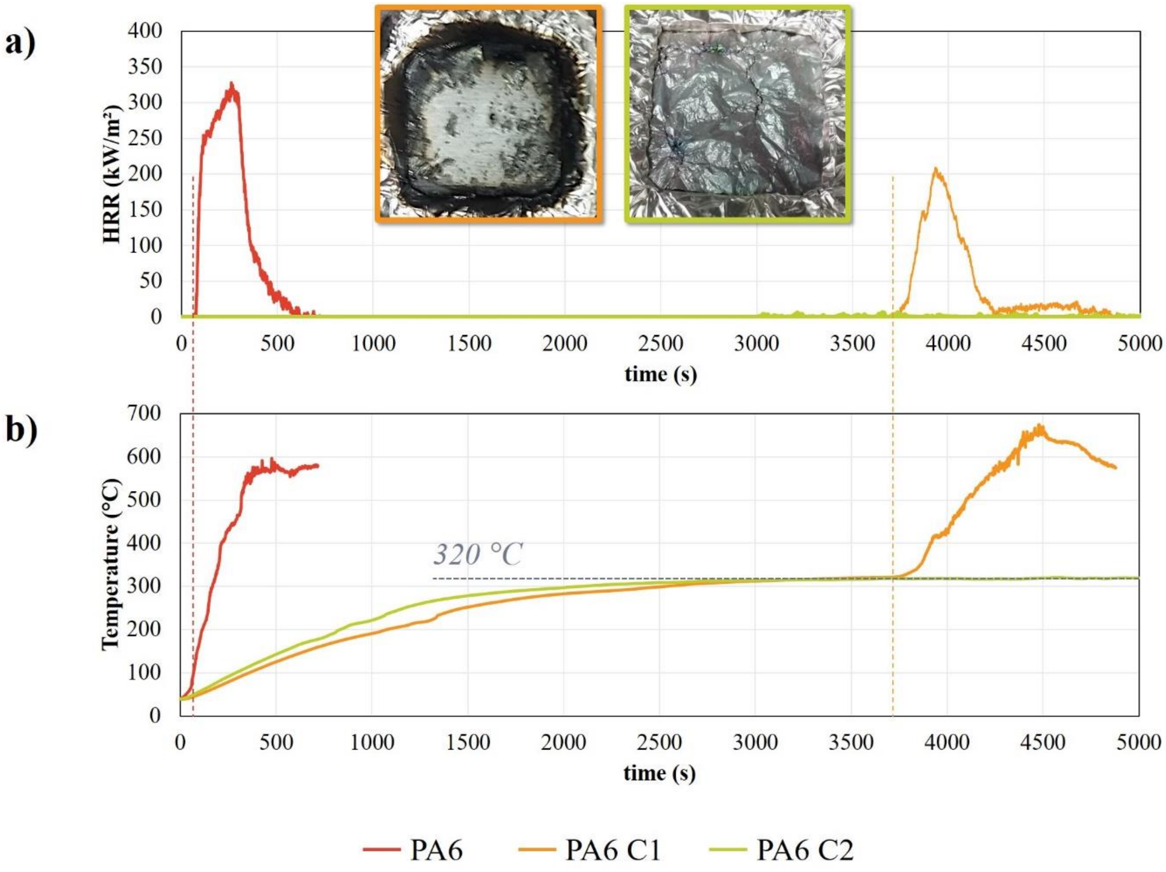

Figure 80. a) MLC test results of Al/Al_2O_3-coated PA6 with two different alumina deposition time: PA6 C1 (60 min) and PA6 C2 (210 min), compared with PA6 (heat flux: 50 kW/m² and distance to heater: 35 mm). a) HRR curve vs time and b) temperature at the back of the sample plate vs time. The inserted digital images show PA6 C1 and PA6 C2 after the test.

Several elements of the temperature curves are to be stressed out (see Figure 80 b)). First, the rise in temperature of both samples is lower than what was presented in section I and II of this chapter, which highlights the importance of the boundary conditions.[381], [441] Secondly, for both PA6 C1 and PA6 C2, an inflexion point is observed around 220°C, which probably corresponds to the fusion of the polymer. Then, interestingly, C2 is at first less efficient than C1 at limiting the rise in temperature. Indeed, the increase in temperature at the back of the sample is quicker at first for PA6 C2 than for PA6 C1, meaning temperatures are kept low for a longer time in the case of PA6 C1. Finally, the temperature is stabilized and a thermal equilibrium is reached as the curve reaches a plateau at 320°C for both samples, until the ignition for PA6 C1, and after removal of the sample after 1h30 without any indication of an evolution for PA6 C2. This leads to the long time to ignition observed, as the temperature is maintained under the critical point for a long period of time.

Table 31. MLC results for PA6, PA6 C1 and PA6 C2.

	TTI ± σ [s] (variation, %)	**PkHRR ± σ [kW/m²] (variation, %)**	**THR ± σ [MJ/m²] (variation, %)**
PA6	73 ± 11	313,0 ± 35,9	82,6 ± 9,5
PA6 C1	4138 ± 284 (5238 %)	236 (-25 %)	63 (-24%)
PA6 C2	No ignition		

3) Discussion and conclusion

The evolution of the emissivity of PA6 C2 as a function of temperature is not different than the one observed for PA6 C1, meaning that the values are stabilized around 0.06 from 60°C to 200°C. This shows the durability of the protection of the coating when exposed to a thermal constraint (Figure 81).

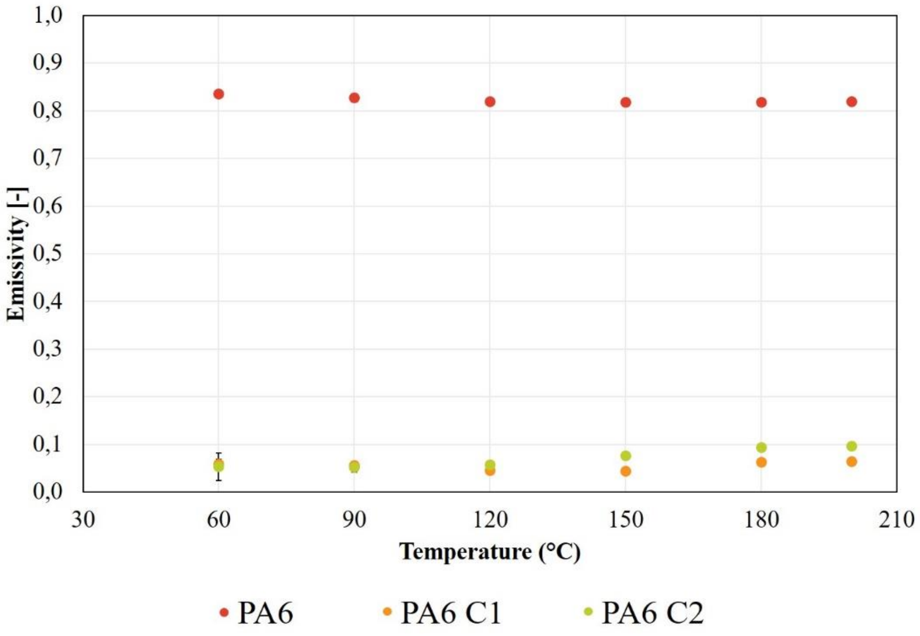

Figure 81. Emissivity of PA6, PA6 C1 and PA6 C2 as a function of temperature.

To conclude, a coating with a thicker alumina layer still provides exceptional protection thanks to the reflection of infrared rays and the resulting limit of heat absorption. Even better, no combustion was observed, even as it reached the same temperature plateau as PA6 C1, and despite the fact that the rise in temperature was at first higher than PA6 C1. This once again triggers the thought that despite radiative heat shielding being the main mechanism of protection, there are other parameters at play in the performance of low emissivity coatings, especially mechanical robustness. Indeed, despite the presence of cracks (Figure 80), they did not propagate on the surface, which kept the degradation under a critical level.

IV. Perspectives: application to other substrates – example of Polypropylene (PP)

1) PP and fire retardant PP

Polypropylene is one of the most used commodity polymers, but also very flammable, and as such a fire retardant treatment is necessary. Effective fire retardants molecules or fire retardant systems have been found throughout the years but the fact remains that PP has a low time to ignition which is part of its fire hazard. Here, a low emissivity Al/Al_2O_3 coating was deposited on virgin PP plates and the influence of Al_2O_3 deposition time was investigated (final samples are named PP C1 and PP C2 in the following). Then, it was deposited on FR PP plates filled with 10 wt. % of expandable graphite (the name of the uncoated and coated FR PP plates are called PP EG and PP EG C1 respectively in the following).

Figure 82 a_1 and b_1) shows digital pictures of PP C1 and PP C2, and Figure 83 shows PP EG C1 after deposition of the low emissivity coating.

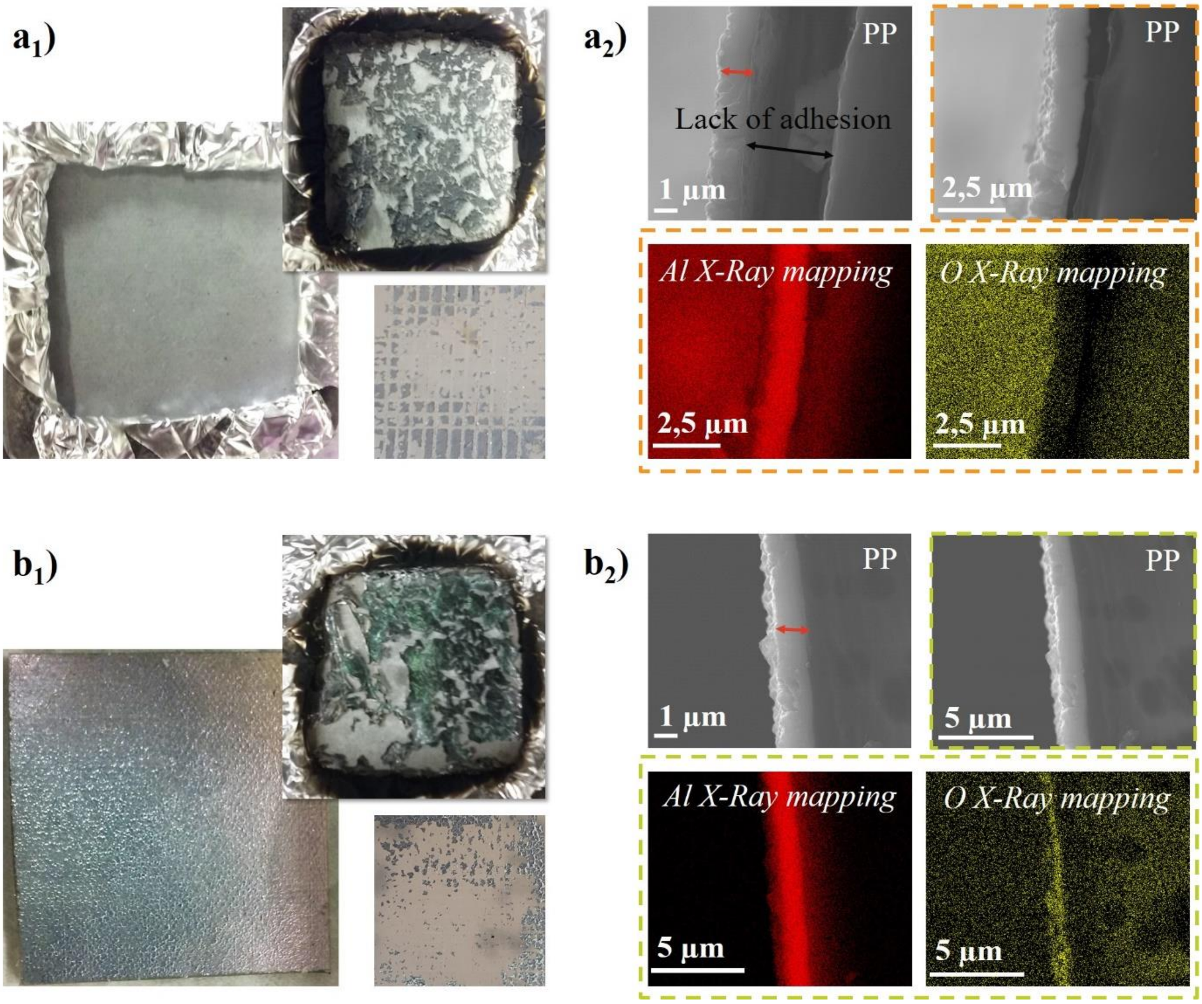

Figure 82. a_1) Digital images of PP C1 before (left) and after (insert) test. The bottom right image is the result of the tape peel test. a_2) SEM images of PP C1. Framed images are Al and O X-ray mapping. b_1) Digital images of PP C2 before (left) and after (insert) test. The bottom right image is the result of the tape peel test. b_2) SEM images of PP C2. Framed images are Al and O X-ray mapping.

They exhibit a shiny and metallic aspect with the aluminum grey color, slightly attenuated by a milky hue due to the alumina layer. They have a matter aspect than what was observed for PA6, which might be due to a higher roughness. Peel tape adhesion tests showed that the coating adheres poorly to PP plates despite the plasma pre-treatment and is rated 0B for PP C1 PP C2 and PP EG C1 which is the lowest rating (this problem can also be seen on SEM images in Figure 82 a_2), where the coating delaminated upon sampling). This would be a point to address if the system had to be used commercially. However, the coating resists light stresses and does not delaminate when the plates are cut, and adheres to the substrate enough for the tests.

SEM images in Figure 82 a_2) and b_2) show that the Al/Al_2O_3 coating is uniform and continuous. The adhesion issue prevented the measurements of the thickness of C1 but it is expected to be similar to PA6 C1. PP C2 is 1.26 ± 0.06 µm thick with an Al_2O_3 layer around 0.38 ± 0.04 µm thickness (measured by EDS O X-Ray mapping). Because of this, the same slight pink/blue hue as PA6 C2 is observed for PP C2, because of thin film interferences.

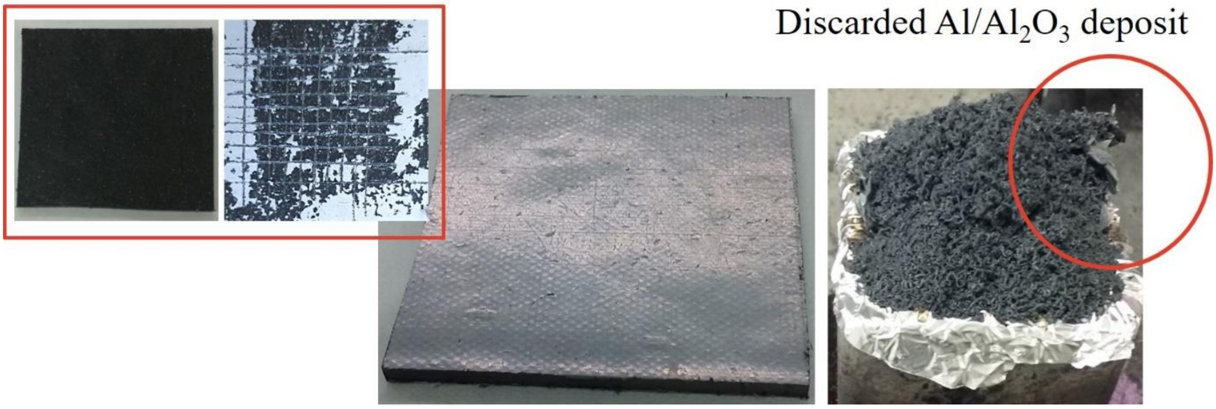

Figure 83. Digital images of PP EG C1 before(left) and after test (right). The inserts on the left show PP EG (left) and the result of the tape peel test (right).

Measuring the emissivity of uncoated and coated PP and PP EG shows that the reflectivity of infrared rays is indeed enhanced with Al/Al_2O_3. The calculated values are gathered in Figure 84. Surprisingly, the emissivity of PP C2 (0.19) is lower than that of PP C1 (0.31). It could be linked to the difference in term of roughness between the two tested samples. In addition, the variation and the value of the emissivity, especially for PP C1 and PP EG C1 (0.34) is higher than for PA6 C1, which is probably due to an increased surface roughness.

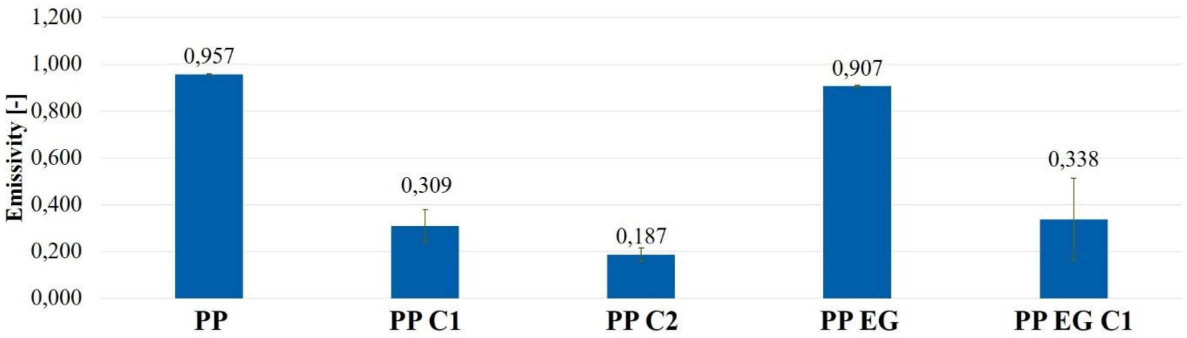

Figure 84. Emissivity of PP, PP C1 and PP C2, as well as PP EG and PP EG C1, as calculated by infrared diffuse reflectance measurement through an integrating sphere at room temperature.

The emissivity of PP is constant (~0.83) even as the temperature increases from 60°C to 150°C, whereas for PP EG, it stabilizes around 0.8 (see Figure 85). For all coated samples the emissivity stabilizes between 60°C and 150°C at 0.1, with no difference between PP C1, PP EG C1 and PP C2.

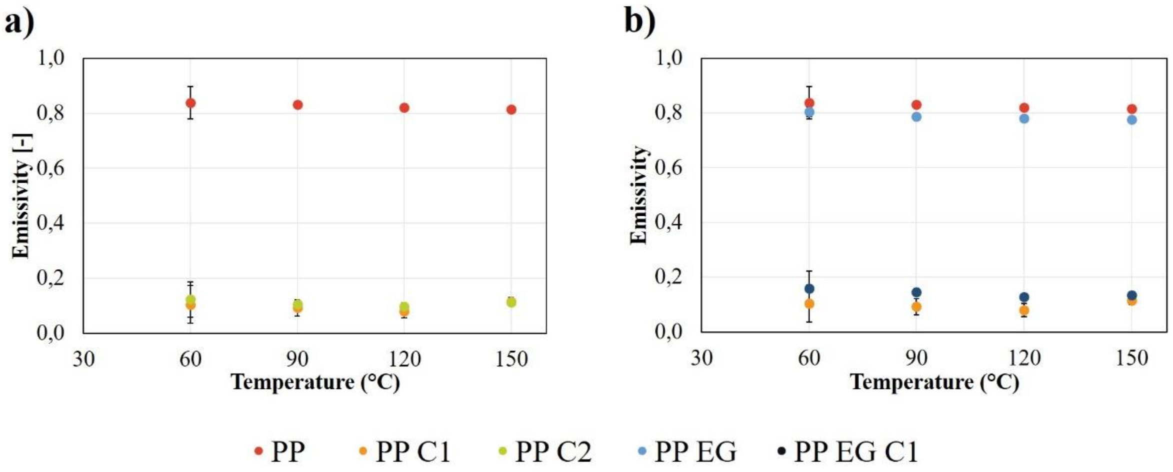

Figure 85. a) Emissivity of PP, PP C1 and PP C2 as a function of temperature. The emissivity of PP EG and PP EG C1 as a function of temperature are presented in b).

2) Fire testing

HRR curves versus time are plotted in Figure 86 a). Neat PP ignited after only 40 s of exposure, whereas PP C1 and PP C2 ignited after 7 min and 6 min respectively. The ignition occurred after the failure of the coating, which was followed by the release of combustible decomposition products. Afterwards, the protective effect was completely lost and no influence on the burning behavior of the polymer was observed (whether in terms of pHRR, THR or shape of the curve, cf Table 32).

The material decomposed with the deposit floating on top of the boiling fuel pool until it was completely consumed, and there was no residue except for the degraded coating (Figure 82 a_1)). The residue of PP-C1 still had the aspect of an oxidized aluminum foil, whereas the residue of PP-C2 showed a blue hue (Figure 82 b_1)), which was assumed to be linked to interference colors due to the evolution of Al_2O_3 under the harsh conditions. The coating remained glossy before ignition, and it is safe to say that aluminum was successfully protected by the alumina layer. Additionally, no delamination was observed during the test, despite the poor adhesion of the coating.

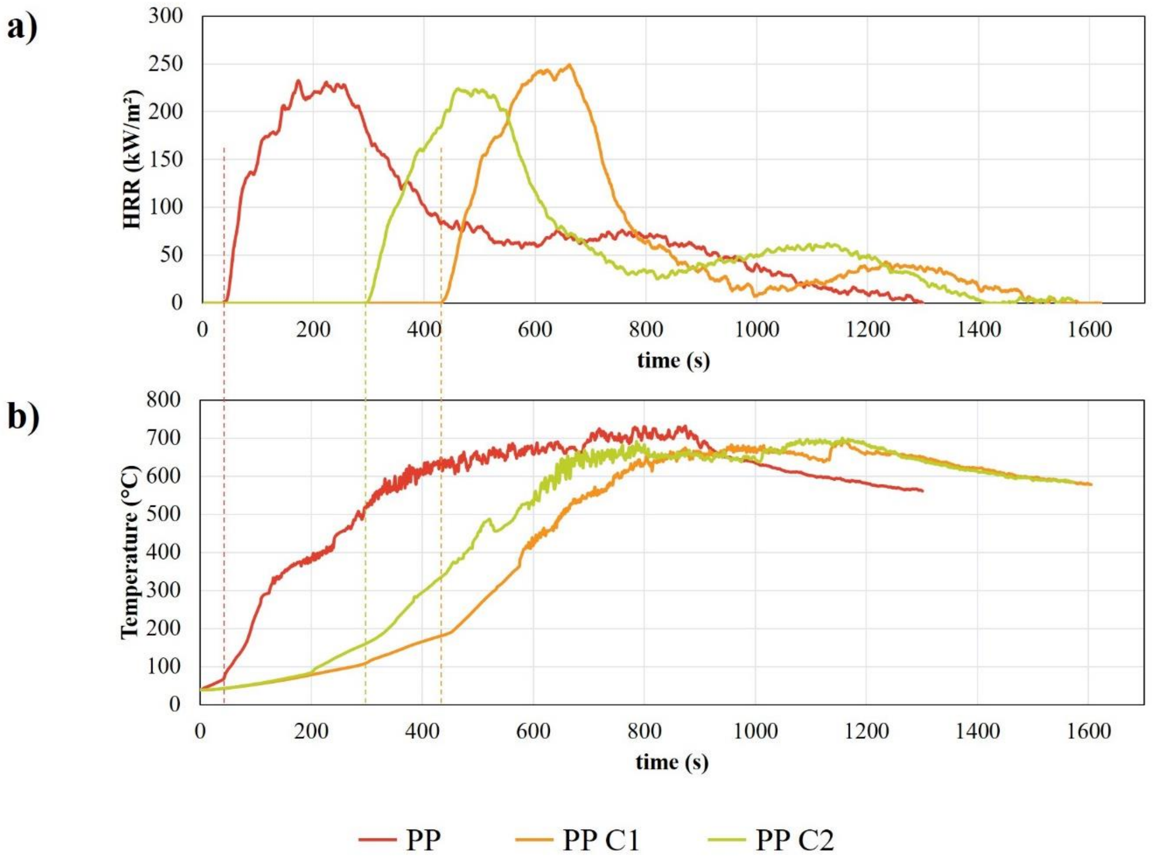

Figure 86. a) MLC test results of Al/Al_2O_3-coated PP with two different alumina deposition time: PP C1 (60 min) and PP C2 (210 min), compared with PP (heat flux: 50 kW/m² and distance to heater: 35 mm). a) HRR curve vs time and b) temperature at the back of the sample plate vs time.

The temperature measurements in Figure 86 b) show the slowdown of the temperature rise at the back of the coated sample when compared to an uncoated PP. The coating with the lowest alumina deposition time kept temperature at lower levels than that with higher deposition time, and for a longer time. Nevertheless, it is less noticeable than with PA6 substrates. Interestingly, according to the data from PP C1, the temperature at the back of the PP sample was kept under 200°C for approximately 7 min thanks to the low-emissivity surface. It is important because the EG particles selected for the FR PP formulation activate between 200 °C and 230 °C. Therefore, it can be expected that the low emissivity surface will keep the FR filler from activating for the same time, effectively increasing the time to ignition of the FR plate.

Table 32. MLC results for PP, PP C1 and PP C2.

	TTI ± σ [s] (variation, %)	**PkHRR ± σ [kW/m²] (variation, %)**	**THR ± σ [MJ/m²] (variation, %)**
PP	40 ± 2	219 ± 20	96 ± 6
PP C1	437 ± 3 (+986 %)	244 ± 11 (+12 %)	77 ± 12 (-20 %)
PP C2	349 ± 73 (766%)	213 ± 22 (-3%)	85 ± 0 (-12 %)

Figure 87 a) shows the HRR curves of PP, PP-EG and PP-EG-C1. Polypropylene filled with 10 wt. % EG ignites very quickly, even when compared to control. The time to ignition is only 23 seconds, which is 44% less than that of the neat PP. However, pHRR is reduced from 219 kW/m² to 96 kW/m², corresponding to a 56% reduction. THR is also reduced by 47%, decreasing from 96 to 51 MJ/m². These values, summarized in Table 33, show how effective expandable graphite is at reducing flammability of polypropylene, with the exception of the short time to ignition.

The mode of action of expandable graphite is physical intumescence. Upon heating, the molecules inserted between the graphite layer sublimate, leading to graphite worms forming an intumescent protective entangled network. The swelling and formation of the interpenetrating network smother the flame and dissipate heat.[442] This effect is not lost upon modification of the polymer surface with the low-emissivity Al/Al_2O_3 layer, and a complementary effect is observed: the graphite worms do not expand right away thanks to the reduction of heat absorption. Instead, the coating remains flat and glossy, and after a while, some individual worms start to pierce their way through the film, and swelling starts to occur at the edges of the sample. However, no release of combustible gases was observed until the swelling increased and reached the middle of the sample. Ignition occurred after 7 min on average, and the reduction in pHRR and THR brought by EG particle was maintained (see Table 33). The important swelling caused the coating to be completely discarded on the sides, leaving the PP-EG sample to burn and swell as if without coating (Figure 83).

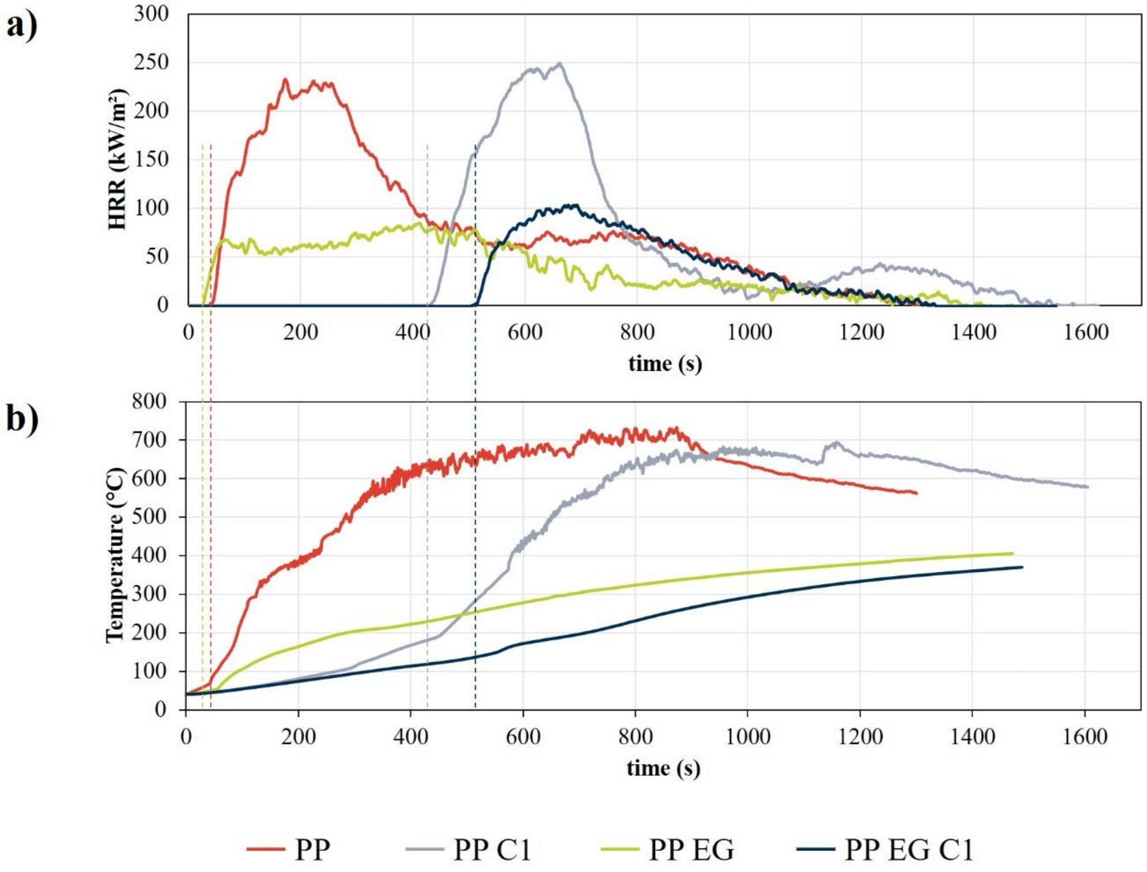

Figure 87. MLC test results of PP formulated with 10 wt% of EG, without (PP EG) and with (PP EG C1) Al/Al_2O_3 coating, compared with PP and PP C1 (heat flux: 50 kW/m² and distance to heater: 35 mm). a) HRR curve vs time and b) temperature at the back of the sample plate vs time.

As summarized in Figure 87 b), the addition of EG already provides some thermal protection, as it prevents the temperature to rise too high, even after ignition. This is due to the interpenetrating network and heat dissipation mechanism of the graphite worms providing an insulating effect. As previously observed, the presence of the thin low-emissivity coating hinders heat absorption, which further limits the increase in temperature at the back of the sample. Therefore, the temperature is kept below the activation temperature of the selected FR fillers for a longer time, effectively increasing the time to ignition. It is interesting, however, to observe that both mechanisms act completely independently to one another. The swelling completely destroys the coating, which has no further effect on the combustion behavior.

Table 33. MLC results for PP, PP EG and PP EG C1.

	TTI ± σ [s] (variation, %)	**pHRR ± σ [s] (variation, %)**	**THR ± σ [s] (variation, %)**
PP	40 ± 2	219 ± 20	96 ± 6
PP EG	23 ± 2 (-44%)	96 ± 9 (-56%)	51 ± 5 (-47%)
PP EG C1	435 ± 95 (+980%)	116 ± 11 (-47%)	44 ± 3 (-54%)

V. General discussion, conclusion and perspective

It was shown in this chapter how low emissivity metal/dielectric coatings lower heat absorption by reflecting infrared radiation over the range corresponding to high temperature radiation. The combination of a thin layer of metal protected by a thin layer of transparent dielectric material creates a broad range mirror that adheres to polymers and increases their time to ignition considerably. They complement or even improve fire retardant fillers by delaying their activation without inhibiting their effect, producing materials with both long time to ignition and low pHRR and THR. Measurements of the evolution of the emissivity as a function of temperature show that they keep their protective effect constant at least until the substrate starts to degrade (200°C for PA6).

This study raises several questions, some of them having already been stressed out throughout this chapter. First, two coatings with different metallic layers have similar fire performances despite the differences of behavior during the test. Then, the temperature at the back of a sample with a thicker dielectric layer will increase faster, but will show a better fire performance than a coating with a thinner dielectric top coating. The influence of adhesion, mechanical robustness…was not addressed and is probably of importance. Moreover, the action of the coating on impeding mass transfer also has a significant role. Then, the effect of low heat absorption on the degradation of the substrate, and its evolution during the test should be studied to have more insight on the behavior of the system against the thermal constraints. Especially in FR filled plates, it could have an effect on the quality of the protective ceramic layer, in particular in the case of PA6 MDH.

The behavior of the polymer right at the interface between the coating and the bulk before and during the test could also be particularly interesting. A point to clarify would be the influence on the optical and barrier properties of the coating of:

- The state of the surface of the substrate and its evolution during the test
- The nature of the interface between metal and polymer and between metal and dielectric, and its evolution during the test.
- The structure of the coating (number and stack of layers, presence of anti-diffusion layers, of an adhesion layer…)
- The nature of the dielectric material (for example, using nitrides instead of oxides).

Selective surfaces are systems that are good reflectors in a certain range of the electromagnetic spectrum, and highly absorbing in another. This is the principle behind radiative cooling of materials: the coating is reflective in the infrared range of interest, and absorbs in the other. Consequently, it simultaneously reflects heat and radiates it away, which eventually cools the material. Using such selective surfaces would be a very interesting lead to follow afterwards for the fire protection of substrates (for example, design a coating that reflects radiations in the 1-13 µm range but absorbs light outside of it). This problem of heat loss from re radiation also raises the question whether it exists an optimum emissivity or whether it should be as low as possible. Our results tend to be in favor of the latter, but it is to be explored further.

Durability of the coatings was not addressed, although it is a very important point when considering applying low emissivity coatings to fire protection. The point of using such coatings is only valid if they keep their reflective properties in the environment they are subjected to. Normally the dielectric layer is there to keep the metal from degrading, and it filled its role for the duration of our study, but it would be necessary to test it against various constraints to attest for it.

As was seen in this chapter, the influence of the emissivity of the surface has a great influence on the ignitability of polymers and on radiative heat transfer between a heat source and a material. Improvement of the surface treatment is always possible, either to broaden the high reflectivity range of the coating, to target a specific range for a specific thermal constraint with filters, or to improve the mechanical properties. It is also possible to adjust the thickness of each layer to obtain a transparent film in the visible range or to adapt the properties. A simplification of the coating to make only one layer would also be interesting, and a lead could be to use alloys of metals with a high durability, as proposed by Hu et al. They proposed an alloy of a metal with another transition metal compound (in their study Ag and HfN) which greatly improved Ag durability in harsh environments and preserved the broad range reflective properties of the metallic coating. This approach has the merit of eliminating the risk of element interdiffusion between the metal and the dielectric, as well as simplifying the system.[443] The study of other design or method of deposition to make low emissivity coatings could also be interesting to look into. It should also be interesting to have a photonic, or metamaterial approach to see if patterning the surface to reach original optical properties is interesting for fire protection. It is very likely that this concept can be applied and extended to other flammable substrates as well. The only caution would be to check how the roughness of the substrate affects the radiative properties of the film and its fire performances. It was applied on rough 3D printed multimaterial, for instance and the result was very promising, showing the high potential of low emissivity coatings. The results were submitted and accepted in ACS Omega. Finally, as both fire retardant surface treatment and infrared mirror, they have the potential to be used as multifunctional coating for fire protection and energy saving application, for example.

Conclusion and Outlook

This work was dedicated to the study and design of thin coatings for the fire protection of polymeric substrates. The interest was directed in understanding the systems in order to design new ones, with an interdisciplinary approach and the smart combination of concepts.

The review of literature gathered in the first chapter identified layer-by-layer coatings as a first promising approach for the fire protection of polymeric substrates, especially for porous substrates with complex surfaces. This method is extensively studied because of it high efficiency, ease of use and versatility. However, the reason for the good performances of these systems were still not fully understood.

The focus of the second chapter was therefore to try and gain more insight into the mode of action of layer by layer composite coatings deposited on FPUF, in collaboration with Dr Lazar and Prof. Grunlan from Texas Agricultural and Mechanical University (TAMU). In a first part, a coating composed of 8 BL of CH and VMT was found to sustain various thermal constraint ranging from a simple torch with a low heat flux and butane flow, to a butane torch with a 116 kW/m² heat flux. The coating was found to act as a physical barrier to heat and mass transfer and its effect was reinforced by the open-cell structure of the foam (formation of an exoskeleton). In a second part, the use of h-BN in a LbL coating on PUF showed that it is possible to obtain good fire performance with only a single bilayer, shortening the tedious and time-consuming process of the layer-by-layer process. In addition, its UV protection and preservation of FPUF mechanical properties paved the way for multifunctional and less invasive systems.

The third chapter aimed at applying the concepts uncovered by the mechanistic study of layer-by-layer coatings. Two axes of improvements were carried out. First, high filler content composite coatings composed of alginate and clays were deposited in a one pot process on PA66 fabrics. They exhibited self-extinguishing behavior, reaching the best ranking in UL94 test (V-0 rating). Moreover, the systems were found to act as layer-by-layer coatings evidencing the approach. Then, the concept of hydrogel was applied to improve the thermal stability and barrier effect of the coatings. In addition, the effect of combining different types of clays with different morphologies was studied. It was found that, whereas VMT platelets could provide a barrier effect on their own, SEP needles could create compact charred composite structures that acted the same way. Combining the two effects allowed to reach a higher protective effect.

The fourth chapter was dedicated to the study of protected infrared mirrors (metal/dielectric coatings) as radiative heat barriers for the fire protection of PA6 plates and other flat surfaces. They were found to enhance the reflectivity (lower the emissivity) of the substrate for infrared rays and therefore considerably limit radiative heat transfer. As a consequence, the time to ignition of PA6 was considerably increased, to the point of near incombustibility. However, they failed in limiting the HRR of protected substrates once they ignited. The combination with bulk fire retardants showed the complementarity of the two approaches. The coating acts in the first stages by reflecting infrared rays and limiting heat absorption, therefore keeping the substrate at relatively low temperature (lower than its decomposition temperature) for a long amount of time, delaying the activation of the fillers. Once it fails, the fire retardants take over with their respective mechanisms to limit the heat release rate in a radiative fire scenario. Three different fire retardant systems were studied, and it appeared that the association of low emissivity coatings with magnesium hydroxide (heat sink mechanism and formation of ceramic-like physical barrier) induced a beneficial chain of events leading to an improvement of the performance of the coating and FR PA6 both.

To summarize, three promising systems of thin coatings for the fire protection of polymeric substrates were studied and developed. These include two innovative approaches that proved their potential for the development of surface-based fire protective treatments.

Following this work, several leads can be envisioned. First, layer-by-layer systems consisting of only one bilayer have proven their relevance and new systems with other high-performing nanoparticles should be studied. Hydrogels as passive fire retardant solution can also be pursued, however, the mechanical properties should be improved, especially by optimizing the cross-linking system and the interaction with the filler. Moreover, having a system that restrained water durably could be an interesting lead for development, and improve the time to ignition of the systems. In this regards, having a look at soft robotics and skin biomimetic research could be interesting, as they are currently looking for ways to do this. Moreover, hydrogels are used to design systems that are self-healing. When dealing with surface treatment, the key point is the prevention of cracks that could cancel the protective effect of the coating. Self-healing systems would be a good step in the direction of durability. Finally, infrared reflective systems have proven their great potential and more research is needed to design optimized systems and to understand how they are reacting to fire.

As a concluding note, durability and non-invasiveness of the treatment are the points to address. As a result, designing multifunctional systems in order to have only one treatment for a variety of applications would be extremely interesting, especially with the outlook of going to the industrial scale.

Materials and methods

This paragraph is meant to present the different materials used in this part, as well as the characterizations methods. Each section corresponds to one previous chapter, and the last section is dedicated to the fire tests.

I. Layer-by-layer coatings for fire protection of porous substrates

1) Materials

Branched polyethylenimine (PEI, 25 000 g/mol) and poly(acrylic acid) (PAA, 100 000 g/mol, 35 wt % in water), and hexagonal boron nitride powder (h-BN, 98%, ∼1μm) were purchased from Sigma-Aldrich (Milwaukee, WI, United States of America). Chitosan (CH, 60 000 g/mol, deacetylation 95%) was purchased from G.T.C. Union Group Ltd. (Qingdao, China) and Microlite 963++ vermiculite clay (VMT, 7.8 wt % in water) was purchased from Specialty Vermiculite Corp. (Cambridge, MA). All solutions were prepared with 18 MΩ deionized (DI) water, and the pHs of solutions were adjusted using diluted solutions that were prepared from 37% hydrochloric acid, 97% sodium hydroxide pellets, or 70% nitric acid purchased from Sigma-Aldrich. Open cell, polyether-based polyurethane foam (type 1850, 1.75 lbs/ft3 density) was purchased from Future Foam (High Point, NC). All products were used without further purification and were prepared by using 18 MΩ deionized (DI) water.

Vermiculite is a type of naturally occurring clay. It is a 2:1 phyllosilicate (one octahedral sheet sandwiched between two tetrahedral sheets), with Mg^{2+} and a bit of Ca^{2+}, Na^{+} and K^{+} cations in the interlayer space (see Figure 88).

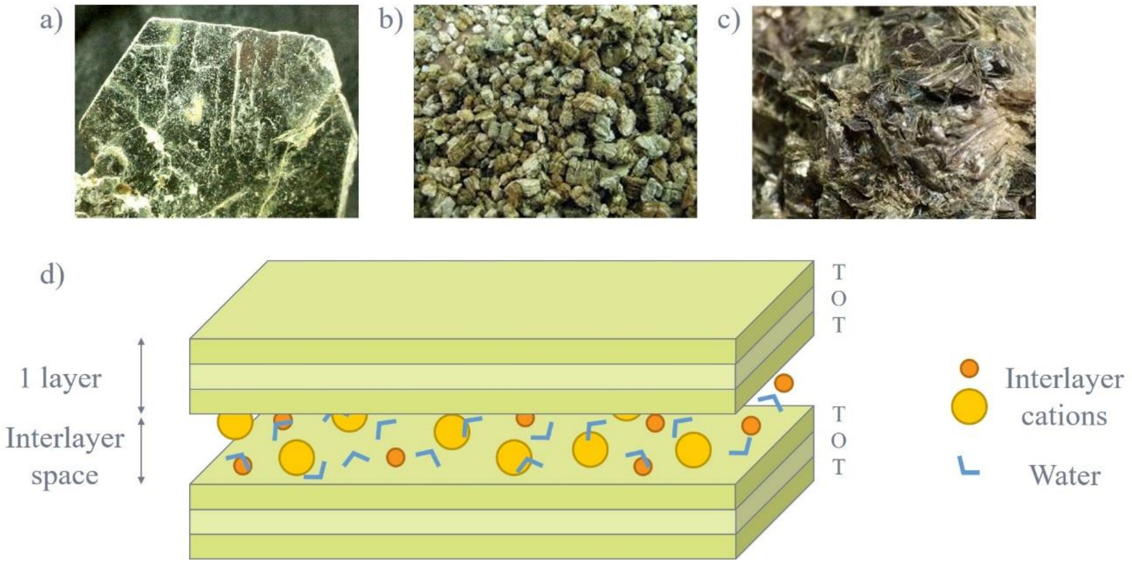

Figure 88. Illustration of a) a natural vermiculite mineral, b) vermiculite granulates for agricultural or adsorbance purposes and c) the foil-like nature of vermiculite. d) Schematic describing the structure of vermiculite, showing two layers with interlayers materials. The layers are composed of one octahedral sheet (O) sandwiched between two tetrahedral sheets. Source of the photographs: ©Wikipediacommons.

h-BN is a graphene-like particle that is starting to attract the attention of the field of fire science. Like graphite, it is a particle composed of a stack of planar sheets, one sheet being composed of B and N atoms covalently linked together in a honeycomb structure (see Figure 89). Its advantage when compared to graphene is its high thermal stability, which is why it is used in high temperature equipment.

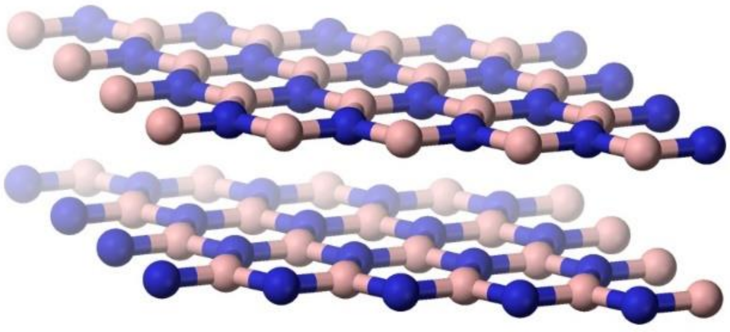

Figure 89. Structure of h-BN, showing two stacked nanosheets. Boron and nitrogen atoms are presented with two different colors. © Wikipedia Commons.

Because of its chemical inertness, electrical insulation properties, and high in-plane thermal conductivity, it is used in lots of other applications as well.[396], [398], [444] They do not have any net surface charge but boron atoms are electron acceptors due to the high polarity of the B-N bond. Therefore, they have a strong affinity for electron-rich amine moiety and can form Lewis adducts with amine-rich molecules such as PEI.

Chitosan is a material derived from chitin, constituted of several units of β-(1→4)-N-acetyl-D-glucosamine. Chitin is a natural polysaccharide whose abundance is second only to cellulose. It is found as ordered crystalline microfibrils as a structural component of the cell walls of fungi or yeast, in squid pens and more importantly in the exoskeleton (cuticle) of arthropods, the main ones being the shell of crustaceans such as krill, crabs or shrimps, which are the main resources of chitin. A chain of chitosan is randomly composed of a fraction of β-(1→4)-N-acetyl-D-glucosamine, the rest being units of β-(1→4)-D-glucosamine (see Figure 90). In the field of fire science, chitosan is favored as an environmentally-benign char forming material, as some other polysaccharides such as starch and alginate.

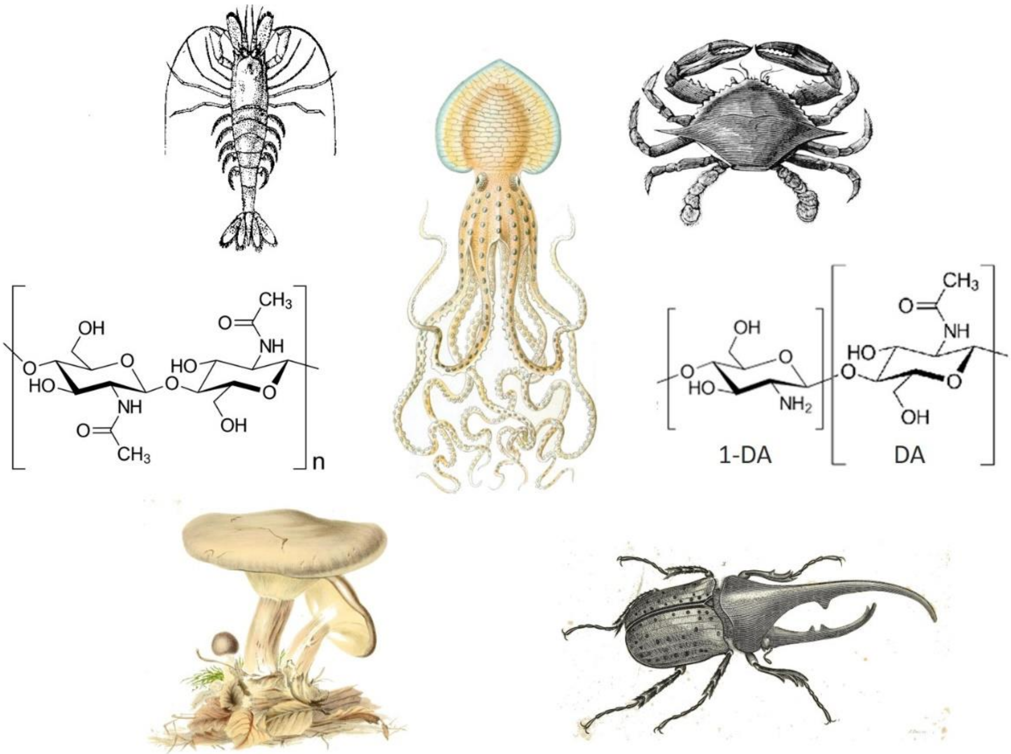

Figure 90. Structures of chitin (left) and chitosan (right). Illustrations represents examples of natural sources of chitin such as shrimp (up left), crab (up right), squid (middle), fungi (bottom left) and other arthropods (here a beetle, bottom right). DA is the acetylated fraction. All pictures are in the public domain and put online by the. Biodiversity Heritage Library.

2) Preparation of the solutions

The h-BN dispersion was sonicated for 8 h by using a 5510 Branson ultrasonic bath to prepare a 1.0 wt% dispersion in water (pH 8). This allowed the hydrolysis of B-N bonds to produce B-OH pendant groups (with the release of NH_3) and render the h-BN nanosheets soluble in water.[399] Microlite 963++ being already a stable dispersion of VMT in distilled water, it was only diluted to reach a 1.0 wt% dispersion (pH 7.8). 0.1 wt% PEI (pH 11) and 1.0 wt% PAA solutions (whose pH was adjusted to 2 using 2 M nitric acid) in distilled water were also prepared via magnetic stirring to ensure proper dissolution. Chitosan was dissolved in distilled water whose pH was adjusted to 1.6 using 5 M hydrochloric acid. After stirring overnight, chitosan was completely dissolved to produce a 0.1 wt% solution, and the pH was once again adjusted to 6 using 5 M sodium hydroxide. The pH of PEI, h-BN and VMT was not altered.

3) Preparation of the substrates

The foams used in this work are open cell, polyether-based polyurethane foam (type 1850,1.75 lbs/ft3 density) purchased from Future Foam (High Point, NC, USA). To ensure the proper adsorption of the layer-by-layer coating, the foam samples were first washed with distilled water and dried in an oven at 70°C. A layer of PAA was then applied as a primer by immersing the material in the solution for 1 min (it was squeezed three times to get rid of air). The foam was then extensively rinsed with distilled water, and the excess solution was wrung out using mechanical rollers. The polymer adheres to the foam through hydrogen bonds and form a negatively charged surface.

4) Deposition

For each system, the first bilayer was deposited by immersing the foam for 5 min in the solution of PEI, followed by 5 min exposure to the solutions of either h-BN or VMT. This produced PEI/h-BN coated PUFs and PEI/VMT PUFs. To obtain CH/VMT PUFs, the PEI/VMT sample was immersed alternatively in CH and VMT solutions for 1 min the necessary number of times to obtain 8 bilayers. All deposition steps consist in squeezing the foam three times in a given solution, waiting for the appropriate time for adsorption to occur, before rinsing the sample extensively in distilled water and wringing out the excess solution between mechanical rollers. The process produced CH/VMT PUFs. The resulting samples were then dried at 70°C in an oven overnight. The process is summarized in Figure 91.

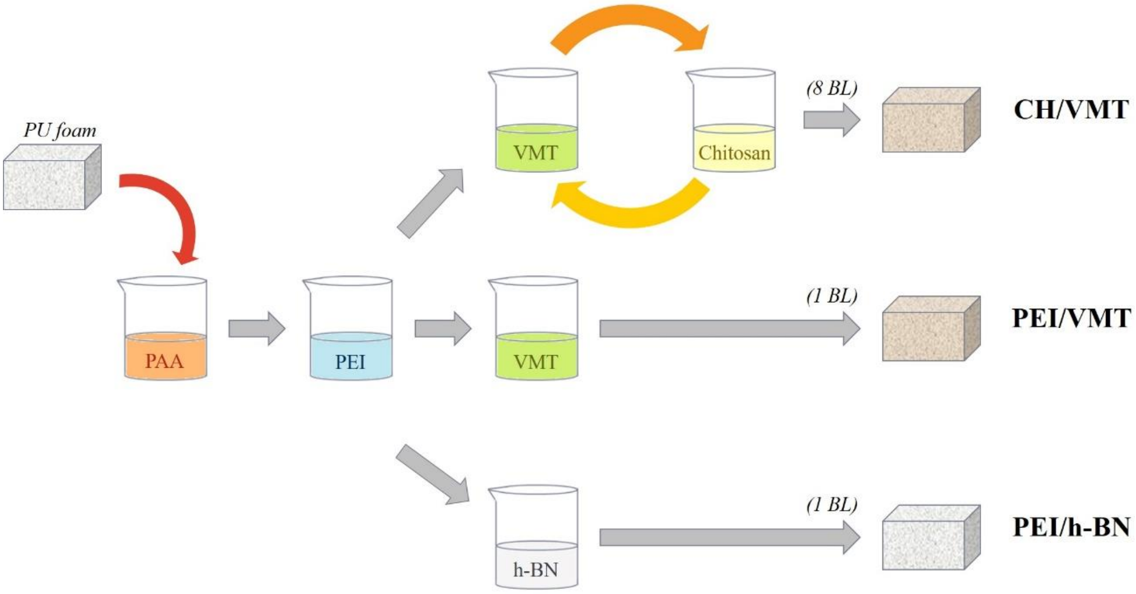

Figure 91. Schematic of layer-by-layer deposition of CH/VMT, PEI/VMT and PEI/h-BN nanocoatings.

5) Characterizations

a. *Growth profile and thickness*

The growth profile and the thickness of the layer-by-layer coatings were determined with an Alpha-SE ellipsometer (J.A. Woollman Co., Inc., Lincoln, NE, USA), equipped with a laser emitting at 632.8 nm. To this end, the coating was deposited on polished silicon wafers (University Wafer, Boston, MA, USA).

b. *Scanning Electron Microscopy*

High magnification images of the surface morphology of the coated and uncoated PUFs before and after fire tests were performed with either a Hitachi S4700 field emission scanning electron microscope (SEM) or a JSM-7500 (JEOL, Tokyo, Japan) SEM. The samples were sputter-coated with 5 nm of platinum/palladium alloy prior to imaging.

c. Transmission Electron Microscopy

The nanostructure of the coatings was disclosed by observing the cross section of the coated PUFs using transmission electron microscopy (TEM). The samples were observed with a Tecnai G2-20 twin TEM (FEI company, Hillsboro, OR, USA).

d. Electron Probe Micro-Analysis

To monitor the deposition and the evolution of the coating through the test, Aluminum and Boron X-ray mapping was performed on cross sections of the treated and control foams and on residues by Electron Probe Micro-Analysis at 15 and 10 kV respectively, using a CAMECA SX100 (Gennevilliers, France). To this end, the samples were embedded in epoxy resin and polished up to 0.25 µm. They were then covered with a 5 nm thick layer of carbon using a Bal-Tec SCD 005 sputter coater.

e. Thermogravimetric Analysis

Thermogravimetric analysis (TGA) is a routine technic used to examine the thermal decomposition of materials. The samples are placed in an alumina crucible in an oven with a controlled atmosphere ensured by a continuous flow of nitrogen (with the optional addition of oxygen for thermo-oxidative conditions rather than pyrolysis), and the degradation is monitored by the mass loss of the sample. Similar to the previously mentioned fire tests, it is possible to follow the gases produced by the degradation by coupling the oven with a FTIR apparatus. In this work, a Discovery thermogravimetric analyser from TA instruments is used, coupled with a Nicolet iS10 was used. A mass of around 6 mg was weighed and the samples were placed in alumina crucibles. Analysis under nitrogen atmosphere were performed between 40°C and 800°C at 10°C/min and 60°C/min with a purge flow and a nitrogen flow set at 15 and 50 mL/min respectively. The temperature was kept at 40°C for 1h before test to have a truly inert atmosphere. As for FTIR analyses, the gases were transferred to the 10 cm pathway gas cell, equipped with KBr windows and heated at 215°C, by a transferline heated at 225°C to avoid condensation (8 scans were performed with a resolution of 4 cm^{-1}, with pre-test background analysis).

f. Solid State Nuclear Magnetic Resonance

Solid state NMR was used to observe the chemical structure of the treated and untreated samples, before and after fire tests. It is a tool used to observe the change in the environment of atoms. It consists in placing the sample in an intense magnetic field and forcing the nuclear spins out of equilibrium by applying a radiofrequency electromagnetic field. The return to an equilibrium state depends on the environment of the atom and generate a signal that can be picked up and interpreted. Contrary to liquid state NMR, solid state NMR must take into account the anisotropy of the atoms' environment in the material. As a consequence, the atoms are submitted to several interactions, namely chemical shift anisotropy, first- and second-order nuclear quadrupolar interaction (in the case of atoms with a spin > 1/2), and first-order dipolar interaction, which have a strong effect on the signal, causing a broadening of the peaks. These interactions have an angular dependency with respect to the applied magnetic field, and can be nullified at certain points. Therefore, the material is reduced ideally in a fine powder and placed in a rotor closed with a fanned lid. The rotor itself is placed in a probe, inclined at a specific angle (54.74° with respect to the magnetic field) and sent spinning. The rotation and the inclination at this so-called “magic angle” average the broadening dipolar interaction and the first order quadrupolar interaction to the point of cancelling it. This technique is appropriately called Magic Angle Spinning (MAS) NMR spectroscopy. However, quadrupolar nuclei such as boron, can also have large second order quadrupolar interaction that cause impractical broadening of the peaks, mismatch between chemical shift (ppm) and apparent position of the signal, and wavy-shaped peaks. In that case, increasing the magnetic field can average weak quadrupolar interaction down, even if cancelling it is impossible at an angle of 54.74°.

In this work, PUFs samples were reduced to small pieces and analyzed using Advance II spectrophotometer from Bruker (Billerica, MA, USA) at different magnetic fields. The signals were collected and interpreted using TopSpin.

i. ^{11}B solid state MAS NMR

^{11}B is quite abundant (its natural abundance is 80.1% according to IUPAC Periodic Table of the Elements and Isotopes) but it has a large quadrupolar interaction which is not easily cancelled. ^{11}B solid state MAS NMR experiments were carried out at 256.7 MHz on an Advance II 800 MHz spectrophotometer. The samples were placed in a 3.2mm probe and spun at 20 000 Hz. The chemical shifts were determined in regards to a $NaBH_4$ standard. The spectra were obtained after 128 scans and simulated using DMFit (v20150521).[445] The pulse was set at π/2 and the relaxation delay D1 at 10 s (respects D1 > $5T_1$).

ii. ^{13}C solid state MAS NMR

^{13}C solid state MAS NMR experiments were carried out at 100.61 MHz on an Advance II 400 MHz spectrophotometer equipped with a low-field 4 mm probe. 512 scans were acquired at a rotating speed of 10 000 Hz. Since ^{13}C carbon nuclei are not very abundant (its natural abundance is 1.07%), cross-polarization experiments with ^{1}H nuclei were also performed. These observations were performed at a speed of 12 500 Hz and with 512 scans. Glycerin was used as standard. The pulse was set at π/2 and the relaxation delay D1 at 5 s (respects D1 > $5T_1$).

iii. ^{29}Si solid state MAS NMR

^{29}Si solid state MAS NMR experiments were carried out at 79.49 MHz on an Advance II 400 MHz spectrophotometer equipped with a 7 mm probe. This was made to have the maximum quantity of material since ^{29}Si is not very abundant (its natural abundance is 4.685%). The rotor was rotating at 5000 Hz. 64 scans were acquired and proton cross-polarization was performed whenever possible at the same settings with 2048 scans. Tetramethylsilane was used as a standard. The pulse was set at π/6 (this choice pulse was a compromise between having a strong signal and limiting the time required for the analysis) and the relaxation delay D1 at 300 s (respects D1 > $5T_1$).

iv. ^{27}Al solid state MAS NMR

Solid state MAS NMR of ^{27}Al is easy since it is very abundant (it is the only stable isotope of aluminum), however, it has a 5/2 spins which complicates the observation, as it has a large quadrupolar interaction. The experiments were carried out at 104.26 MHz on an Advance II 400 MHz spectrophotometer equipped with a 3.2 mm probe at a rotating speed of 20 000 Hz; and 4096 scans were acquired. $Al(H_2O)_6^{3+}$ was used as a standard. The pulse was set at π/2 and the relaxation delay D1 at 1 s (respects D1 > $5T_1$).

II. One-pot high-filler content coatings for fire protection of textiles.

1) Materials

Commercial polyamide 6.6 (52/36 threads/cm, 78dtex, 75gr/sm²) supplied by Delcotex (Bielefeld, Germany) was used in this study. BPEI, PAA, alginate, citric acid, Sepiolite, Halloysite and calcium chloride ($CaCl_2$) were purchased from Sigma-Aldrich (Milwaukee, WI, United States of America). Microlite 963++ vermiculite clay (VMT, 7.8 wt % in water) was purchased from Specialty Vermiculite Corp. (Cambridge, MA). All solutions were prepared in distilled water at unaltered pH.

Sepiolite is a fibrous clay, composed of tetrahedral SiO_4 layers arranged in a lath structure, that gives its needle-like structure. Additional atoms such as Mg are situated on the edge of the layers. Halloysite is another type of phyllosilicate clay with a tubular structure, composed of one layer of aluminium oxide (inner layer of the tube) and one layer of silicon oxide (outer layer of the tube).

Alginate is polysaccharide occurring naturally in nature and extracted from brown algae. An alginate chain is composed of alternating (1→4)-α-L-guluronic acid and (1→4)-β-D-mannuronic acid blocks (MM) units (see Figure 92). It is mainly used for its gel-forming ability but have a lot of application in health, food and cosmetics sectors. As chitosan, its main interest for fire protection is its char forming ability. In this study, alginate was chosen as it easily forms hydrogel, but also because it is known to be used as clay surfactants, both because of its viscosity and because of its interaction with the particles surface. Therefore, stable dispersion of clay and alginate could be obtained, which is mandatory for their use in one-pot processes.

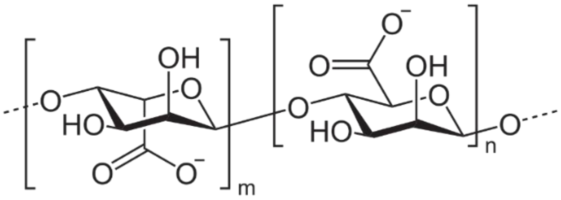

Figure 92. chemical structure of alginate.

2) Preparation of the solutions

Alginate/clay dispersion were prepared in two steps. First, 7 wt% of clay was dispersed in distilled water by stirring the solution overnight with a magnetic stirrer, followed by a 30 min treatment in an ultrasonic bath. The dispersion was then heated to around 70°C and 3 wt% alginate was introduced. The solution was stirred until the alginate was dissolved, before it was cooled down to room temperature (in the case of vermiculite, the viscosity of the solution increased to the point where it looked like a paste and magnetic stirring was not possible anymore. The solution was therefore mixed rigorously by hand until the viscosity decreased and the solution went back to a viscous liquid state, allowing magnetic stirring). When two types of clays were mixed, they were added in a 50/50 ratio. When three clays were mixed, they were added in equal proportions (each clay representing a third of the total clay mass). To ensure proper dispersion, the stirring was pursued overnight and the final solution submitted to a 30 min ultrasonic treatment. Once formed, the solutions were stable and no sedimentation was observed for at least a day. 2 wt% PEI and 2 wt% PAA solutions were prepared in distilled water. 2 wt% $CaCl_2$ and 0.5 M citric acid were dissolved together in distilled water to prepare the baths for alginate gelation.

3) Deposition

Prior to deposition, the substrates were washed 15 min in an ultrasonic bath, first in ethanol then in water. After they were dried, they were immersed 60 s in a PAA solution followed by 60 s immersion in a PEI solution after a rinsing step. A first thin layer of Alginate/Clay was then deposited on the fabrics by soaking them in the alginate/clay dispersion for 60s and removing the excess solution by a padding step. The fabrics were then mounted on a self-made frame so that the whole surface was accessible, and the alginate/clay composite coating was casted on both sides with a paint brush to reach a wet add-on of 600 wt%. In the case of composite coatings, the samples were hung horizontally in ambient conditions to ensure uniform drying. In the case of xerogel composite coatings, the coated samples were immersed in the $CaCl_2$/citric acid solution overnight in order to form an alginate composite hydrogel. Afterwards, they were rinsed extensively with distilled water to get rid of excess ions, and hung horizontally to dry in ambient conditions.

4) Characterizations

a. Scanning Electron Microscopy

High magnification images of the cross-section morphology of coated and uncoated PA66 fabrics before and after fire tests were performed with a JSM-7500 (JEOL, Tokyo, Japan) SEM, as well as Energy Dispersive X-Ray mappings. The samples were sputter-coated with 5 nm of platinum/palladium alloy prior to imaging. The analyses were done at 5kV, 7µA and at a working distance of 10mm.

b. Thermogravimetric analysis

Thermogravimetric analysis were performed from 40°C to 1000°C in N_2 atmosphere on a TG 209F1 Libra (Netzsch, Selb, Germany), at a speed of 10°C/min. The nitrogen flow was set at 50 cm^3/min, and around 5 mg of sample was placed in open alumina crucibles.

c. Fourier Transform Infrared spectroscopy (FTIR)

Attenuated Total Reflectance (ATR) FTIR spectra of uncoated and coated PA66 samples were acquired on a IS50 spectrometer (Thermofischer, Waltham, MA, United States of America) from 400 cm^{-1} to 4000 cm^{-1} with a resolution of 4 cm^{-1} and 64 scans. The number of background scans was set at 64. The acquired spectra were interpreted using the software OMNIC.

III. Low-emissivity coatings for the fire protection of raw and formulated polymer substrates

1) Materials

Commercial polyamide 6 (Domamid H24) supplied by Domo Caproleuna GmbH from Domo Chemicals (Leuna, Germany) was used in this study. Different fire retardant systems were used:

- a mixture of aluminum diethylphosphinate (DEPAL) and melamine polyphosphate (MPP) commercialized under the name Exolit ® OP1311 by Clariant GmbH (Frankfurt am Main, Germany) was used as an intumescent fire-retardant additive for PA6 with a loading of 23 wt. % (the selection of this loading is based on our previous work).[433], [434]

- Cloisite 30B from Southern Clay Product (San Antonio, TX - USA) was used with a loading of 5 wt. % combined with 18 wt. % of OP1311 in PA6.[433], [434]
- Magnifin H5A from Huber (Bergheim, Germany) was used with a loading of 50 wt. % in PA6.[437]

Commercial polypropylene (PP 089Y1E) was supplied by Repsol (Madrid, Spain). An intumescent polypropylene compound was obtained by loading 10 wt. % of ES350F5 expandable graphite (EG) (Graphitwerk, Kropfmühl, Germany), based on our previous work.[442]

200mm metallic targets (99.99 % purity) from A.M.P.E.R.E Industrie (Saint-Ouen-l'Aumône, France) (99.99 % purity) were used for PVD deposition.

2) Processing

Virgin polymers pellets and compounds pellets were processed using a HAAKE Rheomix OS PTW 16 twin-screw extruder (co-rotating intermeshing twin crew, barrel length of 400 mm, screw diameter 16 mm, 10zones). Raw ingredients were dosed and introduced into the extruder with separate gravimetric side feeders. Polymer flow rate was fixed at about 420 g/h with a rotating speed of 250 rpm. Temperature in the different zones in the extruder were fixed at the following values: 270/270/260/260/260/250/250/230/230/210 °C for PA6 and PA-FR, 190/190/190/190/190/190/190/190/190/190 °C for PP. This temperature profile had to be adapted in the case of PP filled with expandable graphite in order to have a homogeneous distribution of EG particles: 200/200/200/200/200/170/185/180/200/200 °C (the adapted profile did not impact the behavior of raw PP samples during MLC). PA6 can degrade during the extrusion process in presence of water. To prevent it, polymer pellets and OP1311 powder were put at 70°C in an oven overnight prior to extrusion. Once air-cooled, the filaments obtained were cut into pellets with a pelletizer from Thermo Scientific (Waltham, Massachusetts, USA). 10 x 10 x 0.3 cm^3 plates were then molded by thermocompression using a Fontune press from Fontijne Grotnes B.V. (Niles, Michigan, United States).

3) Deposition

a. Physical Vapor Deposition: pulsed DC magnetron sputtering

The physical vapor deposition (PVD) methods are a set of coating synthesis techniques of metallurgical or ceramic films for various applications as in mechanics, optics, microelectronics, chemical and aeronautical industries, etc... In a general way, coatings are deposited at low pressure (<10 Pa) following mainly three stages: creation of a metallic vapor from a source (or target), its transport in the target - substrates space and its condensation on the surface of a substrate to be coated.

Magnetron sputtering consists in sputtering a solid target (cathode), which is the material to be deposited, with positive ions of inert gas plasma.

First, the chamber is evacuated down to a pressure of about 10^{-4} Pa, before an inert gas (argon) is injected to obtain the working pressure. Plasma is generated by a discharge between the target that acts as the cathode (between –1 to -3 kV), and the walls of the chamber, which are grounded. Argon ions (Ar^+) of the discharge are then accelerated towards the target. The discharge is maintained in the vicinity of the target's surface thanks to secondary electrons generated by the target's bombardment.

Positive ions are accelerated towards the negatively polarized target under the effect of an electric field and these ions bombard the target's surface. Several mechanisms can occur on the target's surface:

1) The impact creates a charge transfer between the target and the incident ions which is neutralized and reflected.
2) The Ar^+ ion implantation in the target
3) A secondary electron is ejected which will contribute to maintain the discharge. Therefore, the plasma is self-sustained.
4) The momentum transfer from the incident ion ejects atoms from the target: this is the sputtering process. This phenomenon occurs under the condition that the energy of the incident ion exceed the "sputtering threshold" (between 15 and 30 eV for metals).

Once the species of the target are ejected, they travel to the cold substrate and condense to form a thin film.

Magnets (the magnetron) with opposing polarity are placed underneath the target, as well as a pole piece. They generate a magnetic field around it, which traps the electrons of plasma. The increasing concentration of electrons increase the probability of collision with Ar atoms which creates a high density plasma around the target. As a result, the deposition speed is increased to reasonable levels, allowing its application in industry.

Pure metallic targets are used for this study. Two methods exist in order to deposit ceramic layers such as oxides, nitrides or carbides. The first one is to sputter a ceramic target in argon, and the other one is to sputter a metallic target in reactive plasma (a mixture of argon and reactive gas). In this study, we focus on the latter, which is the reactive mode. The gas (O_2 for oxides, N_2 for nitrides…) will react with the metal (essentially the target where the plasma is localized, this is target poisoning) and the resulting material is sputtered. The contamination of target's surface during the deposition of the dielectric is a problem that leads to electrical instabilities. This can lead to two phenomena:

- The breakdown of the dielectric layer; as it breaks, scraps of the material can impact the substrate and provoke defects during the film growth.
- The formation of electric arcs between the dielectric and a metallic surface can project droplets on the substrate.
- The formation of electric arcs between the dielectric and a metallic surface at negative potential can damage the structure.

Several solutions can be used to prevent these problems. Here, the target is submitted to a pulsed direct current at a frequency of 50 kHz. The process is summarized in Figure 93.[446], [447]

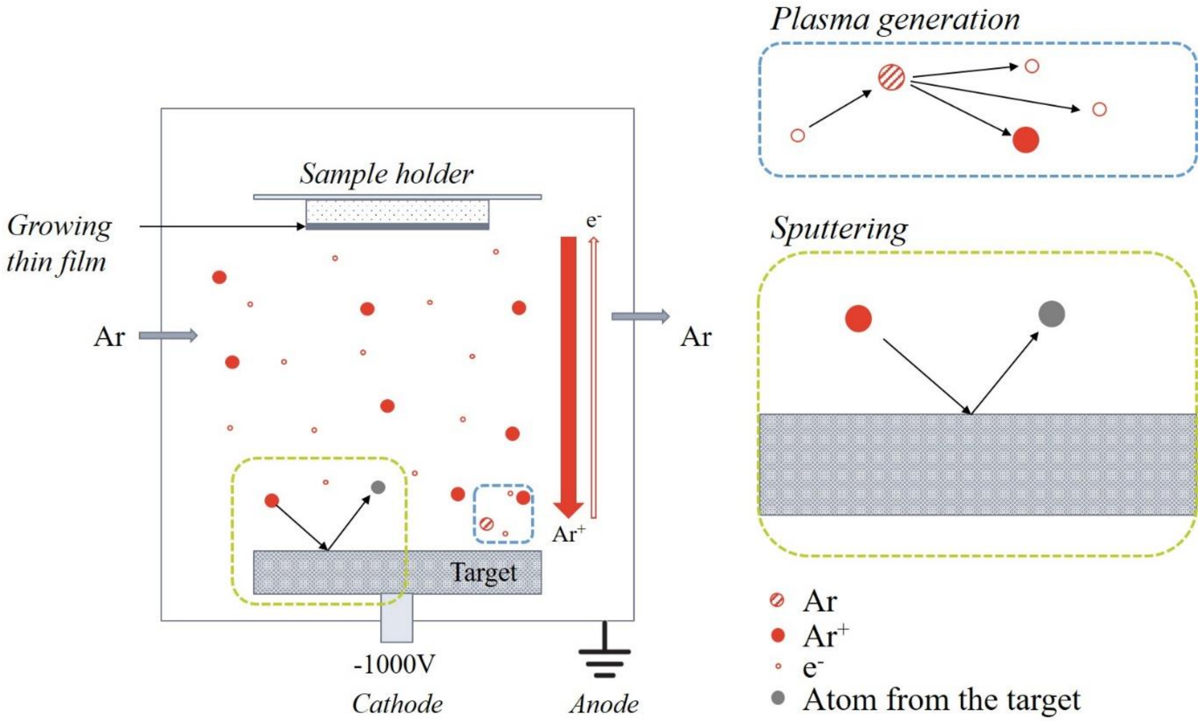

Figure 93. Scheme of the PVD pulsed DC magnetron sputtering process. Left is a scheme of the chamber during metal deposition (for ceramic deposition, a reactive gas is added along with Ar). It shows the acceleration of Ar^+ ions towards the target due to the establishment of an electric field between the negative target and the grounded anode. Close-ups on the right describe the main mechanisms during metal deposition, namely plasma generation and sputtering as Ar^+ ions bombard the target.

b. Deposition parameters

Bilayered films of aluminum and alumina (Al/Al_2O_3) or copper and alumina (Cu/Al_2O_3) were deposited on polyamide 6 plates (10 x 10 x 0.3 cm^3) by pulsed DC magnetron sputtering (DEPHIS4, DEPHIS, Etupes, France). Prior to treatment, the polymer plates were cleaned in ethanol in an ultrasonic bath for 5 min. The deposition was simultaneously made on glass substrates for Scanning Electron Microscopy (SEM) observation and X-Ray Diffraction (XRD) characterization. The substrates were maintained on the sample holder in front of the target with Kapton adhesive. The chamber was evacuated down to a pressure of 2.10^{-4} Pa, which took approximately 1 h. To enhance the adhesion between the deposit and the polymers, the substrates were sputter-cleaned for 20 min using Ar^+ ions (0,3 Pa, RF power: 200 W for a 600 mm in diameter substrates holder). The aluminum layer was deposited by sputtering a pure aluminum target in pure argon for 30 min. The copper layer was deposited by sputtering a pure copper target in pure argon for 10 min. The Al_2O_3 layer was subsequently deposited via reactive sputtering of a pure aluminum target in an argon and oxygen atmosphere with different deposition times (60 min for cycle 1, and 210 min for cycle 2 – see Table 34). Argon and oxygen flows were fixed at 100 sccm and 20 sccm respectively. No bias is performed during deposition. Considering the duration of all steps (evacuation of the chamber, sputter-cleaning, deposition of aluminum and deposition of aluminum oxide), cycle 1 lasted for about 3 h and cycle 2 lasted for about 5 h. The deposition parameters are summarized in Table 34.

Al/Al_2O_3 coatings were deposited on polypropylene surface using the same procedure as described above.

Table 34. Sputtering parameters during the deposition of Al/Al_2O_3 bilayered film on PP and PA6 plates.

	Cycle 1	**Cycle 2**
Metal discharge current (A)	1	
Argon flow rate (sccm)	100	
Oxygen flow rate (sccm) (*only during Al_2O_3 deposition*)	20	
Metal time of deposition (min)	Cu: 10 Al: 30	Cu: / Al: 30
Al_2O_3 time of deposition (min)	60	210

4) Characterization

a. Scanning Electron Microscopy

Observation of the cross-section of the coating and thickness determination was carried out on polyamide 6 and polypropylene substrates by Scanning Electron Microscopy with Energy Dispersive X-Ray mapping (SEM-EDX) on a JEOL JSM-7500 field-emission scanning electron microscope (Tokyo, Japan). To obtain a flat surface, all the samples were ultramicrotomed at room temperature on a Leica ultracut UCT microtome using a Diatome diamond knife. The samples were covered with a carbon deposit by sputtering prior to observation. The analyses were done at 5kV, 7µA and at a working distance of 10mm.

b. *X-Ray Diffraction*

X-Ray Diffraction was performed on glass substrates in Bragg-Brentano geometry on a Rigaku SmartLab High Resolution X-Ray Diffractometer (HR-XRD). The X-ray source is a 9 kW rotating anode (Cu $\lambda K\alpha_1 = 1.54056$ Å). The scans for Al/Al_2O_3 were performed in θ/2θ from 15° to 90° with a speed of 10°/min and a step of 0.01°, with the Kβ wavelength of the Cu anode filtered. The scans for Cu/Al_2O_3 were performed in 2θ from 15° to 90° with a speed of 10°/min and a step of 0.01°, with the Kβ wavelength of the Cu anode unfiltered in order to see the diffraction peaks of Cu. This also suppressed the hump shape due to the glass substrate.

c. *Emissivity at room temperature*

Total hemispherical emissivity was measured at 20°C by infrared diffuse reflectance measurements on a Bruker Vertex 70v spectrophotometer. It is equipped with an integrating sphere (Bruker A562) with a diameter of 75 mm and gold-coated for analysis in the NIR and MIR spectral range (see Figure 94).

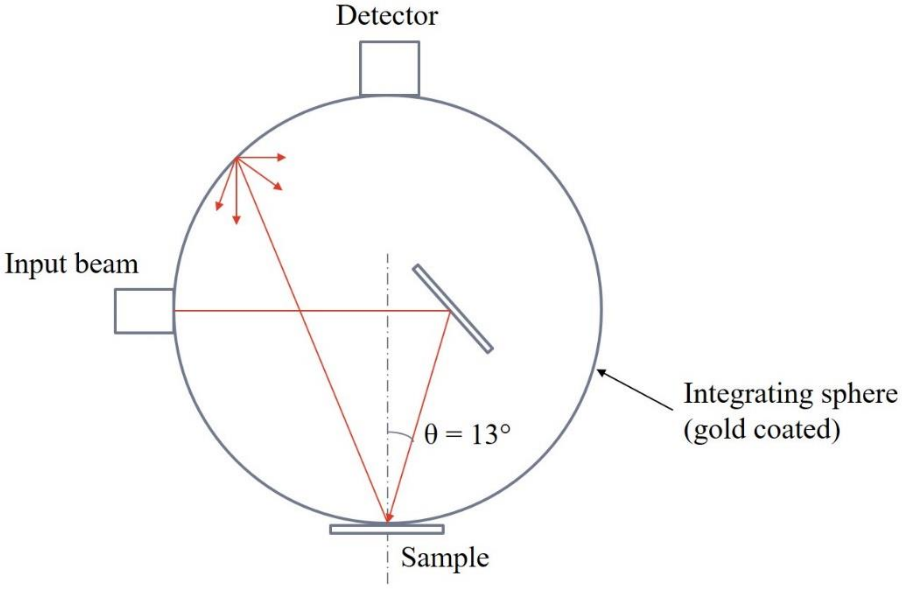

Figure 94. Scheme of total hemispherical emissivity measurement by infrared diffuse reflectance

The beam impacts the sample at an angle of 13°, integrated in the sphere, and the resulting signal is intercepted by a DLaTGS detector. The system operated in the MIR using a SiC light source, with a KBr beam splitter, and a 6 mm aperture. The resolution was set at 4 cm^{-1} and 128 scans were acquired from 350 cm^{-1} to 3000 cm^{-1}. This spectral range was selected because it included the maximum of radiation intensity emitted by a conical resistance with a 50 kW/m^2 heat flux, without having to change the light source to go to the NIR spectral range. Before each series of measurements, the spectrometer is calibrated with a gold reference. All measurements were made four times for repeatability on different places of the sample (error lower than 1%). The apparatus was run from Bruker OPUS software, which was also used to interpret the spectra. The emissivity was measured by integrating the spectra between 7.5 and 13 µm.

d. Total normal emissivity as a function of temperature

The emissivity of the samples at high temperature is determined through radiometric emission measurements. It is determined by calculating the ratio of the signal measured from the sample (proportional to the emitted intensity) to the signal measured from a separate black body kept at the same temperature, over an identical optical path. To this means, a mirror is moved back and forth a trail in order to catch the signal from either the black body, or the sample, as explained in Figure 95.

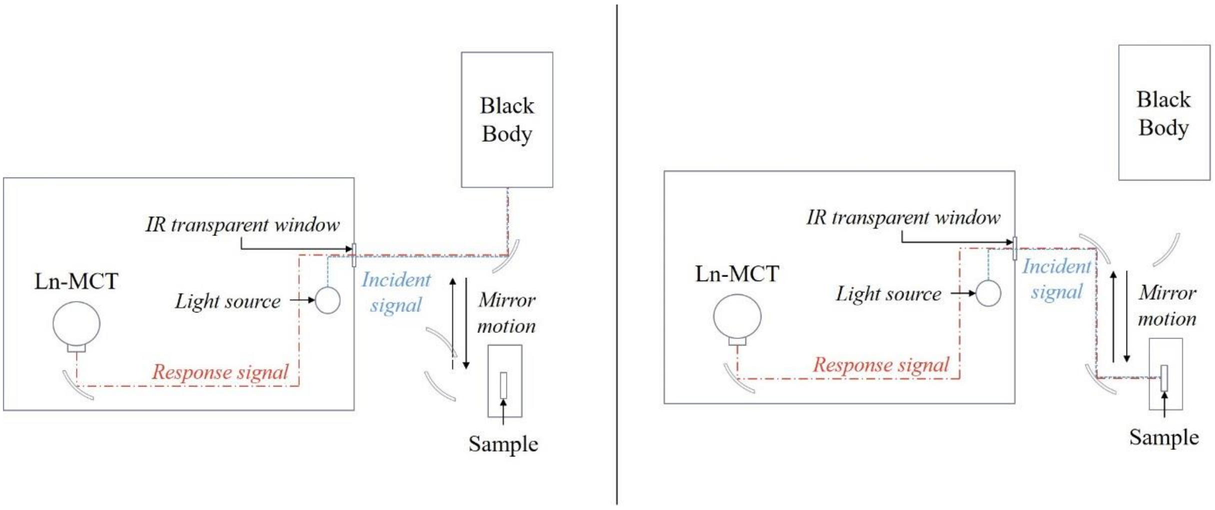

Figure 95. Scheme of radiometric emission measurements for the determination of the total normal emissivity as a function of temperature. Left: position for the measurement of the signal of the black body. Right: position for the measurement of the signal of the sample.

In this configuration, the total normal emissivity is calculated, which can differ a little from the total hemispherical emissivity because of the directional dependence of this property. The signal is emitted from a SiC source, and lead to either the sample and the black body through an optical path (KBr beam splitter, aperture of 2 mm), before being received by an Mercury Cadmium Telluride detector (Ln-MCT)[6]. The resolution was set at 4 cm^{-1}, and the number of scans acquired for both black body and sample was 128, over the 350-5000 cm^{-1} spectral range. Reflectance spectra were acquired and interpreted using the OPUS software, and integrated between 7.5 and 13 µm.

IV. Fire tests

1) Bench scale high heat flux burn-through fire test

(Layer-by-layer coatings for fire protection of porous substrates)

This homemade fire test is designed to test the resistance of a material to high heat flux in the presence of a flame. Since fire tests are destructive, the successful scaling down of fire tests is one of the major issues of fire science in order to spare resources in materials and space as well as to improve work safety. Here, the bench is meant to mimic the standards ISO2685:1998(E) and FAR25.856(b):2003 at a laboratory scale.[385] It is composed of two panels placed vertically on a rail to be able to switch easily between the two.

A flux meter is adjusted on one of the panels for calibration purposes and to check the heat flux. The second panel is the sample holder. It is composed of two refractory ceramic plates (calcium silicate, hereafter referred to as calsil) pierced with a 10 x 10 cm² window that hold the tested material in place. A butane torch is placed in front of the panel so that it impacts the sample at a right angle. The flow of butane is set so that a heat flux of 116 ± 10 kW/m² is delivered with a temperature of flame of about 1100°C. The sample is exposed to the flame for at least 15 min or until it is pierced. Thermocouples can be placed in the samples whether needed to monitor temperature changes, and a space is meant to put an infrared camera behind

---

[6] MCT detector are photon detectors. They have a fast response time and high detectivity, but a low spectral range. They must be cooled in order to function, usually with liquid nitrogen.

the sample. The fumes are evacuated by a hood, where a FTIR apparatus can be fixed to analyze the evolving gases. It is composed of a sampling gun adjusted on the hood with a 2µm air filter. The gases then travel down a 2m polytetrafluoroethylene transferline with a 0.1µm air filter, kept at 200 °C to prevent their condensation, and are brought to a gas cell with two KBr window for analysis (10 scans with a resolution of 0.5 cm^{-1} from 650 to 4500 cm^{-1} and with pre-test background analysis). The gas cell has a 2m long optical pathways and is placed in a chamber filled with dry air at a temperature of 186°C and at a pressure of 653 Torr. It is then possible to monitor the evolved quantities of carbon dioxide, sulfur dioxide, nitric oxide, nitrogen dioxide, water, hydrogen bromide, hydrogen chloride, hydrogen cyanide, ammonia, ethane, acetylene, carbon monoxide, and propane with a quantitative method used via the software OMNIC. In this work, PUF blocks of 20 x 20 x 2.5 cm^3 were exposed to the 116 kW/m^2 heat flux for 15min, with 4 thermocouples planted at 5, 10, 15 and 20 mm away from the exposed surface. A description of the apparatus and the set-up is presented in Figure 96.

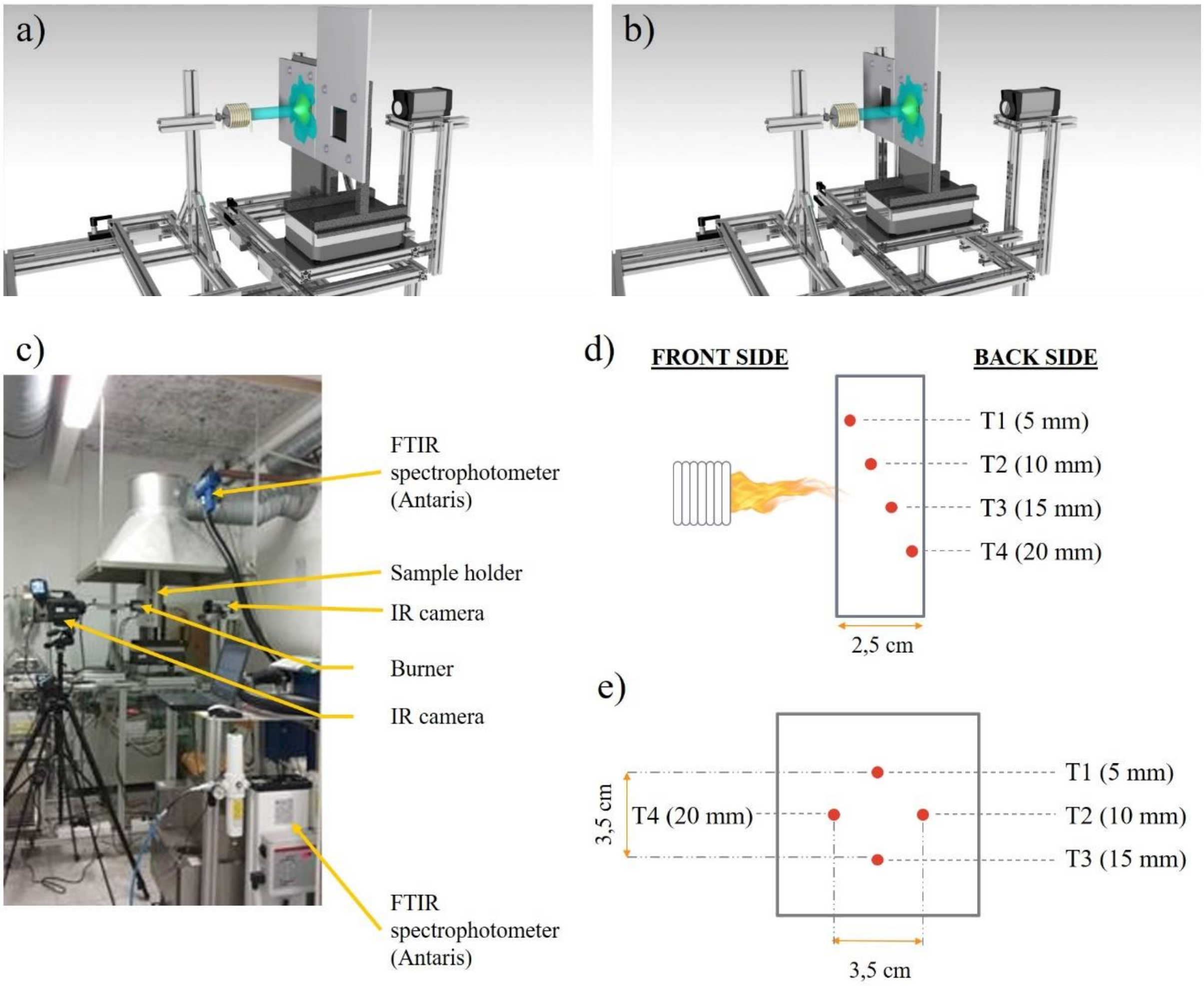

Figure 96. 3D view of the burn-through fire test, in calibration mode (a) and during test (b). c) Digital photograph of the test and set-up. Schematic showing the position of the thermocouples in the sample: side view (d) and front view (e).

2) Hand-held butane torch test

(Layer-by-layer coatings for fire protection of porous substrates)

This non-standard fire test is designed as a screening tool to test the validity of the systems and have first elements on their reaction against fire. A small sample is put on a wired grid and exposed to the flame (1400°C, measured by a thermocouple at the center of the flame) of a butane hand torch for 10s.

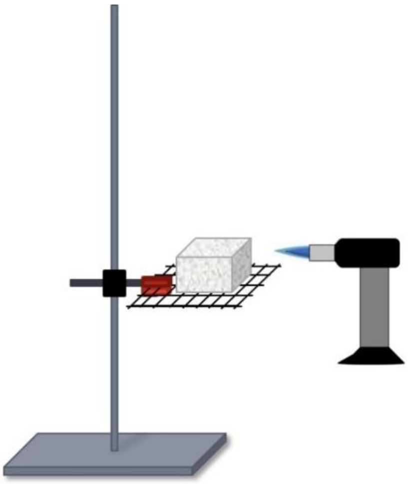

Figure 97. Schematic of a hand held fire test.

Its flame resistance is evaluated by calculating the lost mass by weighing it before and after the test, as well as by observing its morphology. In this work, 5 x 5 x 2.5 cm^3 samples of polyurethane foam were used. A schematic of the installation is presented in Figure 97.

3) UL94

(One-pot high-filler content coatings for fire protection of textiles)

This standardized test allows the rapid screening of fire retardant solution by rating them according to several parameters characterizing the ease of extinction of the samples. The test consists in submitting the sample to the flame of a methane burner tilted at 45° and measuring the residual burning or afterglow time once the flame is removed. The flame is applied twice for 10 s. The flux of methane is adapted so that the flame is 2 cm high, and a cotton is placed underneath the sample to evaluate the hazard of an eventual melt-dripping. The studied material is then rated V-0 (highest rating), V-1, V-2 or not classified according to its behavior (depending on the time of residual burning or afterglow after the removal of the flame, melt-dripping, complete combustion etc.). In this work, 8x16 cm^2 PA66 fabric samples were placed in a steel frame before being tested. A schematic of the installation is presented in Figure 98. The combustion spread was calculated by considering the time to reach a 5 cm decomposed length.

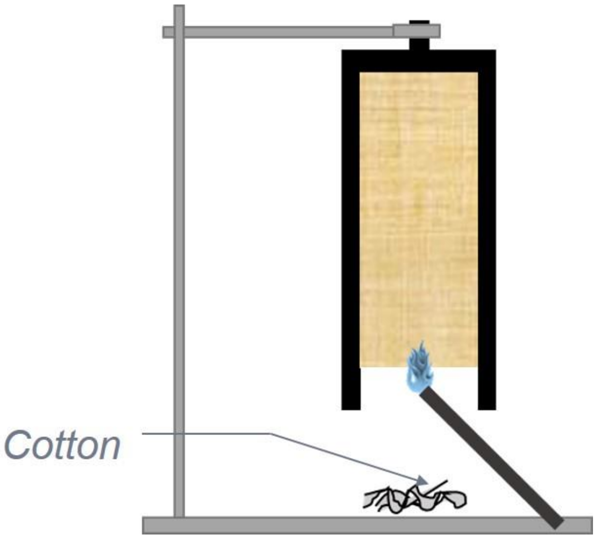

Figure 98. Schematic of a UL94 test adapted for textiles.

During the test, the temperature on the surface of the sample was measured by a X6540SC infrared camera (FLIR systems, Wilsonville, OR, United States of America), positioned 80 cm away from the fabric. The camera is calibrated from 20°C to 1500°C and equipped with a filter eliminating the specific wavelengths emitted by the flame, allowing to see through it.

4) Heat release during flame spread: small-scale EN 50399

(One-pot high-filler content coatings for fire protection of textiles)

This test is a small scale lab-made version of the test used to evaluate and rate the flammability of materials used for cable sheaths. The sample (in this work, 50 x 5 cm² PA66 fabric) is placed on a grid in a closed box and maintained by two clamps at the top and at the bottom. It is impacted at 10 cm from its bottom by the flame of a methane burner tilted at 45°, for 60 s. The heat release rate is calculated by measuring the depletion of oxygen thanks to a zirconia based oxygen analyzer (BA100, Bühler Technologies, Ratingen, Germany), placed in the exhaust chimney, alongside an anemometer and a 0.5 mm K-type thermocouple. The flux of methane is set at 650 mL/min.[448] All experiments were done five times, except for plain PA66 that was done once. A schematic of the set-up is presented in Figure 99.

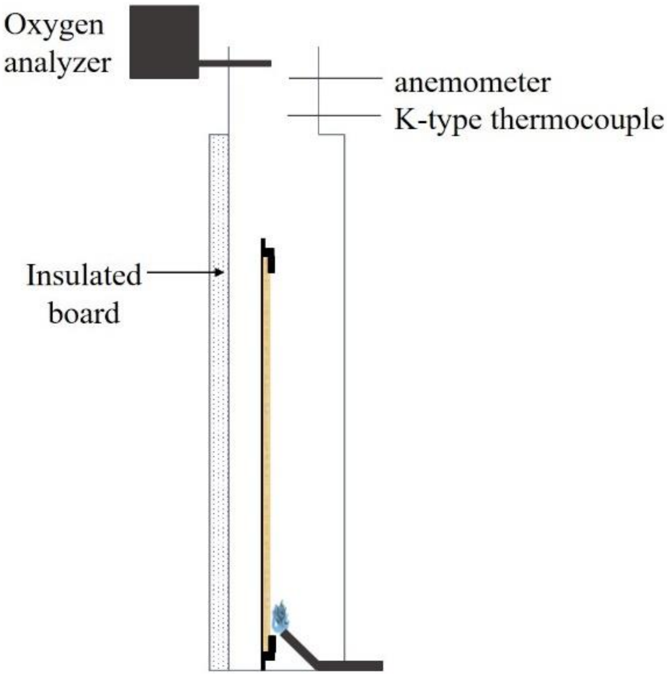

Figure 99. Schematic of the small scale EN 50399 test (heat release during flame spread).

5) Mass loss cone calorimeter

The mass loss cone calorimeter (Fire Testing Technology (FTT), East Grinstead, UK) is a routine bench scale test, following the ISO 5660 standard. The test consists in exposing the sample to a uniform heat flux generated by a conical resistance, at a given distance. The sample is wrapped in aluminum foil, placed on a ceramic backing board in a stainless steel frame. It is then placed horizontally under the resistance so that only the upper surface (usually 10 x 10 cm^2) is exposed to the heat. The sample will decompose, and release flammable gases which will ignite (auto-ignition) or be ignited (piloted ignition) with an external energy source. Each standard heat flux corresponds to those encountered in different fire scenario, from different step of developing fires to fully developed fires. For example, the most used heat flux are $35 kW/m^2$ and $50 kW/m^2$ which corresponds to a developing fire and a more fully developed fire respectively [381]. It should be noted that, even if thermo-oxidative processes dominate in the absence of a flame, once the sample is burning, the material decomposes essentially through pyrolysis. During a test, the HRR [kW/m^2] is monitored as a function of time.

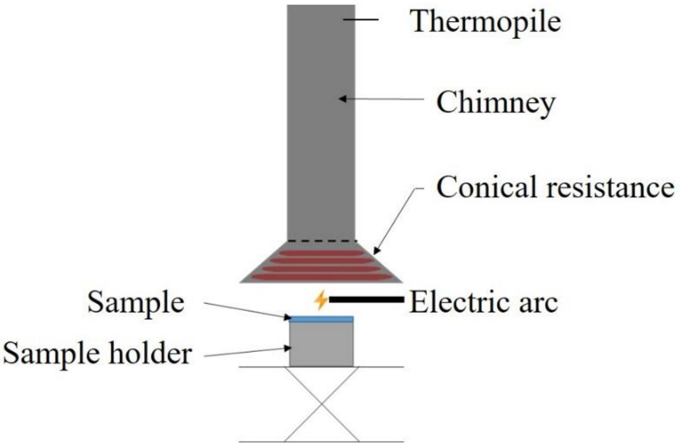

Figure 100. Schematic of the mass loss cone calorimeter.

This allows to determine important flammability parameters such as the pHRR [kW/m²], the THR [MJ/m²] as well as the TTI [s]. It is sometimes also possible to monitor the Smoke production rate (SPR [m²/s]) and Total Smoke Release (TSR [m²/m²]). The time to reach the pHRR is also important as it is one of the parameters of importance in fire safety to limit the number of victims. Furthermore, the test can be equipped to measure the smoke release and its density, as well as evolving species of interest such as CO_2 or CO. In the standard, the HRR of a sample is calculated through the determination of the quantity of oxygen consumed. The instrument used in this work derives a bit from this, as the HRR is determined by a thermopile situated on top of a chimney. The evolved decomposition gases are ignited with an electric arc

A schematic of the installation is presented in Figure 100.

a. Layer-by-layer coatings for fire protection of porous substrates

The samples tested here are 10 x 10 x 2.5 cm^3 PUF blocks tested at 35 kW/m² heat flux. The distance between the sample and the radiant conical heater was set at 25 mm. and the evolved gases are analyzed using the Fourier Transformed Infrared (FTIR) spectrometer described in the section IV.1). The distance between the sample and the radiant conical heater was set at 25 mm. Tests were performed 2 times to ensure repeatability of the results.

b. Low-emissivity coatings for the fire protection of raw and formulated polymer substrates

The coated and uncoated polymer plates were cut into 5 x 5 x 0.3 cm^3 samples and tested at a 50 kW/m² heat flux. The sample size, while deviating from the ISO standard, allows to compromise between representative fire behavior and fast screening. The evolution of the temperature at the back of the sample was monitored with a K-type thermocouple with a diameter of 0.5 mm from Omega (Manchester, United Kingdom). To prevent it from piercing the deposit during the test, it was maintained in place with a 1 cm-thick calcium silicate plate pierced with a 1 mm hole to ensure contact with the polymer (see Figure 62 in chapter 4). To prevent early decomposition from the sides of the sample, non-flammable glue (Pyrocol F, Marly, France) was deposited along the edges of the sample and of the calcium silicate plate to hold them together (except when stated otherwise). PA6 samples were conditioned at 50°C overnight before testing to get rid of humidity. The distance between the sample and the radiant conical heater was set at 35 mm in order to prevent contact with the igniter and/or the heating element in case of strong swelling due to intumescence. Tests were performed 3 to 4 times.

References

[1] "Les statistiques des Services d'Incendie et de Secours - Edition 2019," 2019.

[2] N. N. Brushlinsky, M. Ahrens, S. V. Sokolov, and P. Wagner, "World Fire Statistics 2019," Paris, France, 2019.

[3] A. Ramgobin, G. Fontaine, and S. Bourbigot, "Thermal Degradation and Fire Behavior of High Performance Polymers," *Polym. Rev.*, vol. 59, no. 1, pp. 55–123, 2019, doi: 10.1080/15583724.2018.1546736.

[4] S. Bourbigot and S. Duquesne, "Fire retardant polymers: Recent developments and opportunities," *J. Mater. Chem.*, vol. 17, no. 22, pp. 2283–2300, 2007, doi: 10.1039/b702511d.

[5] H. Ge, W. Wang, Y. Pan, X. Yu, W. Hu, and Y. Hu, "An inherently flame-retardant polyamide containing a phosphorus pendent group prepared by interfacial polymerization," *RSC Adv.*, vol. 6, no. 85, pp. 81802–81808, 2016, doi: 10.1039/c6ra17108g.

[6] W. Hu *et al.*, "Flame retardant polystyrene copolymers: Preparation, thermal properties, and fire toxicities," *Polym. Adv. Technol.*, vol. 25, no. 6, pp. 631–637, 2014, doi: 10.1002/pat.3261.

[7] A. B. Morgan and A. Z. Worku, *Flame Retardants: Overview*. 2015.

[8] A. B. Morgan, "The Future of Flame Retardant Polymers–Unmet Needs and Likely New Approaches," *Polym. Rev.*, vol. 59, no. 1, pp. 25–54, 2019, doi: 10.1080/15583724.2018.1454948.

[9] S. Bourbigot and S. Duquesne, "Intumescence and Nanocomposites: A Novel Route for Flame-Retarding Polymeric Materials," in *Flame Retardant Polymer Nanocomposites*, A. B. Morgan and C. A. Wilkie, Eds. John Wiley & Sons, Inc., 2006, pp. 131–162.

[10] S. Liang, N. M. Neisius, and S. Gaan, "Recent developments in flame retardant polymeric coatings," *Prog. Org. Coatings*, vol. 76, no. 11, pp. 1642–1665, 2013, doi: 10.1016/j.porgcoat.2013.07.014.

[11] S. T. Lazar, T. J. Kolibaba, and J. C. Grunlan, "Flame-retardant surface treatments," *Nat. Rev. Mater.*, vol. 5, no. 4, pp. 259–275, 2020, doi: 10.1038/s41578-019-0164-6.

[12] H. Dislich and P. Hinz, "History and principles of the sol-gel process, and some new multicomponent oxide coatings," *J. Non. Cryst. Solids*, vol. 48, no. 1, pp. 11–16, 1982, doi: 10.1016/0022-3093(82)90242-3.

[13] U. Schubert, "Chemistry and Fundamentals of the Sol-Gel Process," in *The Sol-Gel Handbook : Synthesis, Characterization, and Applications*, 1st ed., D. Levy and M. Zayat, Eds. Weinheim, Germany: Wiley-VCH Verlag GmbH & Co. KGaA, 2015, pp. 1–28.

[14] J. Livage, “Basic Principles of Sol-Gel Chemistry,” in *Sol-Gel Technologies for Glass Producers and Users*, M. A. Aegerter and M. Mennig, Eds. Boston, MA: Springer US, 2004, pp. 3–14.

[15] S. Karataş, Z. Hoşgör, Y. Menceloğlu, N. Kayaman-Apohan, and A. Güngör, “Synthesis and characterization of flame retarding UV-curable organic–inorganic hybrid coatings,” *J. Appl. Polym. Sci.*, vol. 102, no. 2, pp. 1906–1914, Oct. 2006, doi: 10.1002/app.24274.

[16] S. Karataş, N. Kayaman-Apohan, O. Turunç, and A. Güngör, “Synthesis and characterization of UV-curable phosphorus containing hybrid materials prepared by sol-gel technique,” *Polym. Adv. Technol.*, vol. 22, no. 5, pp. 567–576, May 2011, doi: 10.1002/pat.1546.

[17] C. Kizilkaya, S. Karataş, N. K. Apohan, and A. Güngör, “Synthesis and characterization of novel polyimide/SiO2 nanocomposite materials containing phenylphosphine oxide via sol-gel technique,” *Journal of Applied Polymer Science*, vol. 115, no. 6. pp. 3256–3264, 2010, doi: 10.1002/app.31404.

[18] Y. Mülazim, M. V. Kahraman, N. K. Apohan, S. Kiziltaş, and A. Güngör, “Preparation and characterization of UV-curable, boron-containing, transparent hybrid coatings,” *Journal of Applied Polymer Science*, vol. 120, no. 4. pp. 2112–2121, 2011, doi: 10.1002/app.33358.

[19] Y. Mülazim, E. Çakmakçi, and M. V. Kahraman, “Preparation of photo curable highly hydrophobic coatings using a modified castor oil derivative as a sol-gel component,” *Prog. Org. Coatings*, vol. 72, no. 3, pp. 394–401, 2011, doi: 10.1016/j.porgcoat.2011.05.012.

[20] E. Baştürk, B. Oktay, M. V. Kahraman, and N. Kayaman Apohan, “UV cured thiol-ene flame retardant hybrid coatings,” *Prog. Org. Coatings*, vol. 76, no. 6, pp. 936–943, 2013, doi: 10.1016/j.porgcoat.2012.10.012.

[21] D. Shang, X. Sun, J. Hang, L. Jin, and L. Shi, “Flame resistance, physical and mechanical properties of UV-cured hybrid coatings containing low-hydroxyl-content sols via an anhydrous sol-gel process,” *Prog. Org. Coatings*, vol. 105, pp. 267–276, 2017, doi: 10.1016/j.porgcoat.2017.01.015.

[22] M. Messoria *et al.*, “Flame retarding poly(methyl methacrylate) with nanostructured organic-inorganic hybrids coatings,” *Polymer (Guildf).*, vol. 44, no. 16, pp. 4463–4470, 2003, doi: 10.1016/S0032-3861(03)00396-3.

[23] K. Satoh, H. Nakazumi, and M. Morita, “Novel Fluorinated Inorganic-Organic Finishing Materials for Nylon Carpeting,” *Text. Res. J.*, vol. 74, no. 12, pp. 1079–1084, 2004, doi: 10.1177/004051750407401209.

[24] S. Bellayer, M. Jimenez, S. Barrau, and S. Bourbigot, “Fire retardant sol–gel coatings for flexible polyurethane foams,” *RSC Adv.*, vol. 6, no. 34, pp. 28543–28554, 2016, doi: 10.1039/C6RA02094A.

[25] Z. M. Zhu, Y. J. Xu, W. Liao, S. Xu, and Y. Z. Wang, “Highly Flame Retardant Expanded Polystyrene Foams from Phosphorus-Nitrogen-Silicon Synergistic Adhesives,” *Ind. Eng. Chem. Res.*, vol. 56, no. 16, pp. 4649–4658, 2017, doi:

10.1021/acs.iecr.6b05065.

[26] E. Baştürk, T. Inan, and A. Güngör, "Flame retardant UV-curable acrylated epoxidized soybean oil based organic-inorganic hybrid coating," *Prog. Org. Coatings*, vol. 76, no. 6, pp. 985–992, 2013, doi: 10.1016/j.porgcoat.2012.10.007.

[27] F. Girardi *et al.*, "Hybrid organic-inorganic materials as coatings for protecting wood," *Prog. Org. Coatings*, vol. 77, no. 2, pp. 449–457, 2014, doi: 10.1016/j.porgcoat.2013.11.010.

[28] J. Alongi and G. Malucelli, "Cotton fabrics treated with novel oxidic phases acting as effective smoke suppressants," *Carbohydr. Polym.*, vol. 90, no. 1, pp. 251–260, 2012, doi: 10.1016/j.carbpol.2012.05.032.

[29] J. Alongi, M. Ciobanu, and G. Malucelli, "Sol-gel treatments for enhancing flame retardancy and thermal stability of cotton fabrics: Optimisation of the process and evaluation of the durability," *Cellulose*, vol. 18, no. 1, pp. 167–177, 2011, doi: 10.1007/s10570-010-9470-2.

[30] J. Alongi, M. Ciobanu, and G. Malucelli, "Sol-gel treatments on cotton fabrics for improving thermal and flame stability: Effect of the structure of the alkoxysilane precursor," *Carbohydr. Polym.*, vol. 87, no. 1, pp. 627–635, 2012, doi: 10.1016/j.carbpol.2011.08.036.

[31] J. Alongi, M. Ciobanu, and G. Malucelli, "Cotton fabrics treated with hybrid organic-inorganic coatings obtained through dual-cure processes," *Cellulose*, vol. 18, no. 5, pp. 1335–1348, 2011, doi: 10.1007/s10570-011-9564-5.

[32] C. Colleoni, I. Donelli, G. Freddi, E. Guido, V. Migani, and G. Rosace, "A novel sol-gel multi-layer approach for cotton fabric finishing by tetraethoxysilane precursor," *Surf. Coatings Technol.*, vol. 235, pp. 192–203, 2013, doi: 10.1016/j.surfcoat.2013.07.033.

[33] G. Brancatelli, C. Colleoni, M. R. Massafra, and G. Rosace, "Effect of hybrid phosphorus-doped silica thin films produced by sol-gel method on the thermal behavior of cotton fabrics," *Polym. Degrad. Stab.*, vol. 96, no. 4, pp. 483–490, 2011, doi: 10.1016/j.polymdegradstab.2011.01.013.

[34] S. Deh, F. Gähr, and M. R. Buchmeiser, "Synergistic effects in the pyrolysis of phosphorus-based flame-retardants: The role of Si- and N-based compounds," *Polym. Degrad. Stab.*, vol. 130, pp. 155–164, 2016, doi: 10.1016/j.polymdegradstab.2016.06.009.

[35] V. Rajendran, N. R. Dhineshbabu, R. R. Kanna, and K. V. I. S. Kaler, "Enhancement of thermal stability, flame retardancy, and antimicrobial properties of cotton fabrics functionalized by inorganic nanocomposites," *Ind. Eng. Chem. Res.*, vol. 53, no. 50, pp. 19512–19524, 2014, doi: 10.1021/ie502584m.

[36] R. S. Kappes, T. Urbainczyk, U. Artz, T. Textor, and J. S. Gutmann, "Flame retardants based on amino silanes and phenylphosphonic acid," *Polym. Degrad. Stab.*, vol. 129, pp. 168–179, 2016, doi: 10.1016/j.polymdegradstab.2016.04.012.

[37] J. Alongi, M. Ciobanu, and G. Malucelli, "Thermal stability, flame retardancy and

mechanical properties of cotton fabrics treated with inorganic coatings synthesized through sol-gel processes," *Carbohydr. Polym.*, vol. 87, no. 3, pp. 2093–2099, 2012, doi: 10.1016/j.carbpol.2011.10.032.

[38] J. Alongi, M. Ciobanu, J. Tata, F. Carosio, and G. Malucelli, "Thermal stability and flame retardancy of polyester, cotton, and relative blend textile fabrics subjected to sol-gel treatments," *J. Appl. Polym. Sci.*, vol. 119, no. 4, pp. 1961–1969, Feb. 2011, doi: 10.1002/app.32954.

[39] C. K. Kundu, X. Wang, Y. Hou, and Y. Hu, "Construction of flame retardant coating on polyamide 6.6 via UV grafting of phosphorylated chitosan and sol–gel process of organo-silane," *Carbohydr. Polym.*, vol. 181, no. November 2017, pp. 833–840, 2018, doi: 10.1016/j.carbpol.2017.11.069.

[40] E. Guido *et al.*, "Thermal stability and flame retardancy of polyester fabrics sol-gel treated in the presence of boehmite nanoparticles," *Polym. Degrad. Stab.*, vol. 98, no. 9, pp. 1609–1616, 2013, doi: 10.1016/j.polymdegradstab.2013.06.021.

[41] C. K. Kundu, X. Wang, L. Liu, L. Song, and Y. Hu, "Few layer deposition and sol-gel finishing of organic-inorganic compounds for improved flame retardant and hydrophilic properties of polyamide 66 textiles: A hybrid approach," *Prog. Org. Coatings*, vol. 129, no. November 2018, pp. 318–326, 2019, doi: 10.1016/j.porgcoat.2019.01.010.

[42] J. Alongi, C. Colleoni, G. Malucelli, and G. Rosace, "Hybrid phosphorus-doped silica architectures derived from a multistep sol-gel process for improving thermal stability and flame retardancy of cotton fabrics," *Polym. Degrad. Stab.*, vol. 97, no. 8, pp. 1334–1344, 2012, doi: 10.1016/j.polymdegradstab.2012.05.030.

[43] J. Alongi, C. Colleoni, G. Rosace, and G. Malucelli, "The role of pre-hydrolysis on multi step sol-gel processes for enhancing the flame retardancy of cotton," *Cellulose*, vol. 20, no. 1, pp. 525–535, 2013, doi: 10.1007/s10570-012-9806-1.

[44] J. Alongi, C. Colleoni, G. Rosace, and G. Malucelli, "Sol-gel derived architectures for enhancing cotton flame retardancy: Effect of pure and phosphorus-doped silica phases," *Polym. Degrad. Stab.*, vol. 99, no. 1, pp. 92–98, 2014, doi: 10.1016/j.polymdegradstab.2013.11.020.

[45] J. Alongi, C. Colleoni, G. Rosace, and G. Malucelli, "Phosphorus- and nitrogen-doped silica coatings for enhancing the flame retardancy of cotton: Synergisms or additive effects?," *Polym. Degrad. Stab.*, vol. 98, no. 2, pp. 579–589, 2013, doi: 10.1016/j.polymdegradstab.2012.11.017.

[46] J. Alongi, M. Ciobanu, and G. Malucelli, "Novel flame retardant finishing systems for cotton fabrics based on phosphorus-containing compounds and silica derived from sol-gel processes," *Carbohydr. Polym.*, vol. 85, no. 3, pp. 599–608, 2011, doi: 10.1016/j.carbpol.2011.03.024.

[47] F. Samyn, M. Vandewalle, S. Bellayer, and S. Duquesne, "Sol-gel treatments to flame retard PA11/flax composites," *Fibers*, vol. 7, no. 10, 2019, doi: 10.3390/fib7100086.

[48] X. W. Cheng, R. C. Tang, J. P. Guan, and S. Q. Zhou, "An eco-friendly and effective flame retardant coating for cotton fabric based on phytic acid doped silica sol approach,"

Prog. Org. Coatings, vol. 141, no. January, p. 105539, 2020, doi: 10.1016/j.porgcoat.2020.105539.

[49] Y. Ren, Y. Zhang, Y. Gu, and Q. Zeng, “Flame retardant polyacrylonitrile fabrics prepared by organic-inorganic hybrid silica coating via sol-gel technique,” *Prog. Org. Coatings*, vol. 112, no. August, pp. 225–233, 2017, doi: 10.1016/j.porgcoat.2017.07.022.

[50] M. Barbalini, L. Bertolla, J. Toušek, and G. Malucelli, “Hybrid silica-phytic acid coatings: Effect on the thermal stability and flame retardancy of cotton,” *Polymers (Basel).*, vol. 11, no. 10, 2019, doi: 10.3390/polym11101664.

[51] D. Zhang *et al.*, “Flame retardant and hydrophobic coatings on cotton fabrics via sol-gel and self-assembly techniques,” *J. Colloid Interface Sci.*, vol. 505, pp. 892–899, 2017, doi: 10.1016/j.jcis.2017.06.087.

[52] D. Lin, X. Zeng, H. Li, X. Lai, and T. Wu, “One-pot fabrication of superhydrophobic and flame-retardant coatings on cotton fabrics via sol-gel reaction,” *J. Colloid Interface Sci.*, vol. 533, pp. 198–206, 2019, doi: 10.1016/j.jcis.2018.08.060.

[53] H. Nabipour, X. Wang, L. Song, and Y. Hu, “Hydrophobic and flame-retardant finishing of cotton fabrics for water–oil separation,” *Cellulose*, vol. 27, no. 7, pp. 4145–4159, 2020, doi: 10.1007/s10570-020-03057-1.

[54] Y. Liu *et al.*, “Effect of phosphorus-containing inorganic-organic hybrid coating on the flammability of cotton fabrics: Synthesis, characterization and flammability,” *Chem. Eng. J.*, vol. 294, pp. 167–175, 2016, doi: 10.1016/j.cej.2016.02.080.

[55] Y. S. Zhu, F. You, H. T. Zhou, W. H. Huangfu, and Z. H. Wang, “Pyrolysis Properties and Flame Retardant Effects of Fabrics Finished by Hybrid Silica-based Sols,” *Procedia Eng.*, vol. 211, pp. 1091–1101, 2018, doi: 10.1016/j.proeng.2017.12.114.

[56] J. Vasiljević *et al.*, “Functionalization of cellulose fibres with DOPO-polysilsesquioxane flame retardant nanocoating,” *Cellulose*, vol. 22, no. 3, pp. 1893–1910, 2015, doi: 10.1007/s10570-015-0599-x.

[57] J. Vasiljević *et al.*, “Study of flame-retardant finishing of cellulose fibres: Organic-inorganic hybrid versus conventional organophosphonate,” *Polym. Degrad. Stab.*, vol. 98, no. 12, pp. 2602–2608, 2013, doi: 10.1016/j.polymdegradstab.2013.09.020.

[58] A. M. Grancaric, C. Colleoni, E. Guido, L. Botteri, and G. Rosace, “Thermal behaviour and flame retardancy of monoethanolamine-doped sol-gel coatings of cotton fabric,” *Prog. Org. Coatings*, vol. 103, pp. 174–181, 2017, doi: 10.1016/j.porgcoat.2016.10.035.

[59] Z. Jiang, D. Xu, X. Ma, J. Liu, and P. Zhu, “Facile synthesis of novel reactive phosphoramidate siloxane and application to flame retardant cellulose fabrics,” *Cellulose*, vol. 26, no. 9, pp. 5783–5796, 2019, doi: 10.1007/s10570-019-02465-2.

[60] J. Alongi and G. Malucelli, “Thermal stability, flame retardancy and abrasion resistance of cotton and cotton-linen blends treated by sol-gel silica coatings containing alumina micro- or nano-particles,” *Polym. Degrad. Stab.*, vol. 98, no. 8, pp. 1428–1438, 2013, doi: 10.1016/j.polymdegradstab.2013.05.002.

[61] M. H. Fallah, S. A. Fallah, and M. A. Zanjanchi, “Synthesis and characterization of nano-sized zinc oxide coating on cellulosic fibers: Photoactivity and flame-retardancy study,” *Chinese J. Chem.*, vol. 29, no. 6, pp. 1239–1245, 2011, doi: 10.1002/cjoc.201190230.

[62] Q. hua Zhang, J. Gu, G. qiang Chen, and T. ling Xing, “Durable flame retardant finish for silk fabric using boron hybrid silica sol,” *Appl. Surf. Sci.*, vol. 387, pp. 446–453, 2016, doi: 10.1016/j.apsusc.2016.06.119.

[63] Q. Zhang *et al.*, “Flame retardance and thermal stability of wool fabric treated by boron containing silica sols,” *Mater. Des.*, vol. 85, pp. 796–799, 2015, doi: 10.1016/j.matdes.2015.07.163.

[64] A. Šehić, B. Tomšič, I. Jerman, J. Vasiljević, J. Medved, and B. Simončič, “Synergistic inhibitory action of P- and Si-containing precursors in sol-gel coatings on the thermal degradation of polyamide 6,” *Polym. Degrad. Stab.*, vol. 128, pp. 245–252, 2016, doi: 10.1016/j.polymdegradstab.2016.03.026.

[65] A. A. Younis, “Optimization of mechanical, thermal, and ignition properties of polyester fabric using urea and phosphoric acid,” *J. Ind. Text.*, vol. 49, no. 6, pp. 791–808, 2020, doi: 10.1177/1528083718798636.

[66] G. Akovali and F. Takrouri, “Studies on modification of some flammability characteristics by plasma. II. Polyester fabric,” *J. Appl. Polym. Sci.*, vol. 42, no. 10, pp. 2717–2725, 1991, doi: 10.1002/app.1991.070421010.

[67] G. Akovali and G. Gundogan, “Studies on flame retardancy of polyacrylonitrile fiber treated by flame-retardant monomers in cold plasma,” *Journal of Applied Polymer Science*, vol. 41, no. 9–10. pp. 2011–2019, 1990, doi: 10.1002/app.1990.070410907.

[68] A. Quédé *et al.*, “Elaboration of fire retardant coatings on polyamide-6 using a cold plasma polymerization process,” *Surf. Coatings Technol.*, vol. 151–152, pp. 424–428, 2002, doi: 10.1016/S0257-8972(01)01646-2.

[69] A. Quédé *et al.*, “Thermal stability and flammability studies of coated polymer powders using a plasma fluidized bed process,” *J. Mater. Sci.*, vol. 37, no. 7, pp. 1395–1399, 2002, doi: 10.1023/A:1014576730732.

[70] S. Bourbigot, C. Jama, M. Le Bras, R. Delobel, O. Dessaux, and P. Goudmand, “New approach to flame retardancy using plasma assisted surface polymerisation techniques,” *Polym. Degrad. Stab.*, vol. 66, no. 1, pp. 153–155, 1999, doi: 10.1016/S0141-3910(99)00059-2.

[71] C. Jama *et al.*, “Fire Retardancy and Thermal Stability of Materials Coated by Organosilicon Thin Films Using a Cold Remote Plasma Process,” pp. 200–213, 2001, doi: 10.1021/bk-2001-0797.ch016.

[72] J. Bardon *et al.*, “Characterization of a plasma polymer coating from an organophosphorus silane deposited at atmospheric pressure for fire-retardant purposes,” *Prog. Org. Coatings*, vol. 88, pp. 39–47, 2015, doi: 10.1016/j.porgcoat.2015.06.005.

[73] B. Schartel, G. Kühn, R. Mix, and J. Friedrich, “Surface controlled fire retardancy of polymers using plasma polymerisation,” *Macromol. Mater. Eng.*, vol. 287, no. 9, pp.

579–582, 2002, doi: 10.1002/1439-2054(20020901)287:9<579::AID-MAME579>3.0.CO;2-6.

[74] F. Hilt, N. Gherardi, D. Duday, A. Berné, and P. Choquet, “Efficient Flame Retardant Thin Films Synthesized by Atmospheric Pressure PECVD through the High Co-deposition Rate of Hexamethyldisiloxane and Triethylphosphate on Polycarbonate and Polyamide-6 Substrates,” *ACS Appl. Mater. Interfaces*, vol. 8, no. 19, pp. 12422–12433, May 2016, doi: 10.1021/acsami.6b01819.

[75] J. Li, W. Tong, and L. Yi, “Flame-retardant composite coatings for cotton fabrics fabricated by using oxygen plasma-induced polymerization of vinyl phosphonic acid/cyclotetrasiloxane,” *Text. Res. J.*, vol. 89, no. 23–24, pp. 5053–5066, 2019, doi: 10.1177/0040517519848158.

[76] A. R. Horrocks, S. Nazaré, R. Masood, B. Kandola, and D. Price, “Surface modification of fabrics for improved flash-fire resistance using atmospheric pressure plasma in the presence of a functionalized clay and polysiloxane,” *Polymers for Advanced Technologies*, vol. 22, no. 1. pp. 22–29, 2011, doi: 10.1002/pat.1707.

[77] A. Quédé, B. Mutel, P. Supiot, C. Jama, O. Dessaux, and R. Delobel, “Characterization of organosilicon films synthesized by N2-PACVD. Application to fire retardant properties of coated polymers,” *Surf. Coatings Technol.*, vol. 180–181, pp. 265–270, 2004, doi: 10.1016/j.surfcoat.2003.10.067.

[78] M. J. Tsafack and J. Levalois-Grützmacher, “Plasma-induced graft-polymerization of flame retardant monomers onto PAN fabrics,” *Surf. Coatings Technol.*, vol. 200, no. 11, pp. 3503–3510, 2006, doi: 10.1016/j.surfcoat.2004.11.030.

[79] M. J. Tsafack and J. Levalois-Grützmacher, “Towards multifunctional surfaces using the plasma-induced graft-polymerization (PIGP) process: Flame and waterproof cotton textiles,” *Surf. Coatings Technol.*, vol. 201, no. 12, pp. 5789–5795, 2007, doi: 10.1016/j.surfcoat.2006.10.027.

[80] B. Paosawatyanyong, P. Jermsutjarit, and W. Bhanthumnavin, “Graft copolymerization coating of methacryloyloxyethyl diphenyl phosphate flame retardant onto silk surface,” *Prog. Org. Coatings*, vol. 77, no. 10, pp. 1585–1590, 2014, doi: 10.1016/j.porgcoat.2014.01.023.

[81] K. Kamlangkla, S. K. Hodak, and J. Levalois-Grützmacher, “Multifunctional silk fabrics by means of the plasma induced graft polymerization (PIGP) process,” *Surf. Coatings Technol.*, vol. 205, no. 13–14, pp. 3755–3762, 2011, doi: 10.1016/j.surfcoat.2011.01.006.

[82] S. Zanini, C. Riccardi, M. Orlandi, C. Colombo, and F. Croccolo, “Plasma-induced graft-polymerisation of ethylene glycol methacrylate phosphate on polyethylene films,” *Polym. Degrad. Stab.*, vol. 93, no. 6, pp. 1158–1163, 2008, doi: 10.1016/j.polymdegradstab.2008.03.009.

[83] H. Yavuz, Z. Rzaev, and N. Dilsiz, “Characterisation of flame retardant plasma polymer deposited BOPP film,” *Plast. Rubber Compos.*, vol. 37, no. 5–6, pp. 268–275, 2008, doi: 10.1179/174328908X309385.

[84] I. Errifai *et al.*, “Elaboration of a fire retardant coating for polyamide-6 using cold plasma polymerization of a fluorinated acrylate,” *Surf. Coatings Technol.*, vol. 180–181, pp. 297–301, 2004, doi: 10.1016/j.surfcoat.2003.10.074.

[85] F. Carosio, J. Alongi, and A. Frache, “Influence of surface activation by plasma and nanoparticle adsorption on the morphology, thermal stability and combustion behavior of PET fabrics,” *Eur. Polym. J.*, vol. 47, no. 5, pp. 893–902, 2011, doi: 10.1016/j.eurpolymj.2011.01.009.

[86] B. K. Kandola and P. Luangtriratana, “Thermo-physical performance of organoclay coatings deposited on the surfaces of glass fibre-reinforced epoxy composites using an atmospheric pressure plasma or a resin binder,” *Appl. Clay Sci.*, vol. 99, pp. 62–71, 2014, doi: 10.1016/j.clay.2014.06.013.

[87] Z. Ömeroğulları and D. Kut, “Application of low-frequency oxygen plasma treatment to polyester fabric to reduce the amount of flame retardant agent,” *Text. Res. J.*, vol. 82, no. 6, pp. 613–621, 2012, doi: 10.1177/0040517511420758.

[88] Z. R. Farag, S. Krüger, G. Hidde, A. Schimanski, C. Jäger, and J. Friedrich, “Deposition of thick polymer or inorganic layers with flame-retardant properties by combination of plasma and spray processes,” *Surf. Coatings Technol.*, vol. 228, pp. 266–274, 2013, doi: 10.1016/j.surfcoat.2013.04.039.

[89] V. Totolin, M. Sarmadi, S. O. Manolache, and F. S. Denes, “Environmentally friendly flame-retardant materials produced by atmospheric pressure plasma modifications,” *J. Appl. Polym. Sci.*, vol. 124, no. 1, pp. 116–122, Apr. 2012, doi: 10.1002/app.35087.

[90] V. Totolin, M. Sarmadi, S. O. Manolache, and F. S. Denes, “Atmospheric pressure plasma enhanced synthesis of flame retardant cellulosic materials,” *J. Appl. Polym. Sci.*, vol. 117, no. 5, pp. 281–289, 2010, doi: 10.1002/app.31987.

[91] G. Decher, J. D. Hong, and J. Schmitt, “Buildup of ultrathin multilayer films by a self-assembly process: III. Consecutively alternating adsorption of anionic and cationic polyelectrolytes on charged surfaces,” *Thin Solid Films*, vol. 210–211, no. PART 2, pp. 831–835, 1992, doi: 10.1016/0040-6090(92)90417-A.

[92] G. Decher, “Layer-by-Layer Assembly (Putting Molecules to Work),” *Multilayer Thin Film. Seq. Assem. Nanocomposite Mater. Second Ed.*, vol. 1, pp. 1–21, 2012, doi: 10.1002/9783527646746.ch1.

[93] R. K. Iler, “Multilayers of colloidal particles,” *J. Colloid Interface Sci.*, vol. 21, no. 6, pp. 569–594, 1966.

[94] J. M. Lehn, “Towards complex matter: Supramolecular chemistry and self-organization,” *Eur. Rev.*, vol. 17, no. 2, pp. 263–280, 2009, doi: 10.1017/S1062798709000805.

[95] G. M. Whitesides, J. P. Mathias, and C. T. Seto, “Molecular self-assembly and nanochemistry: A chemical strategy for the synthesis of nanostructures,” *Science (80-.).*, vol. 254, no. 5036, pp. 1312–1319, 1991, doi: 10.1126/science.1962191.

[96] R. S. Tu and M. Tirrell, “Bottom-up design of biomimetic assemblies,” *Adv. Drug Deliv.*

Rev., vol. 56, no. 11, pp. 1537–1563, 2004, doi: 10.1016/j.addr.2003.10.047.

[97] R. Mérindol, “Layer-by-layer assembly of strong bio-inspired nanocomposites,” Université de Strasbourg, 2014.

[98] P. Lavalle *et al.*, “Comparison of the structure of polyelectrolyte multilayer films exhibiting a linear and an exponential growth regime: An in situ atomic force microscopy study,” *Macromolecules*, vol. 35, no. 11, pp. 4458–4465, 2002, doi: 10.1021/ma0119833.

[99] P. Podsiadlo *et al.*, “Exponential growth of LBL films with incorporated inorganic sheets,” *Nano Lett.*, vol. 8, no. 6, pp. 1762–1770, 2008, doi: 10.1021/nl8011648.

[100] X. Li, P. Fan, X. Tuo, Y. He, and X. Wang, “Photoresponsive layer-by-layer ultrathin films prepared from a hyperbranched azobenzene-containing polymeric diazonium salt,” *Thin Solid Films*, vol. 517, no. 6, pp. 2055–2062, 2009, doi: 10.1016/j.tsf.2008.10.136.

[101] K. Araki, M. J. Wagner, and M. S. Wrighton, “Layer-by-layer growth of electrostatically assembled multilayer porphyrin films,” *Langmuir*, vol. 12, no. 22, pp. 5393–5398, 1996, doi: 10.1021/la960024c.

[102] A. Martin *et al.*, “Controlled release of encapsulated methylene blue in a multilayered textile coating,” *MATEC Web Conf.*, vol. 7, 2013, doi: 10.1051/matecconf/20130704012.

[103] S. J. Percival, L. J. Small, E. D. Spoerke, and S. B. Rempe, “Polyelectrolyte layer-by-layer deposition on nanoporous supports for ion selective membranes,” *RSC Adv.*, vol. 8, no. 57, pp. 32992–32999, 2018, doi: 10.1039/c8ra05580g.

[104] F. Ben Dhieb, S. H. Tabatabaei, F. Mighri, and A. Ajji, “Comparison of Crosslinking Efficiency in Dip and Roll-Deposited Coatings on Their Oxygen Barrier,” *ACS Omega*, vol. 4, no. 14, pp. 15772–15779, 2019, doi: 10.1021/acsomega.9b00950.

[105] D. Lin, X. Zeng, H. Li, and X. Lai, “Facile fabrication of superhydrophobic and flame-retardant coatings on cotton fabrics via layer-by-layer assembly,” *Cellulose*, vol. 25, no. 5, pp. 3135–3149, 2018, doi: 10.1007/s10570-018-1748-9.

[106] J. Janesch, I. Czabany, C. Hansmann, A. Mautner, T. Rosenau, and W. Gindl-Altmutter, “Transparent layer-by-layer coatings based on biopolymers and CeO2 to protect wood from UV light,” *Prog. Org. Coatings*, vol. 138, no. August 2019, p. 105409, 2020, doi: 10.1016/j.porgcoat.2019.105409.

[107] Y. Zhang *et al.*, “Eco-friendly flame retardant and electromagnetic interference shielding cotton fabrics with multi-layered coatings,” *Chem. Eng. J.*, vol. 372, no. May, pp. 1077–1090, 2019, doi: 10.1016/j.cej.2019.05.012.

[108] F. Fadhillah, S. M. Javaid Zaidi, Z. Khan, M. Khaled, F. Rahman, and P. Hammond, “Development of multilayer polyelectrolyte thin-film membranes fabricated by spin assisted layer-by-layer assembly,” *Journal of Applied Polymer Science*, vol. 126, no. 4. pp. 1468–1474, 2012, doi: 10.1002/app.36879.

[109] C. J. Lefaux, J. A. Zimberlin, A. V. Dobrynin, and P. T. Mather, “Polyelectrolyte spin assembly: Influence of ionic strength on the growth of multilayered thin films,” *J. Polym.*

Sci. Part B Polym. Phys., vol. 42, no. 19, pp. 3654–3666, 2004, doi: 10.1002/polb.20209.

[110] F. Oytun and F. Basarir, “Spin-assisted layer-by-layer assembled oppositely charged reduced graphene oxide films,” *Mater. Lett.*, vol. 257, p. 126756, 2019, doi: 10.1016/j.matlet.2019.126756.

[111] W. Yu, J. Koc, J. A. Finlay, J. L. Clarke, A. S. Clare, and A. Rosenhahn, “Layer-by-layer constructed hyaluronic acid/chitosan multilayers as antifouling and fouling-release coatings,” *Biointerphases*, vol. 14, no. 5, p. 051002, 2019, doi: 10.1116/1.5110887.

[112] M. J. Serpe and L. A. Lyon, “Optical and acoustic studies of pH-dependent swelling in microgel thin films,” *Chem. Mater.*, vol. 16, no. 22, pp. 4373–4380, 2004, doi: 10.1021/cm048844v.

[113] V. Vertlib, M. Dietiker, M. Plötze, L. Yezek, R. Spolenak, and A. M. Puzrin, “Fast assembly of bio-inspired nanocomposite films,” *J. Mater. Res.*, vol. 23, no. 4, pp. 1026–1035, 2008, doi: 10.1557/jmr.2008.0147.

[114] F. Xiang, T. M. Givens, and J. C. Grunlan, “Fast spray deposition of super gas barrier polyelectrolyte multilayer thin films,” *Ind. Eng. Chem. Res.*, vol. 54, no. 19, pp. 5254–5260, 2015, doi: 10.1021/acs.iecr.5b01367.

[115] Z. Zhou *et al.*, “Layer-by-layer assembly of MXene and carbon nanotubes on electrospun polymer films for flexible energy storage,” *Nanoscale*, vol. 10, no. 13, pp. 6005–6013, 2018, doi: 10.1039/c8nr00313k.

[116] S. Chang, R. P. Slopek, B. Condon, and J. C. Grunlan, “Surface coating for flame-retardant behavior of cotton fabric using a continuous layer-by-layer process,” *Ind. Eng. Chem. Res.*, vol. 53, no. 10, pp. 3805–3812, 2014, doi: 10.1021/ie403992x.

[117] K. Fujimoto, S. Fujita, B. Ding, and S. Shiratori, “Fabrication of layer-by-layer self-Assembly films using roll-to-roll process,” *Japanese J. Appl. Physics, Part 2 Lett.*, vol. 44, no. 1–7, pp. 1–4, 2005, doi: 10.1143/JJAP.44.L126.

[118] F. S. Gittleson, D. J. Kohn, X. Li, and A. D. Taylor, “Improving the assembly speed, quality, and tunability of thin conductive multilayers,” *ACS Nano*, vol. 6, no. 5, pp. 3703–3711, 2012, doi: 10.1021/nn204384f.

[119] S. Seo, S. Lee, and Y. T. Park, “Note: Automatic layer-by-layer spraying system for functional thin film coatings,” *Rev. Sci. Instrum.*, vol. 87, no. 3, 2016, doi: 10.1063/1.4945043.

[120] A. J. Mateos, A. A. Cain, and J. C. Grunlan, “Large-scale continuous immersion system for layer-by-layer deposition of flame retardant and conductive nanocoatings on fabric,” *Ind. Eng. Chem. Res.*, vol. 53, no. 15, pp. 6409–6416, 2014, doi: 10.1021/ie500122u.

[121] F. Carosio and J. Alongi, “Ultra-Fast Layer-by-Layer Approach for Depositing Flame Retardant Coatings on Flexible PU Foams within Seconds,” *ACS Appl. Mater. Interfaces*, vol. 8, no. 10, pp. 6315–6319, 2016, doi: 10.1021/acsami.6b00598.

[122] S. Miyauchi, H. Imoto, and K. Naka, “Fabrication of polymer-calcite composite thin films by phase transition of vaterite composite particles with octacarboxy-terminated T8-

caged silsesquioxane," *Polym. J.*, vol. 48, no. 10, pp. 1019–1027, 2016, doi: 10.1038/pj.2016.69.

[123] S. Nag, A. Sachan, M. Castro, V. Choudhary, and J. F. Feller, "Spray layer-by-layer assembly of POSS functionalized CNT quantum chemo-resistive sensors with tuneable selectivity and ppm resolution to VOC biomarkers," *Sensors Actuators, B Chem.*, vol. 222, pp. 362–373, 2016, doi: 10.1016/j.snb.2015.08.038.

[124] B. Song, L. Meng, and Y. Huang, "Preparation and characterization of (POSS/TiO2)n multi-coatings based on PBO fiber surface for improvement of UV resistance," *Fibers Polym.*, vol. 14, no. 3, pp. 375–381, 2013, doi: 10.1007/s12221-013-0375-1.

[125] H. Yang, K. Li, W. Liu, X. Liu, W. Xu, and B. Deng, "Development of structural colored cotton fabric via the layer-by-layer electrostatic self-assembling of SiO2 nanoparticles," *Cellulose*, vol. 27, no. 7, pp. 4133–4144, 2020, doi: 10.1007/s10570-020-03040-w.

[126] M. Xiong, Z. Ren, and W. Liu, "Fabrication of UV-resistant and superhydrophobic surface on cotton fabric by functionalized polyethyleneimine/SiO2 via layer-by-layer assembly and dip-coating," *Cellulose*, vol. 26, no. 16, pp. 8951–8962, 2019, doi: 10.1007/s10570-019-02705-5.

[127] K. Han, T. Y. Park, K. Yong, and H. J. Cha, "Combinational Biomimicking of Lotus Leaf, Mussel, and Sandcastle Worm for Robust Superhydrophobic Surfaces with Biomedical Multifunctionality: Antithrombotic, Antibiofouling, and Tissue Closure Capabilities," *ACS Appl. Mater. Interfaces*, vol. 11, no. 10, pp. 9777–9785, 2019, doi: 10.1021/acsami.8b21122.

[128] D. Patra, P. Vangal, A. A. Cain, C. Cho, O. Regev, and J. C. Grunlan, "Inorganic nanoparticle thin film that suppresses flammability of polyurethane with only a single electrostatically-assembled bilayer," *ACS Appl. Mater. Interfaces*, vol. 6, no. 19, pp. 16903–16908, 2014, doi: 10.1021/am504455k.

[129] K. M. Holder, R. J. Smith, and J. C. Grunlan, "A review of flame retardant nanocoatings prepared using layer-by-layer assembly of polyelectrolytes," *J. Mater. Sci.*, vol. 52, no. 22, pp. 12923–12959, 2017, doi: 10.1007/s10853-017-1390-1.

[130] K. Srikulkit, C. Iamsamai, and S. T. Dubas, "Development of Flame Retardant Polyphosphoric Acid Coating Based on the Polyelectrolyte Multilayers Technique," *J. Met. Mater. Miner.*, vol. 16, no. 2, pp. 41–45, 2006.

[131] Y. C. Li, J. Schulz, and J. C. Grunlan, "Polyelectrolyte/nanosilicate thin-film assemblies: Influence of pH on growth, mechanical behavior, and flammability," *ACS Appl. Mater. Interfaces*, vol. 1, no. 10, pp. 2338–2347, 2009, doi: 10.1021/am900484q.

[132] Y.-C. Li *et al.*, "Flame Retardant Behavior of Polyelectrolyte−Clay Thin Film Assemblies on Cotton Fabric," *ACS Nano*, vol. 4, no. 6, pp. 3325–3337, Jun. 2010, doi: 10.1021/nn100467e.

[133] Y. C. Li *et al.*, "Intumescent all-polymer multilayer nanocoating capable of extinguishing flame on fabric," *Advanced Materials*, vol. 23, no. 34. pp. 3926–3931, 2011, doi: 10.1002/adma.201101871.

[134] A. Laachachi, V. Ball, K. Apaydin, V. Toniazzo, and D. Ruch, “Diffusion of polyphosphates into (poly(allylamine)-montmorillonite) multilayer films: Flame retardant-intumescent films with improved oxygen barrier,” *Langmuir*, vol. 27, no. 22, pp. 13879–13887, 2011, doi: 10.1021/la203252q.

[135] K. Apaydin *et al.*, “Intumescent coating of (polyallylamine-polyphosphates) deposited on polyamide fabrics via layer-by-layer technique,” *Polym. Degrad. Stab.*, vol. 106, pp. 158–164, 2014, doi: 10.1016/j.polymdegradstab.2014.01.006.

[136] K. Apaydin, A. Laachachi, V. Ball, M. Jimenez, S. Bourbigot, and D. Ruch, “Layer-by-layer deposition of a TiO2-filled intumescent coating and its effect on the flame retardancy of polyamide and polyester fabrics,” *Colloids Surfaces A Physicochem. Eng. Asp.*, vol. 469, pp. 1–10, 2015, doi: 10.1016/j.colsurfa.2014.12.021.

[137] M. Haile, M. Leistner, O. Sarwar, C. M. Toler, R. Henderson, and J. C. Grunlan, “A wash-durable polyelectrolyte complex that extinguishes flames on polyester-cotton fabric,” *RSC Adv.*, vol. 6, no. 40, pp. 33998–34004, 2016, doi: 10.1039/c6ra03637f.

[138] G. Laufer, C. Kirkland, A. B. Morgan, and J. C. Grunlan, “Intumescent multilayer nanocoating, made with renewable polyelectrolytes, for flame-retardant cotton,” *Biomacromolecules*, vol. 13, no. 9, pp. 2843–2848, 2012, doi: 10.1021/bm300873b.

[139] Y. Pan and H. Zhao, “A novel blowing agent polyelectrolyte for fabricating intumescent multilayer coating that retards fire on cotton fabric,” *J. Appl. Polym. Sci.*, vol. 135, no. 32, pp. 1–8, 2018, doi: 10.1002/app.46583.

[140] C. K. Kundu, X. Wang, L. Song, and Y. Hu, “Borate cross-linked layer-by-layer assembly of green polyelectrolytes on polyamide 66 fabrics for flame-retardant treatment,” *Prog. Org. Coatings*, vol. 121, no. March, pp. 173–181, 2018, doi: 10.1016/j.porgcoat.2018.04.031.

[141] C. Kumar Kundu *et al.*, “A green approach to constructing multilayered nanocoating for flame retardant treatment of polyamide 66 fabric from chitosan and sodium alginate,” *Carbohydr. Polym.*, vol. 166, pp. 131–138, 2017, doi: 10.1016/j.carbpol.2017.02.084.

[142] X. W. Cheng, J. P. Guan, X. H. Yang, R. C. Tang, and F. Yao, “A bio-resourced phytic acid/chitosan polyelectrolyte complex for the flame retardant treatment of wool fabric,” *J. Clean. Prod.*, vol. 223, pp. 342–349, 2019, doi: 10.1016/j.jclepro.2019.03.157.

[143] M. Jimenez, T. Guin, S. Bellayer, R. Dupretz, S. Bourbigot, and J. C. Grunlan, “Microintumescent mechanism of flame-retardant water-based chitosan-ammonium polyphosphate multilayer nanocoating on cotton fabric,” *J. Appl. Polym. Sci.*, vol. 133, no. 32, pp. 1–12, 2016, doi: 10.1002/app.43783.

[144] F. Fang *et al.*, “Intumescent flame retardant coatings on cotton fabric of chitosan and ammonium polyphosphate via layer-by-layer assembly,” *Surf. Coatings Technol.*, vol. 262, pp. 9–14, 2015, doi: 10.1016/j.surfcoat.2014.11.011.

[145] F. Carosio, J. Alongi, and G. Malucelli, “Layer by Layer ammonium polyphosphate-based coatings for flame retardancy of polyester-cotton blends,” *Carbohydr. Polym.*, vol. 88, no. 4, pp. 1460–1469, 2012, doi: 10.1016/j.carbpol.2012.02.049.

[146] I. Jordanov *et al.*, “Flame retardant polyester fabric from nitrogen-rich low molecular weight additives within intumescent nanocoating,” *Polym. Degrad. Stab.*, vol. 170, p. 108998, 2019, doi: 10.1016/j.polymdegradstab.2019.108998.

[147] F. Carosio and J. Alongi, “Few durable layers suppress cotton combustion due to the joint combination of layer by layer assembly and UV-curing,” *RSC Adv.*, vol. 5, no. 87, pp. 71482–71490, 2015, doi: 10.1039/c5ra11856e.

[148] T. Guin, M. Krecker, A. Milhorn, and J. C. Grunlan, “Maintaining hand and improving fire resistance of cotton fabric through ultrasonication rinsing of multilayer nanocoating,” *Cellulose*, vol. 21, no. 4, pp. 3023–3030, 2014, doi: 10.1007/s10570-014-0286-3.

[149] S. Lazar, B. Eberle, E. Bellevergue, and J. Grunlan, “Amine Salt Thickening of Intumescent Multilayer Flame Retardant Treatment,” *Ind. Eng. Chem. Res.*, vol. 59, no. 7, pp. 2689–2695, 2020, doi: 10.1021/acs.iecr.9b06359.

[150] H. Pan, W. Wang, Y. Pan, L. Song, Y. Hu, and K. M. Liew, “Formation of self-extinguishing flame retardant biobased coating on cotton fabrics via Layer-by-Layer assembly of chitin derivatives,” *Carbohydr. Polym.*, vol. 115, pp. 516–524, 2015, doi: 10.1016/j.carbpol.2014.08.084.

[151] C. K. Kundu, X. Wang, L. Song, and Y. Hu, “Chitosan-based flame retardant coatings for polyamide 66 textiles: One-pot deposition versus layer-by-layer assembly,” *Int. J. Biol. Macromol.*, vol. 143, pp. 1–10, 2020, doi: 10.1016/j.ijbiomac.2019.11.220.

[152] F. Carosio, A. Di Blasio, J. Alongi, and G. Malucelli, “Green DNA-based flame retardant coatings assembled through Layer by Layer,” *Polymer (Guildf).*, vol. 54, no. 19, pp. 5148–5153, 2013, doi: 10.1016/j.polymer.2013.07.029.

[153] Y. Pan *et al.*, “Effect of genipin crosslinked layer-by-layer self-assembled coating on the thermal stability, flammability and wash durability of cotton fabric,” *Carbohydr. Polym.*, vol. 206, no. November 2018, pp. 396–402, 2019, doi: 10.1016/j.carbpol.2018.11.037.

[154] L. Liu, Y. Pan, Z. Wang, Y. Hou, Z. Gui, and Y. Hu, “Layer-by-Layer Assembly of Hypophosphorous Acid-Modified Chitosan Based Coating for Flame-Retardant Polyester-Cotton Blends,” *Ind. Eng. Chem. Res.*, vol. 56, no. 34, pp. 9429–9436, 2017, doi: 10.1021/acs.iecr.7b02303.

[155] X. Wang, M. Q. Romero, X. Q. Zhang, R. Wang, and D. Y. Wang, “Intumescent multilayer hybrid coating for flame retardant cotton fabrics based on layer-by-layer assembly and sol-gel process,” *RSC Adv.*, vol. 5, no. 14, pp. 10647–10655, 2015, doi: 10.1039/c4ra14943b.

[156] L. Liu, Z. Huang, Y. Pan, X. Wang, L. Song, and Y. Hu, “Finishing of cotton fabrics by multi-layered coatings to improve their flame retardancy and water repellency,” *Cellulose*, vol. 25, no. 8, pp. 4791–4803, 2018, doi: 10.1007/s10570-018-1866-4.

[157] Z. Jiang, C. Wang, S. Fang, P. Ji, H. Wang, and C. Ji, “Durable flame-retardant and antidroplet finishing of polyester fabrics with flexible polysiloxane and phytic acid through layer-by-layer assembly and sol–gel process,” *J. Appl. Polym. Sci.*, vol. 135, no. 27, pp. 1–10, 2018, doi: 10.1002/app.46414.

[158] F. Fang *et al.*, "Environmentally friendly assembly multilayer coating for flame retardant and antimicrobial cotton fabric," *Prog. Org. Coatings*, vol. 90, pp. 258–266, 2016, doi: 10.1016/j.porgcoat.2015.09.025.

[159] F. Fang *et al.*, "Boron-containing intumescent multilayer nanocoating for extinguishing flame on cotton fabric," *Cellulose*, vol. 23, no. 3, pp. 2161–2172, 2016, doi: 10.1007/s10570-016-0928-8.

[160] F. Fang *et al.*, "Construction of intumescent flame retardant and antimicrobial coating on cotton fabric via layer-by-layer assembly technology," *Surf. Coatings Technol.*, vol. 276, pp. 726–734, 2015, doi: 10.1016/j.surfcoat.2015.05.023.

[161] J. C. Yang, W. Liao, S. B. Deng, Z. J. Cao, and Y. Z. Wang, "Flame retardation of cellulose-rich fabrics via a simplified layer-by-layer assembly," *Carbohydr. Polym.*, vol. 151, pp. 434–440, 2016, doi: 10.1016/j.carbpol.2016.05.087.

[162] T. Zhang, H. Yan, L. Wang, and Z. Fang, "Controlled formation of self-extinguishing intumescent coating on ramie fabric via layer-by-layer assembly," *Ind. Eng. Chem. Res.*, vol. 52, no. 18, pp. 6138–6146, 2013, doi: 10.1021/ie3031554.

[163] L. Zhao, H. Yan, Z. Fang, J. Wang, and H. Wang, "On the flameproof treatment of ramie fabrics using a spray-assisted layer-by-layer technique," *Polym. Degrad. Stab.*, vol. 121, pp. 11–17, 2015, doi: 10.1016/j.polymdegradstab.2015.08.007.

[164] F. Carosio, J. Alongi, and G. Malucelli, "Flammability and combustion properties of ammonium polyphosphate-/ poly(acrylic acid)-based layer by layer architectures deposited on cotton, polyester and their blends," *Polym. Degrad. Stab.*, vol. 98, no. 9, pp. 1626–1637, 2013, doi: 10.1016/j.polymdegradstab.2013.06.019.

[165] F. Carosio, C. Negrell-Guirao, A. Di Blasio, J. Alongi, G. David, and G. Camino, "Tunable thermal and flame response of phosphonated oligoallylamines layer by layer assemblies on cotton," *Carbohydr. Polym.*, vol. 115, pp. 752–759, 2015, doi: 10.1016/j.carbpol.2014.06.066.

[166] M. Narkhede, S. Thota, R. Mosurkal, W. S. Muller, and J. Kumar, "Layer-by-layer assembly of halogen-free polymeric materials on nylon/cotton blend for flame retardant applications," *Fire Mater.*, vol. 40, no. 2, pp. 206–218, 2016, doi: 10.1002/fam.

[167] F. Carosio, F. Cuttica, A. Di Blasio, J. Alongi, and G. Malucelli, "Layer by layer assembly of flame retardant thin films on closed cell PET foams: Efficiency of ammonium polyphosphate versus DNA," *Polym. Degrad. Stab.*, vol. 113, pp. 189–196, 2015, doi: 10.1016/j.polymdegradstab.2014.09.018.

[168] S. B. Deng, W. Liao, J. C. Yang, Z. J. Cao, and Y. Z. Wang, "Flame-Retardant and Smoke-Suppressed Silicone Foams with Chitosan-Based Nanocoatings," *Ind. Eng. Chem. Res.*, vol. 55, no. 27, pp. 7239–7248, 2016, doi: 10.1021/acs.iecr.6b00532.

[169] F. Carosio, M. Ghanadpour, J. Alongi, and L. Wågberg, "Layer-by-layer-assembled chitosan/phosphorylated cellulose nanofibrils as a bio-based and flame protecting nano-exoskeleton on PU foams," *Carbohydr. Polym.*, vol. 202, no. July, pp. 479–487, 2018, doi: 10.1016/j.carbpol.2018.09.005.

[170] H. Xuan, J. Ren, X. Wang, J. Zhang, and L. Ge, "Flame-retardant, non-irritating and self-healing multilayer films with double-network structure," *Compos. Sci. Technol.*, vol. 145, pp. 15–23, 2017, doi: 10.1016/j.compscitech.2017.03.038.

[171] O. Köklükaya, F. Carosio, J. C. Grunlan, and L. Wågberg, "Flame-Retardant Paper from Wood Fibers Functionalized via Layer-by-Layer Assembly," *ACS Appl. Mater. Interfaces*, vol. 7, no. 42, pp. 23750–23759, 2015, doi: 10.1021/acsami.5b08105.

[172] O. Köklükaya, F. Carosio, and L. Wågberg, "Tailoring flame-retardancy and strength of papers via layer-by-layer treatment of cellulose fibers," *Cellulose*, vol. 25, no. 4, pp. 2691–2709, 2018, doi: 10.1007/s10570-018-1749-8.

[173] Y. Pan, L. Liu, and H. Zhao, "Recyclable flame retardant paper made from layer-by-layer assembly of zinc coordinated multi-layered coatings," *Cellulose*, vol. 25, no. 9, pp. 5309–5321, 2018, doi: 10.1007/s10570-018-1922-0.

[174] Y. Pan, W. Wang, L. Liu, H. Ge, L. Song, and Y. Hu, "Influences of metal ions crosslinked alginate based coatings on thermal stability and fire resistance of cotton fabrics," *Carbohydr. Polym.*, vol. 170, pp. 133–139, 2017, doi: 10.1016/j.carbpol.2017.04.065.

[175] Y. Pan, L. Liu, L. Song, Y. Hu, W. Wang, and H. Zhao, "Durable flame retardant treatment of polyethylene terephthalate (PET) fabric with cross-linked layer-by-layer assembled coating," *Polym. Degrad. Stab.*, vol. 165, pp. 145–152, 2019, doi: 10.1016/j.polymdegradstab.2019.05.009.

[176] F. Carosio, G. Fontaine, J. Alongi, and S. Bourbigot, "Starch-Based Layer by Layer Assembly: Efficient and Sustainable Approach to Cotton Fire Protection," *ACS Appl. Mater. Interfaces*, vol. 7, no. 22, pp. 12158–12167, 2015, doi: 10.1021/acsami.5b02507.

[177] M. Leistner, A. A. Abu-Odeh, S. C. Rohmer, and J. C. Grunlan, "Water-based chitosan/melamine polyphosphate multilayer nanocoating that extinguishes fire on polyester-cotton fabric," *Carbohydr. Polym.*, vol. 130, pp. 227–232, 2015, doi: 10.1016/j.carbpol.2015.05.005.

[178] S. Li, X. Lin, Y. Liu, R. Li, X. Ren, and T. S. Huang, "Phosphorus-nitrogen-silicon-based assembly multilayer coating for the preparation of flame retardant and antimicrobial cotton fabric," *Cellulose*, vol. 26, no. 6, pp. 4213–4223, 2019, doi: 10.1007/s10570-019-02373-5.

[179] G. Laufer, C. Kirkland, A. B. Morgan, and J. C. Grunlan, "Exceptionally flame retardant sulfur-based multilayer nanocoating for polyurethane prepared from aqueous polyelectrolyte solutions," *ACS Macro Lett.*, vol. 2, no. 5, pp. 361–365, 2013, doi: 10.1021/mz400105e.

[180] Y. Pan *et al.*, "Effect of Fully Biobased Coatings Constructed via Layer-by-Layer Assembly of Chitosan and Lignosulfonate on the Thermal, Flame Retardant, and Mechanical Properties of Flexible Polyurethane Foam," *ACS Sustain. Chem. Eng.*, vol. 4, no. 3, pp. 1431–1438, 2016, doi: 10.1021/acssuschemeng.5b01423.

[181] F. Carosio, A. Di Blasio, F. Cuttica, J. Alongi, and G. Malucelli, "Self-assembled hybrid nanoarchitectures deposited on poly(urethane) foams capable of chemically adapting to

extreme heat," *RSC Adv.*, vol. 4, no. 32, pp. 16674–16680, 2014, doi: 10.1039/c4ra01343c.

[182] F. Carosio, C. Negrell-Guirao, J. Alongi, G. David, and G. Camino, "All-polymer Layer by Layer coating as efficient solution to polyurethane foam flame retardancy," *Eur. Polym. J.*, vol. 70, pp. 94–103, 2015, doi: 10.1016/j.eurpolymj.2015.07.001.

[183] J. Chen, S. D. Jiang, Z. Q. Huang, G. Tang, and Y. Hu, "Self-assembly of hydroxyapatite with polyelectrolyte as a green flame retardant for poly(vinyl alcohol)," *J. Fire Sci.*, vol. 35, no. 6, pp. 507–520, 2017, doi: 10.1177/0734904117720476.

[184] S. D. Jiang, G. Tang, J. Chen, Z. Q. Huang, and Y. Hu, "Biobased polyelectrolyte multilayer-coated hollow mesoporous silica as a green flame retardant for epoxy resin," *J. Hazard. Mater.*, vol. 342, pp. 689–697, 2018, doi: 10.1016/j.jhazmat.2017.09.001.

[185] H. Yan, N. Li, J. Cheng, P. Song, Z. Fang, and H. Wang, "Fabrication of flame retardant benzoxazine semi-biocomposites reinforced by ramie fabrics with bio-based flame retardant coating," *Polym. Compos.*, vol. 39, pp. E480–E488, 2018, doi: 10.1002/pc.24617.

[186] N. Li *et al.*, "Flame retarding and reinforcing modification of ramie/polybenzoxazine composites by surface treatment of ramie fabric," *Compos. Sci. Technol.*, vol. 121, pp. 82–88, 2015, doi: 10.1016/j.compscitech.2015.07.013.

[187] H. Yan, N. Li, Z. Fang, and H. Wang, "Application of poly(diphenolic acid-phenyl phosphate)-based layer by layer nanocoating in flame retardant ramie fabrics," *J. Appl. Polym. Sci.*, vol. 134, no. 20, pp. 1–13, 2017, doi: 10.1002/app.44795.

[188] X. H. Shi *et al.*, "Layer-by-layer assembled flame-retardant architecture toward high-performance carbon fiber composite," *Chem. Eng. J.*, vol. 353, no. April, pp. 550–558, 2018, doi: 10.1016/j.cej.2018.07.146.

[189] F. Carosio, G. Laufer, J. Alongi, G. Camino, and J. C. Grunlan, "Layer-by-layer assembly of silica-based flame retardant thin film on PET fabric," *Polym. Degrad. Stab.*, vol. 96, no. 5, pp. 745–750, 2011, doi: 10.1016/j.polymdegradstab.2011.02.019.

[190] J. Alongi, F. Carosio, A. Frache, and G. Malucelli, "Layer by Layer coatings assembled through dipping, vertical or horizontal spray for cotton flame retardancy," *Carbohydr. Polym.*, vol. 92, no. 1, pp. 114–119, 2013, doi: 10.1016/j.carbpol.2012.08.086.

[191] F. Carosio, A. Di Blasio, F. Cuttica, J. Alongi, A. Frache, and G. Malucelli, "Flame retardancy of polyester fabrics treated by spray-assisted layer-by-layer silica architectures," *Ind. Eng. Chem. Res.*, vol. 52, no. 28, pp. 9544–9550, 2013, doi: 10.1021/ie4011244.

[192] F. Carosio, A. Di Blasio, J. Alongi, and G. Malucelli, "Layer by layer nanoarchitectures for the surface protection of polycarbonate," *Eur. Polym. J.*, vol. 49, no. 2, pp. 397–404, 2013, doi: 10.1016/j.eurpolymj.2012.10.032.

[193] J. Alongi, F. Carosio, and G. Malucelli, "Layer by layer complex architectures based on ammonium polyphosphate, chitosan and silica on polyester-cotton blends: Flammability and combustion behaviour," *Cellulose*, vol. 19, no. 3, pp. 1041–1050, 2012, doi:

10.1007/s10570-012-9682-8.

[194] H. Yan, L. Zhao, Z. Fang, and H. Wang, “Construction of multilayer coatings for flame retardancy of ramie fabric using layer-by-layer assembly,” *Journal of Applied Polymer Science*, vol. 134, no. 48. 2017, doi: 10.1002/app.45556.

[195] T. Zhang, H. Yan, M. Peng, L. Wang, H. Ding, and Z. Fang, “Construction of flame retardant nanocoating on ramie fabric via layer-by-layer assembly of carbon nanotube and ammonium polyphosphate,” *Nanoscale*, vol. 5, no. 7, pp. 3013–3021, 2013, doi: 10.1039/c3nr34020a.

[196] G. Huang, H. Liang, X. Wang, and J. Gao, “Poly(acrylic acid)/clay thin films assembled by layer-by-layer deposition for improving the flame retardancy properties of cotton,” *Ind. Eng. Chem. Res.*, vol. 51, no. 38, pp. 12299–12309, 2012, doi: 10.1021/ie300820k.

[197] S. Li, X. Lin, Z. Li, and X. Ren, “Hybrid organic-inorganic hydrophobic and intumescent flame-retardant coating for cotton fabrics,” *Compos. Commun.*, vol. 14, no. March, pp. 15–20, 2019, doi: 10.1016/j.coco.2019.05.005.

[198] G. Huang, J. Yang, J. Gao, and X. Wang, “Thin films of intumescent flame retardant-polyacrylamide and exfoliated graphene oxide fabricated via layer-by-layer assembly for improving flame retardant properties of cotton fabric,” *Ind. Eng. Chem. Res.*, vol. 51, no. 38, pp. 12355–12366, 2012, doi: 10.1021/ie301911t.

[199] W. Wang *et al.*, “Synthesis of Phosphorylated Graphene Oxide Based Multilayer Coating: Self-Assembly Method and Application for Improving the Fire Safety of Cotton Fabrics,” *Ind. Eng. Chem. Res.*, vol. 56, no. 23, pp. 6664–6670, 2017, doi: 10.1021/acs.iecr.7b01293.

[200] X. Chen *et al.*, “Flame-retardant, electrically conductive and antimicrobial multifunctional coating on cotton fabric via layer-by-layer assembly technique,” *RSC Adv.*, vol. 6, no. 33, pp. 27669–27676, 2016, doi: 10.1039/c5ra26914h.

[201] X. Ding *et al.*, “Carbon nanotube-filled intumescent multilayer nanocoating on cotton fabric for enhancing flame retardant property,” *Surf. Coatings Technol.*, vol. 305, pp. 184–191, 2016, doi: 10.1016/j.surfcoat.2016.08.035.

[202] F. Fang *et al.*, “Unique nanobrick wall nanocoating for flame-retardant cotton fabric via layer-by-layer assembly technique,” *Cellulose*, vol. 23, no. 5, pp. 3341–3354, 2016, doi: 10.1007/s10570-016-1013-z.

[203] F. Carosio, J. Alongi, C. Paravidino, and A. Frache, “Improving the flame retardant efficiency of layer by layer coatings containing deoxyribonucleic acid by post-diffusion of hydrotalcite sanoparticles,” *Materials (Basel).*, vol. 10, no. 7, 2017, doi: 10.3390/ma10070709.

[204] X. Shi *et al.*, “Bi-phase fire-resistant polyethylenimine/graphene oxide/melanin coatings using layer by layer assembly technique: Smoke suppression and thermal stability of flexible polyurethane foams,” *Polymer (Guildf).*, vol. 170, no. March, pp. 65–75, 2019, doi: 10.1016/j.polymer.2019.03.008.

[205] A. A. Cain, C. R. Nolen, Y. C. Li, R. Davis, and J. C. Grunlan, “Phosphorous-filled

nanobrick wall multilayer thin film eliminates polyurethane melt dripping and reduces heat release associated with fire," *Polym. Degrad. Stab.*, vol. 98, no. 12, pp. 2645–2652, 2013, doi: 10.1016/j.polymdegradstab.2013.09.028.

[206] X. Liu *et al.*, "Combination Intumescent and Kaolin-Filled Multilayer Nanocoatings that Reduce Polyurethane Flammability," *Macromol. Mater. Eng.*, vol. 304, no. 2, pp. 1–7, 2019, doi: 10.1002/mame.201800531.

[207] O. Köklükaya, F. Carosio, V. L. Durán, and L. Wågberg, "Layer-by-layer modified low density cellulose fiber networks: A sustainable and fireproof alternative to petroleum based foams," *Carbohydr. Polym.*, vol. 230, no. September 2019, 2020, doi: 10.1016/j.carbpol.2019.115616.

[208] K. M. Holder, M. E. Huff, M. N. Cosio, and J. C. Grunlan, "Intumescing multilayer thin film deposited on clay-based nanobrick wall to produce self-extinguishing flame retardant polyurethane," *J. Mater. Sci.*, vol. 50, no. 6, pp. 2451–2458, 2014, doi: 10.1007/s10853-014-8800-4.

[209] F. Carosio and A. Fina, "Three organic/inorganic nanolayers on flexible foam allow retaining superior flame retardancy performance upon mechanical compression cycles," *Front. Mater.*, vol. 6, no. February, pp. 1–10, 2019, doi: 10.3389/fmats.2019.00020.

[210] O. Köklükaya, F. Carosio, and L. Wågberg, "Superior Flame-Resistant Cellulose Nanofibril Aerogels Modified with Hybrid Layer-by-Layer Coatings," *ACS Appl. Mater. Interfaces*, vol. 9, no. 34, pp. 29082–29092, 2017, doi: 10.1021/acsami.7b08018.

[211] R. D. Davis, R. H. Harris, and T. Thomas, "Interagency Agreement Report : Exposure and Fire Hazard Assessment of Nanoparticles in Fire Safe Consumer Products NIST Internal Report 7805 Interagency Agreement Report : Exposure and Fire Hazard Assessment of Nanoparticles in Fire Safe Consumer Products," Gaithersburg, 2011.

[212] Y. S. Kim, R. Davis, A. A. Cain, and J. C. Grunlan, "Development of layer-by-layer assembled carbon nanofiber-filled coatings to reduce polyurethane foam flammability," *Polymer (Guildf).*, vol. 52, no. 13, pp. 2847–2855, 2011, doi: 10.1016/j.polymer.2011.04.023.

[213] Y. S. Kim and R. Davis, "Multi-walled carbon nanotube layer-by-layer coatings with a trilayer structure to reduce foam flammability," *Thin Solid Films*, vol. 550, pp. 184–189, 2014, doi: 10.1016/j.tsf.2013.10.167.

[214] K. M. Holder *et al.*, "Carbon Nanotube Multilayer Nanocoatings Prevent Flame Spread on Flexible Polyurethane Foam," *Macromol. Mater. Eng.*, vol. 301, no. 6, pp. 665–673, 2016, doi: 10.1002/mame.201500327.

[215] H. Pan, Y. Pan, W. Wang, L. Song, Y. Hu, and K. M. Liew, "Synergistic effect of layer-by-layer assembled thin films based on clay and carbon nanotubes to reduce the flammability of flexible polyurethane foam," *Ind. Eng. Chem. Res.*, vol. 53, no. 37, pp. 14315–14321, 2014, doi: 10.1021/ie502215p.

[216] H. Pan, Y. Lu, L. Song, X. Zhang, and Y. Hu, "Fabrication of binary hybrid-filled layer-by-layer coatings on flexible polyurethane foams and studies on their flame-retardant and thermal properties," *RSC Adv.*, vol. 6, no. 82, pp. 78286–78295, 2016, doi:

10.1039/c6ra03760g.

[217] H. Pan, Y. Lu, L. Song, X. Zhang, and Y. Hu, “Construction of layer-by-layer coating based on graphene oxide/β-FeOOH nanorods and its synergistic effect on improving flame retardancy of flexible polyurethane foam,” *Compos. Sci. Technol.*, vol. 129, pp. 116–122, Jun. 2016, doi: 10.1016/j.compscitech.2016.04.018.

[218] X. Qiu, C. K. Kundu, Z. Li, X. Li, and Z. Zhang, “Layer-by-layer-assembled flame-retardant coatings from polydopamine-induced in situ functionalized and reduced graphene oxide,” *J. Mater. Sci.*, vol. 54, no. 21, pp. 13848–13862, 2019, doi: 10.1007/s10853-019-03879-w.

[219] X. Zhang, Q. Shen, X. Zhang, H. Pan, and Y. Lu, “Graphene oxide-filled multilayer coating to improve flame-retardant and smoke suppression properties of flexible polyurethane foam,” *J. Mater. Sci.*, vol. 51, no. 23, pp. 10361–10374, 2016, doi: 10.1007/s10853-016-0247-3.

[220] F. Carosio, L. Maddalena, J. Gomez, G. Saracco, and A. Fina, “Graphene Oxide Exoskeleton to Produce Self-Extinguishing, Nonignitable, and Flame Resistant Flexible Foams: A Mechanically Tough Alternative to Inorganic Aerogels,” *Adv. Mater. Interfaces*, vol. 5, no. 23, pp. 1–9, 2018, doi: 10.1002/admi.201801288.

[221] H. Pan, B. Yu, W. Wang, Y. Pan, L. Song, and Y. Hu, “Comparative study of layer by layer assembled multilayer films based on graphene oxide and reduced graphene oxide on flexible polyurethane foam: flame retardant and smoke suppression properties,” *RSC Adv.*, vol. 6, no. 115, pp. 114304–114312, 2016, doi: 10.1039/c6ra15522g.

[222] W. Chen *et al.*, “Non-covalently Functionalized Graphene Oxide-Based Coating to Enhance Thermal Stability and Flame Retardancy of PVA Film,” *Nano-Micro Lett.*, vol. 10, no. 3, pp. 1–13, 2018, doi: 10.1007/s40820-018-0190-8.

[223] H. Pan, Y. Pan, L. Song, and Y. Hu, “Construction of β-FeOOH nanorod-filled layer-by-layer coating with effective structure to reduce flammability of flexible polyurethane foam,” *Polym. Adv. Technol.*, vol. 28, no. 2, pp. 243–251, Feb. 2017, doi: 10.1002/pat.3880.

[224] W. Wang *et al.*, “Sandwichlike Coating Consisting of Alternating Montmorillonite and β-FeOOH for Reducing the Fire Hazard of Flexible Polyurethane Foam,” *ACS Sustain. Chem. Eng.*, vol. 3, no. 12, pp. 3214–3223, 2015, doi: 10.1021/acssuschemeng.5b00805.

[225] H. Pan, W. Wang, Y. Pan, L. Song, Y. Hu, and K. M. Liew, “Formation of layer-by-layer assembled titanate nanotubes filled coating on flexible polyurethane foam with improved flame retardant and smoke suppression properties,” *ACS Appl. Mater. Interfaces*, vol. 7, no. 1, pp. 101–111, 2015, doi: 10.1021/am507045g.

[226] M. Haile, S. Fomete, I. D. Lopez, and J. C. Grunlan, “Aluminum hydroxide multilayer assembly capable of extinguishing flame on polyurethane foam,” *J. Mater. Sci.*, vol. 51, no. 1, pp. 375–381, 2015, doi: 10.1007/s10853-015-9258-8.

[227] W. Wang *et al.*, “Synthesis and characterization of MnO2 nanosheets based multilayer coating and applications as a flame retardant for flexible polyurethane foam,” *Compos. Sci. Technol.*, vol. 123, pp. 212–221, 2016, doi: 10.1016/j.compscitech.2015.12.014.

[228] Y. Pan *et al.*, “Construction of organic–inorganic hybrid nano-coatings containing α-zirconium phosphate with high efficiency for reducing fire hazards of flexible polyurethane foam,” *Mater. Chem. Phys.*, vol. 163, pp. 107–115, Aug. 2015, doi: 10.1016/j.matchemphys.2015.07.020.

[229] H. Pan, Q. Shen, Z. Zhang, B. Yu, and Y. Lu, “MoS2-filled coating on flexible polyurethane foam via layer-by-layer assembly technique: flame-retardant and smoke suppression properties,” *J. Mater. Sci.*, vol. 53, no. 12, pp. 9340–9349, 2018, doi: 10.1007/s10853-018-2199-2.

[230] B. Lin *et al.*, “MXene/chitosan nanocoating for flexible polyurethane foam towards remarkable fire hazards reductions,” *J. Hazard. Mater.*, vol. 381, no. April 2019, 2020, doi: 10.1016/j.jhazmat.2019.120952.

[231] X. Mu *et al.*, “A single α-cobalt hydroxide/sodium alginate bilayer layer-by-layer assembly for conferring flame retardancy to flexible polyurethane foams,” *Mater. Chem. Phys.*, vol. 191, pp. 52–61, 2017, doi: 10.1016/j.matchemphys.2017.01.023.

[232] X. Qiu, Z. Li, X. Li, L. Yu, and Z. Zhang, “Construction and flame-retardant performance of layer-by-layer assembled hexagonal boron nitride coatings on flexible polyurethane foams,” *J. Appl. Polym. Sci.*, vol. 136, no. 29, pp. 1–9, 2019, doi: 10.1002/app.47839.

[233] Y. Pan, W. Cai, J. Du, L. Song, Y. Hu, and H. Zhao, “Lanthanum phenylphosphonate–based multilayered coating for reducing flammability and smoke production of flexible polyurethane foam,” *Polym. Adv. Technol.*, vol. 31, no. 6, pp. 1330–1339, 2020, doi: 10.1002/pat.4862.

[234] L. Liu, W. Wang, and Y. Hu, “Layered double hydroxide-decorated flexible polyurethane foam: Significantly improved toxic effluent elimination,” *RSC Adv.*, vol. 5, no. 118, pp. 97458–97466, 2015, doi: 10.1039/c5ra19414h.

[235] Y. H. Yang, Y. C. Li, J. Shields, and R. D. Davis, “Layer double hydroxide and sodium montmorillonite multilayer coatings for the flammability reduction of flexible polyurethane foams,” *J. Appl. Polym. Sci.*, vol. 132, no. 14, pp. 1–8, 2015, doi: 10.1002/app.41767.

[236] Y. C. Li, Y. H. Yang, J. R. Shields, and R. D. Davis, “Layered double hydroxide-based fire resistant coatings for flexible polyurethane foam,” *Polymer (Guildf).*, vol. 56, pp. 284–292, 2015, doi: 10.1016/j.polymer.2014.11.023.

[237] H. Pan *et al.*, “Fabrication of flame retardant coating on cotton fabric by alternate assembly of exfoliated layered double hydroxides and alginate,” *RSC Adv.*, vol. 6, no. 113, pp. 111950–111958, 2016, doi: 10.1039/c6ra21804k.

[238] Y. C. Li, S. Mannen, J. Schulz, and J. C. Grunlan, “Growth and fire protection behavior of POSS-based multilayer thin films,” *J. Mater. Chem.*, vol. 21, no. 9, pp. 3060–3069, 2011, doi: 10.1039/c0jm03752d.

[239] J. Alongi, A. Di Blasio, F. Carosio, and G. Malucelli, “UV-cured hybrid organic-inorganic Layer by Layer assemblies: Effect on the flame retardancy of polycarbonate films,” *Polym. Degrad. Stab.*, vol. 107, pp. 74–81, 2014, doi:

10.1016/j.polymdegradstab.2014.05.005.

[240] F. Carosio and J. Alongi, "Influence of layer by layer coatings containing octapropylammonium polyhedral oligomeric silsesquioxane and ammonium polyphosphate on the thermal stability and flammability of acrylic fabrics," *J. Anal. Appl. Pyrolysis*, vol. 119, pp. 114–123, 2016, doi: 10.1016/j.jaap.2016.03.010.

[241] Y. Ren, T. Huo, Y. Qin, and X. Liu, "Preparation of flame retardant polyacrylonitrile fabric based on sol-gel and layer-by-layer assembly," *Materials (Basel).*, vol. 11, no. 4, pp. 1–14, 2018, doi: 10.3390/ma11040483.

[242] F. Carosio, A. Di Pierro, J. Alongi, A. Fina, and G. Saracco, "Controlling the melt dripping of polyester fabrics by tuning the ionic strength of polyhedral oligomeric silsesquioxane and sodium montmorillonite coatings assembled through Layer by Layer," *J. Colloid Interface Sci.*, vol. 510, pp. 142–151, 2018, doi: 10.1016/j.jcis.2017.09.059.

[243] K. Choi, S. Seo, H. Kwon, D. Kim, and Y. T. Park, "Fire protection behavior of layer-by-layer assembled starch–clay multilayers on cotton fabric," *J. Mater. Sci.*, vol. 53, no. 16, pp. 11433–11443, 2018, doi: 10.1007/s10853-018-2434-x.

[244] Y. Pan, W. Wang, H. Pan, J. Zhan, and Y. Hu, "Fabrication of montmorillonite and titanate nanotube based coatings: Via layer-by-layer self-assembly method to enhance the thermal stability, flame retardancy and ultraviolet protection of polyethylene terephthalate (PET) fabric," *RSC Adv.*, vol. 6, no. 59, pp. 53625–53634, 2016, doi: 10.1039/c6ra05213d.

[245] S. Batool, R. Gill, C. Ma, G. C. S. Reddy, W. Guo, and Y. Hu, "Epoxy-based multilayers for flame resistant flexible polyurethane foam (FPUF)," *J. Appl. Polym. Sci.*, vol. 137, no. 29, pp. 1–10, 2020, doi: 10.1002/app.48890.

[246] T. Xu, L. Zhang, Y. Zhong, and Z. Mao, "Fire retardancy and durability of poly(N-benzyloxycarbonyl-3,4- dihydroxyphenylalanine)-montmorillonite composite film coated polyimide fabric," *J. Appl. Polym. Sci.*, vol. 131, no. 1, pp. 1–8, 2014, doi: 10.1002/app.39608.

[247] Y. S. Kim, R. Harris, and R. Davis, "Innovative approach to rapid growth of highly clay-filled coatings on porous polyurethane foam," *ACS Macro Lett.*, vol. 1, no. 7, pp. 820–824, 2012, doi: 10.1021/mz300102h.

[248] Y. C. Li, Y. S. Kim, J. Shields, and R. Davis, "Controlling polyurethane foam flammability and mechanical behaviour by tailoring the composition of clay-based multilayer nanocoatings," *J. Mater. Chem. A*, vol. 1, no. 41, pp. 12987–12997, 2013, doi: 10.1039/c3ta11936j.

[249] Y. S. Kim, Y. C. Li, W. M. Pitts, M. Werrel, and R. D. Davis, "Rapid growing clay coatings to reduce the fire threat of furniture," *ACS Appl. Mater. Interfaces*, vol. 6, no. 3, pp. 2146–2152, 2014, doi: 10.1021/am405259n.

[250] G. Laufer, C. Kirkland, A. A. Cain, and J. C. Grunlan, "Clay-chitosan nanobrick walls: Completely renewable gas barrier and flame-retardant nanocoatings," *ACS Applied Materials and Interfaces*, vol. 4, no. 3. pp. 1643–1649, 2012, doi: 10.1021/am2017915.

[251] W. O. Yah, A. Takahara, and Y. M. Lvov, “Selective modification of halloysite lumen with octadecylphosphonic acid: New inorganic tubular micelle,” *J. Am. Chem. Soc.*, vol. 134, no. 3, pp. 1853–1859, 2012, doi: 10.1021/ja210258y.

[252] R. J. Smith *et al.*, “Environmentally Benign Halloysite Nanotube Multilayer Assembly Significantly Reduces Polyurethane Flammability,” *Adv. Funct. Mater.*, vol. 28, no. 27, pp. 1–8, 2018, doi: 10.1002/adfm.201703289.

[253] Y. Pan, L. Liu, W. Cai, Y. Hu, S. Jiang, and H. Zhao, “Effect of layer-by-layer self-assembled sepiolite-based nanocoating on flame retardant and smoke suppressant properties of flexible polyurethane foam,” *Appl. Clay Sci.*, vol. 168, no. November 2018, pp. 230–236, 2019, doi: 10.1016/j.clay.2018.11.014.

[254] A. A. Cain, M. G. B. Plummer, S. E. Murray, L. Bolling, O. Regev, and J. C. Grunlan, “Iron-containing, high aspect ratio clay as nanoarmor that imparts substantial thermal/flame protection to polyurethane with a single electrostatically-deposited bilayer,” *J. Mater. Chem. A*, vol. 2, no. 41, pp. 17609–17617, 2014, doi: 10.1039/c4ta03541k.

[255] T. Guin, M. Krecker, A. Milhorn, D. A. Hagen, B. Stevens, and J. C. Grunlan, “Exceptional Flame Resistance and Gas Barrier with Thick Multilayer Nanobrick Wall Thin Films,” *Adv. Mater. Interfaces*, vol. 2, no. 11, pp. 1–7, 2015, doi: 10.1002/admi.201500214.

[256] S. Qin *et al.*, “Super Gas Barrier and Fire Resistance of Nanoplatelet/Nanofibril Multilayer Thin Films,” *Adv. Mater. Interfaces*, vol. 6, no. 2, pp. 1–6, 2019, doi: 10.1002/admi.201801424.

[257] F. Carosio, J. Kochumalayil, A. Fina, and L. A. Berglund, “Extreme Thermal Shielding Effects in Nanopaper Based on Multilayers of Aligned Clay Nanoplatelets in Cellulose Nanofiber Matrix,” *Adv. Mater. Interfaces*, vol. 3, no. 19, pp. 1–5, 2016, doi: 10.1002/admi.201600551.

[258] K. Apaydin *et al.*, “Polyallylamine-montmorillonite as super flame retardant coating assemblies by layer-by layer deposition on polyamide,” *Polym. Degrad. Stab.*, vol. 98, no. 2, pp. 627–634, 2013, doi: 10.1016/j.polymdegradstab.2012.11.006.

[259] K. Apaydin, A. Laachachi, T. Fouquet, M. Jimenez, S. Bourbigot, and D. Ruch, “Mechanistic investigation of a flame retardant coating made by layer-by-layer assembly,” *RSC Adv.*, vol. 4, no. 82, pp. 43326–43334, 2014, doi: 10.1039/c4ra08500k.

[260] B. Prieur *et al.*, “Phosphorylation of lignin: characterization and investigation of the thermal decomposition,” *RSC Adv.*, vol. 7, no. 27, pp. 16866–16877, 2017, doi: 10.1039/c7ra00295e.

[261] M. Le Bras, S. Bourbigot, Y. Le Tallec, and J. Laureyns, “Synergy in intumescence - Application to β-cyclodextrin carbonisation agent in intumescent additives for fire retardant polyethylene formulations,” *Polymer Degradation and Stability*, vol. 56, no. 1. pp. 11–21, 1997, doi: 10.1016/S0141-3910(96)00190-5.

[262] B. Schartel, “Phosphorus-based Flame Retardancy Mechanisms—Old Hat or a Starting Point for Future Development?,” *Materials (Basel).*, vol. 3, no. 10, pp. 4710–4745, Sep.

2010, doi: 10.3390/ma3104710.

[263] M. Lewin and E. D. Weil, "Mechanisms and modes of action in flame retardancy of polymers," in *Fire Retardant Materials*, A. R. Horrocks and D. Price, Eds. Boca Raton: Woodhead Publishing Limited, 2001, pp. 31–68.

[264] C. A. Wilkie and A. B. Morgan, *Fire Retardancy of Polymeric Materials*, CRC Press. Boca Raton: CRC Press Taylor and Francis Group, 2010.

[265] K. M. Gibov, L. N. Shapovalova, and B. A. Zhubanov, "Movement of destruction products through the carbonized layer upon combustion of polymers," *Fire Mater.*, vol. 10, no. 3–4, pp. 133–135, 1986, doi: 10.1002/fam.810100306.

[266] A. A. Cain, S. Murray, K. M. Holder, C. R. Nolen, and J. C. Grunlan, "Intumescent nanocoating extinguishes flame on fabric using aqueous polyelectrolyte complex deposited in single step," *Macromol. Mater. Eng.*, vol. 299, no. 10, pp. 1180–1187, 2014, doi: 10.1002/mame.201400022.

[267] M. Haile, C. Fincher, S. Fomete, and J. C. Grunlan, "Water-soluble polyelectrolyte complexes that extinguish fire on cotton fabric when deposited as pH-cured nanocoating," *Polym. Degrad. Stab.*, vol. 114, pp. 60–64, 2015, doi: 10.1016/j.polymdegradstab.2015.01.022.

[268] X. W. Cheng, R. C. Tang, F. Yao, and X. H. Yang, "Flame retardant coating of wool fabric with phytic acid/polyethyleneimine polyelectrolyte complex," *Prog. Org. Coatings*, vol. 132, no. March, pp. 336–342, 2019, doi: 10.1016/j.porgcoat.2019.04.018.

[269] I. S. Zope, S. Foo, D. G. J. Seah, A. T. Akunuri, and A. Dasari, "Development and Evaluation of a Water-Based Flame Retardant Spray Coating for Cotton Fabrics," *ACS Appl. Mater. Interfaces*, vol. 9, no. 46, pp. 40782–40791, 2017, doi: 10.1021/acsami.7b09863.

[270] E. M. Elsayed, N. F. Attia, and L. A. Alshehri, "Innovative Flame Retardant and Antibacterial Fabrics Coating Based on Inorganic Nanotubes," *ChemistrySelect*, vol. 5, no. 10, pp. 2961–2965, 2020, doi: 10.1002/slct.201904182.

[271] S. Barthwal, S. Barthwal, B. Singh, and N. Bahadur Singh, "Multifunctional and fluorine-free superhydrophobic composite coating based on PDMS modified MWCNTs/ZnO with self-cleaning, oil-water separation, and flame retardant properties," *Colloids Surfaces A Physicochem. Eng. Asp.*, vol. 597, no. January, p. 124776, 2020, doi: 10.1016/j.colsurfa.2020.124776.

[272] N. F. Attia and M. Mousa, "Synthesis of smart coating for furniture textile and their flammability and hydrophobic properties," *Prog. Org. Coatings*, vol. 110, no. April, pp. 204–209, 2017, doi: 10.1016/j.porgcoat.2017.04.035.

[273] R. Davis, Y. C. Li, M. Gervasio, J. Luu, and Y. S. Kim, "One-pot, bioinspired coatings to reduce the flammability of flexible polyurethane foams," *ACS Appl. Mater. Interfaces*, vol. 7, no. 11, pp. 6082–6092, 2015, doi: 10.1021/acsami.5b01105.

[274] F. Carosio, F. Cuttica, L. Medina, and L. A. Berglund, "Clay nanopaper as multifunctional brick and mortar fire protection coating-Wood case study," *Mater. Des.*,

vol. 93, pp. 357–363, 2016, doi: 10.1016/j.matdes.2015.12.140.

[275] B. Lecouvet, M. Sclavons, S. Bourbigot, and C. Bailly, “Highly loaded nanocomposite films as fire protective coating for polymeric substrates,” *J. Fire Sci.*, vol. 32, no. 2, pp. 145–164, 2014, doi: 10.1177/0734904113500207.

[276] H. Kim, D. W. Kim, V. Vasagar, H. Ha, S. Nazarenko, and C. J. Ellison, “Polydopamine-Graphene Oxide Flame Retardant Nanocoatings Applied via an Aqueous Liquid Crystalline Scaffold,” *Adv. Funct. Mater.*, vol. 28, no. 39, p. 1803172, Sep. 2018, doi: 10.1002/adfm.201803172.

[277] A. Walther *et al.*, “Large-area, lightweight and thick biomimetic composites with superior material properties via fast, economic, and green pathways,” *Nano Lett.*, vol. 10, no. 8, pp. 2742–2748, 2010, doi: 10.1021/nl1003224.

[278] J. George and H. Ishida, “A review on the very high nanofiller-content nanocomposites: Their preparation methods and properties with high aspect ratio fillers,” *Prog. Polym. Sci.*, vol. 86, pp. 1–39, 2018, doi: 10.1016/j.progpolymsci.2018.07.006.

[279] H. Xie *et al.*, “A highly efficient flame retardant nacre-inspired nanocoating with ultrasensitive fire-warning and self-healing capabilities,” *Chem. Eng. J.*, vol. 369, no. 381, pp. 8–17, 2019, doi: 10.1016/j.cej.2019.03.045.

[280] H. Xie, X. Lai, Y. Wang, H. Li, and X. Zeng, “A green approach to fabricating nacre-inspired nanocoating for super-efficiently fire-safe polymers via one-step self-assembly,” *J. Hazard. Mater.*, vol. 365, no. 381, pp. 125–136, 2019, doi: 10.1016/j.jhazmat.2018.10.099.

[281] F. Carosio and J. Alongi, “Flame retardant multilayered coatings on acrylic fabrics prepared by one-step deposition of chitosan/montmorillonite complexes,” *Fibers*, vol. 6, no. 2, pp. 1–11, 2018, doi: 10.3390/fib6020036.

[282] P. Das, S. Schipmann, J. M. Malho, B. Zhu, U. Klemradt, and A. Walther, “Facile access to large-scale, self-assembled, nacre-inspired, high-performance materials with tunable nanoscale periodicities,” *ACS Appl. Mater. Interfaces*, vol. 5, no. 9, pp. 3738–3747, 2013, doi: 10.1021/am400350q.

[283] P. Das, H. Thomas, M. Moeller, and A. Walther, “Large-scale, thick, self-assembled, nacre-mimetic brick-walls as fire barrier coatings on textiles,” *Sci. Rep.*, vol. 7, no. November 2016, pp. 1–13, 2017, doi: 10.1038/srep39910.

[284] F. Ding *et al.*, “Biomimetic nanocoatings with exceptional mechanical, barrier, and flame-retardant properties from large-scale one-step coassembly,” *Sci. Adv.*, vol. 3, no. 7, 2017, doi: 10.1126/sciadv.1701212.

[285] Y. Pan, L. Liu, X. Wang, L. Song, and Y. Hu, “Hypophosphorous acid cross-linked layer-by-layer assembly of green polyelectrolytes on polyester-cotton blend fabrics for durable flame-retardant treatment,” *Carbohydr. Polym.*, vol. 201, no. March, pp. 1–8, 2018, doi: 10.1016/j.carbpol.2018.08.044.

[286] J. Liu and C. Xiao, “Fire-retardant multilayer assembled on polyester fabric from water-soluble chitosan, sodium alginate and divalent metal ion,” *Int. J. Biol. Macromol.*, vol.

119, pp. 1083–1089, 2018, doi: 10.1016/j.ijbiomac.2018.08.043.

[287] W. E. Hennink and C. F. van Nostrum, “Novel crosslinking methods to design hydrogels,” *Adv. Drug Deliv. Rev.*, vol. 64, no. SUPPL., pp. 223–236, 2012, doi: 10.1016/j.addr.2012.09.009.

[288] N. A. Peppas and A. S. Hoffman, *Hydrogels*, Third Edit. Elsevier, 2013.

[289] Z. Wang, Y. Cong, and J. Fu, “Stretchable and tough conductive hydrogels for flexible pressure and strain sensors,” *J. Mater. Chem. B*, vol. 8, no. 16, pp. 3437–3459, 2020, doi: 10.1039/c9tb02570g.

[290] Z. Jiang and G. Dou, “Preparation and Characterization of Chitosan Grafting Hydrogel for Mine-Fire Fighting,” *ACS Omega*, vol. 5, no. 5, pp. 2303–2309, 2020, doi: 10.1021/acsomega.9b03551.

[291] T. Zhang, Z. Xu, H. Gui, and Q. Guo, “Emulsion-templated, macroporous hydrogels for enhancing water efficiency in fighting fires,” *J. Mater. Chem. A*, vol. 5, no. 21, pp. 10161–10164, 2017, doi: 10.1039/c7ta02319g.

[292] Y. Li *et al.*, “A novel high-toughness, organic/inorganic double-network fire-retardant gel for coal-seam with high ground temperature,” *Fuel*, vol. 263, no. August 2019, p. 116779, 2020, doi: 10.1016/j.fuel.2019.116779.

[293] X. Ren *et al.*, “Novel sodium silicate/polymer composite gels for the prevention of spontaneous combustion of coal,” *J. Hazard. Mater.*, vol. 371, no. March, pp. 643–654, 2019, doi: 10.1016/j.jhazmat.2019.03.041.

[294] Y. Tang and H. Wang, “Development of a novel bentonite–acrylamide superabsorbent hydrogel for extinguishing gangue fire hazard,” *Powder Technol.*, vol. 323, pp. 486–494, 2018, doi: 10.1016/j.powtec.2017.09.051.

[295] W. Cheng, X. Hu, J. Xie, and Y. Zhao, “An intelligent gel designed to control the spontaneous combustion of coal: Fire prevention and extinguishing properties,” *Fuel*, vol. 210, no. April, pp. 826–835, 2017, doi: 10.1016/j.fuel.2017.09.007.

[296] A. C. Yu *et al.*, “Scalable manufacturing of biomimetic moldable hydrogels for industrial applications,” *Proc. Natl. Acad. Sci. U. S. A.*, vol. 113, no. 50, pp. 14255–14260, 2016, doi: 10.1073/pnas.1618156113.

[297] Y. Yang, H. Zhu, Y. T. Tsai, L. Bai, and J. Deng, “Study on the Thermal Stability of Thermosensitive Hydrogel,” *Procedia Eng.*, vol. 135, pp. 501–509, 2016, doi: 10.1016/j.proeng.2016.01.162.

[298] Y. Yang, J. Deng, D. L. Zhao, and J. Guo, “Mechanism and property of extinguishing temperature-sensitive hydrogels,” *Proc. - 7th Int. Conf. Intell. Comput. Technol. Autom. ICICTA 2014*, pp. 360–364, 2015, doi: 10.1109/ICICTA.2014.94.

[299] Z. Yu *et al.*, “Preparation and characterisation of fire-resistant PNIPAAm/SA/AgNP thermosensitive network hydrogels and laminated cotton fabric used in firefighter protective clothing,” *Cellulose*, vol. 27, no. 9, pp. 5391–5406, 2020, doi: 10.1007/s10570-020-03146-1.

[300] W. R. K. Illeperuma, P. Rothemund, Z. Suo, and J. J. Vlassak, “Fire-Resistant Hydrogel-Fabric Laminates: A Simple Concept That May Save Lives,” *ACS Appl. Mater. Interfaces*, vol. 8, no. 3, pp. 2071–2077, 2016, doi: 10.1021/acsami.5b10538.

[301] J. Wei, G. Wei, Y. Shang, J. Zhou, C. Wu, and Q. Wang, “Dissolution–Crystallization Transition within a Polymer Hydrogel for a Processable Ultratough Electrolyte,” *Adv. Mater.*, vol. 31, no. 30, pp. 1–10, 2019, doi: 10.1002/adma.201900248.

[302] T. Zhang, Z. Xu, Y. Wu, and Q. Guo, “Assembled Block Copolymer Stabilized High Internal Phase Emulsion Hydrogels for Enhancing Oil Safety,” *Ind. Eng. Chem. Res.*, vol. 55, no. 16, pp. 4499–4505, 2016, doi: 10.1021/acs.iecr.6b00039.

[303] L. Y. Hsiao, L. Jing, K. Li, H. Yang, Y. Li, and P. Y. Chen, “Carbon nanotube-integrated conductive hydrogels as multifunctional robotic skin,” *Carbon N. Y.*, vol. 161, pp. 784–793, 2020, doi: 10.1016/j.carbon.2020.01.109.

[304] X. F. Cui *et al.*, “Water-retaining, tough and self-healing hydrogels and their uses as fire-resistant materials,” *Polym. Chem.*, vol. 10, no. 37, pp. 5151–5158, 2019, doi: 10.1039/c9py01015g.

[305] B. N. Mallick, P. K. Rana, and P. K. Sahoo, “Preparation of Starch-Based Bionanocomposite Hydrogel with Mica for Fire Retardancy,” *Adv. Polym. Technol.*, vol. 34, no. 4, p. 21520, Dec. 2015, doi: 10.1002/adv.21520.

[306] C. Chen *et al.*, “Compressive, ultralight and fire-resistant lignin-modified graphene aerogels as recyclable absorbents for oil and organic solvents,” *Chem. Eng. J.*, vol. 350, no. January, pp. 173–180, 2018, doi: 10.1016/j.cej.2018.05.189.

[307] L. Zuo *et al.*, “Graphene/montmorillonite hybrid synergistically reinforced polyimide composite aerogels with enhanced flame-retardant performance,” *Compos. Sci. Technol.*, vol. 139, pp. 57–63, 2017, doi: 10.1016/j.compscitech.2016.12.008.

[308] Y. Wang *et al.*, “Multifunctional polyimide aerogel textile inspired by polar bear hair for thermoregulation in extreme environments,” *Chem. Eng. J.*, vol. 390, no. January, p. 124623, 2020, doi: 10.1016/j.cej.2020.124623.

[309] Z. Qian *et al.*, “Fire-resistant, ultralight, superelastic and thermally insulated polybenzazole aerogels,” *J. Mater. Chem. A*, vol. 6, no. 42, pp. 20769–20777, 2018, doi: 10.1039/C8TA07204C.

[310] M. Kaya and A. Tabak, “Recycling of an Agricultural Bio-waste as a Novel Cellulose Aerogel: A Green Chemistry Study,” *J. Polym. Environ.*, vol. 28, no. 1, pp. 323–330, 2020, doi: 10.1007/s10924-019-01609-6.

[311] X. Luo, J. Shen, Y. Ma, L. Liu, R. Meng, and J. Yao, “Robust, sustainable cellulose composite aerogels with outstanding flame retardancy and thermal insulation,” *Carbohydr. Polym.*, vol. 230, no. November 2019, p. 115623, 2020, doi: 10.1016/j.carbpol.2019.115623.

[312] Y. Han, X. Zhang, X. Wu, and C. Lu, “Flame Retardant, Heat Insulating Cellulose Aerogels from Waste Cotton Fabrics by in Situ Formation of Magnesium Hydroxide Nanoparticles in Cellulose Gel Nanostructures,” *ACS Sustain. Chem. Eng.*, vol. 3, no. 8,

pp. 1853–1859, 2015, doi: 10.1021/acssuschemeng.5b00438.

[313] M. Kaya, “Super absorbent, light, and highly flame retardant cellulose-based aerogel crosslinked with citric acid,” *J. Appl. Polym. Sci.*, vol. 134, no. 38, p. 45315, Oct. 2017, doi: 10.1002/app.45315.

[314] X. Zhou *et al.*, “Excellent flame retardant and thermal insulated palygorskite/wood fiber composite aerogels with improved mechanical properties,” *Appl. Clay Sci.*, vol. 184, no. August 2019, p. 105402, 2020, doi: 10.1016/j.clay.2019.105402.

[315] M. Farooq, M. H. Sipponen, A. Seppälä, and M. Österberg, “Eco-friendly Flame-Retardant Cellulose Nanofibril Aerogels by Incorporating Sodium Bicarbonate,” *ACS Appl. Mater. Interfaces*, vol. 10, no. 32, pp. 27407–27415, 2018, doi: 10.1021/acsami.8b04376.

[316] D. Wang *et al.*, “Biomimetic structural cellulose nanofiber aerogels with exceptional mechanical, flame-retardant and thermal-insulating properties,” *Chem. Eng. J.*, vol. 389, no. February, p. 124449, 2020, doi: 10.1016/j.cej.2020.124449.

[317] B. Wicklein *et al.*, “Thermally insulating and fire-retardant lightweight anisotropic foams based on nanocellulose and graphene oxide,” *Nat. Nanotechnol.*, vol. 10, no. 3, pp. 277–283, 2015, doi: 10.1038/nnano.2014.248.

[318] L. Wang and M. Sánchez-Soto, “Green bio-based aerogels prepared from recycled cellulose fiber suspensions,” *RSC Adv.*, vol. 5, no. 40, pp. 31384–31391, 2015, doi: 10.1039/c5ra02981c.

[319] L. Guo, Z. Chen, S. Lyu, F. Fu, and S. Wang, “Highly flexible cross-linked cellulose nanofibril sponge-like aerogels with improved mechanical property and enhanced flame retardancy,” *Carbohydr. Polym.*, vol. 179, no. September 2017, pp. 333–340, 2018, doi: 10.1016/j.carbpol.2017.09.084.

[320] Z. Zhou, Y. Yang, Y. Han, Q. Guo, X. Zhang, and C. Lu, “In situ doping enables the multifunctionalization of templately synthesized polyaniline@cellulose nanocomposites,” *Carbohydr. Polym.*, vol. 177, no. August, pp. 241–248, 2017, doi: 10.1016/j.carbpol.2017.08.136.

[321] W. Guo, X. Wang, P. Zhang, J. Liu, L. Song, and Y. Hu, “Nano-fibrillated cellulose-hydroxyapatite based composite foams with excellent fire resistance,” *Carbohydr. Polym.*, vol. 195, no. November 2017, pp. 71–78, 2018, doi: 10.1016/j.carbpol.2018.04.063.

[322] L. Wang, M. Sánchez-Soto, J. Fan, Z. Xia, and Y. Liu, “Boron/nitrogen flame retardant additives cross-linked cellulose nanofibril/montmorillonite aerogels toward super-low flammability and improved mechanical properties,” *Polym. Adv. Technol.*, vol. 30, no. 7, pp. 1807–1817, Jul. 2019, doi: 10.1002/pat.4613.

[323] W. Guo, J. Liu, P. Zhang, L. Song, X. Wang, and Y. Hu, “Multi-functional hydroxyapatite/polyvinyl alcohol composite aerogels with self-cleaning, superior fire resistance and low thermal conductivity,” *Compos. Sci. Technol.*, vol. 158, pp. 128–136, 2018, doi: 10.1016/j.compscitech.2018.01.020.

[324] H. B. Chen, X. L. Li, M. J. Chen, Y. R. He, and H. B. Zhao, “Self-cross-linked melamine-formaldehyde-pectin aerogel with excellent water resistance and flame retardancy,” *Carbohydr. Polym.*, vol. 206, no. October 2018, pp. 609–615, 2019, doi: 10.1016/j.carbpol.2018.11.041.

[325] X. L. Li, Y. R. He, Z. M. Qin, M. J. Chen, and H. B. Chen, “Facile fabrication, mechanical property and flame retardancy of aerogel composites based on alginate and melamine-formaldehyde,” *Polymer (Guildf).*, vol. 181, no. June, p. 121783, 2019, doi: 10.1016/j.polymer.2019.121783.

[326] K. Shang, J. C. Yang, Z. J. Cao, W. Liao, Y. Z. Wang, and D. A. Schiraldi, “Novel Polymer Aerogel toward High Dimensional Stability, Mechanical Property, and Fire Safety,” *ACS Appl. Mater. Interfaces*, vol. 9, no. 27, pp. 22985–22993, 2017, doi: 10.1021/acsami.7b06096.

[327] Y. Huang *et al.*, “Flame-retardant polyvinyl alcohol/cellulose nanofibers hybrid carbon aerogel by freeze drying with ultra-low phosphorus,” *Appl. Surf. Sci.*, vol. 497, no. August, p. 143775, 2019, doi: 10.1016/j.apsusc.2019.143775.

[328] A. H. Kang *et al.*, “Rejuvenated fly ash in poly(vinyl alcohol)-based composite aerogels with high fire safety and smoke suppression,” *Chem. Eng. J.*, vol. 327, pp. 992–999, 2017, doi: 10.1016/j.cej.2017.06.158.

[329] H. B. Chen, Y. Z. Wang, and D. A. Schiraldi, “Preparation and flammability of poly(vinyl alcohol) composite aerogels,” *ACS Appl. Mater. Interfaces*, vol. 6, no. 9, pp. 6790–6796, 2014, doi: 10.1021/am500583x.

[330] Y. Luo *et al.*, “Synergistic effect of ammonium polyphosphate and α-zirconium phosphate in flame-retardant poly(vinyl alcohol) aerogels,” *Polym. Degrad. Stab.*, vol. 170, p. 109019, Dec. 2019, doi: 10.1016/j.polymdegradstab.2019.109019.

[331] X. Sheng, S. Li, Y. Zhao, D. Zhai, L. Zhang, and X. Lu, “Synergistic effects of two-dimensional mxene and ammonium polyphosphate on enhancing the fire safety of polyvinyl alcohol composite aerogels,” *Polymers (Basel).*, vol. 11, no. 12, pp. 1–17, 2019, doi: 10.3390/polym11121964.

[332] Q. Zhang, X. Wang, X. Tao, Z. Li, X. Li, and Z. Zhang, “Polyvinyl alcohol composite aerogel with remarkable flame retardancy, chemical durability and self-cleaning property,” *Compos. Commun.*, vol. 15, no. May, pp. 96–102, 2019, doi: 10.1016/j.coco.2019.07.003.

[333] L. Medina, F. Carosio, and L. A. Berglund, “Recyclable nanocomposite foams of Poly(vinyl alcohol), clay and cellulose nanofibrils – Mechanical properties and flame retardancy,” *Compos. Sci. Technol.*, vol. 182, no. May, p. 107762, 2019, doi: 10.1016/j.compscitech.2019.107762.

[334] Y. T. Wang *et al.*, “Green Approach to Improving the Strength and Flame Retardancy of Poly(vinyl alcohol)/Clay Aerogels: Incorporating Biobased Gelatin,” *ACS Appl. Mater. Interfaces*, vol. 9, no. 48, pp. 42258–42265, 2017, doi: 10.1021/acsami.7b14958.

[335] L. Wang, M. Sánchez-Soto, and M. L. Maspoch, “Polymer/clay aerogel composites with flame retardant agents: Mechanical, thermal and fire behavior,” *Mater. Des.*, vol. 52, pp.

609–614, 2013, doi: 10.1016/j.matdes.2013.05.096.

[336] K. Shang *et al.*, "Robust and fire retardant borate-crosslinked poly (vinyl alcohol)/montmorillonite aerogel via melt-crosslink," *Polymer (Guildf).*, vol. 131, pp. 111–119, 2017, doi: 10.1016/j.polymer.2017.07.022.

[337] A. Liu, L. Medina, and L. A. Berglund, "High-Strength Nanocomposite Aerogels of Ternary Composition: Poly(vinyl alcohol), Clay, and Cellulose Nanofibrils," *ACS Appl. Mater. Interfaces*, vol. 9, no. 7, pp. 6453–6461, 2017, doi: 10.1021/acsami.6b15561.

[338] H. B. Chen *et al.*, "Fabrication and properties of irradiation-cross-linked poly(vinyl alcohol)/clay aerogel composites," *ACS Appl. Mater. Interfaces*, vol. 6, no. 18, pp. 16227–16236, 2014, doi: 10.1021/am504418w.

[339] H. B. Zhao, M. Chen, and H. B. Chen, "Thermally Insulating and Flame-Retardant Polyaniline/Pectin Aerogels," *ACS Sustain. Chem. Eng.*, vol. 5, no. 8, pp. 7012–7019, 2017, doi: 10.1021/acssuschemeng.7b01247.

[340] D. D. Ye *et al.*, "Ultrahigh-Temperature Insulating and Fire-Resistant Aerogels from Cationic Amylopectin and Clay via a Facile Route," *ACS Sustain. Chem. Eng.*, vol. 7, no. 13, pp. 11582–11592, 2019, doi: 10.1021/acssuschemeng.9b01487.

[341] W. Yang *et al.*, "Pectin-assisted dispersion of exfoliated boron nitride nanosheets for assembled bio-composite aerogels," *Compos. Part A Appl. Sci. Manuf.*, vol. 119, no. December 2018, pp. 196–205, 2019, doi: 10.1016/j.compositesa.2019.02.003.

[342] J. Zhu *et al.*, "Lightweight, High-Strength, and Anisotropic Structure Composite Aerogel Based on Hydroxyapatite Nanocrystal and Chitosan with Thermal Insulation and Flame Retardant Properties," *ACS Sustain. Chem. Eng.*, vol. 8, no. 1, pp. 71–83, 2020, doi: 10.1021/acssuschemeng.9b03953.

[343] L. Wang, D. A. Schiraldi, and M. Sánchez-Soto, "Foamlike xanthan gum/clay aerogel composites and tailoring properties by blending with agar," *Ind. Eng. Chem. Res.*, vol. 53, no. 18, pp. 7680–7687, 2014, doi: 10.1021/ie500490n.

[344] L. Wang, M. Sánchez-Soto, and T. Abt, "Properties of bio-based gum Arabic/clay aerogels," *Ind. Crops Prod.*, vol. 91, pp. 15–21, 2016, doi: 10.1016/j.indcrop.2016.05.001.

[345] H. Jin *et al.*, "Ultralight and Hydrophobic Palygorskite-based Aerogels with Prominent Thermal Insulation and Flame Retardancy," *ACS Appl. Mater. Interfaces*, vol. 12, no. 10, pp. 11815–11824, 2020, doi: 10.1021/acsami.9b20923.

[346] K. Shang, W. Liao, J. Wang, Y. T. Wang, Y. Z. Wang, and D. A. Schiraldi, "Nonflammable Alginate Nanocomposite Aerogels Prepared by a Simple Freeze-Drying and Post-Cross-Linking Method," *ACS Appl. Mater. Interfaces*, vol. 8, no. 1, pp. 643–650, 2016, doi: 10.1021/acsami.5b09768.

[347] H. B. Chen, Y. Y. Ao, D. Liu, H. T. Song, and P. Shen, "Novel Neutron Shielding Alginate Based Aerogel with Extremely Low Flammability," *Ind. Eng. Chem. Res.*, vol. 56, no. 30, pp. 8563–8567, 2017, doi: 10.1021/acs.iecr.7b01999.

[348] X. L. Li, M. J. Chen, and H. B. Chen, "Facile fabrication of mechanically-strong and flame retardant alginate/clay aerogels," *Compos. Part B Eng.*, vol. 164, no. November 2018, pp. 18–25, 2019, doi: 10.1016/j.compositesb.2018.11.055.

[349] Q. Wang *et al.*, "Facile construction of cellulose/montmorillonite nanocomposite biobased plastics with flame retardant and gas barrier properties," *Cellulose*, vol. 22, no. 6, pp. 3799–3810, 2015, doi: 10.1007/s10570-015-0758-0.

[350] X. Zhang, B. Wu, S. Sun, and P. Wu, "Hybrid Materials from Ultrahigh-Inorganic-Content Mineral Plastic Hydrogels: Arbitrarily Shapeable, Strong, and Tough," *Adv. Funct. Mater.*, vol. 30, no. 19, p. 1910425, May 2020, doi: 10.1002/adfm.201910425.

[351] O. Gady, M. Poirson, T. Vincent, R. Sonnier, and E. Guibal, "Elaboration of light composite materials based on alginate and algal biomass for flame retardancy: preliminary tests," *J. Mater. Sci.*, vol. 51, no. 22, pp. 10035–10047, 2016, doi: 10.1007/s10853-016-0230-z.

[352] M. Försth, S. Zhao, and A. Roos, "Spectrally selective and adaptive surfaces for protection against radiative heating: ITO and VO2," *Fire Mater.*, vol. 38, pp. 111–124, 2014, doi: 10.1002/fam.2167.

[353] J. F. Sacadura, "Radiative heat transfer in fire safety science," *J. Quant. Spectrosc. Radiat. Transf.*, vol. 93, no. 1-3 SPEC. ISS., pp. 5–24, 2005, doi: 10.1016/j.jqsrt.2004.08.011.

[354] J. de Ris, "Fire radiation-A review," *Symp. Combust.*, vol. 17, no. 1, pp. 1003–1016, 1979, doi: 10.1016/S0082-0784(79)80097-1.

[355] J. De Ris, "A Scientific Approach To Flame Radiation And Material Flammability," *Fire Saf. Sci.*, vol. 2, pp. 29–46, 1989, doi: 10.3801/iafss.fss.2-29.

[356] A. Miller, "Fundamental Optical Properties of Solids," in *Handbook of optics, colume I*, 2nd ed., M. Bass, E. W. Van Stryland, D. R. Williams, and W. L. Wolfe, Eds. New York: McGraw-Hill , Inc, 1995, pp. 1–33.

[357] M. J. Riedl, *Optical Design Fundamentals for Infrared Systems, Second Edition*. Washington D.C.: SPIE Press, 2001.

[358] M. F. Modest, "Fundamentals of Thermal Radiation," in *Radiative Heat Transfer*, 3rd ed., Oxford: Elsevier, 2013, pp. 1–30.

[359] F. Kreith *et al.*, "Heat and mass transfer," in *Mechanical Engineering Handbook*, 1st ed., F. Kreith, Ed. Boca Raton: CRC Press LLC, 1999.

[360] P. Patel, T. R. Hull, A. A. Stec, and R. E. Lyon, "Influence of physical properties on polymer flammability in the cone calorimeter," *Polym. Adv. Technol.*, vol. 22, no. 7, pp. 1100–1107, 2011, doi: 10.1002/pat.1943.

[361] N. Roenner, H. Yuan, R. H. Krämer, and G. Rein, "Computational study of how inert additives affect the flammability of a polymer," *Fire Saf. J.*, vol. 106, no. December 2018, pp. 189–196, 2019, doi: 10.1016/j.firesaf.2019.04.013.

[362] I. Vermesi, N. Roenner, P. Pironi, R. M. Hadden, and G. Rein, “Pyrolysis and ignition of a polymer by transient irradiation,” *Combust. Flame*, vol. 163, pp. 31–41, 2016, doi: 10.1016/j.combustflame.2015.08.006.

[363] T. Nyazika, “Conceptualization of a fire barrier : fundamentals and experimental approach,” Université de Lille, 2019.

[364] M. Boccas, T. Vucina, C. Araya, E. Vera, and C. Ahhee, “Coating the 8-m Gemini telescopes with protected silver,” *Opt. Fabr. Metrol. Mater. Adv. Telesc.*, vol. 5494, no. May, p. 239, 2004, doi: 10.1117/12.548809.

[365] N. L. Thomas, J. D. Wolfe, and J. C. Farmer, “Protected silver coating for astronomical mirrors,” in *Advanced Technology Optical/IR Telescopes VI*, Aug. 1998, vol. 3352, no. May, pp. 580–586, doi: 10.1117/12.319243.

[366] C. Xu *et al.*, “An optically transparent sandwich structure for radar-infrared bi-stealth,” *Infrared Phys. Technol.*, vol. 105, no. September 2019, p. 103108, 2020, doi: 10.1016/j.infrared.2019.103108.

[367] L. Peng, D. Liu, H. Cheng, S. Zhou, and M. Zu, “A Multilayer Film Based Selective Thermal Emitter for Infrared Stealth Technology,” *Adv. Opt. Mater.*, vol. 6, no. 23, pp. 1–8, 2018, doi: 10.1002/adom.201801006.

[368] Z. Mao, X. Yu, L. Zhang, Y. Zhong, and H. Xu, “Novel infrared stealth property of cotton fabrics coated with nano ZnO: (Al, La) particles,” *Vacuum*, vol. 104, pp. 111–115, 2014, doi: 10.1016/j.vacuum.2014.01.011.

[369] G. K. Dalapati *et al.*, “Transparent heat regulating (THR) materials and coatings for energy saving window applications: Impact of materials design, micro-structural, and interface quality on the THR performance,” *Prog. Mater. Sci.*, vol. 95, pp. 42–131, 2018, doi: 10.1016/j.pmatsci.2018.02.007.

[370] M. Ohring, “Mechanical Properties of Thin Films,” in *Materials Science of Thin Films*, 2nd ed., A. Press, Ed. San Diego: Elsevier, 2002, pp. 711–781.

[371] P. H. Berdahl, “Pigments which Reflect Infrared Radiation from Fire,” 5,811,180, 1998.

[372] P. Berdahl, “Pigments to reflect the infrared radiation from fire,” *J. Heat Transfer*, vol. 117, no. 2, pp. 355–358, 1995, doi: 10.1115/1.2822529.

[373] P. Berdahl, “Building energy efficiency and fire safety aspects of reflective coatings,” *Energy Build.*, vol. 22, no. 3, pp. 187–191, 1995, doi: 10.1016/0378-7788(95)00921-J.

[374] J. Zhao *et al.*, “The high-temperature resistance properties of polysiloxane/Al coatings with low infrared emissivity,” *Coatings*, vol. 8, no. 4, 2018, doi: 10.3390/coatings8040125.

[375] L. Qi *et al.*, “Effects of low-melting glass powder on the thermal stabilities of low infrared emissivity Al/polysiloxane coatings,” *Prog. Org. Coatings*, vol. 142, no. January, p. 105579, 2020, doi: 10.1016/j.porgcoat.2020.105579.

[376] R. Sonnier, L. Ferry, B. Gallard, A. Boudenne, and F. Lavaud, “Controlled emissivity

coatings to delay ignition of polyethylene," *Materials (Basel).*, vol. 8, no. 10, pp. 6935–6949, 2015, doi: 10.3390/ma8105349.

[377] B. Schartel, U. Beck, H. Bahr, A. Hertwig, U. Knoll, and M. Weise, "Sub-micrometre coatings as an infrared mirror: A new route to flame retardancy," *Fire Mater.*, vol. 36, pp. 671–677, 2012, doi: 10.1002/fam.1122.

[378] R. Ochoterena and M. Försth, "The effect of thermochromic coatings of VO 2 on the fire performance of windows," *Fire Mater.*, vol. 42, no. 7, pp. 873–876, Nov. 2018, doi: 10.1002/fam.2630.

[379] Y. H. Yang, M. Haile, Y. T. Park, F. A. Malek, and J. C. Grunlan, "Super gas barrier of all-polymer multilayer thin films," *Macromolecules*, vol. 44, no. 6, pp. 1450–1459, 2011, doi: 10.1021/ma1026127.

[380] D. K. Chattopadhyay and D. C. Webster, "Thermal stability and flame retardancy of polyurethanes," *Prog. Polym. Sci.*, vol. 34, no. 10, pp. 1068–1133, 2009, doi: 10.1016/j.progpolymsci.2009.06.002.

[381] B. Schartel and T. R. Hull, "Development of fire-retarded materials — Interpretation of cone calorimeter data," *Fire Mater.*, vol. 31, pp. 327–354, 2007, doi: 10.1002/fam.

[382] I. Corazzari *et al.*, "Advanced physico-chemical characterization of chitosan by means of TGA coupled on-line with FTIR and GCMS: Thermal degradation and water adsorption capacity," *Polym. Degrad. Stab.*, vol. 112, pp. 1–9, 2015, doi: 10.1016/j.polymdegradstab.2014.12.006.

[383] R. G. Gann, "Estimating data for incapacitation of people by fire smoke," *Fire Technol.*, vol. 40, no. 2, pp. 201–207, 2004, doi: 10.1023/B:FIRE.0000016843.38848.37.

[384] G. Socrates, *Infrared and Raman characteristic group frequencies: tables and charts*. Chichester: Wiley, 2001.

[385] P. Tranchard *et al.*, "Fire behaviour of carbon fibre epoxy composite for aircraft: Novel test bench and experimental study," *J. Fire Sci.*, vol. 33, no. 3, pp. 247–266, 2015, doi: 10.1177/0734904115584093.

[386] S. T. McKenna and T. R. Hull, "The fire toxicity of polyurethane foams," *Fire Sci. Rev.*, vol. 5, no. 1, 2016, doi: 10.1186/s40038-016-0012-3.

[387] V. Balek, J. L. Pérez-Rodríguez, L. A. Pérez-Maqueda, J. Šubrt, and J. Poyato, "Thermal behaviour of ground vermiculite," *J. Therm. Anal. Calorim.*, vol. 88, no. 3, pp. 819–823, 2007, doi: 10.1007/s10973-005-7462-5.

[388] Z. Weiss, M. Vaĺǎskov́a, M. Ǩristkov́a, P. ̌Capkov́a, and M. Pospǐsil, "Intercalation and grafting of vermiculite with octadecylamine using low-temperature melting," *Clays Clay Miner.*, vol. 51, no. 5, pp. 555–565, 2003, doi: 10.1346/CCMN.2003.0510509.

[389] S. Duquesne *et al.*, "Mechanism of fire retardancy of polyurethanes using ammonium polyphosphate," *J. Appl. Polym. Sci.*, vol. 82, no. 13, pp. 3262–3274, 2001, doi: 10.1002/app.2185.

[390] S. Bourbigot, M. Le Bras, R. Delobel, and J. M. Trémillon, “Synergistic effect of zeolite in an intumescence process: Study of the interactions between the polymer and the additives,” *J. Chem. Soc. - Faraday Trans.*, vol. 92, no. 18, pp. 3435–3444, 1996, doi: 10.1039/FT9969203435.

[391] R. Brindle, K. Albert, S. J. Harris, C. Tröltzsch, E. Horne, and J. D. Glennon, “Silica-bonded calixarenes in chromatography,” *J. Chromatogr. A*, vol. 731, no. 1–2, pp. 41–46, 1996, doi: 10.1016/0021-9673(95)01079-3.

[392] C. A. Fyfe, Y. Zhang, and P. Aroca, “An Alternative Preparation of Organofunctionalized Silica Gels and Their Characterization by Two-Dimensional High-Resolution Solid-State Heteronuclear NMR Correlation Spectroscopy,” *J. Am. Chem. Soc.*, vol. 114, no. 9, pp. 3252–3255, 1992, doi: 10.1021/ja00035a014.

[393] J. H. Smitrovich and K. A. Woerpel, “Oxidation of sterically hindered alkoxysilanes and phenylsilanes under basic conditions,” *J. Org. Chem.*, vol. 61, no. 17, pp. 6044–6046, 1996, doi: 10.1021/jo960921l.

[394] H. Marsmann, “29Si-NMR Spectroscopic Results,” in *Oxygen-17 and Silicon-29, NMR Basic Principles and Progress / NMR Grundlagen und Fortschritte, volume 17*, P. Diehl, E. Fluck, and R. Kosfeld, Eds. Berlin, Heidelberg: Springer-Verlag GmbH, 1981, pp. 65–235.

[395] M. L. Bocquet, B. Coasne, R. Pellenq, and F. J. Ulm, “Organic-clay interfacial chemical bonds probed by ab initio calculations,” *J. Phys. Chem. C*, vol. 119, no. 12, pp. 6511–6517, 2015, doi: 10.1021/jp510885f.

[396] K. Zhang, Y. Feng, F. Wang, Z. Yang, and J. Wang, “Two dimensional hexagonal boron nitride (2D-hBN): Synthesis, properties and applications,” *J. Mater. Chem. C*, vol. 5, no. 46, pp. 11992–12022, 2017, doi: 10.1039/c7tc04300g.

[397] J. Wang, F. Ma, and M. Sun, “Graphene, hexagonal boron nitride, and their heterostructures: properties and applications,” *RSC Adv.*, vol. 7, no. 27, pp. 16801–16822, 2017, doi: 10.1039/c7ra00260b.

[398] W. Luo, Y. Wang, E. Hitz, Y. Lin, B. Yang, and L. Hu, “Solution Processed Boron Nitride Nanosheets: Synthesis, Assemblies and Emerging Applications,” *Adv. Funct. Mater.*, vol. 27, no. 31, pp. 1–19, 2017, doi: 10.1002/adfm.201701450.

[399] Y. Lin, T. V. Williams, T. B. Xu, W. Cao, H. E. Elsayed-Ali, and J. W. Connell, “Aqueous dispersions of few-layered and monolayered hexagonal boron nitride nanosheets from sonication-assisted hydrolysis: Critical role of water,” *J. Phys. Chem. C*, vol. 115, no. 6, pp. 2679–2685, 2011, doi: 10.1021/jp110985w.

[400] D. Gonzalez Ortiz, C. Pochat-Bohatier, J. Cambedouzou, M. Bechelany, and P. Miele, “Exfoliation of hexagonal boron nitride (h-BN) in liquide phase by ion intercalation,” *Nanomaterials*, vol. 8, no. 9, pp. 1–12, 2018, doi: 10.3390/nano8090716.

[401] S. Y. Xie, W. Wang, K. A. S. Fernando, X. Wang, Y. Lin, and Y. P. Sun, “Solubilization of boron nitride nanotubes,” *Chem. Commun.*, no. 29, pp. 3670–3672, 2005, doi: 10.1039/b505330g.

[402] S. Kumari, O. P. Sharma, and O. P. Khatri, "Alkylamine-functionalized hexagonal boron nitride nanoplatelets as a novel material for the reduction of friction and wear," *Phys. Chem. Chem. Phys.*, vol. 18, no. 33, pp. 22879–22888, 2016, doi: 10.1039/c6cp04741f.

[403] Y. Lin, T. V. Williams, and J. W. Connell, "Soluble, exfoliated hexagonal boron nitride nanosheets," *J. Phys. Chem. Lett.*, vol. 1, no. 1, pp. 277–283, 2010, doi: 10.1021/jz9002108.

[404] P. S. Marchetti, G. E. Maciel, D. Kwon, W. R. Schmidt, and L. V. Interrante, "High-Field 11B Magic-Angle Spinning NMR Characterization of Boron Nitrides," *Chem. Mater.*, vol. 3, no. 3, pp. 482–486, 1991, doi: 10.1021/cm00015a023.

[405] C. Gervais and F. Babonneau, "High resolution solid state NMR investigation of various boron nitride preceramic polymers," *J. Organomet. Chem.*, vol. 657, no. 1–2, pp. 75–82, 2002, doi: 10.1016/S0022-328X(02)01586-3.

[406] C. Gervais, E. Framery, C. Duriez, J. Maquet, M. Vaultier, and F. Babonneau, "11B and 15N solid state NMR investigation of a boron nitride preceramic polymer prepared by ammonolysis of borazine," *J. Eur. Ceram. Soc.*, vol. 25, no. 2-3 SPEC. ISS., pp. 129–135, 2005, doi: 10.1016/j.jeurceramsoc.2004.07.010.

[407] C. J. Jachimowski, "Report NASA TN D-8098 Analytical study of mechanisms for nitric oxide formation during combustion of methane in a jet-stirred combustor," National Aeronautics and Space Administration, Hampton, VA, 1975.

[408] A. L. Davesne *et al.*, "Hexagonal Boron Nitride Platelet-Based Nanocoating for Fire Protection," *ACS Appl. Nano Mater.*, vol. 2, no. 9, pp. 5450–5459, 2019, doi: 10.1021/acsanm.9b01055.

[409] P. Podsiadlo, Z. Tang, B. S. Shim, and N. A. Kotov, "Counterintuitive effect of molecular strength and role of molecular rigidity on mechanical properties of layer-by-layer assembled nanocomposites," *Nano Lett.*, vol. 7, no. 5, pp. 1224–1231, 2007, doi: 10.1021/nl0700649.

[410] P. Podsiadlo *et al.*, "Ultrastrong and stiff layered polymer nanocomposites," *Science (80-.).*, vol. 318, no. 5847, pp. 80–83, 2007, doi: 10.1126/science.1143176.

[411] D. Rosu, L. Rosu, and C. N. Cascaval, "IR-change and yellowing of polyurethane as a result of UV irradiation," *Polym. Degrad. Stab.*, vol. 94, no. 4, pp. 591–596, 2009, doi: 10.1016/j.polymdegradstab.2009.01.013.

[412] T. Van Tran, F. Abedin, A. Usta, and R. Asmatulu, "Polyurethane nanocomposite coating with silanized graphene and hexagonal boron nitride as nanoadditives for improved resistance against ultraviolet degradation," *J. Compos. Mater.*, vol. 53, no. 10, pp. 1387–1399, 2019, doi: 10.1177/0021998318799402.

[413] H. Qin, S. Zhang, C. Zhao, G. Hu, and M. Yang, "Flame retardant mechanism of polymer/clay nanocomposites based on polypropylene," *Polymer (Guildf).*, vol. 46, no. 19 SPEC. ISS., pp. 8386–8395, 2005, doi: 10.1016/j.polymer.2005.07.019.

[414] P. R. Hornsby, J. Wang, R. Rothon, G. Jackson, G. Wilkinson, and K. Cossick, "Thermal decomposition behaviour of polyamide fire-retardant compositions containing

magnesium hydroxide filler," *Polym. Degrad. Stab.*, vol. 51, no. 3, pp. 235–249, 1996, doi: 10.1016/0141-3910(95)00181-6.

[415] J. Zhang, Q. Ji, X. Shen, Y. Xia, L. Tan, and Q. Kong, "Pyrolysis products and thermal degradation mechanism of intrinsically flame-retardant calcium alginate fibre," *Polym. Degrad. Stab.*, vol. 96, no. 5, pp. 936–942, 2011, doi: 10.1016/j.polymdegradstab.2011.01.029.

[416] R. D. Davis, J. W. Gilman, and D. L. VanderHart, "Processing degradation of polyamide 6/montmorillonite clay nanocomposites and clay organic modifier," *Polym. Degrad. Stab.*, vol. 79, no. 1, pp. 111–121, 2003, doi: 10.1016/S0141-3910(02)00263-X.

[417] P. Kiliaris and C. D. Papaspyrides, "Polymer/layered silicate (clay) nanocomposites: An overview of flame retardancy," *Prog. Polym. Sci.*, vol. 35, no. 7, pp. 902–958, 2010, doi: 10.1016/j.progpolymsci.2010.03.001.

[418] H. Qin, Q. Su, S. Zhang, B. Zhao, and M. Yang, "Thermal stability and flammability of polyamide 66/montmorillonite nanocomposites," *Polymer (Guildf).*, vol. 44, no. 24, pp. 7533–7538, 2003, doi: 10.1016/j.polymer.2003.09.014.

[419] H. Bockhorn, A. Hornung, U. Hornung, and J. Weichmann, "Kinetic study on the non-catalysed and catalysed degradation of polyamide 6 with isothermal and dynamic methods," *Thermochim. Acta*, vol. 337, no. 1–2, pp. 97–110, 1999, doi: 10.1016/s0040-6031(99)00151-3.

[420] K. Y. Lee and D. J. Mooney, "Alginate: Properties and biomedical applications," *Prog. Polym. Sci.*, vol. 37, no. 1, pp. 106–126, 2012, doi: 10.1016/j.progpolymsci.2011.06.003.

[421] M. M. Pérez-Madrigal, J. Torras, J. Casanovas, M. Häring, C. Alemán, and D. D. Díaz, "Paradigm Shift for Preparing Versatile M2+-Free Gels from Unmodified Sodium Alginate," *Biomacromolecules*, vol. 18, no. 9, pp. 2967–2979, 2017, doi: 10.1021/acs.biomac.7b00934.

[422] K. Wu, Z. Song, L. He, and Y. Ni, "Analysis of optimal crosslink density and platelet size insensitivity in graphene-based artificial nacres," *Nanoscale*, vol. 10, no. 2, pp. 556–565, 2018, doi: 10.1039/c7nr06748h.

[423] V. Bertolino *et al.*, "Effect of the biopolymer charge and the nanoclay morphology on nanocomposite materials," *Ind. Eng. Chem. Res.*, vol. 55, no. 27, pp. 7373–7380, 2016, doi: 10.1021/acs.iecr.6b01816.

[424] L. Geoffroy *et al.*, "3D printed sandwich materials filled with hydrogels for extremely low heat release rate," *Polym. Degrad. Stab.*, vol. 179, p. 109269, 2020, doi: 10.1016/j.polymdegradstab.2020.109269.

[425] G. Hass, J. B. Heaney, H. Herzig, J. F. Osantowski, and J. J. Triolo, "Reflectance and durability of Ag mirrors coated with thin layers of Al_2O_3 plus reactively deposited silicon oxide," *Appl. Opt.*, vol. 14, no. 11, p. 2639, 1975, doi: 10.1364/ao.14.002639.

[426] W. J. . Tropf, M. E. Thomas, and T. J. . Harris, "Part IV: Optical and Physical Properties of Materials Crystals and Glasses," in *Handbook of Optics, volume II*, 2nd ed., McGraw-Hill, Ed. New York: Optical Society of America, 2009, p. 1152.

[427] W. Sabuga and R. Todtenhaupt, “Effect of roughness on the emissivity of the precious metals silver, gold, palladium, platinum, rhodium, and iridium,” *High Temp. - High Press.*, vol. 33, no. 3, pp. 261–269, 2001, doi: 10.1068/htwu371.

[428] N. Delorme *et al.*, “Experimental evidence of ultrathin polymer film stratification by AFM force spectroscopy,” *Eur. Phys. J. E*, vol. 38, no. 6, 2015, doi: 10.1140/epje/i2015-15056-9.

[429] Y. Bao, J. Gao, and D. T. Gawne, “Crack formation and its prevention in PVD films on epoxy coatings,” *Surf. Coatings Technol.*, vol. 205, no. 1, pp. 15–21, 2010, doi: 10.1016/j.surfcoat.2010.05.037.

[430] R. van Tijum, W. P. Vellinga, and J. T. M. De Hosson, “Surface roughening of metal-polymer systems during plastic deformation,” *Acta Mater.*, vol. 55, no. 8, pp. 2757–2764, 2007, doi: 10.1016/j.actamat.2006.12.013.

[431] R. Van Tijum, W. P. Vellinga, and J. T. M. De Hosson, “Adhesion along metal-polymer interfaces during plastic deformation,” *J. Mater. Sci.*, vol. 42, no. 10, pp. 3529–3536, 2007, doi: 10.1007/s10853-006-1374-z.

[432] W. Viehmann and A. G. Eubanks, “Effects of surface contamination on the infrared emissivity and visible-light scattering of highly reflective surfaces at cryogenic temperatures,” Maryland, 1972.

[433] F. Samyn, “Compréhension des procédés d’ignifugation du polyamide 6 Apport des nanocomposites aux systèmes retardateurs de flamme phosphorés,” Université de Lille, 2007.

[434] F. Samyn and S. Bourbigot, “Protection mechanism of a flame-retarded polyamide 6 nanocomposite,” *J. Fire Sci.*, vol. 32, no. 3, pp. 241–256, 2014, doi: 10.1177/0734904113510685.

[435] U. Braun, B. Schartel, M. A. Fichera, and C. Jäger, “Flame retardancy mechanisms of aluminium phosphinate in combination with melamine polyphosphate and zinc borate in glass-fibre reinforced polyamide 6,6,” *Polym. Degrad. Stab.*, vol. 92, no. 8, pp. 1528–1545, 2007, doi: 10.1016/j.polymdegradstab.2007.05.007.

[436] U. Braun, H. Bahr, and B. Schartel, “Fire retardancy effect of aluminium phosphinate and melamine polyphosphate in glass fibre reinforced polyamide 6,” *E-Polymers*, no. 041, pp. 1–14, 2010, doi: 10.1515/epoly.2010.10.1.443.

[437] M. Casetta, G. Michaux, B. Ohl, S. Duquesne, and S. Bourbigot, “Key role of magnesium hydroxide surface treatment in the flame retardancy of glass fiber reinforced polyamide 6,” *Polym. Degrad. Stab.*, vol. 148, no. December 2017, pp. 95–103, 2018, doi: 10.1016/j.polymdegradstab.2018.01.007.

[438] G. Michaux, “Fire retardancy of Polyamide 6 for electrotechnical applications,” Université de Lille, 2014.

[439] M. A. Kats *et al.*, “Enhancement of absorption and color contrast in ultra-thin highly absorbing optical coatings,” *Appl. Phys. Lett.*, vol. 103, no. 10, 2013, doi: 10.1063/1.4820147.

[440] M. J. Hurley *et al.*, Eds., *SFPE Handbook of Fire Protection Engineering*. New York, NY: Springer New York, 2016.

[441] S. Kang, M. Kwon, J. Y. Choi, and S. Choi, “Thermal boundaries in cone calorimetry testing,” *Coatings*, vol. 9, no. 10, 2019, doi: 10.3390/coatings9100629.

[442] S. Bourbigot, J. Sarazin, T. Bensabath, F. Samyn, and M. Jimenez, “Intumescent polypropylene: Reaction to fire and mechanistic aspects,” *Fire Saf. J.*, vol. 105, no. December 2018, pp. 261–269, 2019, doi: 10.1016/j.firesaf.2019.03.007.

[443] C. Hu *et al.*, “New design for highly durable Infrared-Reflective coatings,” *Light Sci. Appl.*, vol. 7, no. 4, pp. 17111–17175, 2018, doi: 10.1038/lsa.2017.175.

[444] Z. Zheng, M. C. Cox, and B. Li, “Surface modification of hexagonal boron nitride nanomaterials: a review,” *J. Mater. Sci.*, vol. 53, no. 1, pp. 66–99, 2018, doi: 10.1007/s10853-017-1472-0.

[445] D. Massiot *et al.*, “Modelling one- and two-dimensional solid-state NMR spectra,” *Magnetic Resonance in Chemistry*, vol. 40, no. 1. pp. 70–76, 2002, doi: 10.1002/mrc.984.

[446] B. J. H. Stadler, “Vapor processes,” in *Materials Processing - A Unified Approach to Processing of Metals, Ceramics and Polymers*, L. F. Francis, Ed. Amsterdam: Elsevier Science, 2015, pp. 513–582.

[447] A. Billard and F. Perry, “Pulvérisation cathodique magnétron,” *Techniques de l’ingénieur Traitements de surface des métaux par voie sèche et en milieu fondu*, vol. base docum, no. ref. article : m1654. Editions T.I., 2005.

[448] B. Girardin, “Numerical Modelling and Small Scale Testing of Fire Performances for Halogen-Free Cable,” Université de Lille, 2016.

[449] J. G. Thompson, “ 29 Si and 27 Al nuclear magnetic resonance spectroscopy of 2:1 clay minerals ,” *Clay Miner.*, vol. 19, no. 2, pp. 229–236, 1984, doi: 10.1180/claymin.1984.019.2.09.

Conception de nouveaux revêtements fins pour la protection contre le feu

Résumé : L'utilisation intensive de matériaux polymères, hautement inflammables, nécessite le développement de solutions efficaces afin de protéger les hommes et les infrastructures des incendies. Les revêtements fins notamment permettent de réguler les transferts de masse et de chaleur à l'origine du processus de combustion, directement à l'interface entre le matériau et la flamme. En outre, la concentration des retardateurs de flamme à la surface du matériau limite l'utilisation de matière, avec un impact minimum sur les propriétés fonctionnelles du substrat. Le but de cette thèse est de concevoir des revêtements fins innovants, adaptés à plusieurs types de substrats, grâce à une compréhension approfondie du mécanisme de protection de systèmes connus pour être efficaces. Les revêtements en « couche par couche » sont vus comme une solution efficace pour diminuer l'inflammabilité des polymères, et sont particulièrement adaptés aux matériaux poreux. Malgré de nombreuses études, leur mécanisme d'action demeure incertain. Des revêtements « couche par couche », constitués soit de chitosan et de vermiculite, soit de polyethylenimine et de nitrure de bore hexagonal, ont été déposés sur des mousses en polyuréthane. Une analyse détaillée de ces matériaux, avant et après avoir été soumis à différents scénario feu, a permis de rassembler les éléments nécessaires à la compréhension de leur mécanisme d'action. Les résultats de cette analyse ont été appliqués au développement de nouveaux concepts. En premier lieu, des revêtements composites à haut taux de charge composés d'hydrogel alginate/argile ont été appliqués en une seule étape sur des tissus en polyamide 66. La réticulation de la matrice a amélioré la stabilité thermique et l'effet barrière physique du revêtement, ce qui a permis de classer les échantillons V-0 au test UL94. Ensuite, un autre type de barrière physique constituée d'une bicouche métal/diélectrique a été déposé sur des plaques de polyamide 6. L'action de ce revêtement repose sur la réflexion du rayonnement infrarouge, ce qui réduit l'absorption de chaleur par le substrat et augmente considérablement le temps d'ignition du polymère sous une contrainte thermique radiative. Ce concept s'est montré très efficace en combinaison avec des retardateurs de flamme (RF) dans la masse. Les deux approches ont un effet complémentaire. Le revêtement agit en premier en limitant l'absorption de chaleur et en retardant l'action des RF. Lorsqu'il perd son intégrité, les charges prennent le relais sans que leur efficacité ne soit diminuée, et réduisent le pic de débit calorifique et la quantité de chaleur dégagée totale du polyamide 6 grâce à l'action de mécanismes physiques et chimiques.

Mots-clés : Revêtements fins, protection contre le feu, revêtements couche-par-couche, hydrogels, revêtements à basse émissivité

New Design of Thin Coatings for Fire Protection

Abstract: The extensive use of highly flammable polymeric materials requires the development of innovative fire protective solutions to lower the threat on human lives and infrastructures integrity. Thin coatings especially act on the mass and heat transfer responsible for the combustion process directly at the interface between the substrate and the flame. They also have the advantage of concentrating the fire retardant system on one place, therefore using the smallest amount of material as possible, and with minimal impact on the bulk properties of the material. The aim of this Ph.D is to design innovative thin coatings adapted to various substrates, based on an in-depth understanding of the mechanism of action of effective systems. Layer-by-layer coatings are seen as a very efficient solution to lower the flammability of polymers and are particularly adapted to porous substrates. Though extensively studied, their mechanism of action remains unclear. Layer-by-layer coatings, composed either of chitosan and vermiculite or of polyethyleneimine and hexagonal boron nitride, were deposited on flexible polyurethane foam. Extensive analysis of the material before and after being exposed to various thermal constraints allowed to gather more insights on their mechanism of action. This knowledge was applied to develop new concepts. On the first hand, high-filler content composite coatings based on alginate/clay hydrogels were applied in a one pot process on polyamide 66 fabrics. The cross-linked network improved the thermal stability and physical barrier effect of the coating, and the approach was proven to be efficient as the samples were rated V-0 at UL94 test. On the other hand, another kind of thin physical barrier deposited by PVD and composed of protected metal was deposited on polyamide 6 plate. Relying on the reflection of infrared rays, this type of coating reduced the heat absorption by the substrate, and considerably increased the time to ignition in a radiative fire scenario. This concept was proven particularly efficient when combined with thermally triggered bulk fire retardant (FR) fillers. It was found that both approaches have a complementary effect. The coating acts first by reducing the heat absorption, delaying the activation of the FR systems. Once it fails, the fillers take over unhindered, allowing to reduce the peak of Heat Release Rate and Total Heat Release of polyamide 6 thanks to physical and chemical mechanisms.

Key-words: Thin coatings, fire protection, layer-by-layer coatings, hydrogels, low-emissivity coatings